AD-A064 157 AERONAUTICAL RESEARCH ASSOCIATES OF PRINCETON INC N J F/G 1/2
GUST RESPONSE ANALYSES FOR TEN GENERAL AVIATION AIRCRAFT USING --ETC(U)
OCT 78 G G WILLIAMSON DOT-FA77WA-3972
UNCLASSIFIED ARAP-344 FAA-RD-78-117 NL

1 OF 2
AD
A064157

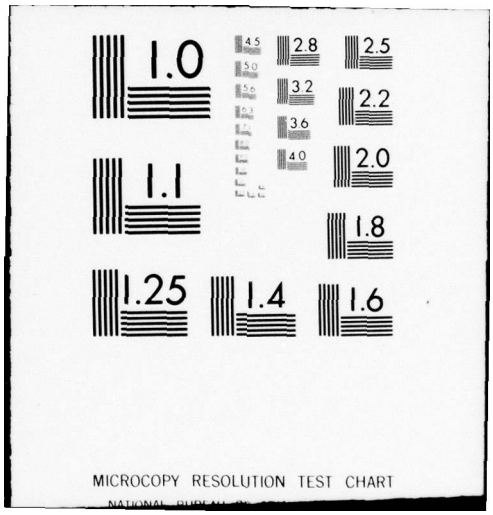
1.0
1.1
1.25
1.4
1.6
1.8
2.0
2.2
2.5
2.8
3.2
3.6
4.0
4.5
5.0
5.6
MICROCOPY RESOLUTION TEST CHART

REPORT NO. FAA-RD-78-117

LEVEL II

GUST RESPONSE ANALYSES FOR TEN GENERAL AVIATION AIRCRAFT USING A TWO-DEGREE-OF-FREEDOM POWER SPECTRAL TECHNIQUE

Guy G. Williamson

AERONAUTICAL RESEARCH ASSOCIATES OF PRINCETON, INC
50 WASHINGTON ROAD, P.O.BOX 2229
PRINCETON, NEW JERSEY 08540

OCTOBER 1978

FINAL REPORT

Document is available to the U.S. public through the National Technical Information Service, Springfield, Virginia 22161.

Prepared for

U.S. DEPARTMENT OF TRANSPORTATION
FEDERAL AVIATION ADMINISTRATION
Systems Research & Development Service
Washington, D.C. 20590

NOTICE

This document is disseminated under the sponsorship of the Department of Transportation in the interest of information exchange. The United States Government assumes no liability for its contents or use thereof.

Technical Report Documentation Page

1. Report No.	2. Government Accession No.	3. Recipient's Catalog No.
FAA-RD-78-117		

4. Title and Subtitle
GUST RESPONSE ANALYSES FOR TEN GENERAL AVIATION AIRCRAFT USING A TWO-DEGREE-OF-FREEDOM POWER SPECTRAL TECHNIQUE.

5. Report Date
October 1978

6. Performing Organization Code

7. Author(s)
Guy G. Williamson

8. Performing Organization Report No.
A.R.A.P. Report No. 344

9. Performing Organization Name and Address
Aeronautical Research Associates of Princeton, Inc., NJ.
50 Washington Road, P.O. Box 2229
Princeton, New Jersey 08540

10. Work Unit No. (TRAIS)

11. Contract or Grant No.
DOT-FA77WA-3972

12. Sponsoring Agency Name and Address
U.S. Department of Transportation
Federal Aviation Administration
Systems Research and Development Services
Washington, D.C. 20590

13. Type of Report and Period Covered
Final Report.
April 1977-April 1978.

14. Sponsoring Agency Code
ALG-313

15. Supplementary Notes
154p.
ARAP-344

16. Abstract

A power spectral technique for estimating gust loads on aircraft is presented, applied to ten general aviation aircraft and the results compared with those obtained by other methods. The technique used employs two-degree-of-freedom models of the longitudinal and lateral aircraft motions due to atmospheric turbulence. The results of this technique are compared with those obtained using Peele's method and simpler one-degree-of-freedom models. The primary conclusion is that this new method would be a useful design tool for the small aircraft manufacturer with access to a digital computer.

17. Key Words	18. Distribution Statement
General Aviation Aircraft Gust Loads Atmospheric Turbulence Power Spectral Density Application	Document is available to the U.S. public through the National Technical Information Service, Springfield, Virginia 22161.

19. Security Classif. (of this report)	20. Security Classif. (of this page)	21. No. of Pages	22. Price
Unclassified	Unclassified	152	

METRIC CONVERSION FACTORS

Approximate Conversions to Metric Measures

Symbol	When You Know	Multiply by	To Find	Symbol
		LENGTH		
in	inches	*2.5	centimeters	cm
ft	feet	30	centimeters	cm
yd	yards	0.9	meters	m
mi	miles	1.6	kilometers	km
		AREA		
in^2	square inches	6.5	square centimeters	cm^2
ft^2	square feet	0.09	square meters	m^2
yd^2	square yards	0.8	square meters	m^2
mi^2	square miles	2.6	square kilometers	km^2
	acres	0.4	hectares	ha
		MASS (weight)		
oz	ounces	28	grams	g
lb	pounds	0.45	kilograms	kg
	short tons (2000 lb)	0.9	tonnes	t
		VOLUME		
tsp	teaspoons	5	milliliters	ml
Tbsp	tablespoons	15	milliliters	ml
fl oz	fluid ounces	30	milliliters	ml
c	cups	0.24	liters	l
pt	pints	0.47	liters	l
qt	quarts	0.95	liters	l
gal	gallons	3.8	liters	l
ft^3	cubic feet	0.03	cubic meters	m^3
yd^3	cubic yards	0.76	cubic meters	m^3
		TEMPERATURE (exact)		
°F	Fahrenheit temperature	5/9 (after subtracting 32)	Celsius temperature	°C

*1 in = 2.54 (exactly). For other exact conversions and more detailed tables, see NBS Misc. Publ. 286, Units of Weights and Measures, Price $2.25, SD Catalog No. C13.10:286.

Approximate Conversions from Metric Measures

Symbol	When You Know	Multiply by	To Find	Symbol
		LENGTH		
mm	millimeters	0.04	inches	in
cm	centimeters	0.4	inches	in
m	meters	3.3	feet	ft
m	meters	1.1	yards	yd
km	kilometers	0.6	miles	mi
		AREA		
cm^2	square centimeters	0.16	square inches	in^2
m^2	square meters	1.2	square yards	yd^2
km^2	square kilometers	0.4	square miles	mi^2
ha	hectares (10,000 m^2)	2.5	acres	
		MASS (weight)		
g	grams	0.035	ounces	oz
kg	kilograms	2.2	pounds	lb
t	tonnes (1000 kg)	1.1	short tons	
		VOLUME		
ml	milliliters	0.03	fluid ounces	fl oz
l	liters	2.1	pints	pt
l	liters	1.06	quarts	qt
l	liters	0.26	gallons	gal
m^3	cubic meters	35	cubic feet	ft^3
m^3	cubic meters	1.3	cubic yards	yd^3
		TEMPERATURE (exact)		
°C	Celsius temperature	9/5 (then add 32)	Fahrenheit temperature	°F

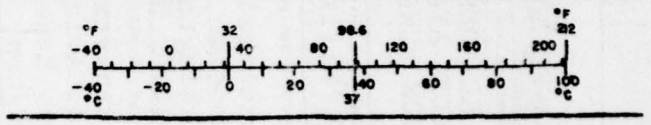

ACKNOWLEDGEMENT

The author would like to thank Dr. John C. Houbolt for his assistance in formulating the two-degree-of-freedom gust load models and for his valuable comments throughout the project.

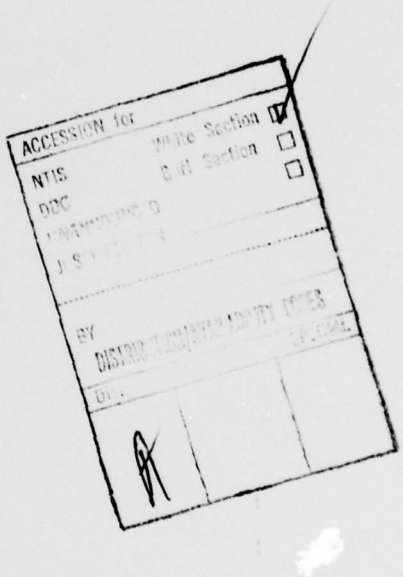

TABLE OF CONTENTS

LIST OF FIGURES

LIST OF SYMBOLS

a	Lift curve slope or Peele's lift attenuation factor.
A	Structural response parameter.
AR	Aspect ratio.
c	Chord of aerodynamic surface.
cg	Center of gravity.
C_i	Integrals as defined in equations (2.16)-(2.28).
C_{ij}	C matrix coefficient in i^{th} row j^{th} column.
C_{L_α}	Lift coefficient variation due to angle of attack.
C_{L_q}	Lift coefficient variation due to pitch rate.
$C_{L_{w_g}}$	Lift coefficient variation due to gust velocity variation along the x axis.
C_{M_α}	Pitching moment coefficient variation due to angle of attack.
C_{M_q}	Pitching moment coefficient variation due to pitch rate.
$C_{M_{w_g}}$	Pitching moment coefficient variation due to gust velocity variation along the x axis.
C_{Y_β}	Yawing moment coefficient variation due to sideslip angle.
C_{N_r}	Yawing moment coefficient variation due to yaw rate.
C_{Y_β}	Side force coefficient variation due to sideslip angle .
C_{Y_r}	Side force coefficient variation due to yaw rate.
d	Diameter
e	Distance from c.g. (Fig. 2.5, 2.7) or natural log base.
e_i	Distance from cg to load P at subscript position i.
F_i	Frequency response function for i^{th} variable proportional to magnitude of the transfer function squared.

g	Gravitational acceleration
h	Altitude
H	Transfer function
j	$\sqrt{-1}$
IAS	Indicated airspeed
I_{ii}	Moment of inertia about i^{th} axis
k	Nondimensional frequency
k_c	Upper Limit of integration for A and No.
L	Scale of turbulence
m	Mass of aircraft
M	Aerodynamic moment about y axis
MAC	Mean aerodynamic chord
N	Aerodynamic moment about z axis
N_{o_i}	Number of zero crossings per second in one direction of the i^{th} function
p, $\dot{\phi}$	roll rate
P	Line load representing aerodynamic force on a section of fuselage, wing, or foil
p#	Airplane # (see Table 301 for geometric and mass properties)
q, $\dot{\theta}$	Pitch rate
$\dot{r}$	Radius of Gyration
$\dot{r}$, $\dot{\psi}$	Yaw rate
s	Nondimensional distance in x direction equation (2.19)
S	Ref area or integral as defined in equations (2.16)-(2.28).
u	Velocity component parallel to x axis
U	Average velocity of aircraft
v	Velocity component parallel to x axis
w	Vertical velocity, downwash vertical velocity, wing
W	Aircraft weight

x	Position parallel forward velocity
X	Aerodynamic force in x direction
y	Lateral position positive out right wing
Y	Aerodynamic force in y direction
z	Position vertical positive upwards
Z	Aerodynamic force in z direction
α	Angle of attack
α_{mn}	Real component of the downwash influence function, Eq. (2.12)
β	Angle of sideslip
β_{mn}	Imaginary component of the downship influence function, Eq. (2.12)
γ	Circulation parameter, $\pi\rho US_w$
$\Delta\ell$	Lateral load factor
Δn	Incremental load factor
θ	Pitch angle
λ	Length of line load
Λ	Sweep angle of wing or tail depending on subscript
π	Pii (3.14157)
σ_i	Root mean square value of the i^{th} variable
ϕ	Power spectral function or in Appendix A, potential function
0DF	Zero degrees of freedom
Ψ	Yaw angle
ω	Temporal frequency
Ω	Spatial frequency
1DF	One degree of freedom
2DF	Two degrees of freedom

SUBSCRIPTS

f	Fuselage
f_i	i^{th} section of fuselage
g	Gust
HT	Horizontal tail
I	Imaginary component
P_{HT}	Horizontal tail force
P_{VT}	Vertical tail force
R	Real component
w	Wing
w_i	i^{th} section of wing
$\ddot{y}$	Lateral acceleration
$\ddot{z}$	Normal acceleration
$\Delta\ell$	Lateral laod factor
Δn	Incremental normal load factor

SUPERSCRIPT

$(\dot{})$	Differentiation w.r.t. time

1. INTRODUCTION

At present the designer of small aircraft must insure that the structure be capable of withstanding the load produced by a single gust of specified form. However, the continuous and random nature of atmospheric turbulence suggests that the designer consider working with histograms of the major loads, i.e., the number of times load levels are reached or exceeded over the useful life of the vehicle. This is necessary for both fatigue design criteria and to insure an acceptably low probability of gust loads in excess of structural yield limits. This load exceedance information can be obtained by the use of power spectral techniques for the representation of atmospheric turbulence and the resultant aircraft load and motion responses.

Several different models have been developed and proposed to represent the aircraft gust load and motion responses. Of particular interest are the one- and two-degree-of-freedom models developed by Houbolt (Refs. 1,2) and the two-degree-of-freedom models by Peele (Ref. 3). Houbolt's one-degree-of-freedom (1DF) models and Peele's two-degree-of-freedom (2DF) models were used to estimate gust loads on ten aircraft representative of those subject to Federal Aviation Regulation 23, at various altitudes, airspeeds, and flight configurations in Reference 4. The purpose of the study reported herein is to:

1. Apply Houbolt's longitudinal and lateral 2DF models to the same aircraft and flight conditions.
2. Quantitatively evaluate the three techniques in order to provide data for possible changes in the Federal Aviation Regulations concerning gust design procedures.
3. Develop a handbook implementing a simplified power spectral gust design procedure.

The major conclusions of this study are:

1. The one-degree-of-freedom Houbolt method is recommended for gust load estimates if the method must be simple enough for handbook-type calculations.
2. Peele's method significantly overestimates the gust loading of the wing on the aircraft investigated.
3. The two-degree-of-freedom method used in this study or one of its variants is a useful design tool for the small aircraft manufacturer with access to a digital computer.

2. DESCRIPTION OF GUST LOAD ESTIMATION TECHNIQUE

2.1 Review of Load Level Exceedance Estimation Based on Structural Response Parameter, A , and Rate of Zero Crossings, N_o

As stated in the introduction, the continuous nature of turbulence produces a distribution of aerodynamic loads in time which can be characterized by the number of times a load level is exceeded per flight hour or over the anticipated life of the aircraft. A suggested use of this load exceedance information (Ref. 1) is to set the maximum design load such that it is not exceeded more than ten times in 30,000 hours of flight. It is not within the scope of this study to develop or evaluate such design load criteria, but merely to point out that this approach is more realistic than the discrete gust design approach required in FAR 23.

The primary goal of this study is the comparative evaluation of three different methods of obtaining these load exceedance rates for each lifting surface. Therefore, a brief review is given of the general manner in which the structural response parameter A , and rate of zero crossings, N_o , are calculated, their physical significance, and how these are used to specify the load exceedance rate. This is then followed by a description of Houbolt's longitudinal and lateral 2DF gust response models.

The symbols used to describe aircraft loads, moments, motions, and their sign conventions are shown in Figure 2.1. The basic physics of the 2DF models used are: 1) that the aircraft responds with vertical motion, z , pitch motion, θ , and horizontal tail load, P_{HT} , to a continuously varying vertical component of atmospheric turbulent velocity w_g (Fig. 2.2), and 2) the aircraft responds with side motion, y , yawing motion, ψ , and lateral tail load, P_{VT} , to a continuously varying lateral component of turbulent velocity, v_g (Fig. 2.3). The basic limitations of this approach are that the effect of the turbulent velocity component in the forward direction, u_g , is neglected, the lateral

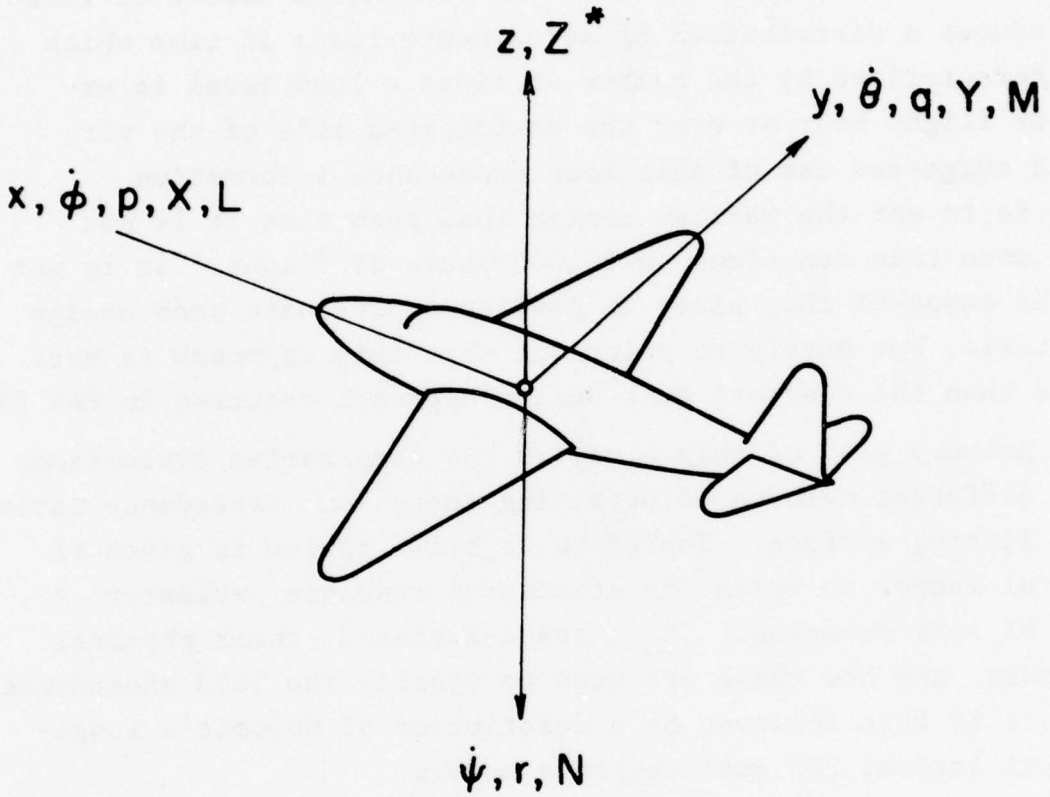

Figure 2.1 Conventions for positive position, angular rate, force and moment about each axis (moment and angular rate follows right hand rule)

* The position and force are defined positive upwards in keeping with the work of Ref. 2.

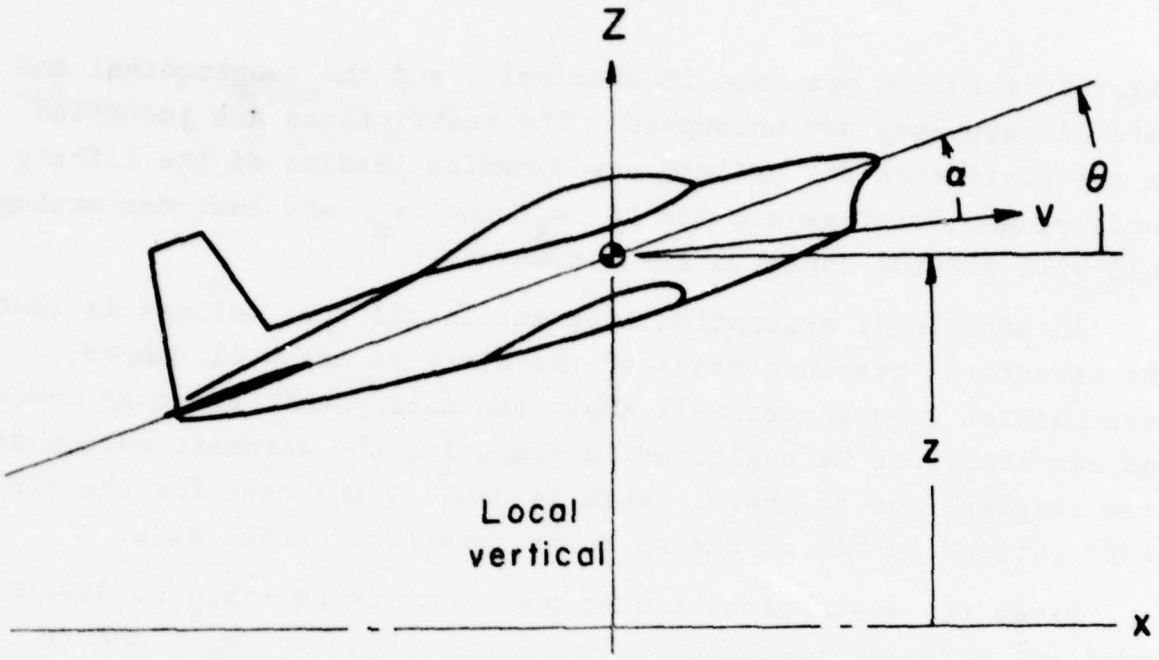

Figure 2.2 Longitudinal response model

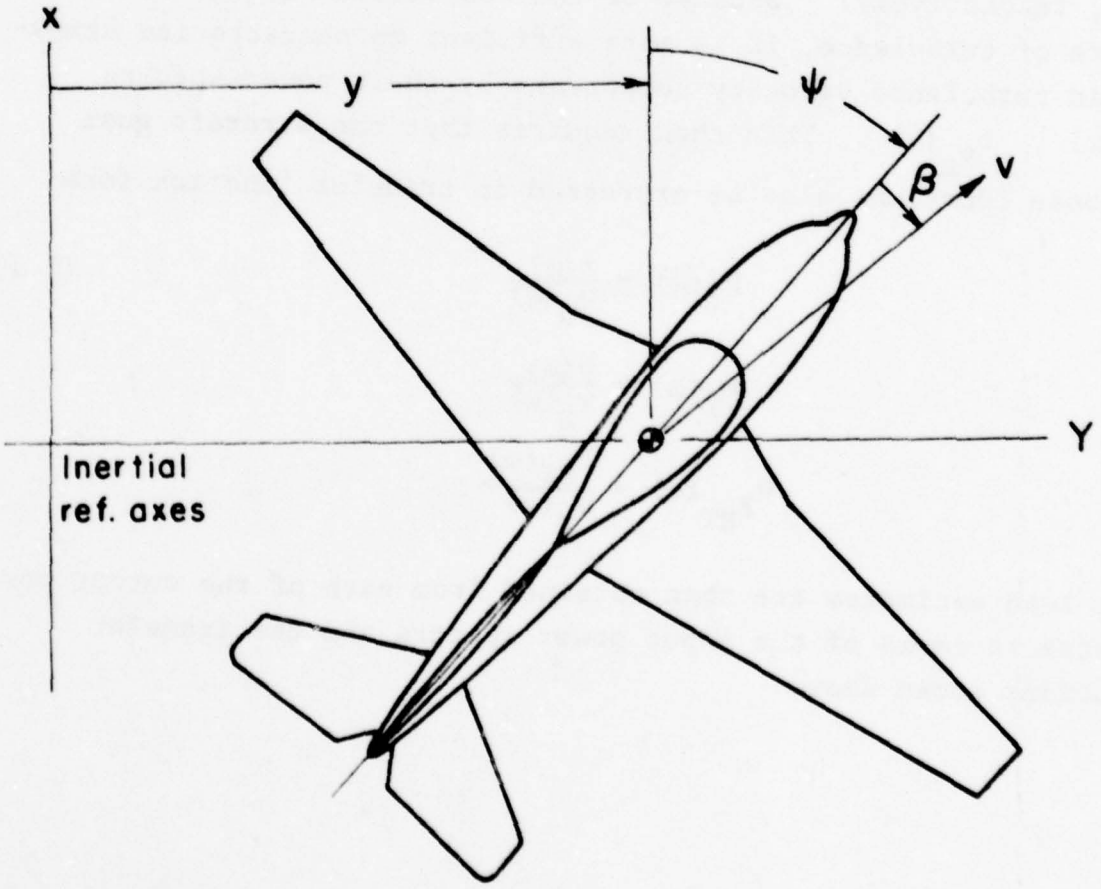

Figure 2.3 Lateral response model

aircraft response does not include roll, and the longitudinal and lateral responses are uncoupled. The restrictions are justified on the basis that the primary aerodynamics loading of the lifting surfaces and fuselage are due to w_g and v_g and that neglecting roll will provide conservative estimates.

An additional assumption inherent in all that follows is that the structural response modes of the aircraft are well damped, have natural frequencies well above the aerodynamic response modes, and can therefore be neglected in computing the aircraft motion and load response due to gusts. This is usually the case for the aircraft covered by FAR 23 due to their relatively small size.

Given the assumptions listed above, it is possible to develop models of aircraft responses z , θ , P_w , P_{HT} to w_g ; and y , ψ , P_{VT} to v_g in either the time or frequency domain (where P_w , P_{HT} , P_{VT} are the loads on the wing, horizontal tail, vertical tail, respectively). Because of the continuous and statistical nature of turbulence, it is more efficient to characterize atmospheric turbulence velocity components by their power spectra $\phi_{w_g}(\omega)$, $\phi_{v_g}(\omega)$. This then requires that the aircraft gust response functions also be expressed in transfer function form

$$H_{\ddot{z}}(\omega) = \frac{\ddot{z}(\omega)}{w_g(\omega)} \qquad (2.1)$$

$$H_{\ddot{y}}(\omega) = \frac{\ddot{y}(\omega)}{v_g(\omega)}$$

$$H_{P_{HT}}(\omega) = \frac{P_{HT}(\omega)}{w_g(\omega)}$$

Gust load estimates are then obtained from each of the output power spectra in terms of the input power spectra and the transfer functions shown above

$$\phi_{\ddot{z}}(\omega) = H_{\ddot{z}}(\omega) \quad H_{\ddot{z}}(-\omega)\phi_{w_g}(\omega)$$

$$\phi_{P_{HT}}(\omega) = H_{P_{HT}}(\omega) \; H_{P_{HT}}(-\omega)\phi_{w_g}(\omega)$$

$$\phi_{\ddot{y}}(\omega) = H_{\ddot{y}}(\omega) \; H_{\ddot{y}}(-\omega)\phi_{v_g}(\omega)$$

$$\phi_{P_{VT}}(\omega) = H_{P_{VT}}(\omega) \; H_{P_{VT}}(-\omega) \; v_g(\omega) \qquad (2.2)$$

While the output power spectra contain all of the necessary structural loading information, it is not in a particularly useful form. The root mean square value of the i^{th} response variable, σ_i, is of more interest for structural design purposes.

$$\sigma_{\Delta n} = \left(\frac{\sigma_{\ddot{z}}}{g}\right)^2 = \left[\int_0^{k_c} \frac{\phi_{\ddot{z}}(k)}{g^2}\, dk\right]^{1/2}$$

$$\sigma_{\Delta \ell} = \frac{\sigma_{\ddot{y}}}{g}^{1/2}\left[\int_0^{k_c} \phi_{\ddot{y}}(k)\, dk\right]^{1/2} \qquad (2.3)$$

These integrals can be written in terms of the dimensional frequency, ω, or its nondimensional equivalent, k.

$$k = \frac{\omega c}{2U} \qquad (2.4)$$

where c is a reference chord length and U is forward flight speed. They are shown here in terms of k, since they are computed in this form in this study.

It should also be noted that the upper limit on these integrals has been changed from infinity to a value k_c for computational purposes. The particular value of cutoff frequency chosen and its effect on A and N_o is discussed in References 1 and 2. The ratio between the rms values of the output $\sigma_{\Delta n}$ and input σ_{w_g} is defined as the structural response parameter $A_{\Delta n}$

substituting (2.2) into (2.3) yields

$$\sigma_{\Delta n} = \left[\int_{\infty}^{k_c} \frac{\phi_z(k)}{g^2}\, dk\right]^{1/2} = \left[\int_0^{k_c} \frac{|H_{\ddot{z}}(k)|}{g^2} \frac{\phi_{w_g}(k)}{\sigma^2_{w_g}}\, dk\right]^{1/2} \sigma_{w_g} = A_{\Delta n}\sigma_{w_g} \tag{2.5}$$

Similarly for the other loading variables

$$\sigma_{HT} = \left[\int_0^{k_c} \frac{|H_{P_{HT}}(k)|^2}{g^2} \frac{\phi_{w_g}(k)}{\sigma^2_{w_g}}\, dk\right]^{1/2} \sigma_{w_g} = A_{HT}\sigma_{HT}$$

$$\sigma_{\Delta \ell} = \left[\int_0^{k_c} \frac{|H_y(k)|^2}{g^2} \frac{\phi_{v_g}(k)}{\sigma^2_{v_g}}\, dk\right]^{1/2} \sigma_{v_g} = A_{\Delta \ell}\sigma_{v_g}$$

$$\sigma_{VT} = \left[\int_0^{k_c} \frac{|H_{P_{VT}}(k)|^2}{g^2} \frac{\phi_{v_g}(k)}{\sigma^2_{v_g}}\, dk\right]^{1/2} \sigma_{v_g} = A_{VT}\sigma_{VT}$$

These structural response parameters, A_i, where $i = \Delta n, \Delta \ell, HT, VT$ give the designer a feel for the magnitude of each major structural component due to turbulence.

Another parameter, important for structural fatigue estimates is the frequency with which any particular load level is exceeded. The number of exceedances of a particular acceleration level, Δn_1, per unit time due to heavy turbulence is given by the relation

$$N_{\Delta n}(\Delta n_1) = N_{o_{\Delta n}} e^{-\frac{\Delta n_1}{\sigma_{\Delta n}}} = N_{o_{\Delta n}} e^{-\frac{\Delta n_1}{A_{\Delta n}\sigma_w}} \tag{2.6}$$

where

$N_{o_{\Delta n}}$ is the rate of zero acceleration crossings in the positive direction.

$N_{o_{\Delta n}}$ is obtained from the relation

$$N_{o_{\Delta n}} = \frac{1}{2\pi} \frac{\dot{\sigma}_{\Delta n}}{\sigma_{\Delta n}} = \frac{U}{\pi c} \left[\frac{\int_0^{\infty} k^2 \, \phi_{\Delta n}(k)\, dk}{\int_0^{k_c} \phi_{\Delta n}(k)\, dk} \right]^{1/2} \tag{2.7}$$

It can be seen from Eq. (2.6) that the gust intensity, σ_{w_g}, structural load parameter, $A_{\Delta n}$, and zero crossing parameter $N_{o_{\Delta n}}$ completely specify the number of times any desired load factor is exceeded per unit time. This same relation also applies for each of the other variables of interest $\Delta \ell$, P_{HT}, and P_{VT}. Comparisons of the gust load estimates by three different aircraft gust response models are therefore presented in terms of the pair of parameters, A, N_o, associated with each of the variables listed above.

The following subsection gives the characteristics of the atmospheric turbulence spectra $\phi_{w_g}(k)$, $\phi_{v_g}(k)$ used in this analysis.

2.2 Model of Atmospheric Turbulence

For all three load estimation techniques examined in this study, atmospheric turbulence is characterized by the von Karman spectrum for both vertical and lateral gust velocities

$$\phi_w(\Omega) = \sigma_{w_g}^2 \frac{L}{\pi} \frac{1 + \frac{8}{3}(1.339L\Omega)^2}{\left[1 + (1.339L\Omega)^2\right]^{11/6}} \tag{2.8}$$

where

Ω = spatial frequency (rad/ft)

σ_{w_g} = root mean squared value of gust velocity (also called gust intensity)

L = scale of turbulence

For an aircraft traversing a patch of turbulence, the spatial distribution appears as a time varying function. For an aircraft flying at velocity U with reference wing semichord $c/2$ the gust input power spectrum can be expressed in terms of the non-dimensional frequency

$$k = \frac{\Omega c}{2} = \frac{\omega c}{2U} \tag{2.9}$$

where

ω = temporal frequency (rad/sec)

$$\phi_{w_g}(k) = \sigma_w^2 \frac{2L}{c} \frac{1 + \frac{8}{3}\left(1.339 \frac{2L}{c} k\right)^2}{\left[1 + \left(1.339 \frac{2L}{c} k\right)^2\right]^{11/6}} \tag{2.10}$$

This same spectral form and turbulence scale are used for the lateral gust velocity, v_g. In addition, the gust velocities are assumed to be uncorrelated. The basic spectral representation plus the assumption concerning relative turbulence scales and lack of correlation are reasonably well justified by experimental data, at least above an altitude of 1000 ft. The scale of atmospheric turbulence varies with altitude, below 1000 ft, atmospheric stability, wind shear and other factors. Estimates of turbulence scale run from less than one hundred to several thousand feet. For the purpose of this study, a value of $L = 2500$ ft was chosen for most analyses. This choice is not crucial since, as shown in Section 3.4, the effect of scale change on the structural loading parameter A is satisfactorily given by the relation

$$A(L_2) = \left(\frac{L_2}{L_1}\right)^{1/3} A(L_1) \tag{2.11}$$

for scale lengths greater than 750 ft.

2.3 Model of Aircraft Response to Gusts

In this section the rationale for estimating the aerodynamic forces on the lifting surfaces and aircraft fuselage due to atmospheric turbulence is reviewed. First, the basic potential flow

model is described. Then the influence coefficient relating the aerodynamic load at one station to downwash velocity at another station is developed. Finally, the aerodynamic loads and resulting moments are incorporated in the two-degree-of-freedom longitudinal and lateral equations of motion in order to calculate gust response transfer functions, structural response parameter, A , and zero crossing parameters, N_o . In addition, equations for the equivalent stability derivatives obtained from this method are developed for comparison with the derivatives used in Peele's methods in Reference 3. These equivalent stability derivatives should also be useful for estimating the inaccuracy of assuming real and constant values for these functions when extracting them from flight test data using high frequency control motion input signals.

The basic premise of Houbolt's technique is that the loads and velocity flow field resulting from gust velocity can be adequately described by potential flow theory. This will not be true if the flow separates from a lifting surface; i.e., if the aircraft stalls or spins. Nor is it likely to accurately account for wing-body interference effects. However, for the prediction of loads on the major surfaces during turbulence encounters at or near cruise conditions (low angle of attack and sideslip) it has great promise. The potential flow model is a series of dipole sources which produce a line load as illustrated in Figure 2.4. The wing load is approximated by two line loads, the fuselage by four, and the tail surfaces by one each. This figure also shows the location of the points where the downwash velocities are computed as well as the motion variables of interest. The one- and two-line load approximations were shown in Reference 2 to adequately estimate the lift curve slope of an elliptically loaded wing with aspect ratio of eight.

The basic relations obtained from the line load model is the downwash velocity at station m due to a load at station n . This is given in terms of the influence functions α_{mn} , β_{mn}

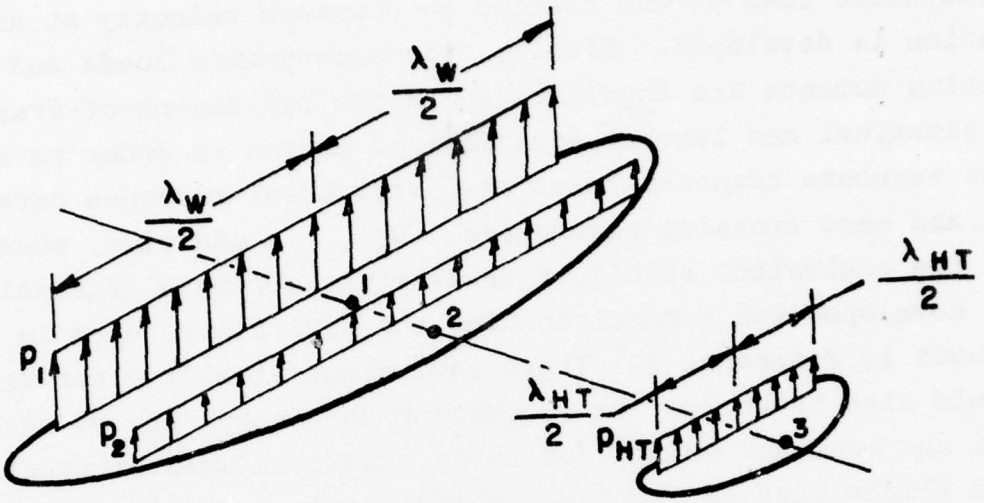

(a) Longitudinal

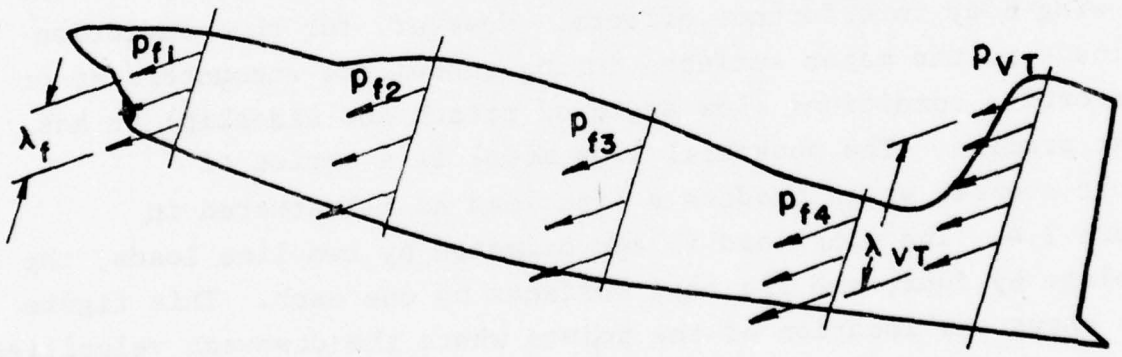

(b) Lateral

Figure 2.4 Distribution of line loads representing aerodynamic forces

$$w_m = \frac{P_n}{\pi \rho U_c \lambda} (\alpha_{mn} + i\beta_{mn}) \tag{2.12}$$

Where for the downwash station ahead of the load

$$\alpha_{mn} + i\beta_{mn} = e^{iks_o} \left[C_1(s_o) + iS_1(s_o) \right] \tag{2.13}$$

and for the downwash station downstream of the load

$$\alpha_{mn} + i\beta_{mn} = -e^{iks_o} \left[C_o + C_1(s_o) + iS_1(s_o) \right] \tag{2.14}$$

where

s_o is the nondimensional distance between load and downwash velocity

$$s_o = |x_{DWNWSH} - x_{LOAD}| 2/c \tag{2.15}$$

and the C and S functions are:

$$C_o = \pi k + 2\int_0^\infty \frac{\cos ks}{s^2} \left(1 - \frac{\lambda/c}{\sqrt{s^2 + (\lambda/c)^2}} \right) ds \tag{2.16}$$

$$C_1(s_o) = \int_{s_o}^\infty \frac{\lambda/c \cos ks}{s^2 \sqrt{s^2 + (\tau/c)^2}} ds \tag{2.17}$$

$$S_1(s_o) = \int_{s_o}^\infty \frac{\lambda/c \sin ks}{s^2 \sqrt{s^2 + (/c)^2}} ds \tag{2.18}$$

where

s is the nondimensional distance variable, positive in the downstream direction

$$s = -\frac{2x}{c} \tag{2.19}$$

Both k and s are a function of the reference chord, c, appropriate to the fuselage or particular aerodynamic surface in

question. For each surface the reference chord, c, spanwise length of line load, λ and lift curve slope, a, are determined as follows. The lift curve slope is a function of aspect ratio, AR, sweep angle, Λ, and Mach number, M

$$a = \frac{\pi \, AR}{1 + \sqrt{1 + \left(\frac{AR}{2 \cos \Lambda}\right)^2 \left(1 - M^2 \cos^2 \Lambda\right)}} \tag{2.20}$$

$$\lambda^2 = \frac{S}{\frac{\pi}{a} - \frac{a}{4\pi}(1 - M^2)} \tag{2.21}$$

$$c = \frac{S}{\lambda} \tag{2.22}$$

where

S is the area of the aerodynamic surface in question.

A different approach is used for the calculation of λ and c for the fuselage.

$$\lambda_f = .707 \, k d_f \tag{2.23}$$

$$c_f = .278 \, \ell_f \tag{2.24}$$

where

subscript f means fuselage

ℓ_f = length of fuselage

d_f = average diameter of fuselage

K = constant set at .75 to produce correct subsonic aerodynamic yawing moment

In the program for computing gust load spectra, the wing, tail, and fuselage loads are all calculated together. This is most easily accomplished with all equations written in terms of the reduced frequency associated with the wing, k_w. In this case the α and β associated for example with the horizontal tail become

$$\alpha_{mn} + i\beta_{mn} = -e^{i \frac{c_{HT}}{c_w} k_w s_{HT}} \left(C_{o_{HT}} + C_{HT} + iS_{HT} \right) \tag{2.25}$$

where

$$C_{o_{HT}} = \pi \frac{c_{HT}}{c_w} k_w + 2 \int_0^{\infty} \frac{\cos \frac{c_{HT}}{c_w} k_w s_{HT}}{s_{HT}^2} \left(\frac{1 - \frac{\lambda_{HT}}{c_{HT}}}{\sqrt{s_{HT}^2 + \left(\frac{\lambda_{HT}}{c_{HT}} \right)^2}} \right) ds_{HT} \tag{2.26}$$

$$C_{HT} = \int_{s_{o_{HT}}}^{\infty} \frac{\frac{\lambda_{HT}}{c_{HT}} \cos \frac{c_{HT}}{c_w} k_w s_{HT}}{s_{HT}^2 \sqrt{s_{HT}^2 + \left(\frac{\lambda_{HT}}{c_{HT}} \right)^2}} ds_{HT} \tag{2.27}$$

$$S_{HT} = \int_{s_{o_{HT}}}^{\infty} \frac{\frac{\lambda_{HT}}{HT} \sin \frac{c_{HT}}{c_w} k_w s_{HT}}{s_{HT}^2 \sqrt{s_{HT}^2 + \left(\frac{HT}{c_{HT}} \right)^2}} ds_{HT} \tag{2.28}$$

Similar relations also apply for the vertical tail and the fuselage.

It should be noted that these equations imply that not only is the magnitude of the downwash velocity-load relation a function of frequency but also the phase angle change in the relationship of these variables. This is unique to this modeling technique and should therefore provide more realism than Peele's method. In particular, Peele's method relates the downwash velocity to load as

$$w_m = P_n K \rho e^{-ak} \tag{2.29}$$

where

- a is a real valued lift attenuation factor which is a function of Mach number and sweep angle given in Reference 3.
- K_p constant of proportionality determined by aircraft stability derivatives

The quantitative significance of including the phase angle variation will be shown in Section 3.1.

The relations presented so far apply to both the longitudinal and lateral gust load responses. At this point the development of these models is separated and the longitudinal response model is described first, followed by the lateral response model.

Referring to Figure 2.5 for the longitudinal load-velocity control points, the three loads produce downwash velocities w_i at the control points

$$w_1 = \frac{1}{\gamma}\left[(\alpha_{11} + i\beta_{11})P_{w_1} + (\alpha_{12} + i\beta_{12})P_{w_2}\right]$$

$$w_2 = \frac{1}{\gamma}\left[(\alpha_{21} + i\beta_{21})P_{w_1} + (\alpha_{11} + i\beta_{22})P_{w_2}\right]$$

$$w_{HT} = \frac{1}{\gamma}\left[(\alpha_{31} + i\beta_{31})P_{w_1} + (\alpha_{32} + i\beta_{32})P_{w_2} + \frac{S_w}{S_{HT}}(\alpha_{33} + i\beta_{33})P_{HT}\right] \qquad (2.30)$$

where

$$\gamma = \pi\rho U S_w \,, \quad \alpha_{22} = \alpha_{11} \,, \quad \beta_{22} = \beta_{11}$$

The downwash at the wing due to the tail load is neglected.

The downwash velocities must also satisfy kinematic contraints in terms of the vertical aircraft velocity, $\dot{z}$, pitch rate, $\dot{\theta}$ and gust velocity magnitude, w_g. (The oscillatory term e^{iwt} is not written in order to keep the notation manageable, but is understood to be part of all input and output variables.)

$$w_1 = \dot{z} + \left(e_w - \frac{c_w}{8}\right)\dot{\theta} - U\theta - w_g$$

$$w_2 = \dot{z} + \left(e_w - \frac{5c_w}{8}\right)\dot{\theta} - U\theta - w_g e^{-i\frac{\omega c_w}{2U}}$$

$$w_{HT} = \dot{z} - \left(e_{HT} + \frac{c_{HT}}{2}\right)\dot{\theta} - U\theta - w_g e^{-i\frac{\omega x_{HT}}{U}} \qquad (2.31)$$

where

$$x_{HT} = e_{HT} + e_w - \frac{c_w}{8} + \frac{c_{HT}}{2}$$

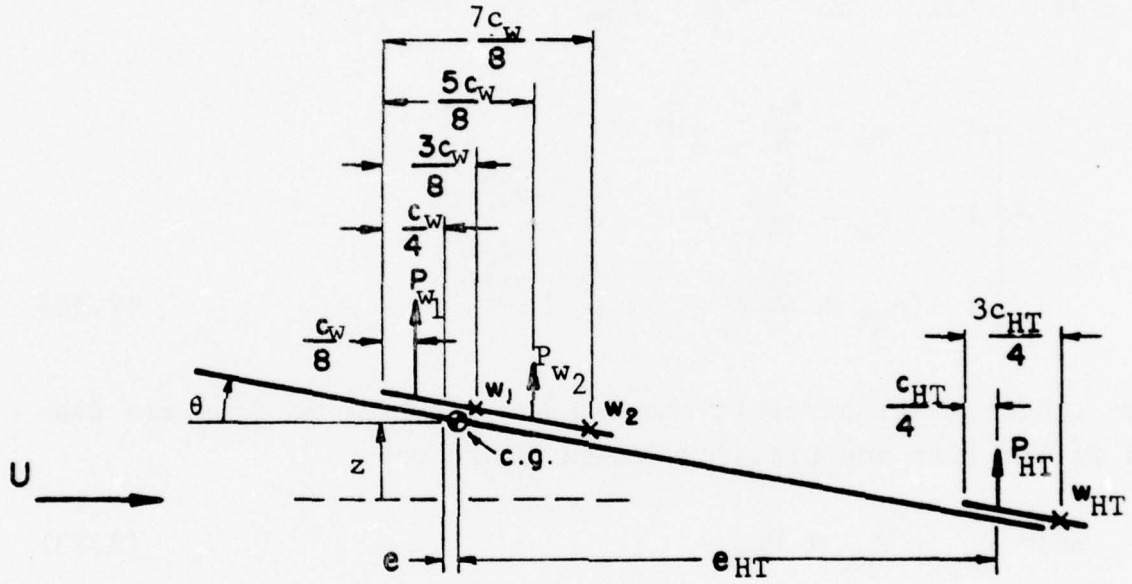

Figure 2.5 Longitudinal loading distribution and notation

The aerodynamic loads can be expressed in terms of the motion variables z, θ and the input gust velocity w by combining Eq. (2.30) and Eq. (2.31).

$$\begin{bmatrix} \alpha_{11} + i\beta_{11} & \alpha_{12} + i\beta_{12} & 0 \\ \alpha_{21} + i\beta_{21} & \alpha_{11} + i\beta_{11} & 0 \\ \alpha_{31} + i\beta_{31} & \alpha_{32} + i\beta_{32} & \frac{S_w}{S_{HT}} \quad \alpha_{33} + i\beta_{33} \end{bmatrix} \begin{matrix} \frac{P_{w_1}}{\gamma} \\ \frac{P_{w_2}}{\gamma} \\ \frac{P_{HT}}{\gamma} \end{matrix}$$

$$= \begin{bmatrix} 1 & e_w - \frac{c_w}{8} & - U - 1 \\ 1 & e_w - \frac{5c_w}{8} & - U - e^{-i \frac{\omega c_w}{2U}} \\ 1 & -(e_{HT} + \frac{c_{HT}}{2}) & - U - e^{-i \frac{\omega x_{HT}}{U}} \end{bmatrix} \tag{2.32}$$

The longitudinal aircraft heaving and pitching motions are described by the lift and pitching moment equations.

$$m\ddot{z} = P_{w_1} + P_{w_2} + P_{HT} \tag{2.33}$$

$$mr_y^2\ddot{\theta} = P_{w_1}\left(e_w + \frac{c_w}{8}\right) + P_{w_2}\left(e_w - \frac{3}{8}c_w\right) - P_{HT}e_{HT} \tag{2.34}$$

where m is aircraft mass and r_y is radius of gyration about the y axis.

Equation (2.32) plus the two equations of motion form a set from which the motion and loads can be determined. This set of equations, suitably nondimensionalized, is Houbolt's longitudinal two-degree-of-freedom gust load response model (Fig. 2.6).

The development of the lateral load gust response model is quite similar to the longitudinal case. Figure 2.4b illustrates the locations for the line dipole sources which are used to represent the forces and moments produced by the fuselage and vertical

$$
\begin{bmatrix}
2\mu k_w & 0 & 1 & 1 & 1 \\
0\ 0\ 0 & 2\mu \frac{r_y^2}{c_w^2} k_w & \frac{e}{c_w} + \frac{1}{8} & \frac{e}{c_w} - \frac{3}{8} & -\frac{e_{HT}}{c_w} \\
-i & -i\left(\frac{e_w}{c_w} - \frac{1}{8}\right) + \frac{1}{2k_w} & \alpha_{11} + i\beta_{11} & \alpha_{12} + i\beta_{12} & 0 \\
-i & -i\left(\frac{e_w}{c_w} - \frac{5}{8}\right) + \frac{1}{2k_w} & \alpha_{21} + i\beta_{21} & \alpha_{11} + i\beta_{11} & 0 \\
-i & -i\left(\frac{e_{HT}}{c_w} - \frac{c_{HT}}{2c_w}\right) + \frac{1}{2k_w} & \alpha_{31} + i\beta_{31} & \alpha_{32} + i\beta_{32} & \frac{S_w}{S_{HT}}\left(\alpha_{33} + i\beta_{33}\right)
\end{bmatrix}
\begin{Vmatrix}
\omega z \\ \omega c\theta \\ \frac{1}{\gamma} P_{w_1} \\ \frac{1}{\gamma} P_{w_2} \\ \frac{1}{\gamma} P_{HT}
\end{Vmatrix}
=
\begin{Vmatrix}
0 \\ 0 \\ 1 \\ e^{-ik_w} \\ e^{-ik_w s_1}
\end{Vmatrix}
$$

$$\mu = \frac{W}{\pi \rho c_w g S_w}$$

$$\gamma = \pi \rho S_w U$$

$$s_1 = \frac{2e_{HT}}{c_w} + \frac{2e}{c_w} - \frac{1}{4} + \frac{c_{HT}}{c_w}$$

$$k_w = \frac{\omega c_w}{2U}$$

Figure 2.6 Longitudinal 2DF Gust Load Model

Kinematic Equations for Sidewash Velocity at Control Points

$$v_1 = \dot{y} + (e_f + c_f/2)\dot{\psi} - U\psi - v_g$$

$$v_2 = \dot{y} + (e_f - c_f/2)\dot{\psi} - U\psi - v_g$$

$$v_3 = \dot{y} + (e_f - 3/2c_f)\dot{\psi} - U\psi - v_g$$

$$v_4 = \dot{y} + (e_f - 5/2c_f)\dot{\psi} - U\psi - v_g$$

$$v_{vt} = \dot{y} - (e_{vt} + c_{vt}/2)\dot{\psi} - U\psi - v_g \qquad 2.35)$$

Sidewash Velocity - Side Load Equations

$$v_1 = \frac{1}{Y_f}\left[(\alpha_{11} + i\beta_{11})P_{f_1} + (\alpha_{12} + i\beta_{12})P_{f_2} + (\alpha_{13} + i\beta_{13})P_{f_3} + (\alpha_{14} + i\beta_{14})P_{f_4}\right]$$

$$v_2 = \frac{1}{Y_f}\left[(\alpha_{21} + i\beta_{21})P_{f_1} + (\alpha_{11} + i\beta_{11})P_{f_2} + (\alpha_{12} + i\beta_{12})P_{f_3} + (\alpha_{13} + i\beta_{13})P_{f_4}\right]$$

$$v_3 = \frac{1}{Y_f}\left[(\alpha_{31} + i\beta_{31})P_{f_1} + (\alpha_{21} + i\beta_{21})P_{f_2} + (\alpha_{11} + i\beta_{11})P_{f_3} + (\alpha_{12} + i\beta_{12})P_{f_4}\right]$$

$$v_4 = \frac{1}{Y_f}\left[(\alpha_{41} + i\beta_{41})P_{f_1} + (\alpha_{31} + i\beta_{31})P_{f_2} + (\alpha_{21} + i\beta_{21})P_{f_3} + (\alpha_{11} + i\beta_{11})P_{f_4}\right]$$

$$v_{vt} = \frac{1}{Y_f}\frac{S_{vt}}{S_f}(\alpha_{vt} + i\beta_{vt}) \qquad (2.36)$$

Side Force Equation

$$m\ddot{y} = P_{f_1} + P_{f_2} + P_{f_3} + P_{f_4} + P_{vt} \qquad (2.37)$$

Yawing Moment Equation

$$I_{zz}\ddot{\psi} = (e_f + c_f)P_{f_1} + e_fP_{f_2} + (e_f - c_f)P_{f_3} + (e_f - 2c_f)P_{f_4} + e_{vt}P_{vt} \qquad (2.38)$$

tail due to lateral gusts. The lateral load and response variables are depicted in Fig. 2.7. The major assumptions in this model are: 1) that the wing contribution to lateral forces is neglected; 2) aerodynamic loads on the body do not significantly contribute to sidewash on the vertical tail and 3) aerodynamic loads on the vertical tail do not significantly contribute to the sidewash on the fuselage. Another frequently used second-order model of lateral motion is a combination of roll and yaw with sideforce neglected. This produces the familiar Dutch roll motion which is of interest for the evaluation of lateral handling qualities. This model, however, is computationally more involved since wing loads must be included. In addition, it is not as close to Peele's lateral model so that comparisons with his method would not be as meaningful. Therefore, while the Dutch roll model is of interest for future studies, it will not be used in this study. Proceeding as in the longitudinal case, equations relating sidewash velocity to aerodynamic loads, Eq. (2.35), and to kinematic constraints, Eq. (2.36), are written along with the side force and moment equations (2.37) and (2.38). In addition to these relations, slender body theory dictates that the wake potential downstream of a body of revolution (the fuselage) should be zero. In order to accomplish this, the four fuselage loads are modified as explained in Appendix A. The side force and moment equations become

$$m\ddot{y} = \sum_{j=1}^{4} P_{f_j}\left[1 - e^{-\frac{i\omega c_f}{2U}(5-j)}\right] + P_{VT} \tag{2.39}$$

$$I_{yy}\ddot{\psi} = \sum_{j=1}^{4} P_{f_j}\left[e_f + (2-j)c_f - e_f - 3c_f\, e^{-\frac{i\omega c_f}{U}(5-j)}\right] + P_{VT}e_{VT} \tag{2.40}$$

This set of seven equations suitably nondimensionalized (Fig. 2.8) forms the lateral two-degree-of-freedom gust load response model used to analyze the gust load exceedance parameters for ten small aircraft as discussed in the next section.

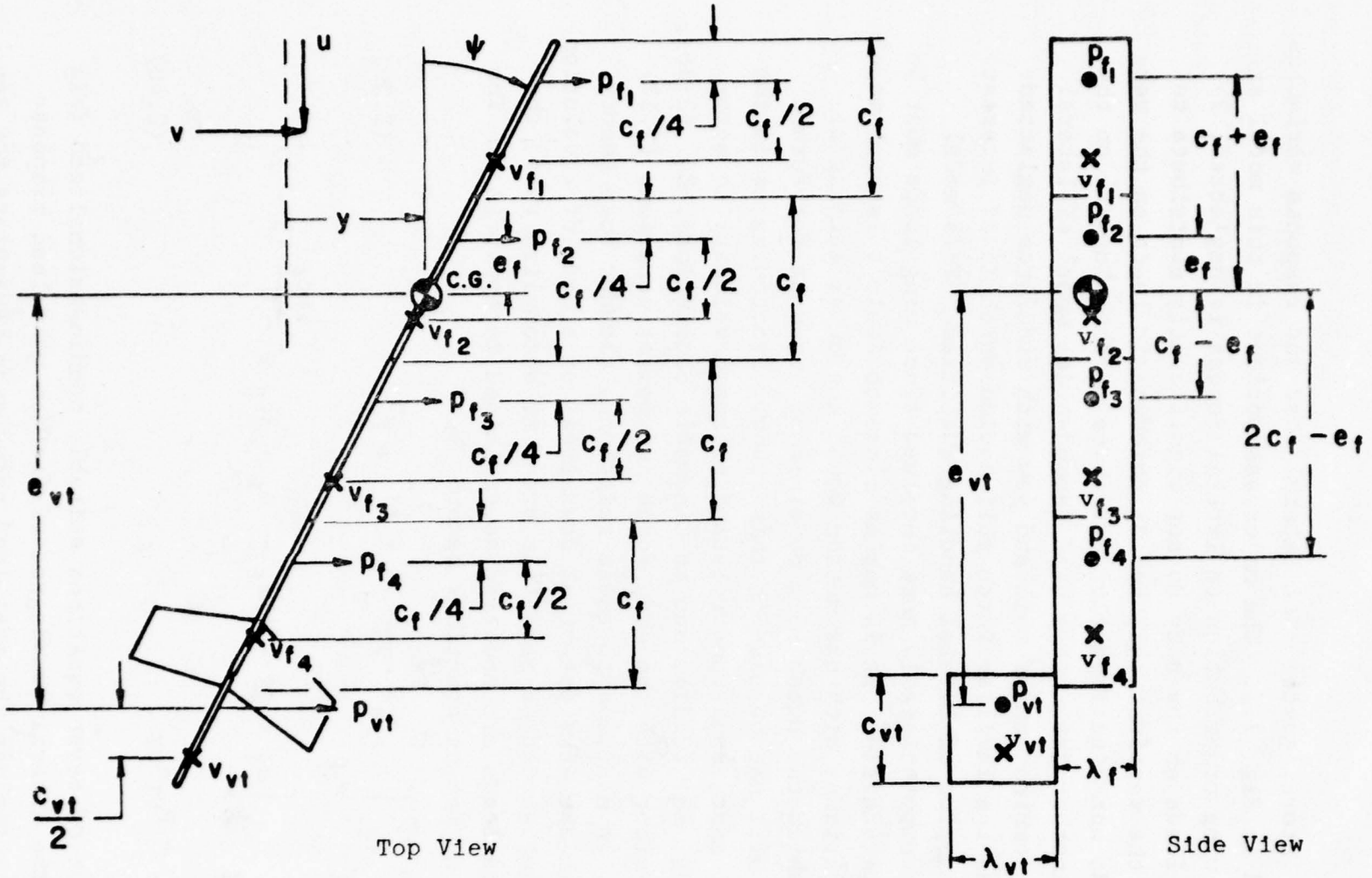

Figure 2.7 Notation and Geometry of Loads for Lateral Response to a Gust v_g .

$$
\begin{bmatrix}
2\mu_f k_f & 0 & 1-e^{-81k_f} & 1-e^{-61k_f} & 1-e^{-41k_f} & 1-e^{-21k_f} & 1 \\
0 & 2\left(\frac{r_z}{c_f}\right)^2 k_f \mu_f & \frac{e_f}{c_f}+1+\left(3-\frac{e_f}{c_f}\right)e^{-81k_f} & \frac{e_f}{c_f}+\left(3-\frac{e_f}{c_f}\right)e^{-61k_f} & \frac{e_f}{c_f}-1+\left(3-\frac{e_f}{c_f}\right)e^{-41k_f} & \frac{e_f}{c_f}-2+\left(3-\frac{e_f}{c_f}\right)e^{-21k_f} & \frac{-e_{vt}}{c_f} \\
-1 & \frac{1}{2k_f}-1\left(\frac{e_f}{c_f}+\frac{1}{2}\right) & \alpha_{f_{11}}+i\beta_{f_{11}} & \alpha_{f_{12}}+i\beta_{f_{12}} & \alpha_{f_{13}}+i\beta_{f_{13}} & \alpha_{f_{14}}+i\beta_{f_{14}} & 0 \\
-1 & \frac{1}{2k_f}-1\left(\frac{e_f}{c_f}-\frac{1}{2}\right) & \alpha_{f_{21}}+i\beta_{f_{21}} & \alpha_{f_{11}}+i\beta_{f_{11}} & \alpha_{f_{12}}+i\beta_{f_{12}} & \alpha_{f_{13}}+i\beta_{f_{13}} & 0 \\
-1 & \frac{1}{2k_f}-1\left(\frac{e_f}{c_f}-\frac{3}{2}\right) & \alpha_{f_{31}}+i\beta_{f_{31}} & \alpha_{f_{21}}+i\beta_{f_{21}} & \alpha_{f_{11}}+i\beta_{f_{11}} & \alpha_{f_{12}}+i\beta_{f_{12}} & 0 \\
-1 & \frac{1}{2k_f}-1\left(\frac{e_f}{c_f}-\frac{5}{2}\right) & \alpha_{f_{41}}+i\beta_{f_{41}} & \alpha_{f_{31}}+i\beta_{f_{31}} & \alpha_{f_{21}}+i\beta_{f_{21}} & \alpha_{f_{11}}+i\beta_{f_{11}} & 0 \\
-1 & \frac{1}{2k_f}+1\left(\frac{e_{vt}}{c_f}+\frac{c_{vt}}{2c_f}\right) & 0 & 0 & 0 & 0 & \frac{S_f}{4S_{vf}}\left(\alpha_{vt}+i\beta_{vt}\right)
\end{bmatrix}
\begin{bmatrix}
\omega_y \\ \omega c_f \psi \\ \frac{P_{f_1}}{\gamma_f} \\ \frac{P_{f_2}}{\gamma_f} \\ \frac{P_{f_3}}{\gamma_f} \\ \frac{P_{f_4}}{\gamma_f} \\ \frac{P_{vt}}{\gamma_f}
\end{bmatrix}
=
\begin{bmatrix}
0 \\ 0 \\ 1 \\ e^{-21k_f} \\ e^{-41k_f} \\ e^{-61k_f} \\ e^{-ik_f e_{vt}}
\end{bmatrix}
v_g
$$

$$
\mu_f = \frac{W}{\pi\rho c_f S_{f/4}} \qquad \gamma_f = \pi\rho S_f U/4
$$

$$
r_z = \sqrt{\frac{gI_{zz}}{W}} \qquad e_{vt} = \frac{2e_t}{c_f} + \frac{2e_f}{c_f} + 1 + \frac{c_{vt}}{c_f}
$$

$$
k_f = \frac{\omega c_f}{2U}
$$

Figure 2.8 Lateral 2DF Gust Load Model

2.4 Equivalent Complex Stability Derivative Model

The relation between longitudinal gust loads and motion variables, Eq. (2.32), can be rewritten replacing z and θ with the angle of attack, α, and pitch rate q.

$$\alpha = \frac{z}{U} - \theta + w_g \tag{2.41}$$

$$q = \dot{\theta} \tag{2.42}$$

$$\begin{bmatrix} \alpha_{11} + i\beta_{11} & \alpha_{12} + i\beta_{12} & 0 \\ \alpha_{21} + i\beta_{21} & \alpha_{11} + i\beta_{11} & 0 \\ \alpha_{31} + i\beta_{31} & \alpha_{32} + i\beta_{32} & \frac{S_w}{S_{HT}} \quad \alpha_{33} + i\beta_{33} \end{bmatrix} \begin{bmatrix} \frac{P_{w_1}}{\gamma} \\ \frac{P_{w_2}}{\gamma} \\ \frac{P_{HT}}{\gamma} \end{bmatrix}$$

$$= \begin{bmatrix} -U\, i2\left(\frac{e}{c_w} - \frac{1}{8}\right)U & 0 \\ -U\, i2\left(\frac{e}{c} - \frac{5}{8}\right)U & 1 - e^{-ik} \\ -U\, i2\left(\frac{e_{HT}}{c_w} - \frac{c_{HT}}{2c_w}\right)U & 1 - e^{-iks_1} \end{bmatrix} \begin{matrix} \alpha \\ q \\ w_g \end{matrix} + \begin{bmatrix} w_g \\ w_g \\ w_g \end{bmatrix} \tag{2.43}$$

Expressing Eq. (2.43) in matrix form

$$\left[A\right] \begin{bmatrix} P_{w_1}/\gamma \\ P_{w_2}/\gamma \\ P_{HT}/\gamma \end{bmatrix} = \left[B\right] \begin{bmatrix} \alpha \\ q \\ w_g \end{bmatrix} + \begin{bmatrix} w_g \\ w_g \\ w_g \end{bmatrix} \tag{2.44}$$

This equation can be solved numerically for the line loads by inverting A.

$$\begin{bmatrix} P_{w_1}/\gamma \\ P_{w_2}/\gamma \\ P_{HT}/\gamma \end{bmatrix} = \begin{bmatrix} A \end{bmatrix}^{-1} \begin{bmatrix} B \end{bmatrix} \begin{bmatrix} \alpha \\ q \\ w_g \end{bmatrix} + \begin{bmatrix} A \end{bmatrix}^{-1} \begin{bmatrix} w_g \\ w_g \\ w_g \end{bmatrix} \tag{2.45}$$

$$\begin{bmatrix} P_{w_1}/\gamma \\ P_{w_2}/\gamma \\ P_{HT}/\gamma \end{bmatrix} = \begin{bmatrix} C \end{bmatrix} \begin{bmatrix} \alpha \\ q \\ w_g \end{bmatrix} + \begin{bmatrix} A \end{bmatrix}^{-1} \begin{bmatrix} w_g \\ w_g \\ w_g \end{bmatrix} \tag{2.46}$$

where

$$\begin{bmatrix} C \end{bmatrix} = \begin{bmatrix} A \end{bmatrix}^{-1} \begin{bmatrix} B \end{bmatrix}$$

The longitudinal stability derivatives can be written in terms of the line loads

$$C_{L_\alpha} = \frac{1}{\frac{\rho U^2}{2} S_w} \frac{\partial (P_{w_1} + P_{w_2} + P_{HT})}{\partial \alpha} \tag{2.47}$$

$$C_{L_q} = \frac{1}{\frac{\rho U^2}{2} S_w} \frac{\partial (P_{w_1} + P_{w_2} + P_{HT})}{\partial \frac{q c_w}{2U}} \tag{2.48}$$

$$C_{M_\alpha} = \frac{1}{\frac{\rho U^2}{2} S_w c_w} \frac{\partial (x_1 P_{w_1} + x_2 P_{w_2} + x_{HT} P_{HT})}{\partial \alpha} \tag{2.49}$$

$$C_{M_q} = \frac{1}{\frac{U^2}{2} S_w c_w} \frac{\partial (x_1 P_{w_1} + x_2 P_{w_2} + x_{HT} P_{HT})}{\partial \frac{q c_w}{2U}} \tag{2.50}$$

The line load derivatives required in Eqs. (2.47) - (2.50) are proportional to the coefficients of the top two rows of matrix [C], Eq. (2.46).

$$
\begin{aligned}
C_{L_\alpha} &= 2\pi \left[C_{11} + C_{21} + C_{31} \right] \\
C_{M_\alpha} &= \frac{2\pi}{c_w} \left[x_{1_w} C_{11} + x_{2_w} C_{24} + x_{HT} C_{31} \right] \\
C_{L_q} &= - \frac{2\pi}{U} \left[C_{12} + C_{22} + C_{32} \right] \\
C_{M_q} &= \frac{2\pi}{U c_w} \left[x_1 C_{12} + x_2 C_{22} + x_{HT} C_{32} \right]
\end{aligned} \tag{2.51}
$$

Note that there are additional pseudo stability derivatives in this model due to the change in the magnitude of the gust velocity along the x axis of the vehicle.

$$
\begin{aligned}
C_{L_{w_g}} &= 2\pi \left[C_{13} + C_{23} + C_{33} \right] \\
C_{M_{w_g}} &= \frac{2\pi}{c_w} \left[x_1 C_{13} + x_2 C_{23} + x_3 C_{33} \right]
\end{aligned} \tag{2.52}
$$

For turbulence wavelengths long compared to the length of the vehicle, these terms should be small.

The equivalent lateral stability derivates C_{y_β}, C_{N_β}, C_{y_r}, and C_{N_r} are obtained by the same procedure. The yaw rate, r, and angle of side slip, β, are substituted into Eq. (2.35) for $\dot{y}$ and v_g. This new equation is combined with Eq. (2.36), solved numerically for the line load derivatives $\partial P_{f_l} / \partial \beta$, etc., which are combined to obtain the lateral stability derivatives.

Numerical results using these equations are given in Section 3.5.

3. GUST RESPONSE OF TEN GENERAL AVIATION AIRCRAFT

The mathematical models of atmospheric turbulence, aircraft gust response, and the calculation of the resulting output power spectra, and load exceedance parameters A and N_o were coded in Fortran IV for solution on A.R.A.P.'s PDP 11/70 digital computer. The program was run for ten general aviation type aircraft in different configurations at cruise airspeed and several altitudes (a total of 69 cases). The aircraft and conditions chosen (Table 3.1) include all of the cases analyzed in Reference 4 by Peele's 2DF, Houbolt's 1DF, and the discrete gust methods. The results of these calculations are presented primarily in terms of pairs of load exceedance parameters

$$A_{\Delta n}, N_{o_{\Delta n}} \quad ; \quad A_{\Delta \ell}, N_{o_{\Delta \ell}} \quad ; \quad A_{HT}, N_{o_{HT}} \quad ; \quad A_{VT}, N_{o_{VT}}$$

as a function of altitude. Additional results are given in terms of frequency response functions which are the square of the amplitude of the transfer functions previously discussed (Section 2.1). The frequency response functions are defined similar to those used in References 2 and 5.

$$F_n(k) \equiv \left(\frac{W}{\pi \rho U S}\right)^2 \left|\frac{\Delta n}{w_g}(k)\right|^2 \tag{3.1}$$

$$F_{\dot{\theta}}(k) \equiv \left|\frac{\dot{\theta}}{w_g}(k)\right|^2 \tag{3.2}$$

$$F_{HT}(k) \equiv \left(\frac{1}{\pi \rho U^2 S_{HT}}\right)^2 \left|\frac{HT}{w_g}(k)\right|^2 \tag{3.3}$$

$$F_{\ell}(k) \equiv \left(\frac{W}{\pi \rho U S}\right)^2 \left|\frac{\ddot{y}}{3 v_g}(k)\right|^2 \tag{3.4}$$

TABLE 3.1 GEOMETRIC AND MASS PROPERTIES OF AIRCRAFT STUDIED

Plane #	CG Loc. ΣMAC	Λ_W deg.	AR_W	S_W ft^2	e_W ft	Λ_{HT} deg.	AR_{HT}	S_{HT} ft^2	e_{HT} ft	Λ_{VT} deg.	AR_{VT} *	S_{VT} ft^2	e_{VT} ft	ℓ_{fus} ft	D_{fus} ft^2	e_{fus} ft	W lb	I_{YY} lb ft^2	I_{ZZ} lb ft^2	IAS fps
1	26.4	0	7.4	174	.116	7.64	3.44	38.7	14.6	17.0	1.78	18.57	14.6	23.2	2.4	-1.46	2,950	43,341	63,337	219
1	28.4				.216				14.65				14.5			-1.36				
2	19.6	0	7.28	178	-.275	0	4.61	32.5	14.36	28.0	1.46	14.90	13.6	24.4	2.6	1.16	3,600	61,180	144,900	285
3	37.9	0	7.52	280	.892	16	5.0	100.0	22.39	50.0	1.29	44.86	20.4	42.7	4.1	4.9	10,200	719,580	1,155,097	418
4	21.1	0	8.15	266	-.087	0	6.67	58.4	21.4	32.0	1.81	44.27	18.7	36.9	3.5	1.85	10,250	427,358	646,479	408
5	10.0	0	7.71	278	-.955	35	3.08	76.0	30.22	42.0	1.83	56.0	29.0	55.5	4.2	6.5	12,500	942,576	1,643,450	372
6	20.9	12	5.02	232	-.288	25	3.97	54.0	20.69	50.0	.828	40.75	15.6	40.0	2.9	7.8	9,000	528,000	681,000	878**
7	27.2	30	5.77	342	-.83	32	3.0	77.0	18.71	35.0	1.41	41.58	24.0	43.4	4.1	6.3	17,375	978,880	1,655,080	932**
7	28.0				-.23				18.11				23.4			6.9				
8	25.0	0	6.2	181	0	0	2.85	35.1	15.0	15.0	1.4	22.8	15.0	24.4	2.7	-.8	3,400	61,400	74,060	279
9	17.0	0	7.28	178	-.39	13	4.73	32.5	14.0	40.0	1.35	13.7	13.1	22.4	2.2	.39	2,127	45,000	76,390	264
10	24.3	0	5.63	171.6	0	0	5.27	31.6	13.8	40.0	1.53	11.56	12.5	21.9	2.3	.31	2,450	45,350	67,900	216
10	15.4				-.5				14.3				13.0			-.19				

* This value is derived from b_{VT}^2/S_{VT} and is multiplied by 1.55 in the program

** or M = .8 , whichever is slower

$$F_{\dot{\psi}}(k) \equiv \left| \frac{\dot{\psi}}{V_g}(k) \right|^2 \tag{3.5}$$

$$F_{VT}(k) \equiv \left(\frac{1}{\pi \rho U^2 S_{VT}} \right)^2 \left| \frac{P_{VT}}{V_g}(k) \right|^2 \tag{3.6}$$

The response function results are useful for determing the approximate second-order natural frequency and damping and for aid in understanding changes in the load exceedance parameters. These have, for the most part, been relegated to Appendix B since they are auxilary in nature.

The load exceedance parameters are shown as function of altitude for each of ten aircraft at the specified flight configurations (Figs. 3.1 - 3.10). Two basic trends are seen in the Houbolt 2DF results contained in these figures: 1) a decrease in $A_{\Delta n}$ and, usually, an increase in $N_{o_{\Delta n}}$ with altitude. This is explained by referring to a typical set of frequency functions as shown in Fig. 3.12a.

For airplane #1 the amplitude squared response function, f_n, increases from sea level to 20K ft by about 30% (Fig. 14a). However, this must be multiplied by $(\pi \rho US/w)^2$ to convert to $|\Delta n/w_g|^2$. The density terms causes the load factor transfer function to decrease with altitude thus resulting in lower values of $A_{\Delta n}$. Again, referring to Fig. 3.12a, it is seen that an increase in altitude amplifies F_n near and above the resonant frequency and attenuates F_n at low frequencies. Therefore, $N_{o_{\Delta n}}$ which is proportional to the radius of gyration of this response increases with altitude.

Another trend evident in the results is that moving the cg aft (Fig. 3.11) increases the structural loading parameters $A_{\Delta n}$, $A_{\Delta \ell}$, and decreases the zero crossing parameters, $N_{o_{\Delta n}}$ and $N_{o_{\Delta \ell}}$. This is due to lowering the short period frequency and comparable lateral frequency. This shift increases the amount of low frequency energy in the output spectrum more than the decrease in high frequency energy.

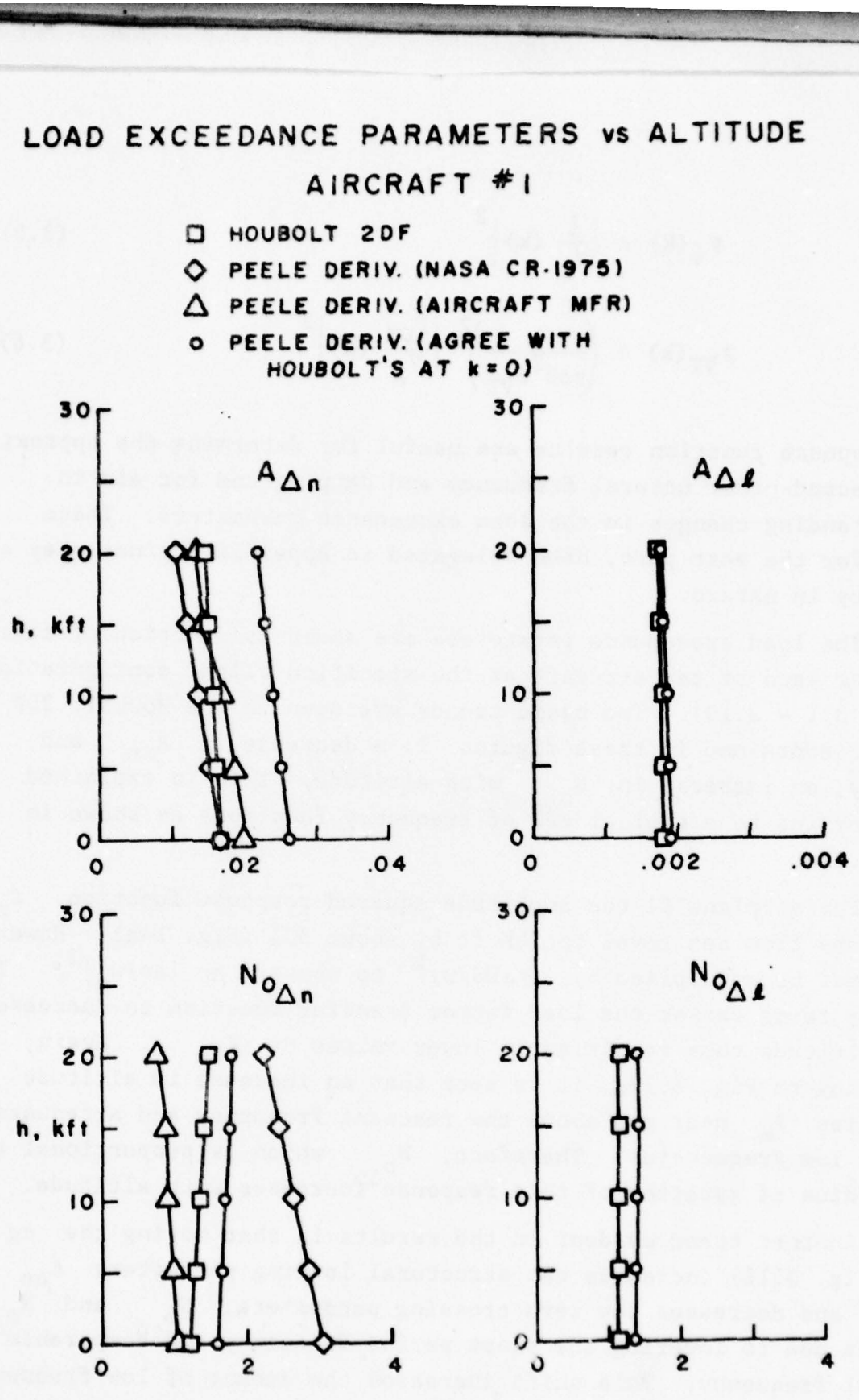
LOAD EXCEEDANCE PARAMETERS vs ALTITUDE
AIRCRAFT #1
HOUBOLT 2DF
PEELE DERIV. (NASA CR-1975)
PEELE DERIV. (AIRCRAFT MFR)
PEELE DERIV. (AGREE WITH HOUBOLT'S AT k = 0)
$A_{\Delta n}$
$A_{\Delta \ell}$
$N_{O_{\Delta n}}$
$N_{O_{\Delta \ell}}$
h, kft
30
20
10
0
.02
.04
.002
.004
2
4

Figure 3.1a

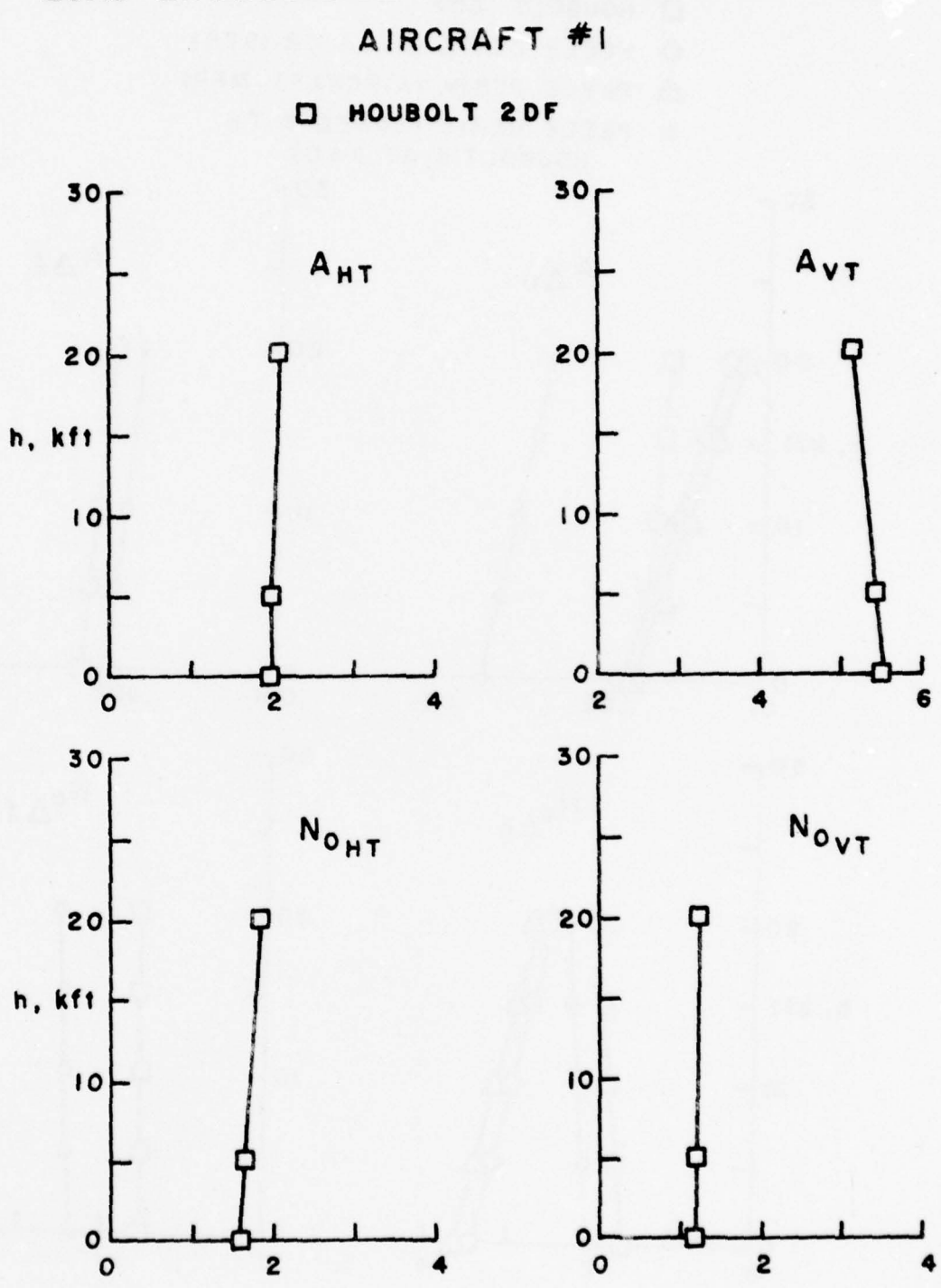
LOAD EXCEEDANCE PARAMETERS vs ALTITUDE
AIRCRAFT #1
HOUBOLT 2DF
A_{HT}
A_{VT}
$N_{O_{HT}}$
$N_{O_{VT}}$
h, kft
30
20
10
0
0
2
4
6

Figure 3.1b

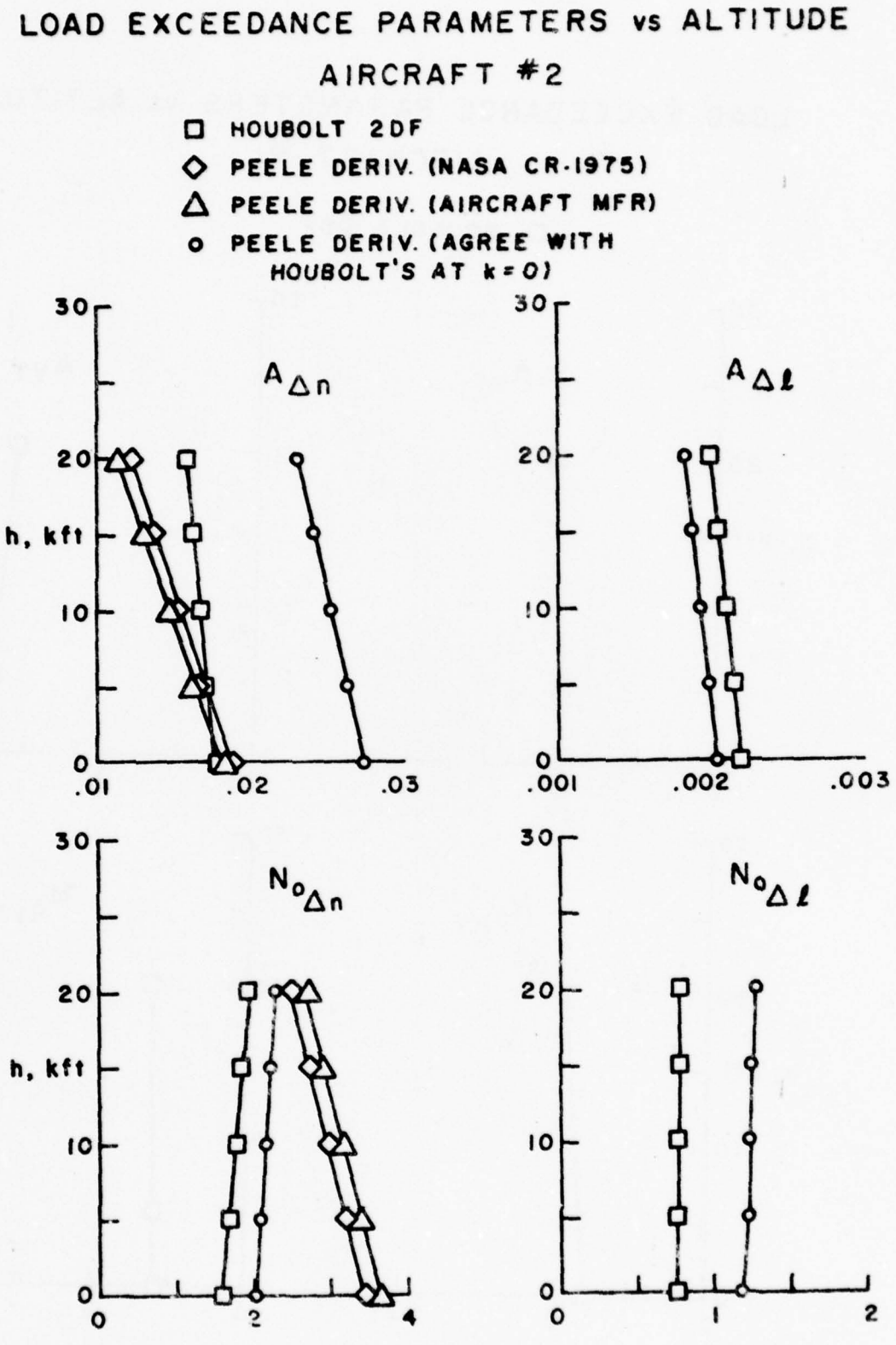
LOAD EXCEEDANCE PARAMETERS vs ALTITUDE
AIRCRAFT #2
HOUBOLT 2DF
PEELE DERIV. (NASA CR-1975)
PEELE DERIV. (AIRCRAFT MFR)
PEELE DERIV. (AGREE WITH HOUBOLT'S AT k=0)
$A_{\Delta n}$
$A_{\Delta \ell}$
$N_{o\Delta n}$
$N_{o\Delta \ell}$
h, kft
30
20
10
0
.01
.02
.03
.001
.002
.003
2
4
1

Figure 3.2a

LOAD EXCEEDANCE PARAMETERS vs ALTITUDE
AIRCRAFT #2

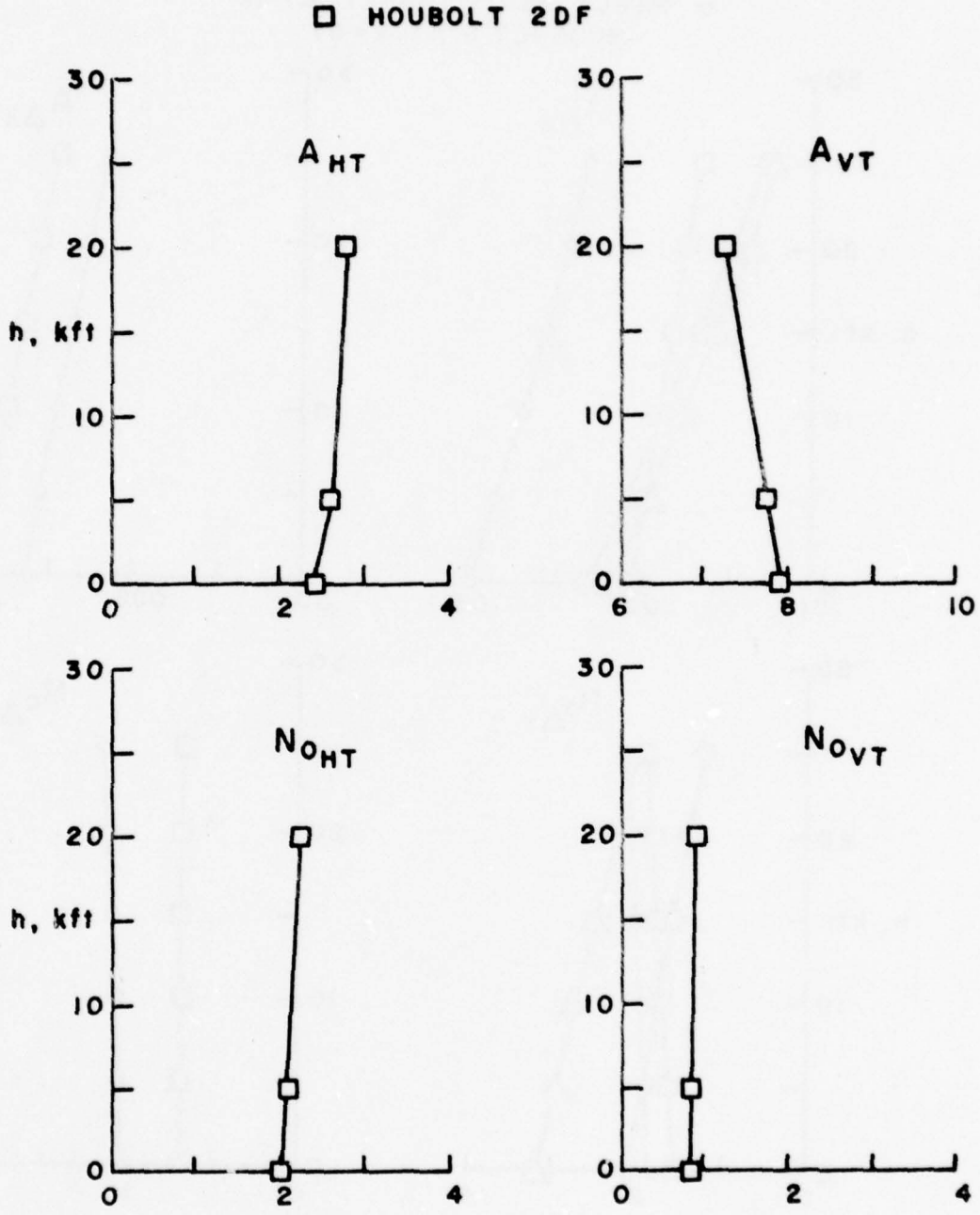

Figure 3.2b

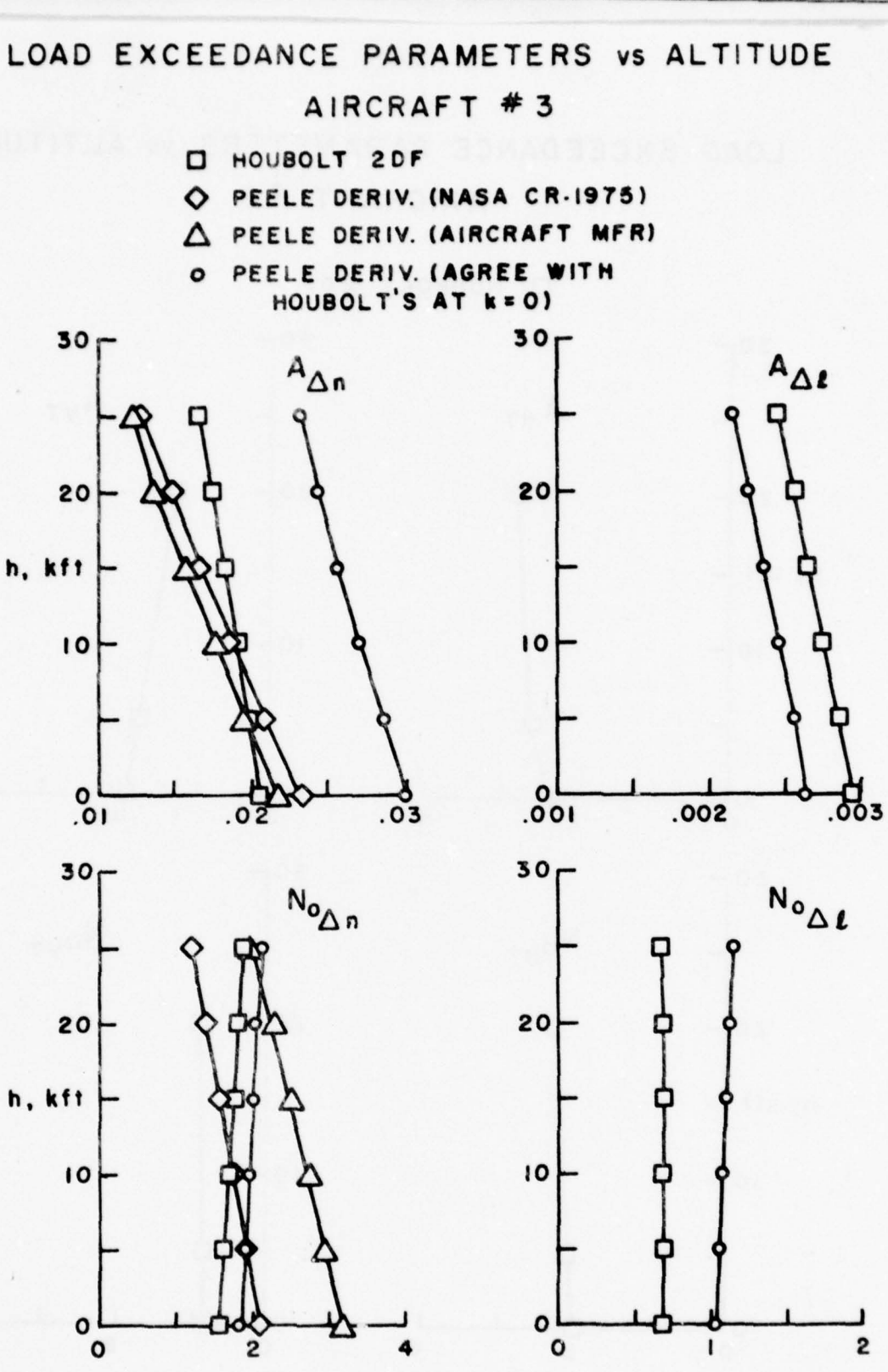
LOAD EXCEEDANCE PARAMETERS vs ALTITUDE
AIRCRAFT # 3
HOUBOLT 2DF
PEELE DERIV. (NASA CR-1975)
PEELE DERIV. (AIRCRAFT MFR)
PEELE DERIV. (AGREE WITH HOUBOLT'S AT k=0)
$A_{\Delta n}$
$A_{\Delta \ell}$
$N_{o\Delta n}$
$N_{o\Delta \ell}$
h, kft
30
20
10
0
.01
.02
.03
.001
.002
.003
2
4
1

Figure 3.3a

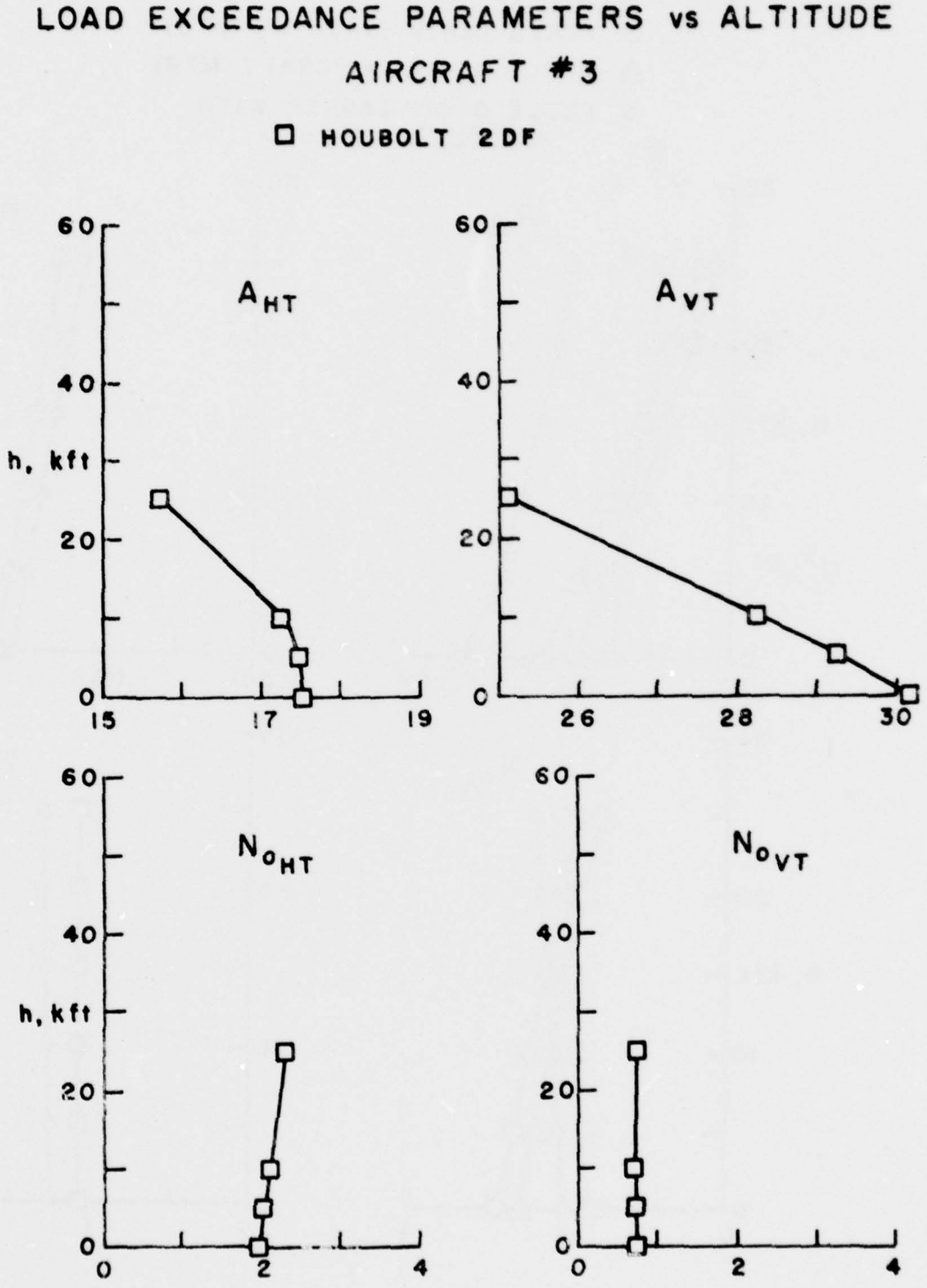
LOAD EXCEEDANCE PARAMETERS vs ALTITUDE
AIRCRAFT #3
HOUBOLT 2DF
A_{HT}
A_{VT}
$N_{O_{HT}}$
$N_{O_{VT}}$
h, kft
60
40
20
0
15
17
19
26
28
30
2
4

Figure 3.3b

LOAD EXCEEDANCE PARAMETERS vs ALTITUDE

AIRCRAFT #4

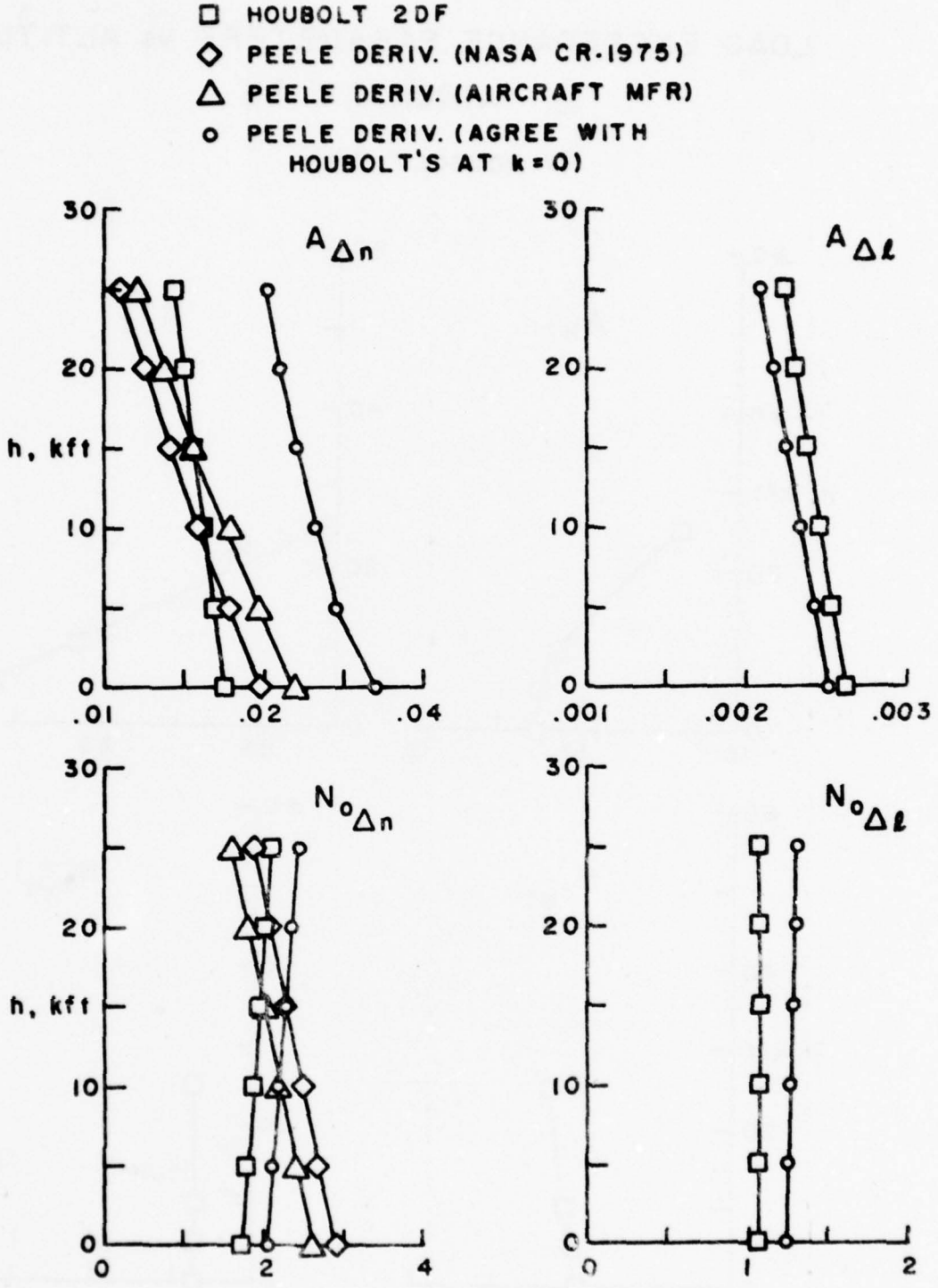

Figure 3.4a

LOAD EXCEEDANCE PARAMETERS vs ALTITUDE
AIRCRAFT #4

□ HOUBOLT 2DF

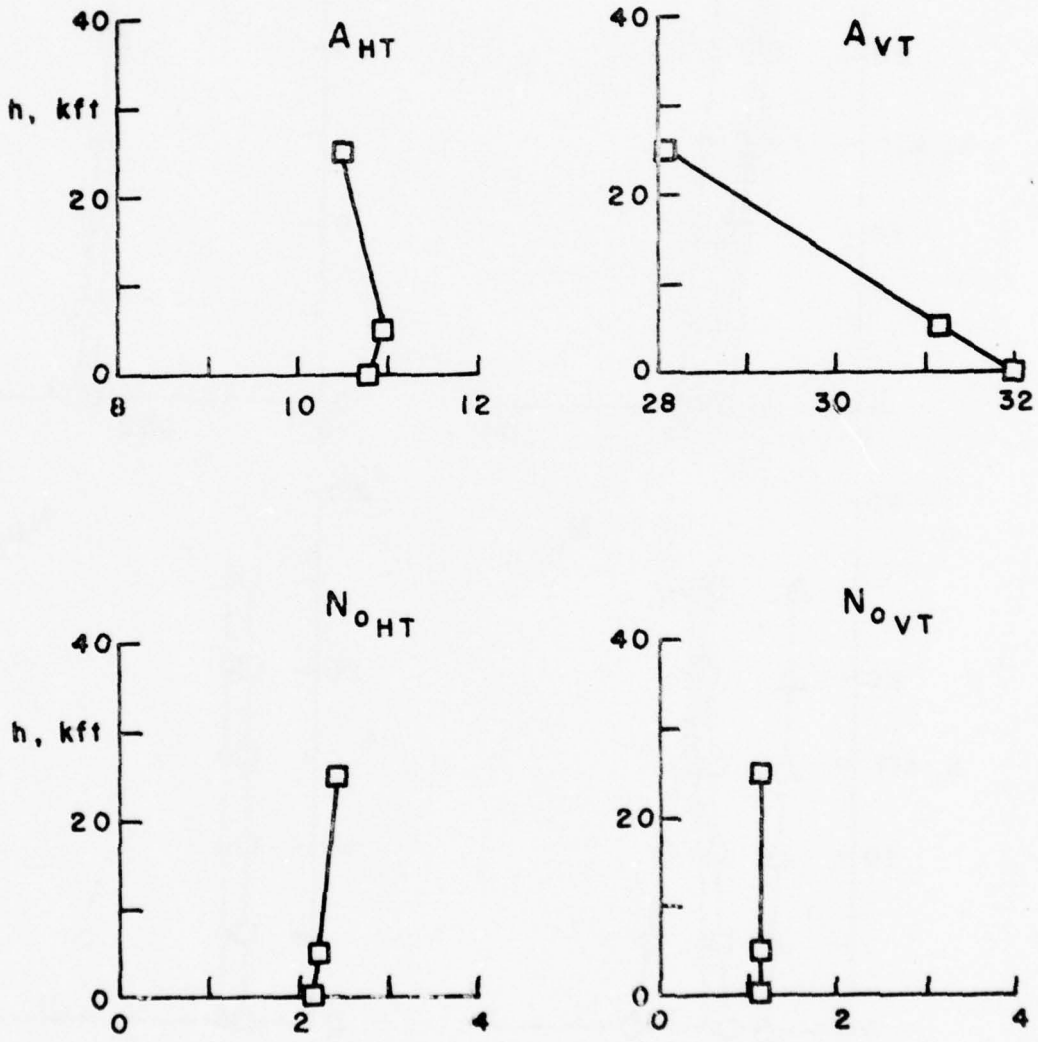

Figure 3.4b

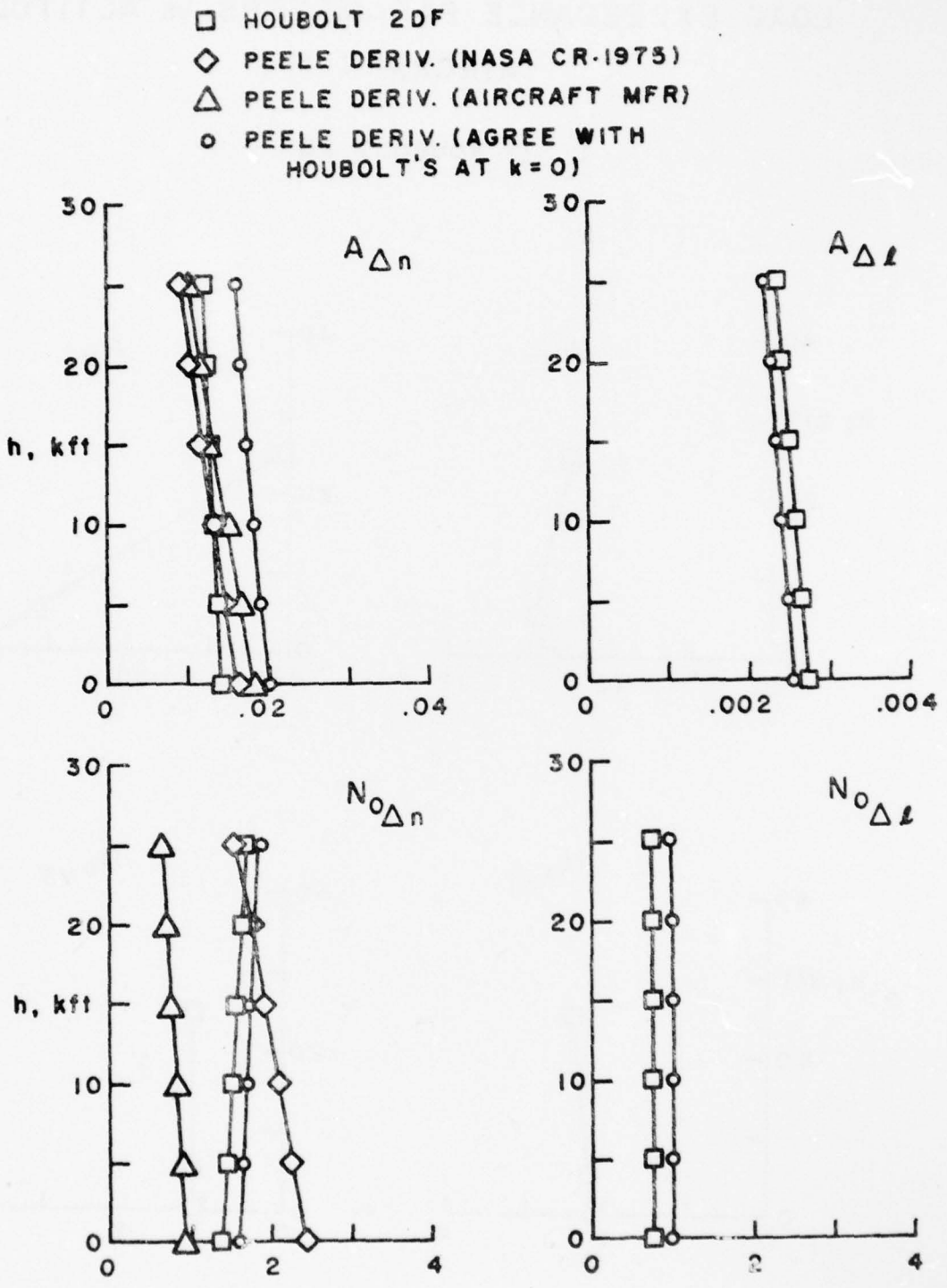
LOAD EXCEEDANCE PARAMETERS vs ALTITUDE
AIRCRAFT # 5
HOUBOLT 2DF
PEELE DERIV. (NASA CR-1975)
PEELE DERIV. (AIRCRAFT MFR)
PEELE DERIV. (AGREE WITH HOUBOLT'S AT k = 0)
$A_{\Delta n}$
$A_{\Delta \ell}$
$N_{O_{\Delta n}}$
$N_{O_{\Delta \ell}}$
h, kft
30
20
10
0
.02
.04
.002
.004
2
4

Figure 3.5a

LOAD EXCEEDANCE PARAMETERS vs ALTITUDE
AIRCRAFT #5

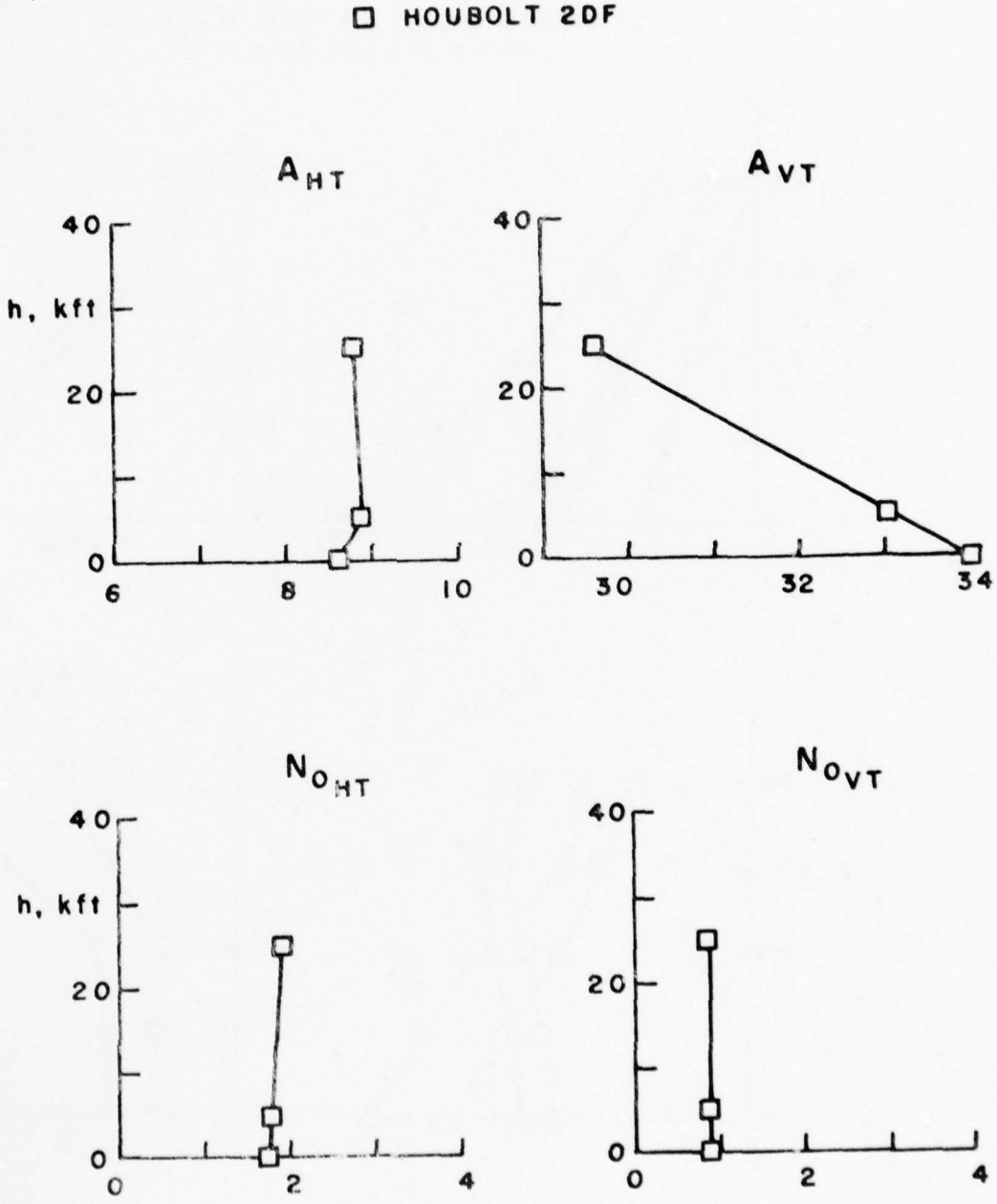

Figure 3.5b

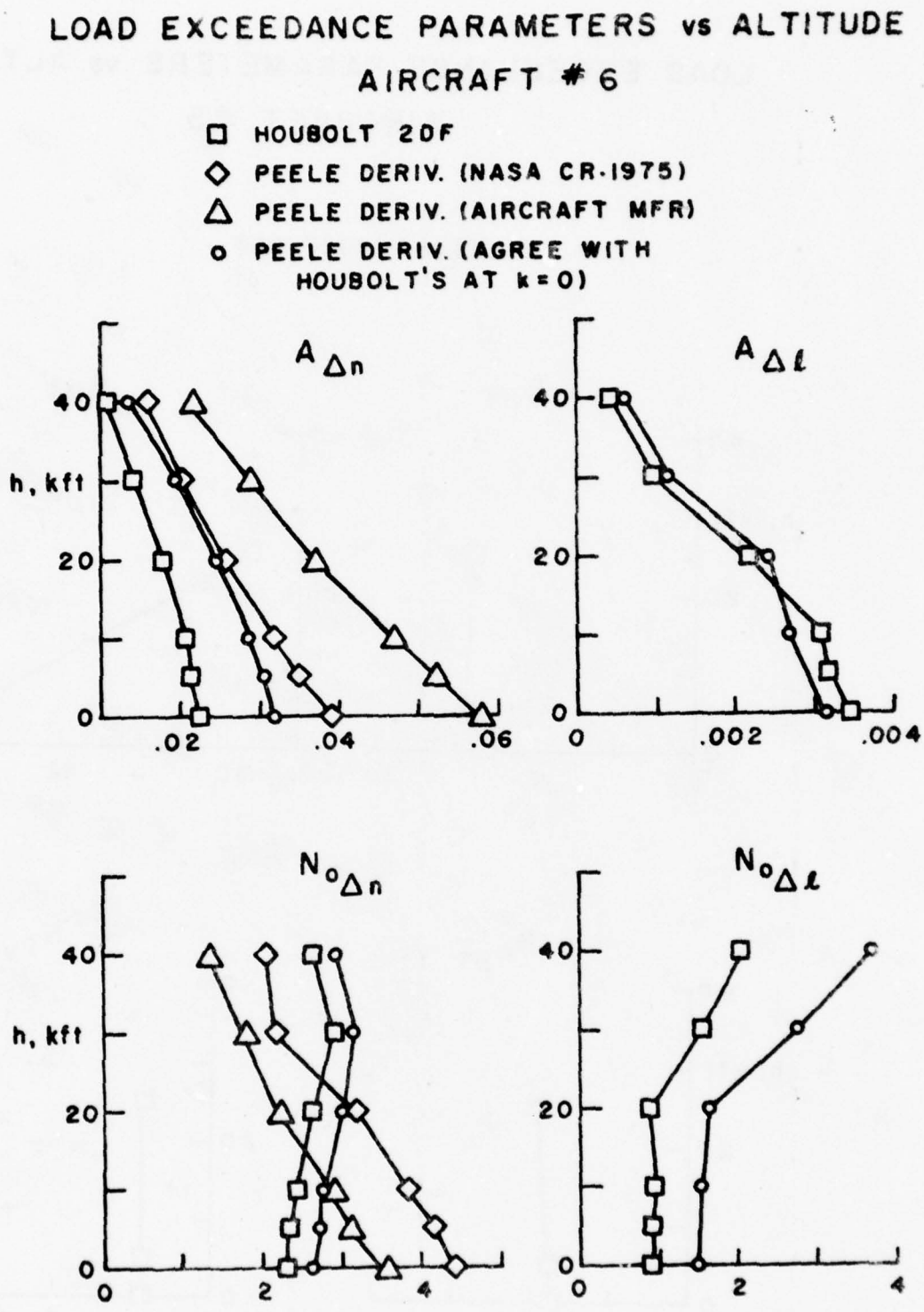
LOAD EXCEEDANCE PARAMETERS vs ALTITUDE
AIRCRAFT # 6
HOUBOLT 20F
PEELE DERIV. (NASA CR-1975)
PEELE DERIV. (AIRCRAFT MFR)
PEELE DERIV. (AGREE WITH HOUBOLT'S AT k=0)
$A_{\Delta n}$
$A_{\Delta \ell}$
$N_{o\Delta n}$
$N_{o\Delta \ell}$
h, kft
40
20
0
.02
.04
.06
.002
.004
2
4

Figure 3.6a

LOAD EXCEEDANCE PARAMETERS vs ALTITUDE
AIRCRAFT #6

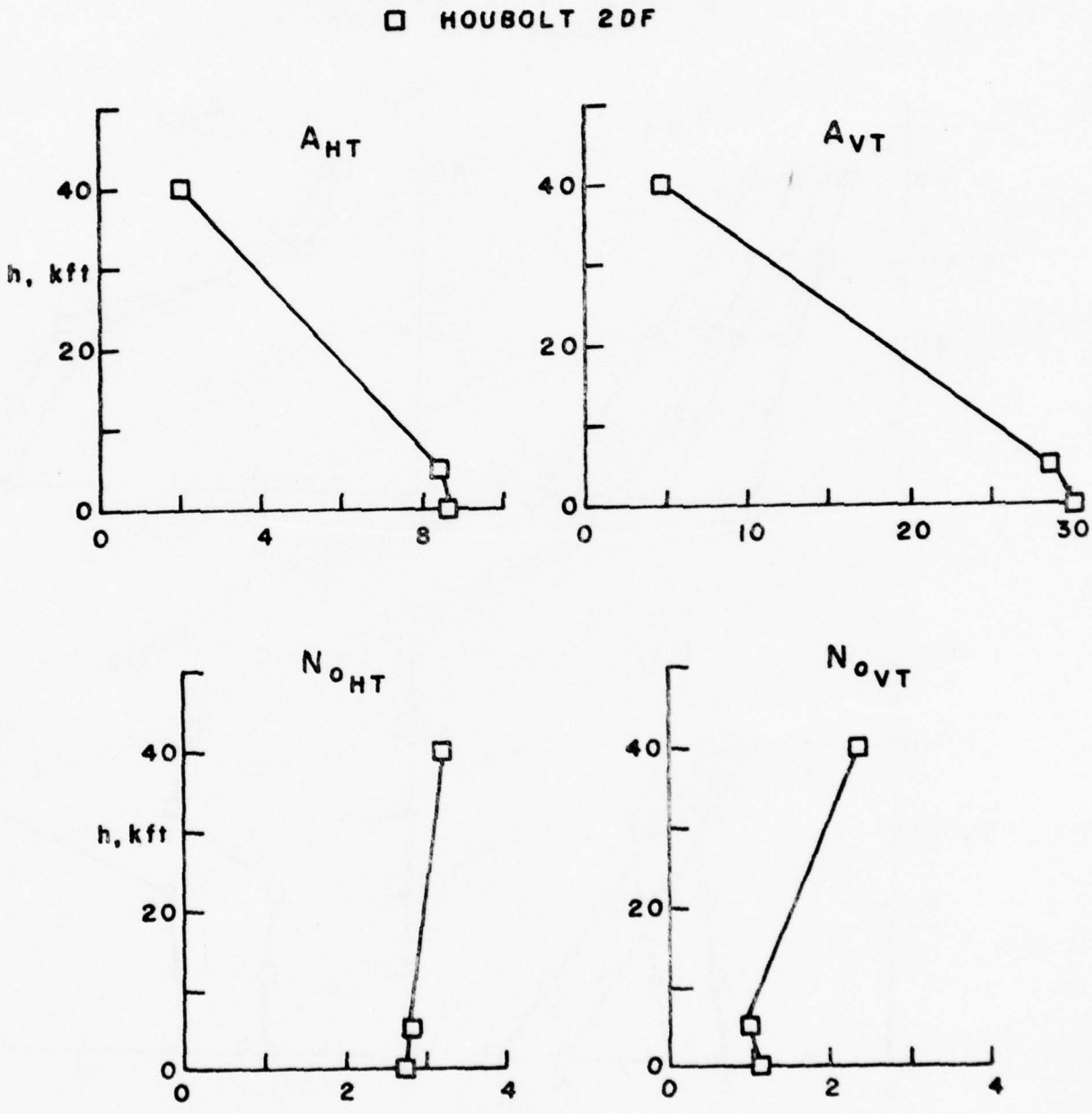

Figure 3.6b

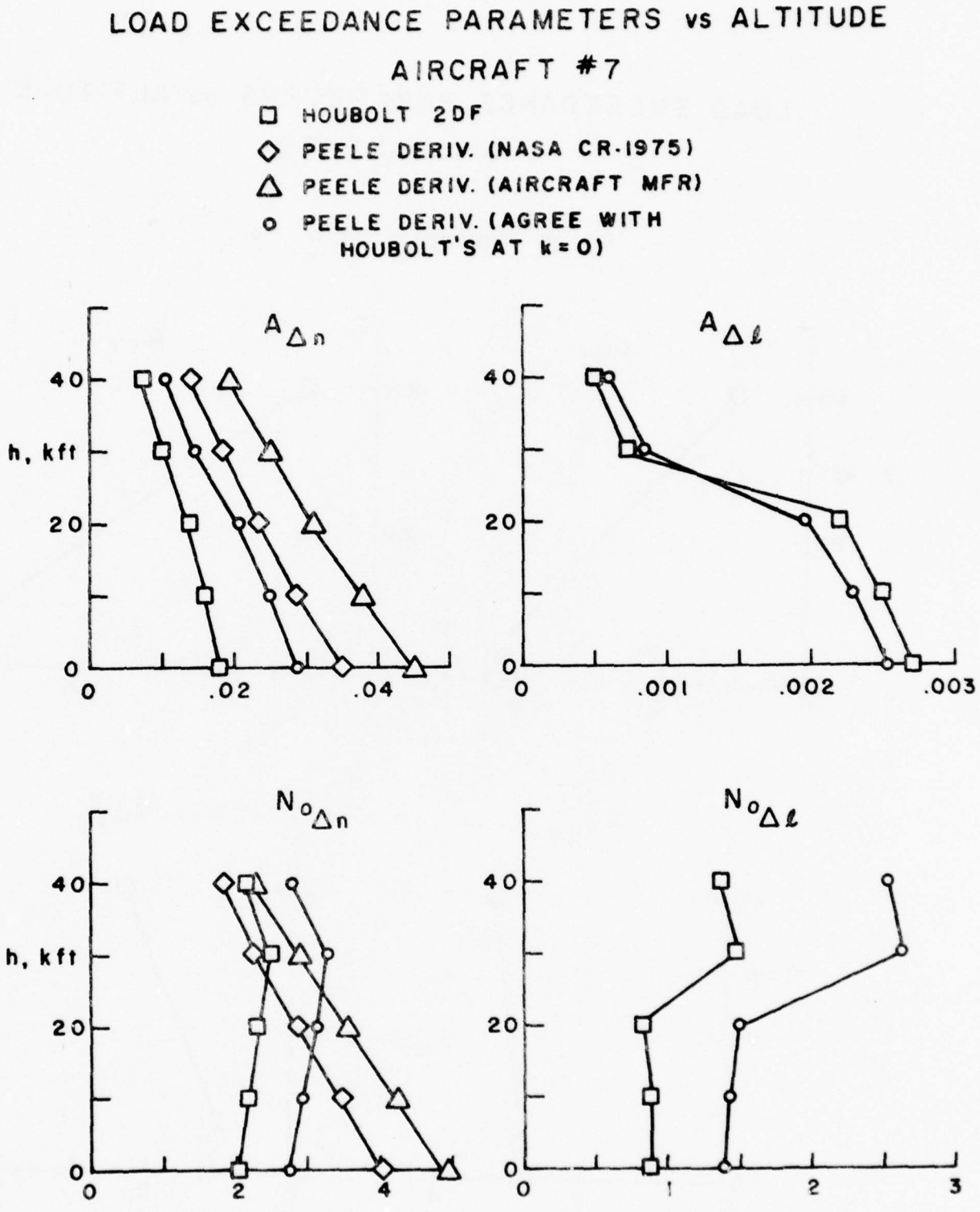
LOAD EXCEEDANCE PARAMETERS vs ALTITUDE
AIRCRAFT #7
HOUBOLT 2DF
PEELE DERIV. (NASA CR-1975)
PEELE DERIV. (AIRCRAFT MFR)
PEELE DERIV. (AGREE WITH HOUBOLT'S AT k=0)
$A_{\Delta n}$
$A_{\Delta \ell}$
$N_{o_{\Delta n}}$
$N_{o_{\Delta \ell}}$
h, kft
40
20
0
.02
.04
.001
.002
.003
2
4
1
3

Figure 3.7a

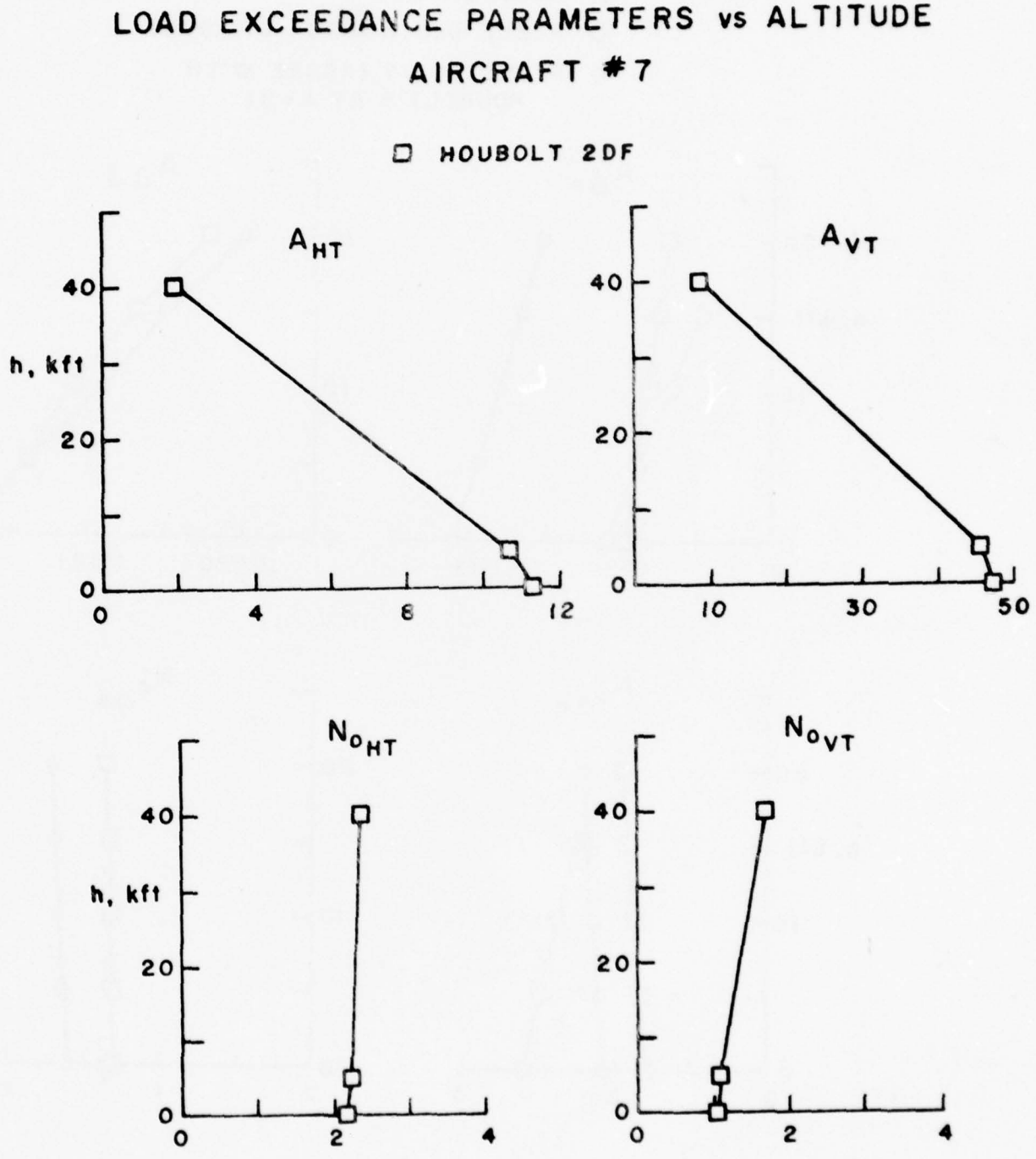
LOAD EXCEEDANCE PARAMETERS vs ALTITUDE
AIRCRAFT #7
HOUBOLT 2DF
A_{HT}
A_{VT}
$N_{O_{HT}}$
$N_{O_{VT}}$
h, kft
40
20
0
0
4
8
12
10
30
50
2

Figure 3.7b

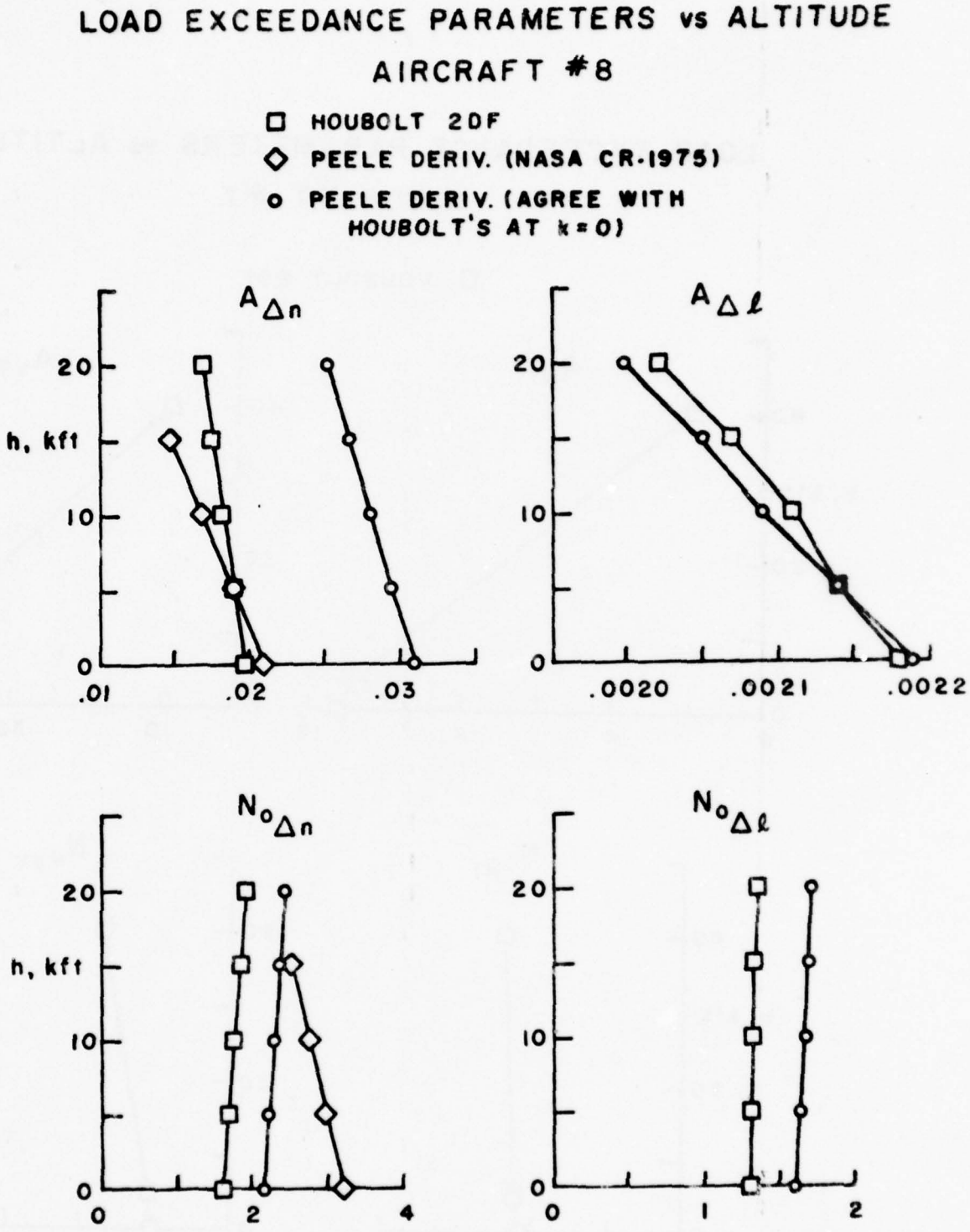
LOAD EXCEEDANCE PARAMETERS vs ALTITUDE
AIRCRAFT #8
HOUBOLT 2DF
PEELE DERIV. (NASA CR-1975)
PEELE DERIV. (AGREE WITH HOUBOLT'S AT k=0)
$A_{\Delta n}$
$A_{\Delta \ell}$
$N_{o_{\Delta n}}$
$N_{o_{\Delta \ell}}$
h, kft
20
10
0
.01
.02
.03
.0020
.0021
.0022
2
4
1

Figure 3.8a

LOAD EXCEEDANCE PARAMETERS vs ALTITUDE
AIRCRAFT #8

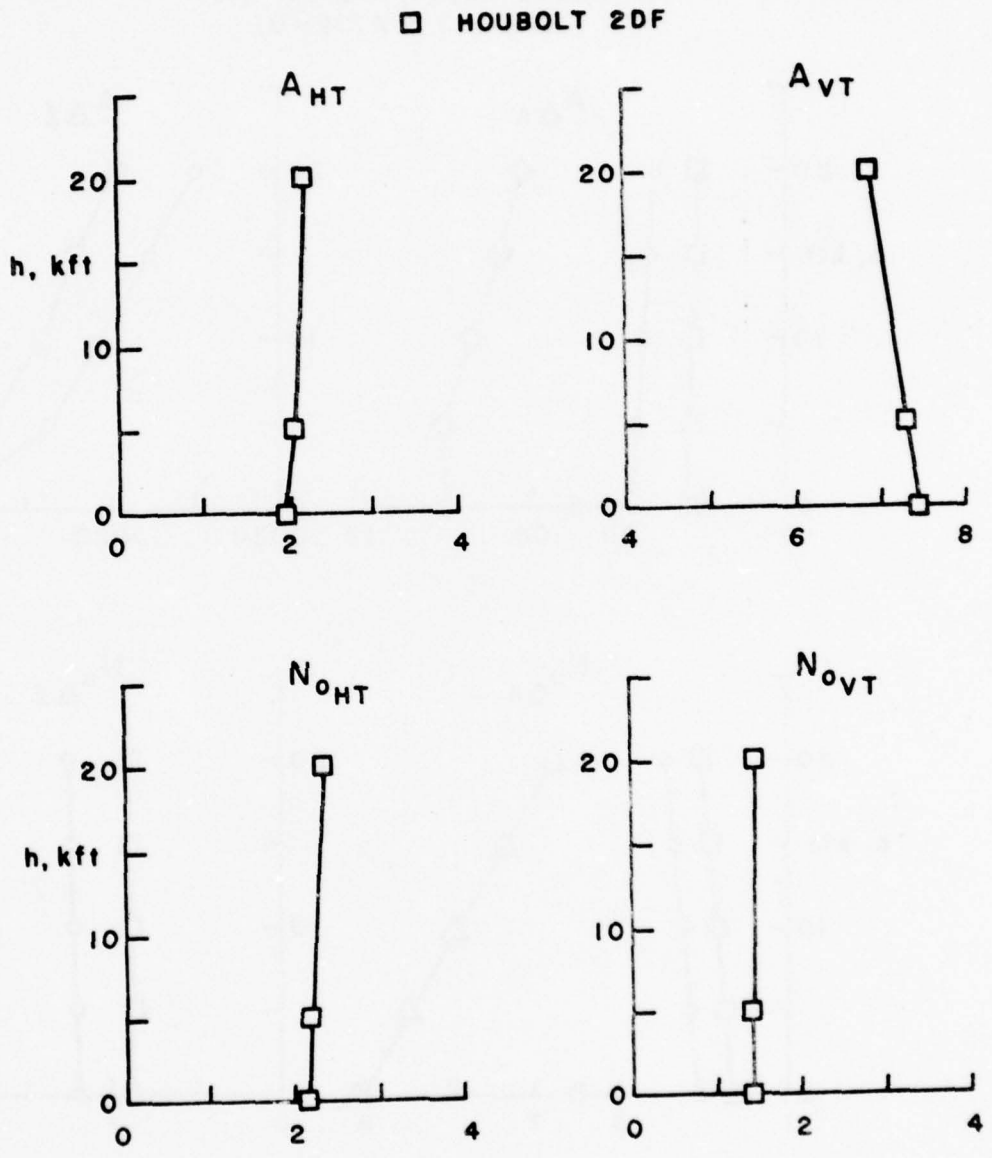

Figure 3.8b

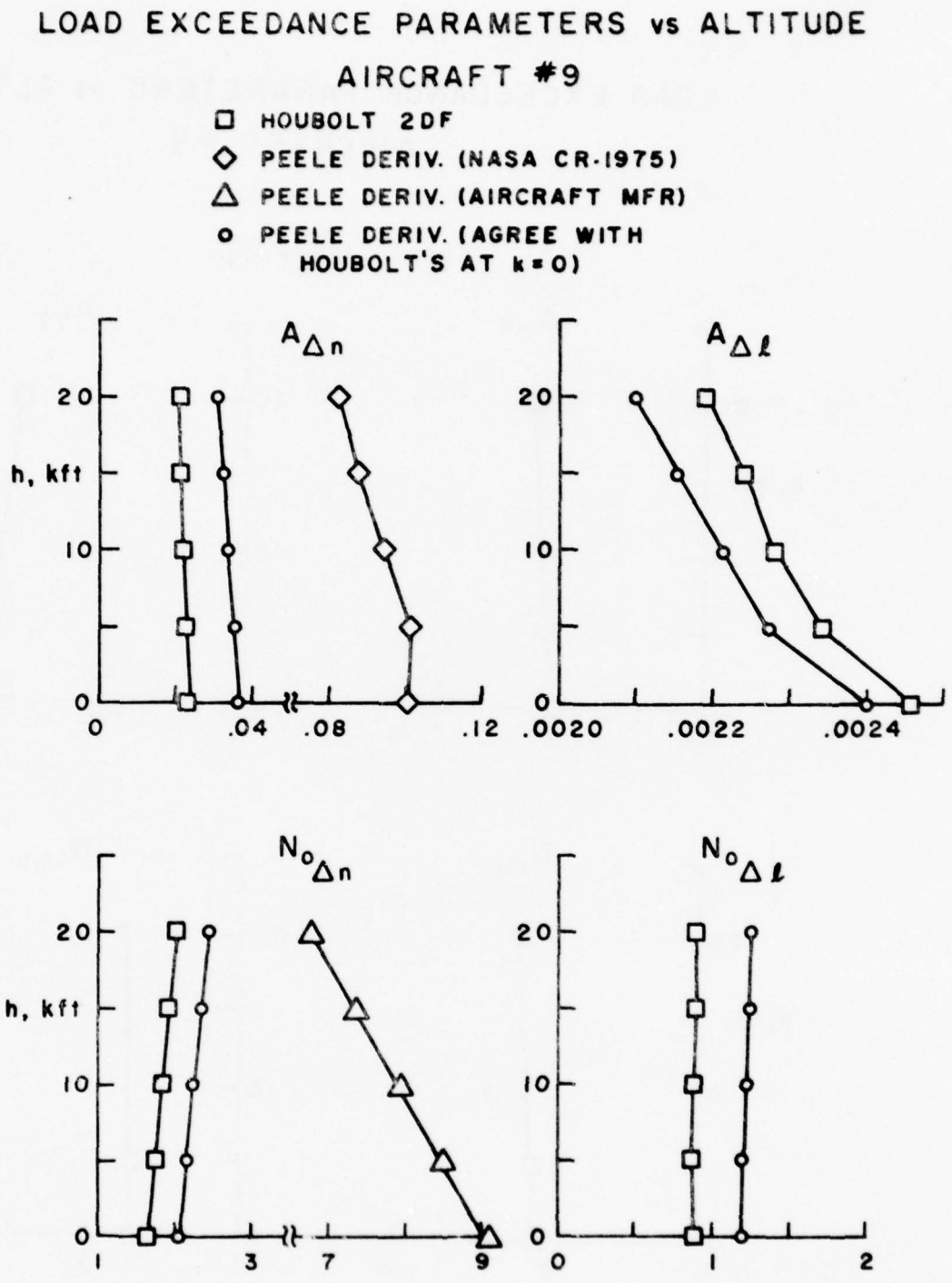

Figure 3.9a

COMPARISON OF TAIL LOAD EXCEEDANCE PARA-

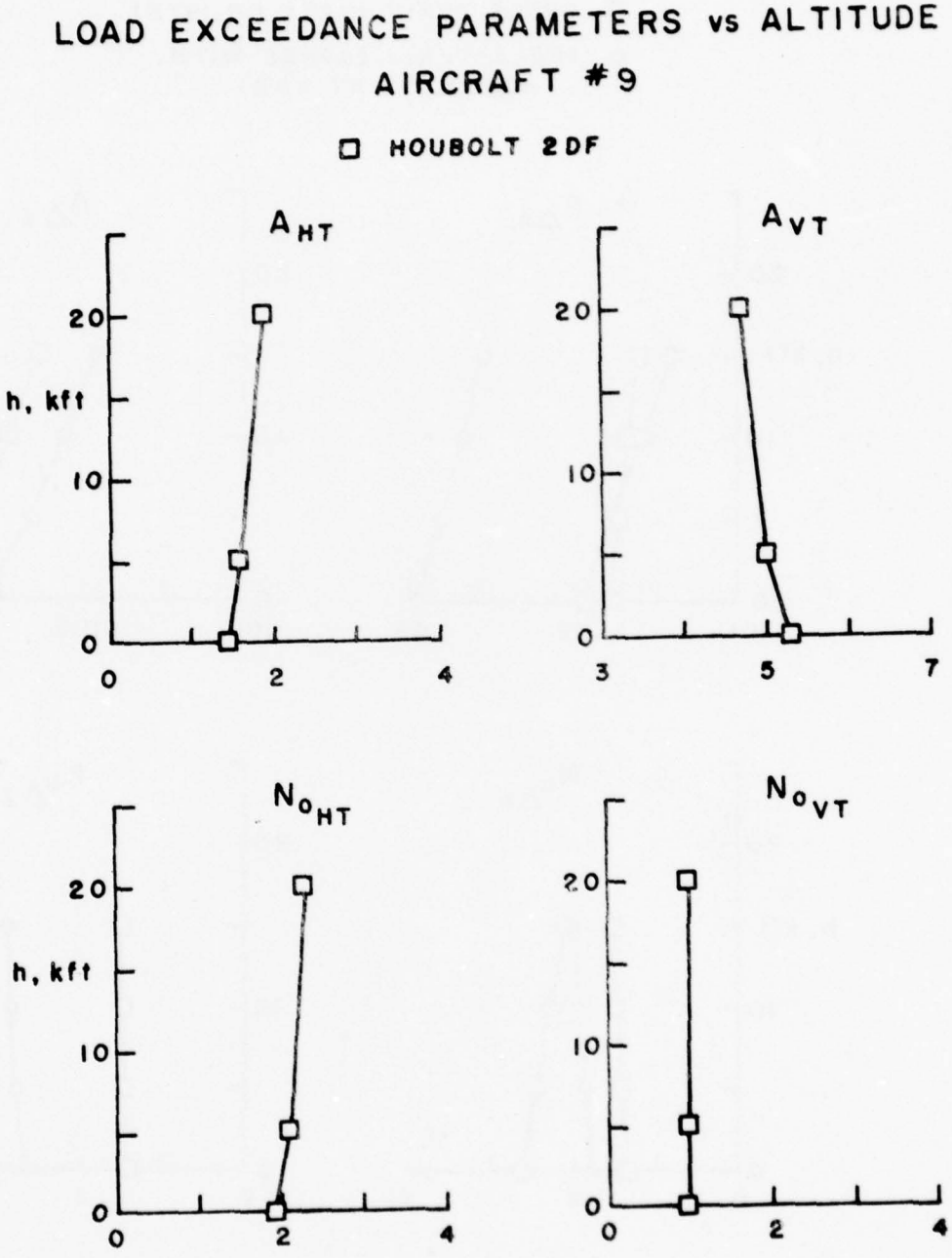
LOAD EXCEEDANCE PARAMETERS vs ALTITUDE
AIRCRAFT #9
HOUBOLT 2DF
A_{HT}
A_{VT}
$N_{O_{HT}}$
$N_{O_{VT}}$
h, kft
20
10
0
0
2
4
3
5
7

Figure 3.9b

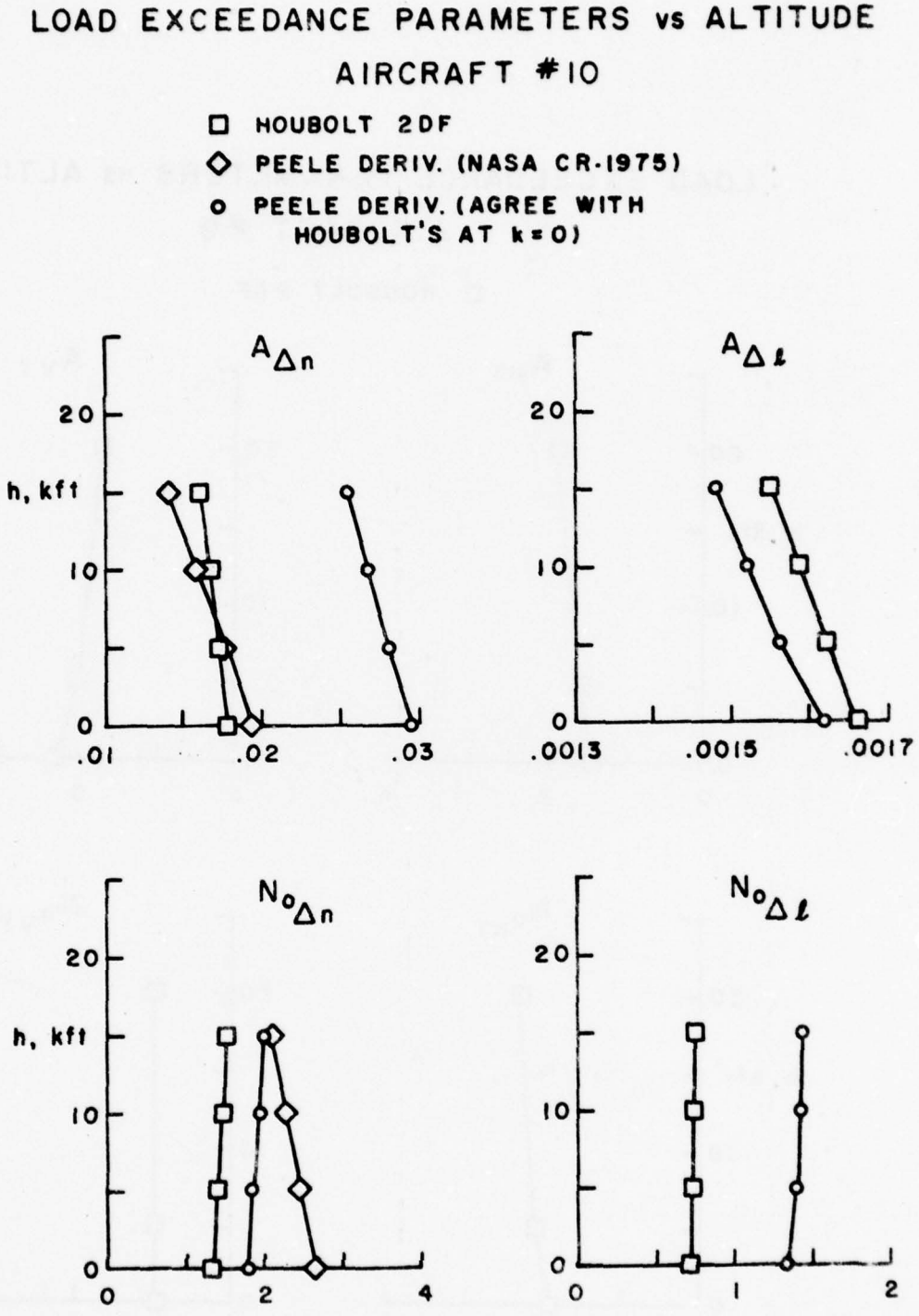
LOAD EXCEEDANCE PARAMETERS vs ALTITUDE
AIRCRAFT #10
HOUBOLT 2DF
PEELE DERIV. (NASA CR-1975)
PEELE DERIV. (AGREE WITH HOUBOLT'S AT k=0)
$A_{\Delta n}$
$A_{\Delta \ell}$
$N_{o_{\Delta n}}$
$N_{o_{\Delta \ell}}$
h, kft
20
10
0
.01
.02
.03
.0013
.0015
.0017
2
4
1

Figure 3.10a

LOAD EXCEEDANCE PARAMETERS vs ALTITUDE
AIRCRAFT #10

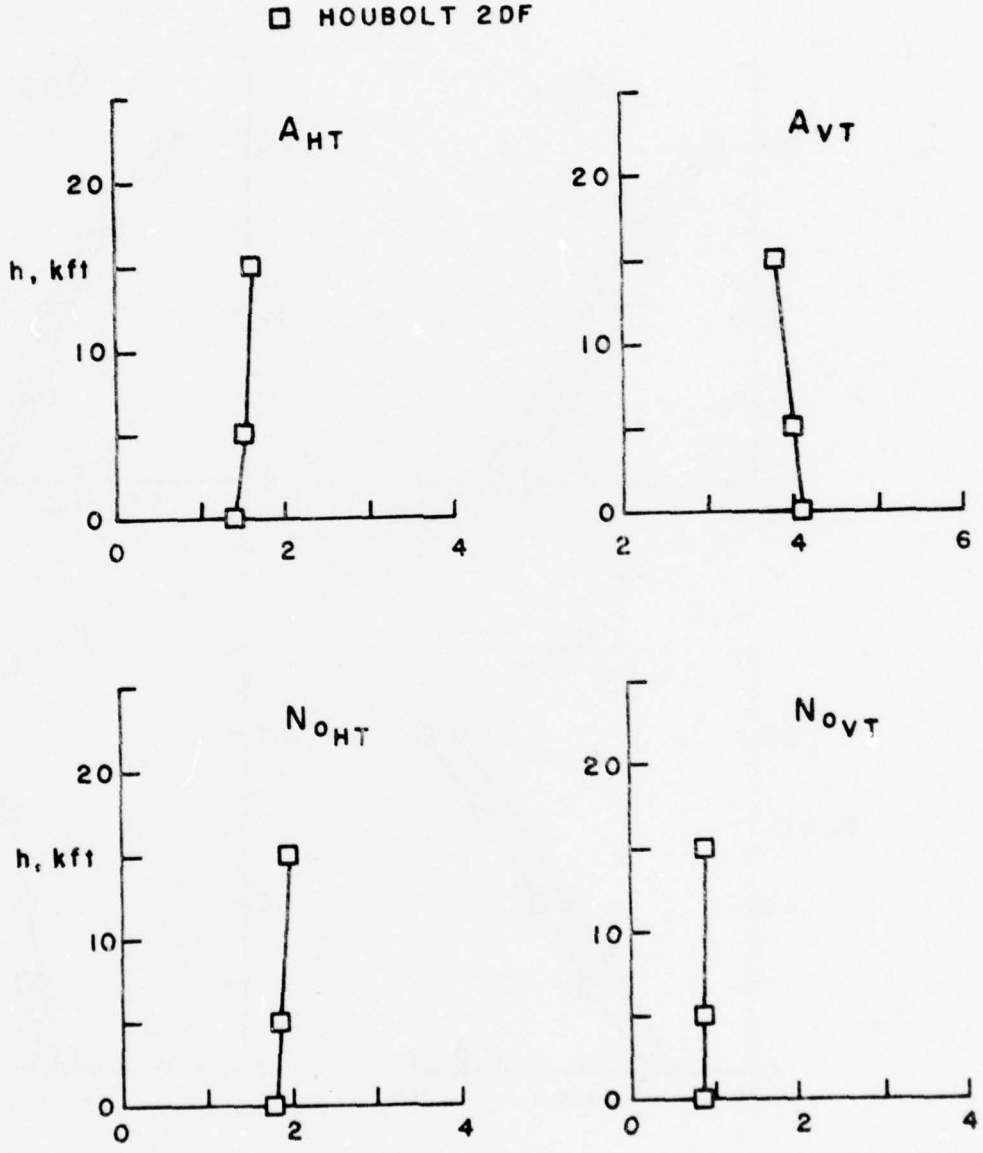

Figure 3.10b

EFFECT OF C.G. POSITION ON
LOAD EXCEEDANCE PARAMETERS
AIRCRAFT # 1
□ Nominal x_{CG} = 26.4 % MAC
○ Aft x_{CG} = 28.4

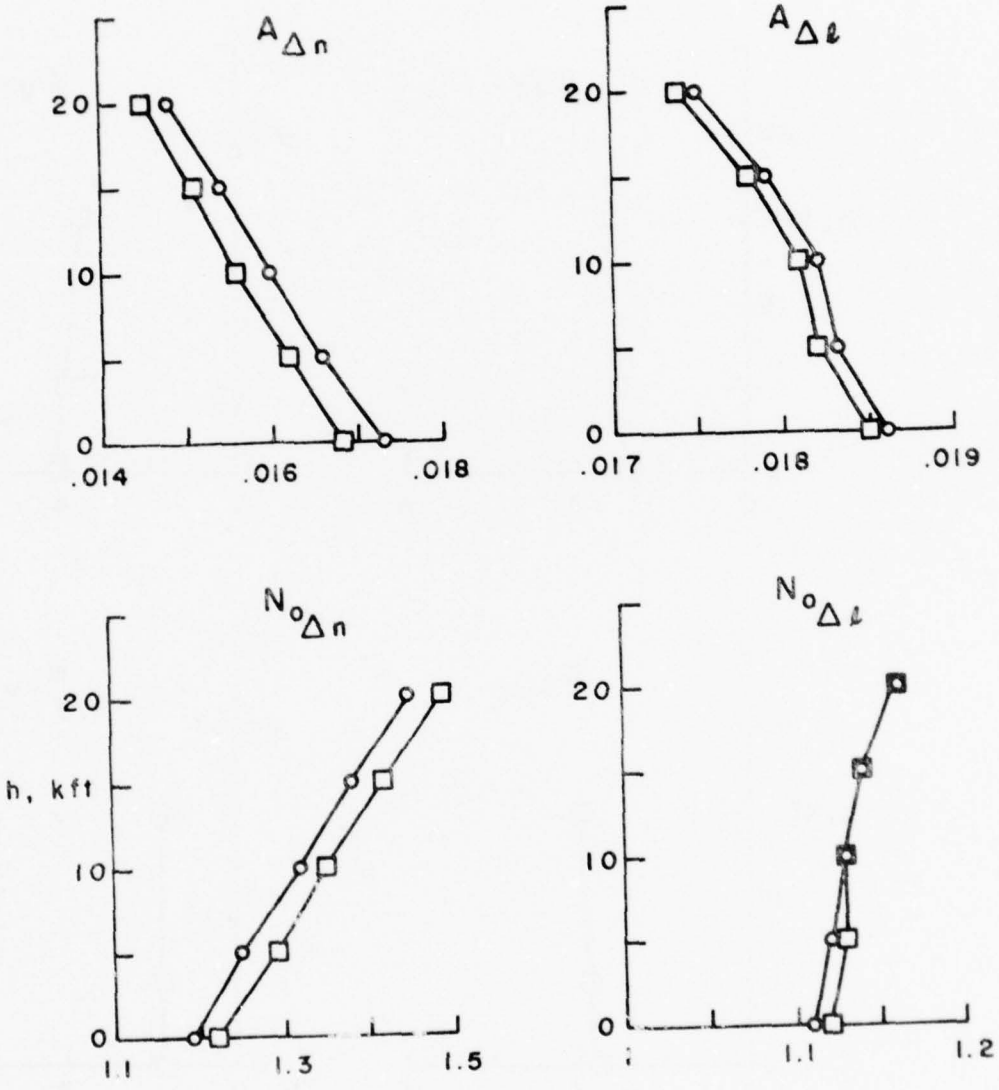

Figure 3.11a

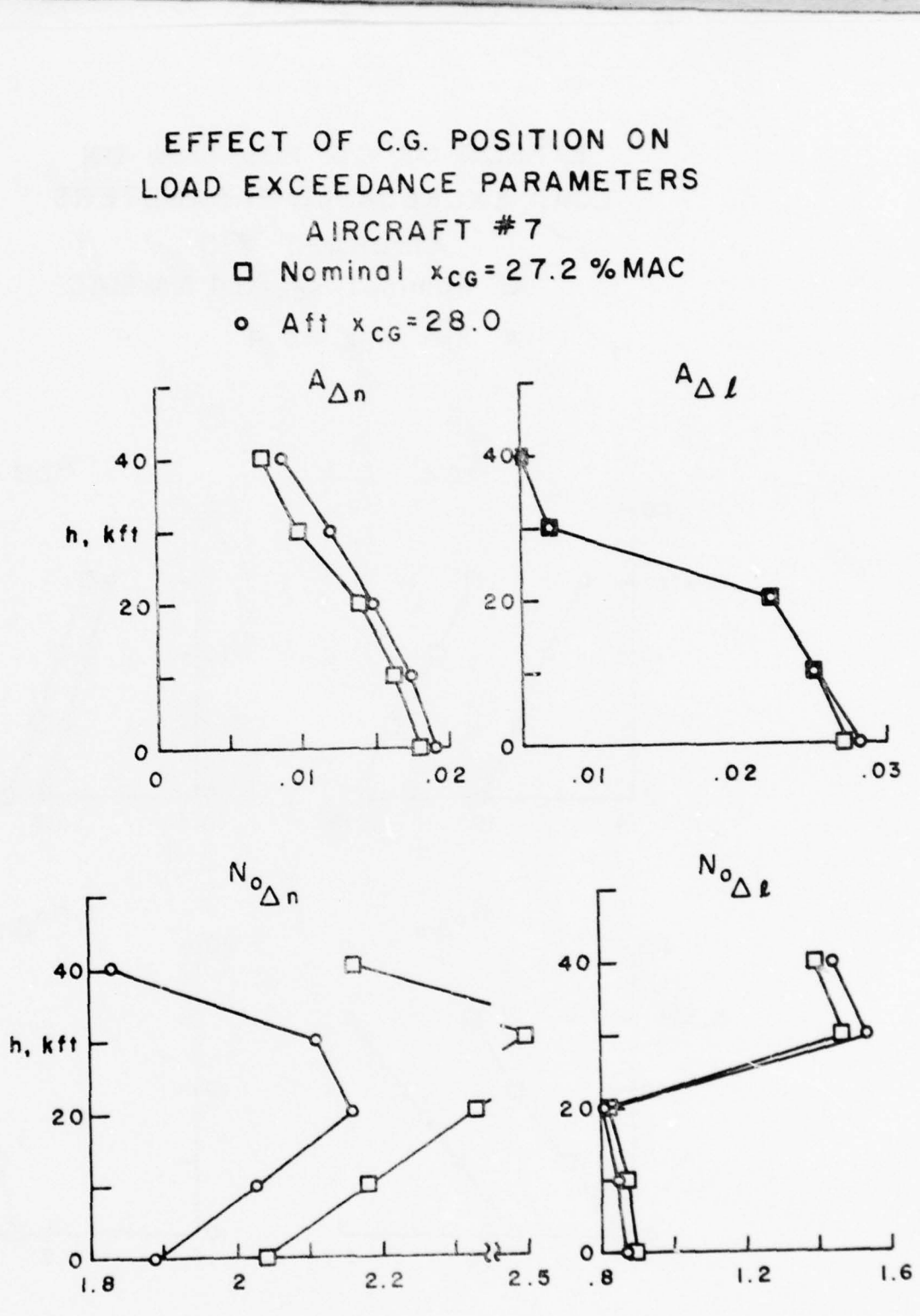
EFFECT OF C.G. POSITION ON
LOAD EXCEEDANCE PARAMETERS
AIRCRAFT #7
□ Nominal x_{CG} = 27.2 %MAC
o Aft x_{CG} = 28.0
$A_{\Delta n}$
$A_{\Delta \ell}$
h, kft
40
20
0
0
.01
.02
.03
$N_{o_{\Delta n}}$
$N_{o_{\Delta \ell}}$
1.8
2
2.2
2.5
.8
1.2
1.6

Figure 3.11b

EFFECT OF C.G. POSITION ON
LOAD EXCEEDANCE PARAMETERS
AIRCRAFT #10
□ Nominal x_{CG} = 24.3 % MAC
○ Fwd x_{CG} = 15.4

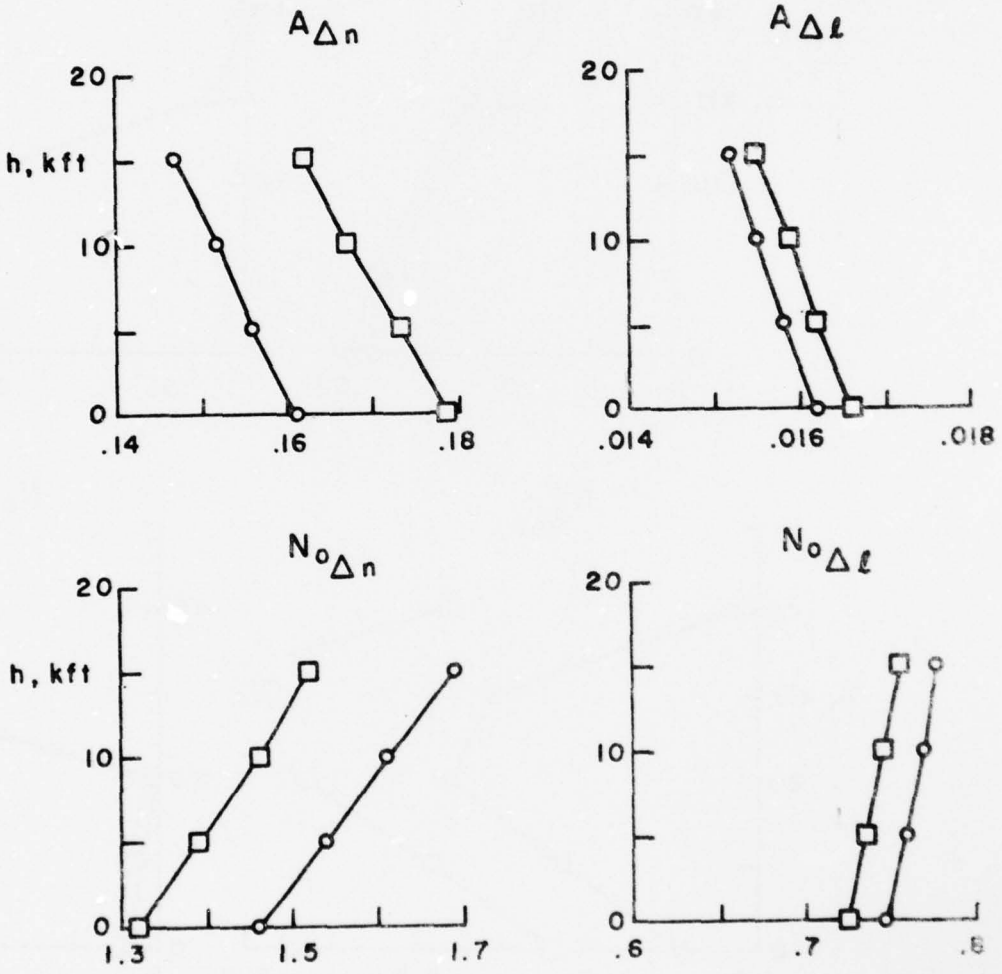

Figure 3.11c

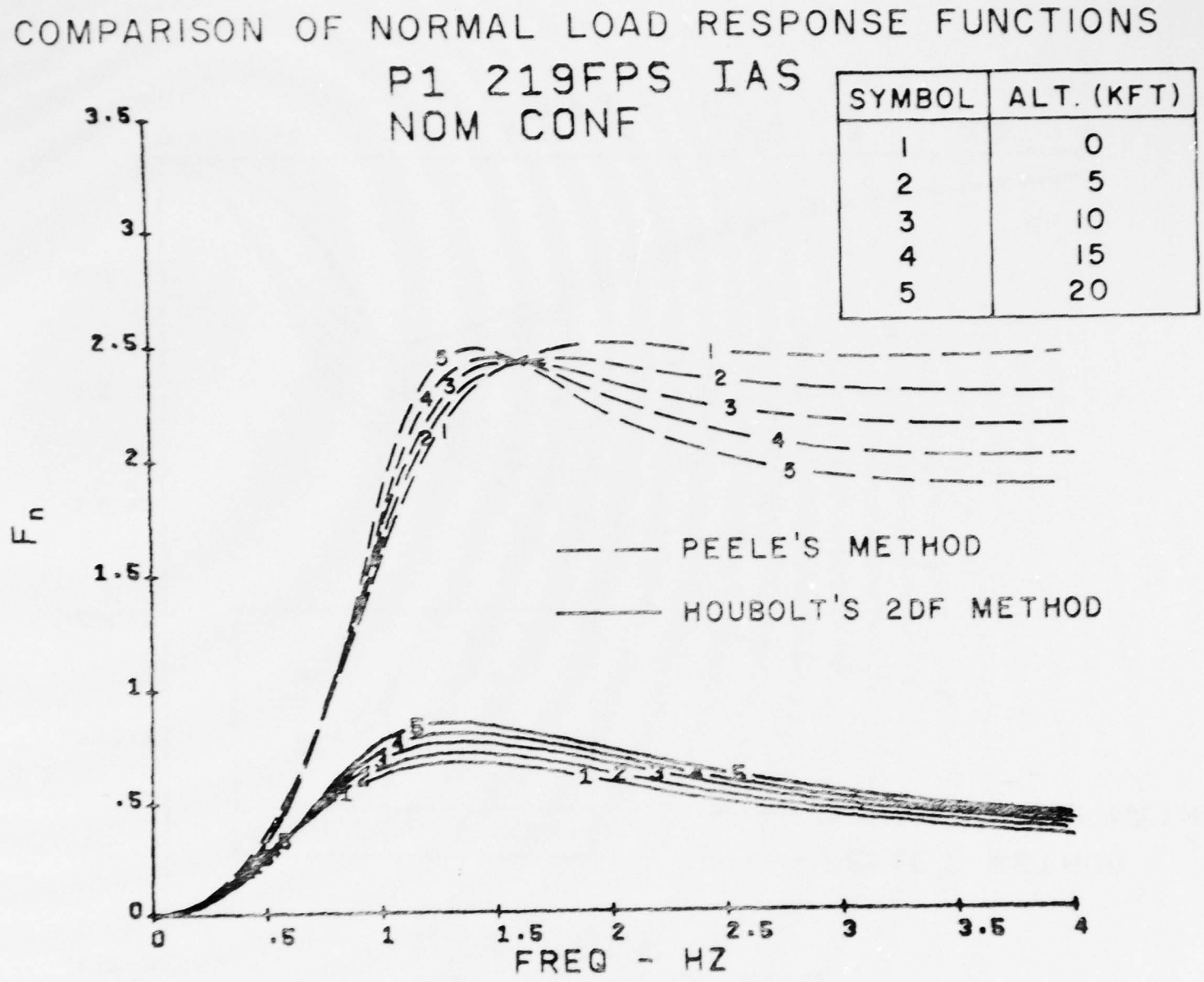
COMPARISON OF NORMAL LOAD RESPONSE FUNCTIONS
P1 219FPS IAS
NOM CONF
SYMBOL | ALT. (KFT)
1 | 0
2 | 5
3 | 10
4 | 15
5 | 20
PEELE'S METHOD
HOUBOLT'S 2DF METHOD
F_c
FREQ - HZ
0
.5
1
1.5
2
2.5
3
3.5
4

Figure 3.12a

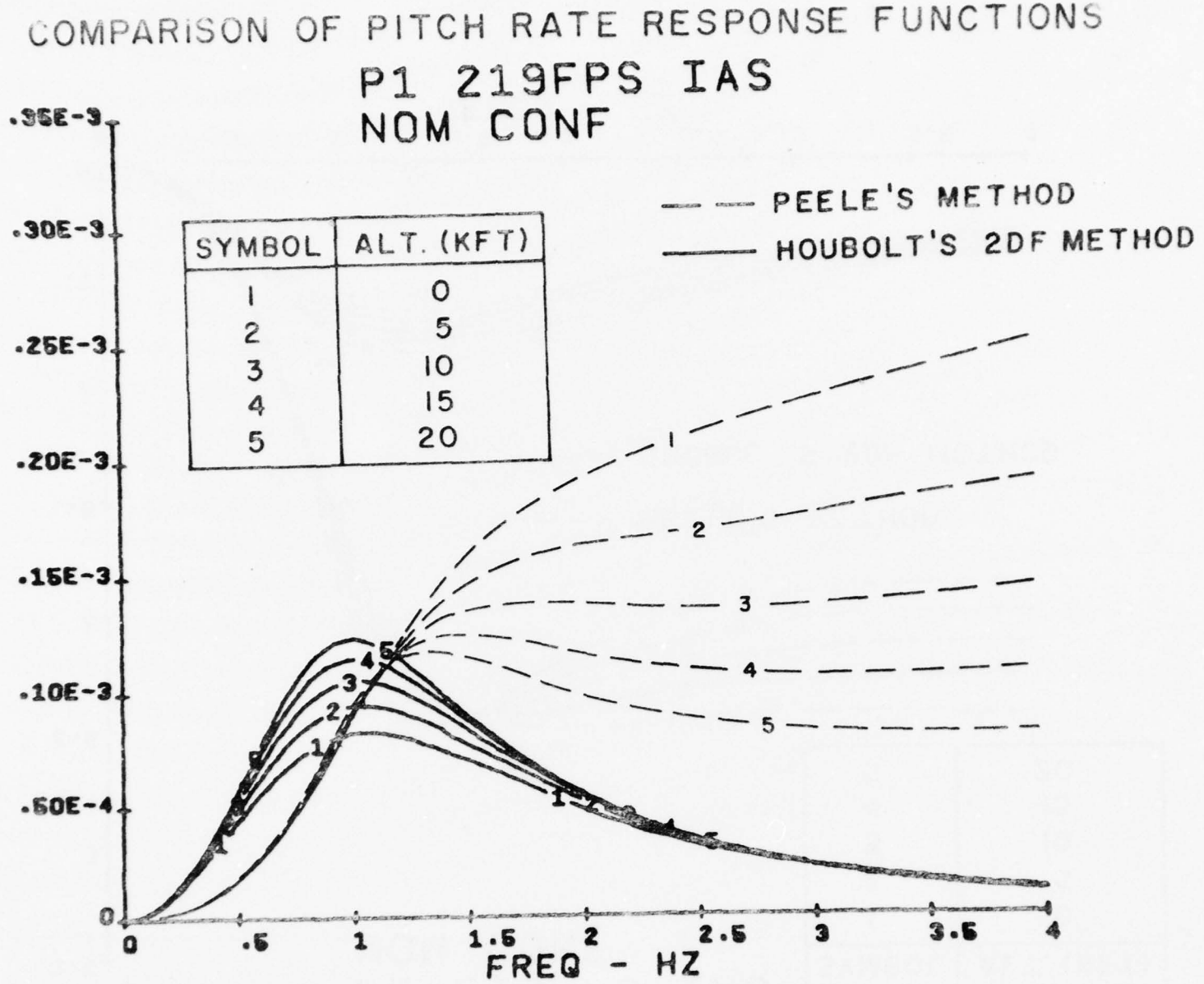
COMPARISON OF PITCH RATE RESPONSE FUNCTIONS
P1 219FPS IAS
NOM CONF
PEELE'S METHOD
HOUBOLT'S 2DF METHOD
SYMBOL | ALT. (KFT)
1 | 0
2 | 5
3 | 10
4 | 15
5 | 20
.35E-3
.30E-3
.25E-3
.20E-3
.15E-3
.10E-3
.50E-4
0
$F_{\dot{\theta}}$
0
.5
1
1.5
2
2.5
3
3.5
4
FREQ - HZ

Figure 3.12b

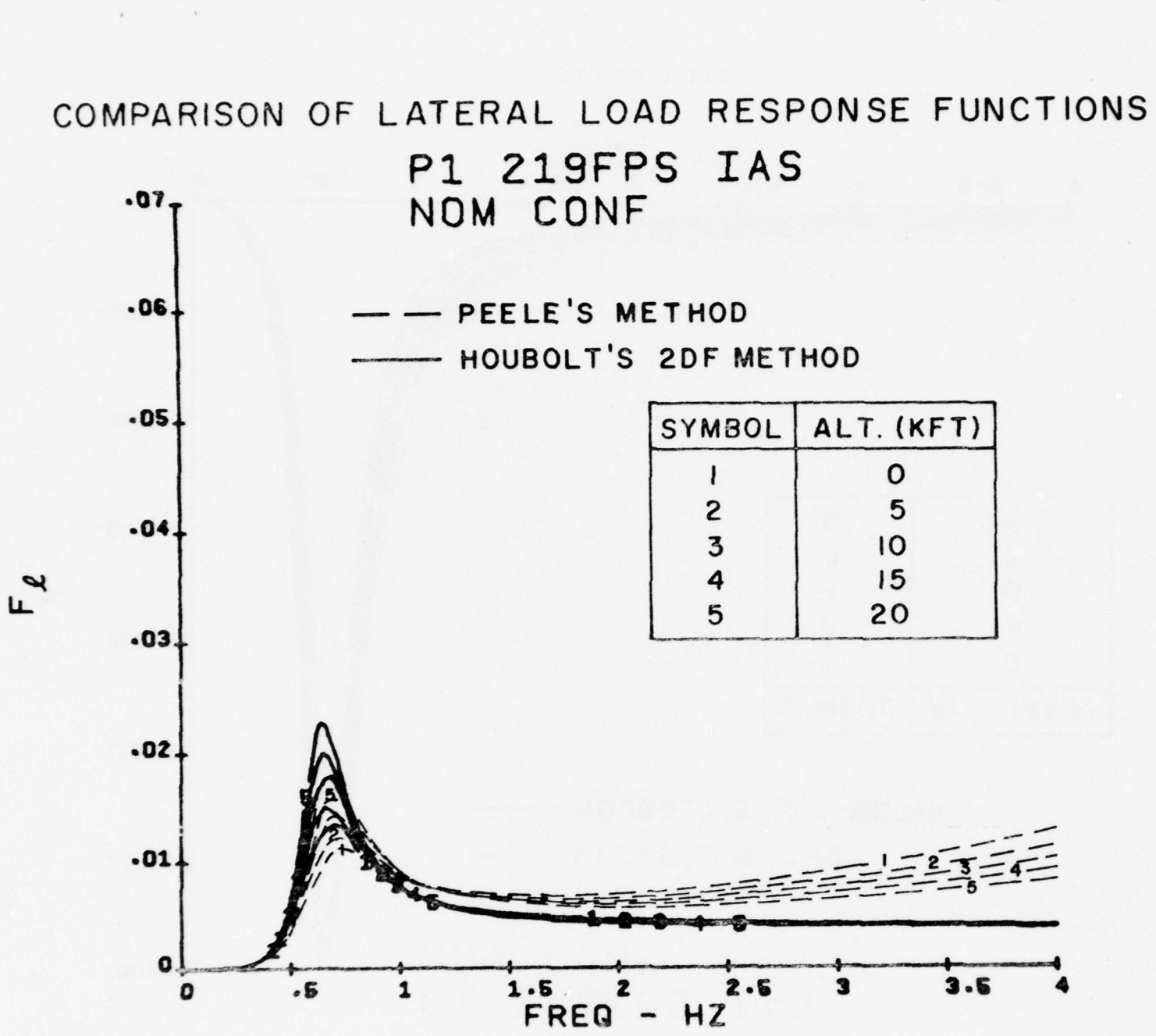
COMPARISON OF LATERAL LOAD RESPONSE FUNCTIONS
P1 219FPS IAS
NOM CONF
— — PEELE'S METHOD
—— HOUBOLT'S 2DF METHOD
SYMBOL | ALT. (KFT)
1 | 0
2 | 5
3 | 10
4 | 15
5 | 20
F_ℓ
.07
.06
.05
.04
.03
.02
.01
0
0
.5
1
1.5
2
2.5
3
3.5
4
FREQ - HZ

Figure 3.12c

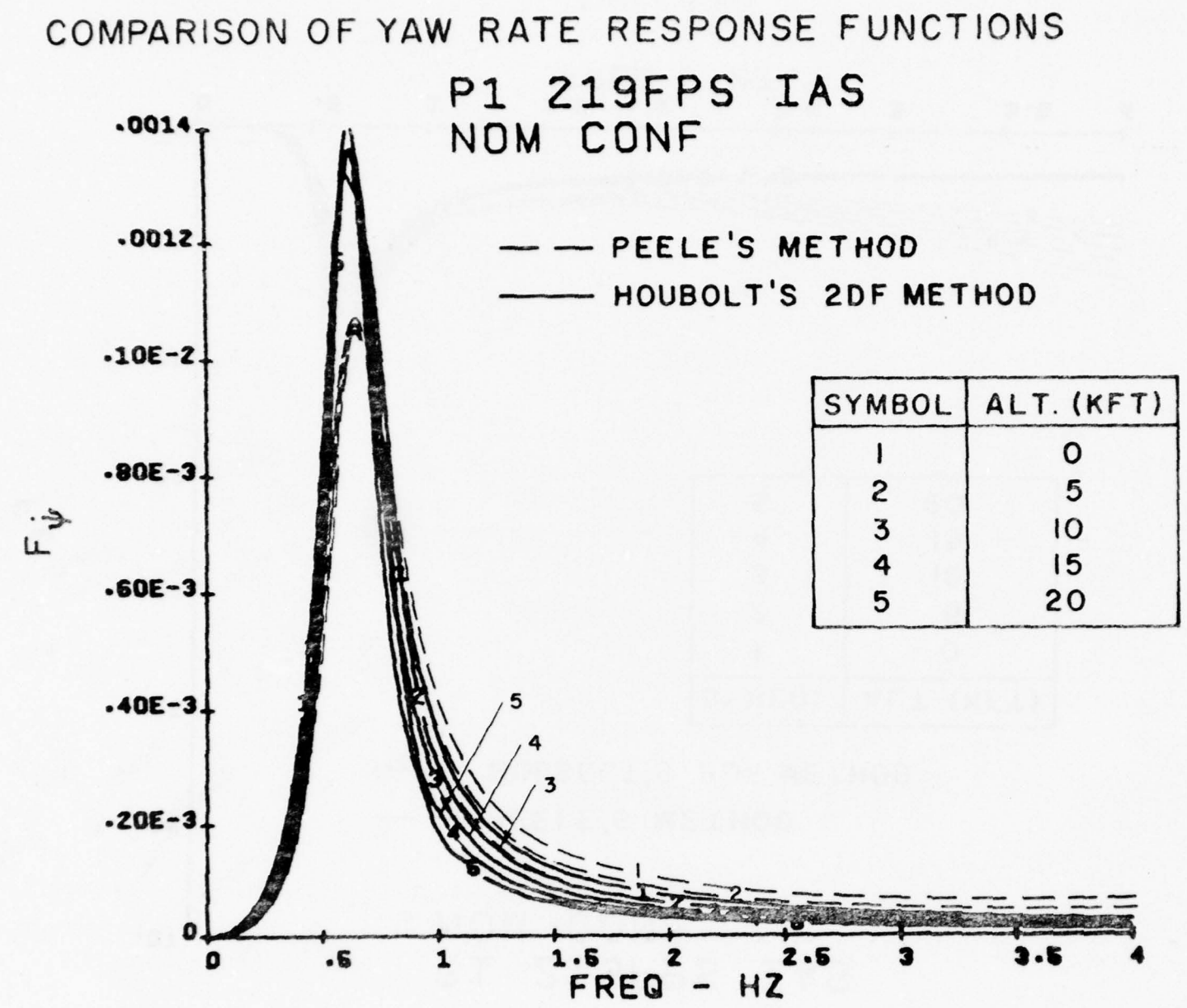
COMPARISON OF YAW RATE RESPONSE FUNCTIONS
P1 219FPS IAS
NOM CONF
— — PEELE'S METHOD
—— HOUBOLT'S 2DF METHOD
SYMBOL | ALT. (KFT)
1 | 0
2 | 5
3 | 10
4 | 15
5 | 20
.0014
.0012
.10E-2
.80E-3
.60E-3
.40E-3
.20E-3
0
Fψ̇
0
.5
1
1.5
2
2.5
3
3.5
4
FREQ - HZ

Figure 3.12d

COMPARISON OF LOAD EXCEEDANCE PARAMETERS USING HOUBOLT'S 1DF AND 2DF METHODS

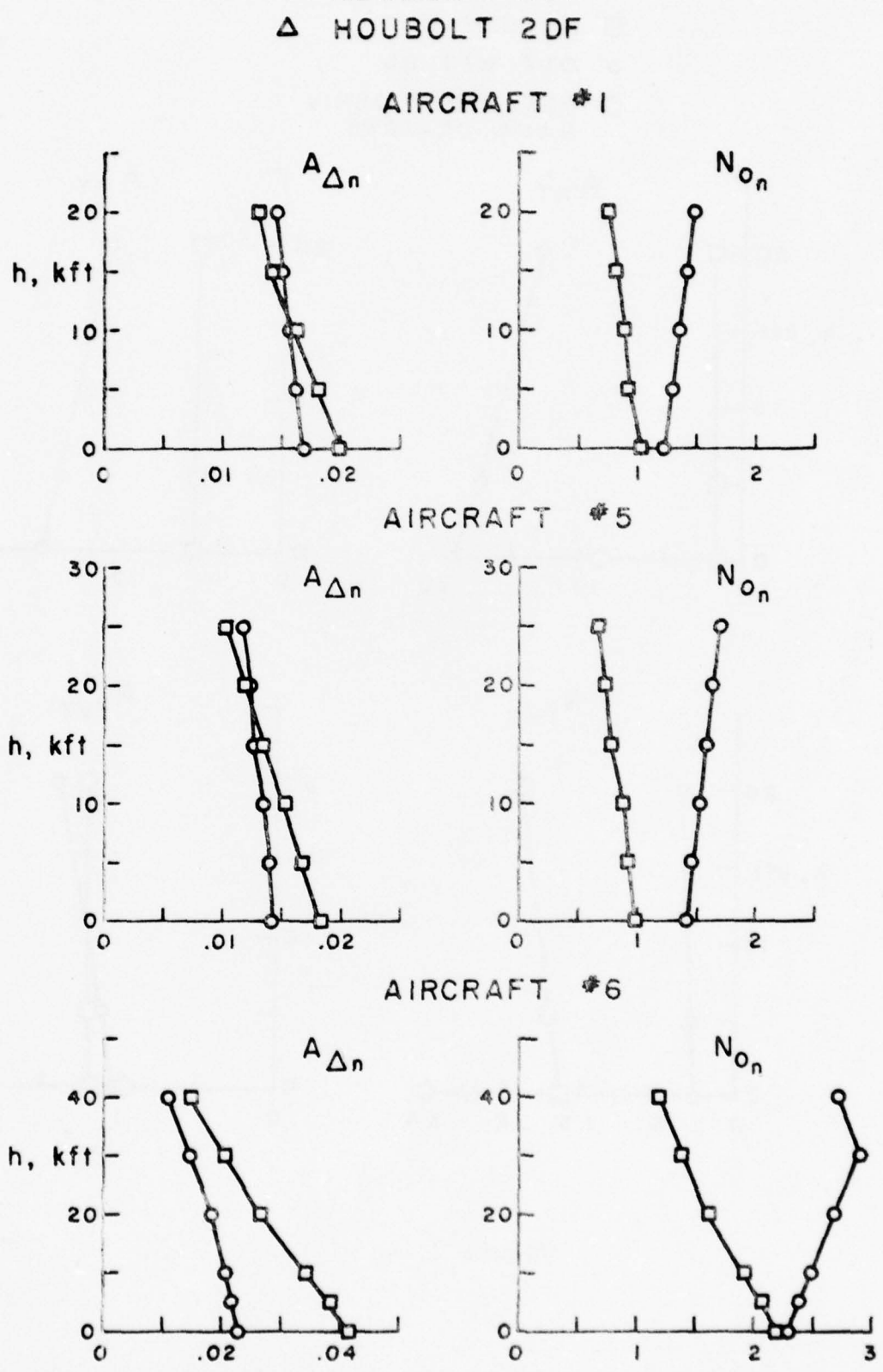

Figure 3.13

COMPARISON OF TAIL LOAD EXCEEDANCE PARAMETERS BY 2DF AND ODF METHODS

AIRCRAFT #1

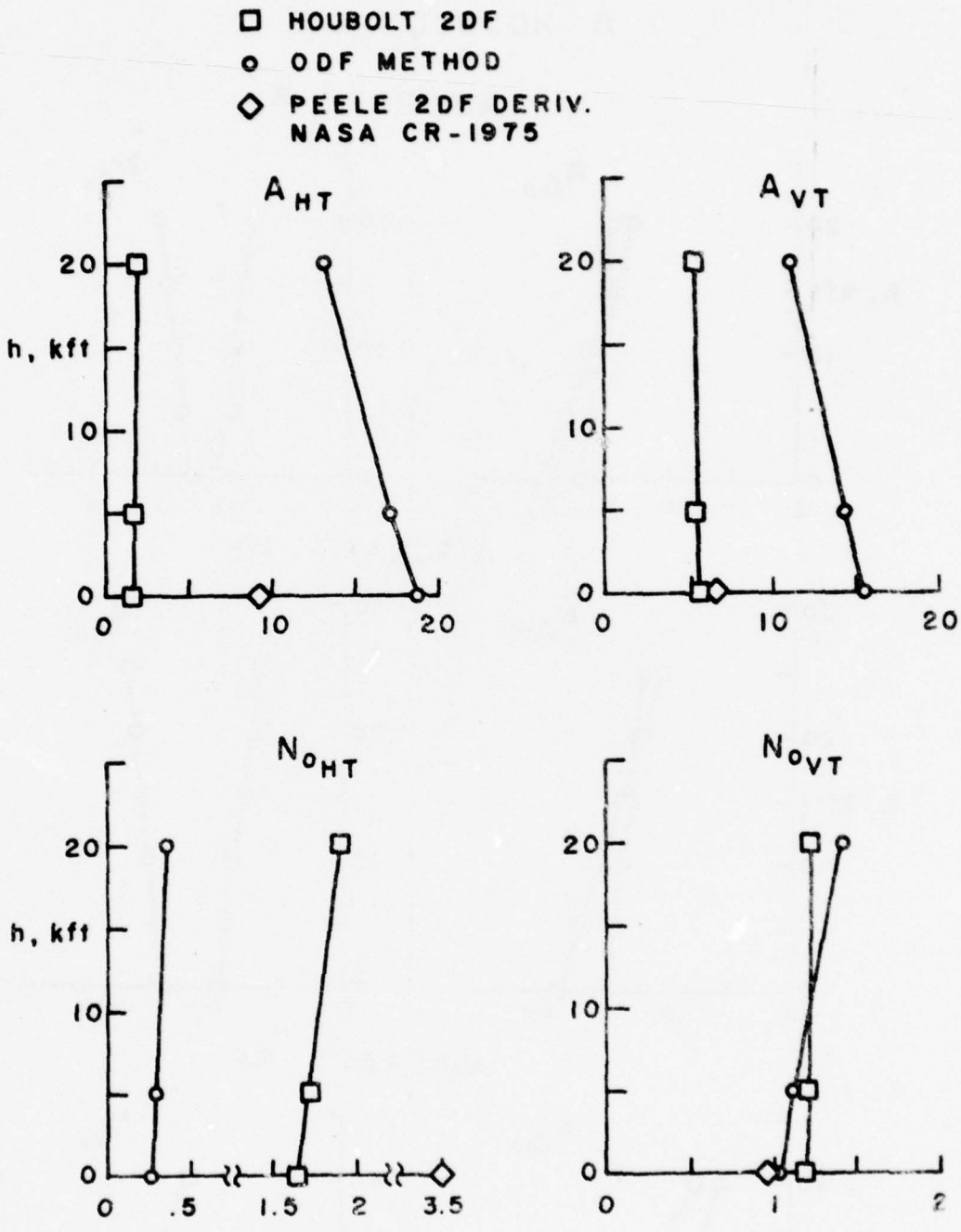

Figure 3.14a

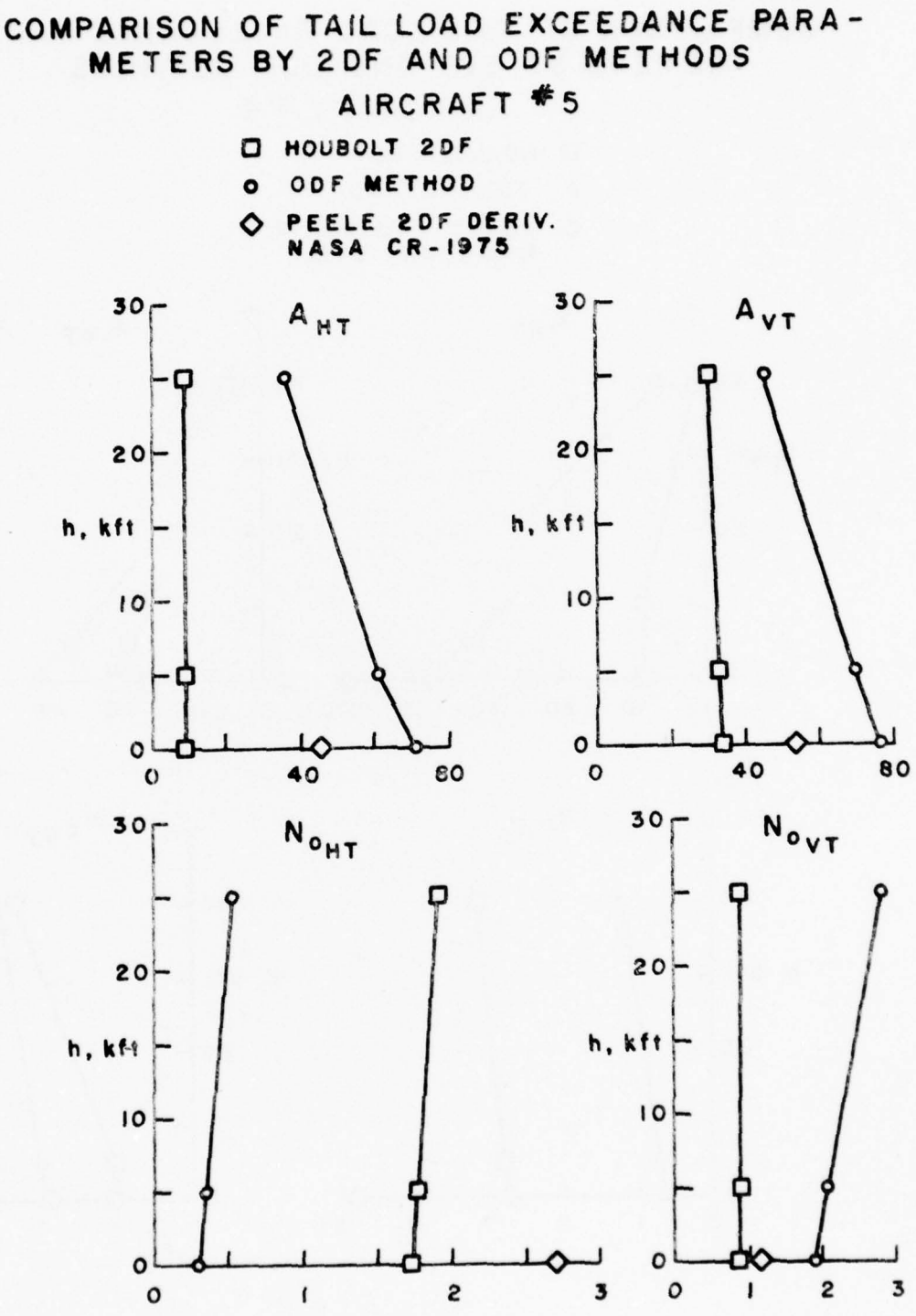
COMPARISON OF TAIL LOAD EXCEEDANCE PARAMETERS BY 2DF AND ODF METHODS
AIRCRAFT #5
HOUBOLT 2DF
ODF METHOD
PEELE 2DF DERIV. NASA CR-1975
A_{HT}
A_{VT}
$N_{o_{HT}}$
$N_{o_{VT}}$
h, kft
30
20
10
0
40
80
1
2
3

Figure 3.14b

COMPARISON OF TAIL LOAD EXCEEDANCE PARAMETERS BY 2DF AND ODF METHODS

AIRCRAFT #6

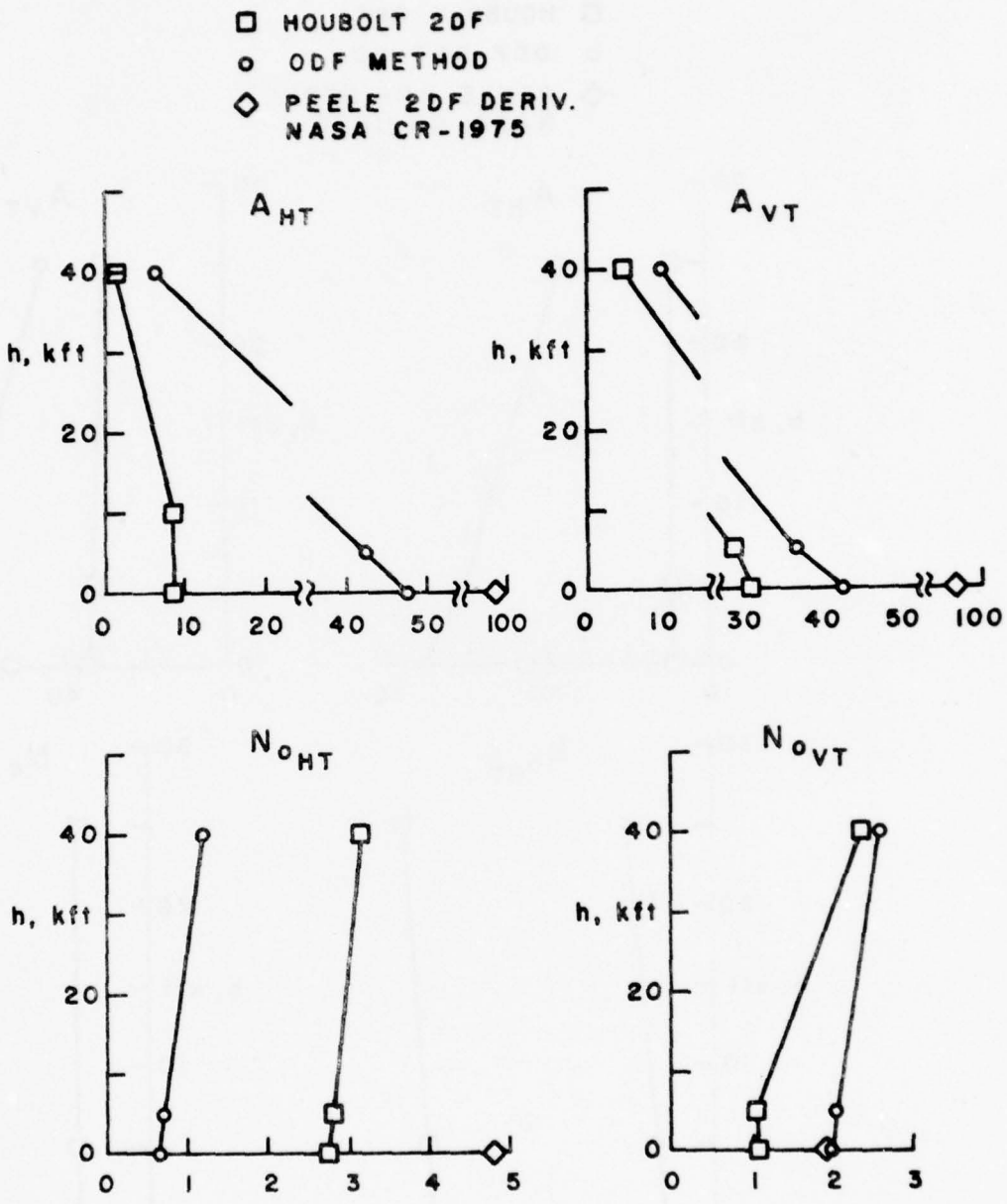

Figure 3.14c

3.1 Comparison of Houbolt's and Peele's 2DF Methods.

Peele's method makes use of the standard longitudinal short period model and lateral snaking model with stability derivatives modified by exponential lift attenuation factors. The results of this approach are obviously dependant on the values of the stability derivatives chosen to represent a particular aircraft. The FAA study, Ref. 4, computes the load exceedance parameters based on derivatives; 1) supplied by the manufacturers, and 2) estimated using methods described in NASA CR 1975 (Ref. 7).

These results, also included on Figs. 3.1 - 3.10, illustrate a major disadvantage of Peele's method, namely the significant variation in the results due to variations in the estimates of the necessary stability derivatives. The requirement to standardize derivative estimation proceedures becomes evident if such a technique is to be incorporated in FAR 23. This in itself would be quite an undertaking. (It should be noted that some of the differences in N_o estimates taken from Ref. 4 are due to an inconsistent choice of cut-off frequency.)

The results of Houbolt's and Peele's techniques differ both because they can start with different derivatives at zero frequency and because the functional dependence of the derivatives on frequency is different. To separate these two effects, additional calculations were run using Peele's method with the derivatives set equal to the equivalent zero frequency values used in Houbolt's 2DF model. These results are also shown in Figs. 3.1 - 3.10.

The basic result of this latter comparison is that in all cases values of $A_{\Delta n}$ and $N_{o_{\Delta n}}$ are larger when computed by Peele's method. This is due to Peele's method predicting a larger normal load response at all frequencies, particularly above 1 hz as illustrated in Fig. 3.12.

Comparisons of the lateral responses indicate that values of $A_{\Delta \ell}$ are smaller and $N_{o_{\Delta \ell}}$ are larger when computed by Peele's method. This also is explained by referring to typical transfer function plots (Fig. 3.12) which indicate that Peele's method underestimates the lateral response at low frequency and overestimates in the high frequency range.

Figure 3.10a

The basic conclusion arising from these comparisons is that, by neglecting the phase angle shift in lift attenuation, Peele's method overestimates the main load exceedance parameter $A_{\Delta n}$. For this reason and because of the sensitivity to stability derivative estimates it is not recommended that Peele's method be incorporated into FAR 23.

3.2 Comparison of Results Obtained Using Houbolt's 1DF and 2DF Models

Reference 1 describes a 1DF model with which the load exceedance parameters can be calculated manually using two charts. In this proceedure the aircraft is assumed to respond longitudinally in heave (only the lift equation is used so the aircraft is characterized completely by the density parameter $\mu = 2w/a\rho cgS$. This method has great appeal since it correctly models the unsteady lift on the wing and is quite simple to apply. The drawback of this approach is that by neglecting the pitch response, the load alleviating tendency of the aircraft to weathercock (hold angle of attack constant) is not included. How important this effect is for FAR 23 aircraft is illustrated in Fig. 3.13. Here the normal load exceedance parameters, calculated using Houbolt's 1DF (Ref. 1) and 2DF (Section 2) methods, are presented. For the sake of brevity the comparison is limited to three aircraft chosen to cover the range of FAR 23 aircraft. They are a light single engine aircraft, a twenty-passenger turboprop, and a small jet business transport.

This comparison of results indicates that the inclusion of the pitch response reduces the rms normal load factor estimate by as much as 50% at sea level, but can even underestimate at high altitude. This is because the damping of the short period mode decreases with altitude, thus increasing the resonant response of the second-order 2DF model. This is a significant difference but it should be noted that manual calculation of the load exceedance parameters by Houbolt's 2DF method using charts is not feasible due to the large number of necessary input parameters. It is, therefore, recommended that the 1DF method be used if manual calculations are to be employed.

3.3 Comparison of Load Exceedance Parameters Based on 2DF and ODF Models.

It is desirable to obtain a simple method for estimating gust load exceedance parameters for the vertical and horizontal tail-surfaces. The loads on the horizontal tail are a strong function of the unsteady wing downwash, therefore, they can not realistically be calculated independent of wing conditions. The vertical tail, however, is somewhat above the fuselage and less strongly influenced by the relatively weak fuselage sidewash. In addition to weak coupling with the flow, induced by other parts of the aircraft, the gust load on the vertical tail produces sideways accelerations which are small relative to the wing induced vertical accelerations. This would indicate that the attenuating effect of the sideways motion can possibly be neglected. If the aircraft also does not develop significant yaw accelerations it is worth considering a ODF model for vertical tail gust loads. For trial purposes this is equivalent to a 2DF model with infinite mass and moment of inertia. The resulting load exceedance parameters, A and N_o, for both the vertical and horizontal tail loads for three typical FAR 23 aircraft are shown in Fig. 3.14 and compared with the results from the standard 2DF model.

The ODF model consistantly overestimates the tail loads due to the overestimation of the low frequency tail load response as shown in Fig. B.6 of appendix B. This suggests that a 1DF response model allowing yaw motion would probably do a better job. In lieu of developing such a model, the ODF model is recommended for the manual estimation of gust loads on vertical tails.

Estimates of A and N_o from Ref. 4 given by Peele's method at sea level are also shown. Structural loading is high compared with Houbolt's 2DF method and not consistently related to Houbolt's 1DF method.

3.4 Effects of the Scale of Atmospheric Turbulence on Gust Load Exceedance Parameters

The actual scale of atmospheric turbulence goes from less than 100 feet (close to the ground) up to five thousand feet. The practical range of interest for aircraft design purposes is roughly

750 ft $\leq$ L $\leq$ 2500 ft. The particular value chosen does have a significant effect on the loading parameter A . Fortunately, in the range of frequencies contributing most to the output power spectra, the von Karman input power spectrum is approximately

$$\phi_\omega(\omega) \sim .522\ \sigma_\omega^2 \left(\frac{L}{U}\right)^{-2/3} \omega^{-5/3} \tag{3.7}$$

The root mean square value for a response variable, such as Δn , is

$$\sigma_{\Delta n} = \left[\int_0^\infty |H_{\Delta n}(\omega)|^2\ \phi_\omega(\omega)\, d\omega\right]^{1/2} \tag{3.8}$$

or approximately

$$\sim .722 \left(\frac{L}{U}\right)^{-1/3} \left[\int |H_{\Delta n}(\omega)|^2\ \omega^{-5/3} d\omega\right]^{1/2} \sigma_\omega \tag{3.9}$$

$\sigma_{\Delta n}$ and, therefore, the structual loading parameter $A_{\Delta n}$ vary inversely with the cube root of the turbulence scale, L .

$$A_{\Delta n}(L_2) = A_{\Delta n}(L_1) \sqrt[3]{\frac{L_1}{L_2}} \tag{3.10}$$

This relationship is accurate to within 5% for all of the FAR 23 aircraft and flight conditions studied. This is illustrated in Fig. 3.15 for aircraft number six which with its high cruise velocity should have the largest errors.

The exact and approximate values of A are shown using Houbolt's 2DF and 1DF models. The error is greater with the 1DF model since this model responds more to low frequency turbulence than the 2DF model does.

The number of zero crossings, $N_{o_{\Delta n}}$, is proportional to the ratio of $\sigma_{\dot{\Delta n}}$ and $\sigma_{\Delta n}$. Since both of these quantities are approximately proportional to $(L)^{-1/3}$ their ratio is independent of scale. Based on the calculations made in this study, for aircraft numbers 1, 5, 6, and 10, this approximation is 95% accurate for the scale range 750 ft $\leq$ L $\leq$ 2500 ft.

VARIATION OF STRUCTURAL LOADING PARAMETER, $A_{\Delta n}$, WITH SCALE OF TURBULENCE, L

AIRCRAFT # 6

H = 40 KFT

IAS = 878 FPS

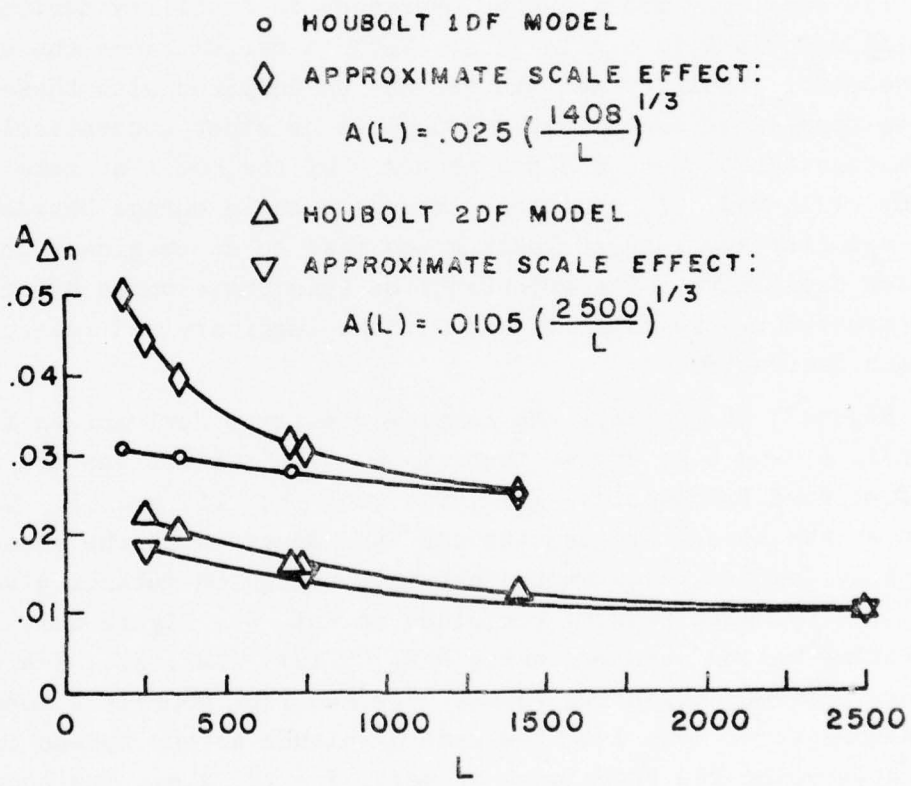

Figure 3.15

The two conclusions to be drawn from this investigation into scale effects for FAR 23 aircraft are:

1) Since A varies significantly with turbulence scale, a particular value of L should be specified for design purposes or comparative analyses.

2) The particular design value chosen for L is not crucial since the variations of A and N_o with scale are well behaved and known.

3.5 Stability Derivative Evaluation

The line load model can be expressed in stability derivative form as described in Section 2.3. This is useful since the equivalent model stability derivatives can be compared with those obtained from experimental data, Houbolt's or other theoretical estimation techniques, and the accuracy of the model at zero frequency evaluated. In addition, the phase angle change between downwash velocity and induced loads gives rise to an imaginary component in each derivative. The importance of this phase angle effect can be estimated by the relative size of the imaginary and real components of each derivative.

Figure 3.16 presents the complex stability derivatives for aircraft 1, 5, and 6 at cruise conditions. The derivatives are evaluated at five frequencies; k_w; .001, .05, .1, .25, and .5. Values shown at the lowest frequencies can be compared with the steady state stability derivative estimates obtained using the methods given in Refs. 7 - 12, with results contained in Ref. 4. Figure 3.16 shows derivative values obtained using NASA CR 1975 (Ref. 7). The difference between derivative values obtained from Houbolt's model and the technique of Ref. 7 is the same magnitude as the spread in estimates using the techniques of Refs. 7 - 12, i.e., its accuracy is comparable to that of other methods. Also, as would be expected, differences in the rotary derivative estimates (C_{L_q} , C_{M_q} , C_{y_r} , C_{N_r}) are generally larger than the differences in the static derivative estimates.

STABILITY DERIVATE VARIATION WITH FREQUENCY

h= 5 kft AIRCRAFT #1

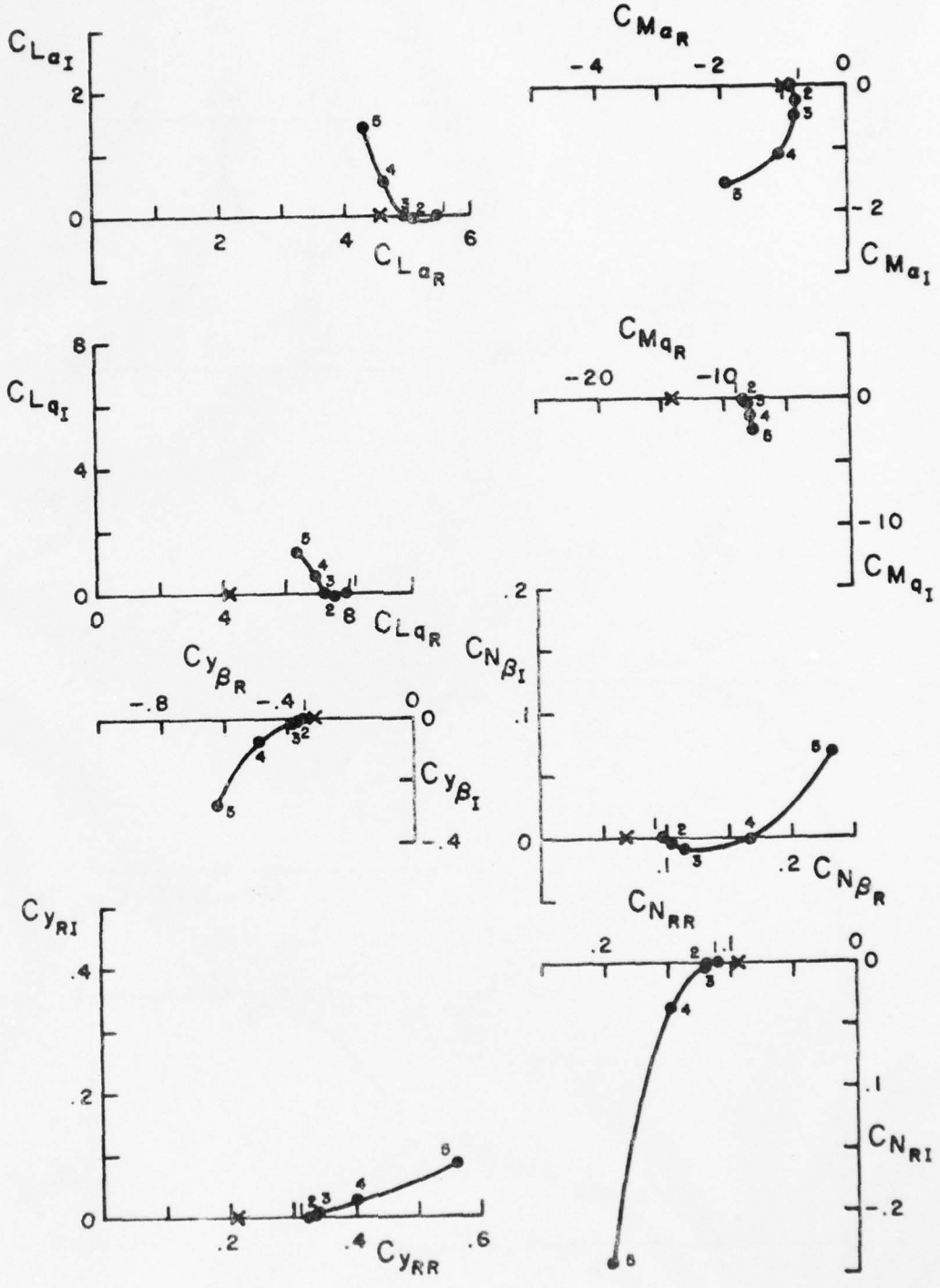

Figure 3.16a

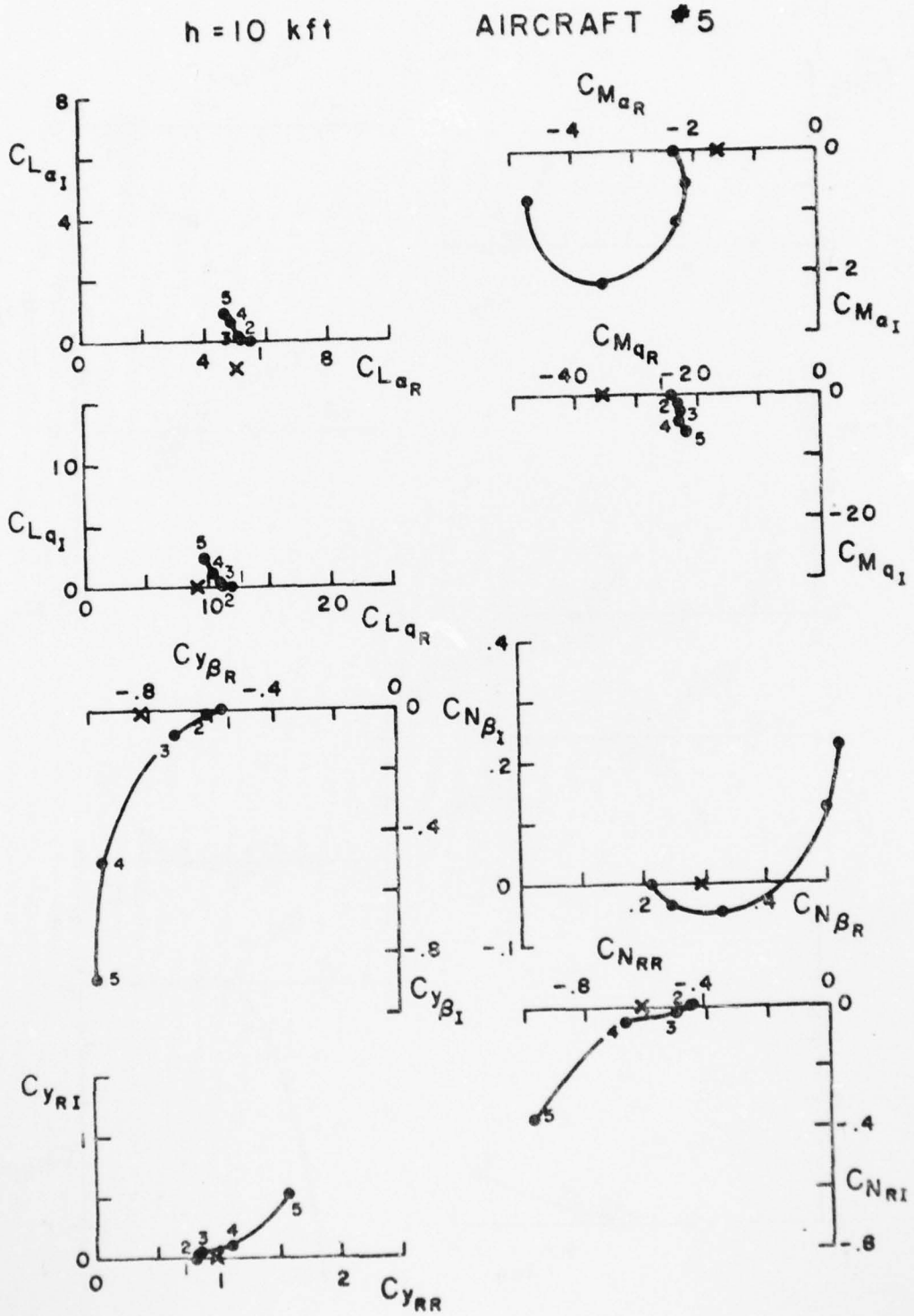
h = 10 kft
AIRCRAFT #5
$C_{L_{a_I}}$
$C_{L_{a_R}}$
$C_{M_{a_R}}$
$C_{M_{a_I}}$
$C_{L_{q_I}}$
$C_{L_{q_R}}$
$C_{M_{q_R}}$
$C_{M_{q_I}}$
$C_{y_{\beta_R}}$
$C_{y_{\beta_I}}$
$C_{N_{\beta_I}}$
$C_{N_{\beta_R}}$
$C_{y_{RI}}$
$C_{y_{RR}}$
$C_{N_{RR}}$
$C_{N_{RI}}$

Figure 3.16b

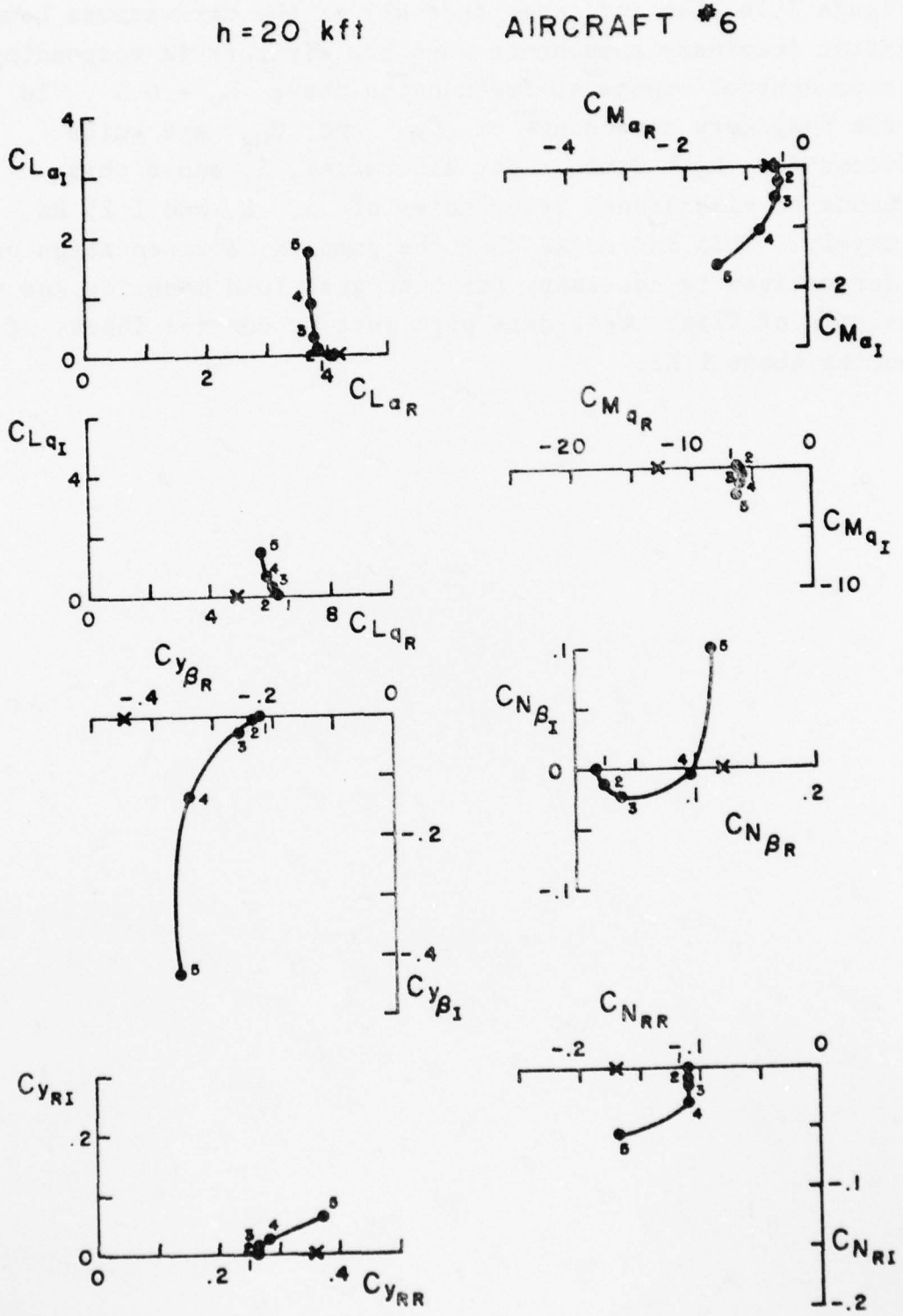
h = 20 kft
AIRCRAFT #6
$C_{L_{a_I}}$
$C_{L_{a_R}}$
$C_{M_{a_R}}$
$C_{M_{a_I}}$
$C_{L_{q_I}}$
$C_{L_{q_R}}$
$C_{M_{q_R}}$
$C_{M_{q_I}}$
$C_{y_{\beta_R}}$
$C_{y_{\beta_I}}$
$C_{N_{\beta_I}}$
$C_{N_{\beta_R}}$
$C_{y_{RI}}$
$C_{y_{RR}}$
$C_{N_{RR}}$
$C_{N_{RI}}$

Figure 3.16c

Figure 3.16 also indicates that all of the derivatives have significant imaginary components when the aircraft is responding to gust or control inputs at frequencies above $k_w = 0.5$. In fact, the imaginary components of C_{M_α} and C_{n_β} are quite significant for $k_w > 0.05$. For aircraft 1, 5, and 6 this corresponds to dimensional frequencies of .5, .8, and 1.25 Hz, respectively. This indicates that the complex representation of these derivatives is necessary for both gust load modeling and the analysis of flight test data with gust or control inputs of frequencies above 1 Hz.

4. SUMMARY AND CONCLUSIONS

At present the gust load estimates specified in FAR 23 are based on encountering a discrete gust. However, commercial and military aircraft use more sophisticated power spectral design techniques which more properly account for the continuous and random nature of turbulence. Should FAR 23 be updated to include power spectral design requirements and, if so, which particular techniques are most appropriate? Answers to these questions must be based on a knowledge of:

1. The accuracy of the various methods in predicting gust load power spectra.
2. The complexity of the different methods.
3. Ultimately, how well does each method discriminate, from the gust load design viewpoint, safe aircraft designs from unsafe ones.

The purpose of this study is to evaluate the relative accuracy and complexity of three power spectral techniques and to make recommendations based on these evaluations. It is believed that these recommendations are limited by the fact that no comparison with experimental data can be made at this time.

In this study, response functions and gust load exceedance parameters have been calculated for ten FAR 23 type aircraft at different flight conditions and configurations using Houbolt's 2DF technique. These results have been compared with similar data obtained by using Peele's 2DF method and Houbolt's 1DF method. The following conclusions are given based on these comparisons.

Peele's 2DF method, while somewhat simpler than Houbolt's 2DF method, requires computerized solutions if the cutoff frequency is related to the aspect ratio of the wing. In addition, this method neglects the significant phase angle shift with

frequency between aerodynamic load and gust velocity. Since the method is not necessarily more accurate than Houbolt's 1DF procedure and it is certainly more complicated, it is not recommended for use in gust load design procedures.

Houbolt's 1DF method overestimates both the rms gust loading and the number of zero crossings. It is, however, simple to apply and is the best candidate for updating from discrete gust load to power spectral techniques.

Houbolt's 2DF method is based on geometric and inertial aircraft characteristics. These are mush easier inputs to specify than the stability derivatives or frequency and damping characteristics required in Peele's method. On the other hand, this method does not easily allow incorporation of flight test data results into the model. Because of the large number of inputs required, manual solution with the aid of charts is not feasible. Depending on the approximations made in determining the influence functions, the computer code can fit in a programmable calculation (400 bytes) or require 21,000 bytes of storage. Further refinements in the 2DF models followed by detailed program documentation are necessary before this method can become a useful design tool.

Houbolt's 2DF model appears to include most of the gust velocity-loading phenomena thought to be significant, although it still remains to be validated with experimental data.

APPENDIX A

REMOVING THE FUSELAGE WAKE WITH A FIFTH LOAD

The strength of the wake potential due to a uniform line load of intensity p downsteram a distance x is

$$\phi_o = - \frac{p}{\rho U} e^{-\frac{i\omega x}{U}}$$

For n line loads a distance c_f apart from each other (see Fig. 2.7), the total strength of the wake potential is

$$\phi_o = - \frac{1}{\rho U} \sum_{j=1}^{n} p_j e^{-\frac{i\omega}{U}[x + c_f(n-j)]}$$

where x is the distance between any desired location downstream of the aircraft and the rearmost line load p_n. For a body of revolution, slender body theory requires that the strength of the wake be zero downstream of the body.

A fictitious 5th load is added to the existing four-panel representation of the fuselage to satisfy this condition. At the point of this added load

$$\phi_o = - \frac{1}{\rho U} \sum_{j=1}^{5} p_j' e^{-\frac{i\omega c_f}{U}(5-j)} = 0$$

The 5th line load intensity must, therefore, be

$$p_5' = - \sum_{j=1}^{4} p_j' e^{-\frac{i\omega c_f}{U}(5-j)}$$

Since all of the line load intensities extend over the same width λ, the total loads p_j are related in the same fashion as the intensities p_j'.

The additional load, p_5, is included in the side force and yawing moment equations implicitly in terms of the original four loads and a moment arm, $e_f - 3c_f$.

$$m\ddot{y} = \sum_{j=1}^{4} p_j \left[1 - e^{-\frac{i\omega c_f}{U}(5-j)}\right] + p_{vt}$$

$$I_{yy}\ddot{\psi} = \sum_{j=1}^{4} p_j \left\{\left[e_f + (2-j)c_f\right] - (e_f - 3c_f)e^{-\frac{i\omega c_f}{U}(5-j)}\right\} + p_{vt}e_{vt}$$

APPENDIX B

This appendix contains all of the frequency response functions calculated using Houbolt's 2DF method. The functions are useful for understanding the trends seen in the load exceedance parameters and for determining each aircraft's approximate lateral and longitudinal damping and natural frequency. The response functions relating the input and output power spectra are proportional to the square of the amplitude of the transfer functions Eq. (3.1) and Eq. (3.6).

NORMAL ACCELERATION RESPONSE FUNCTION

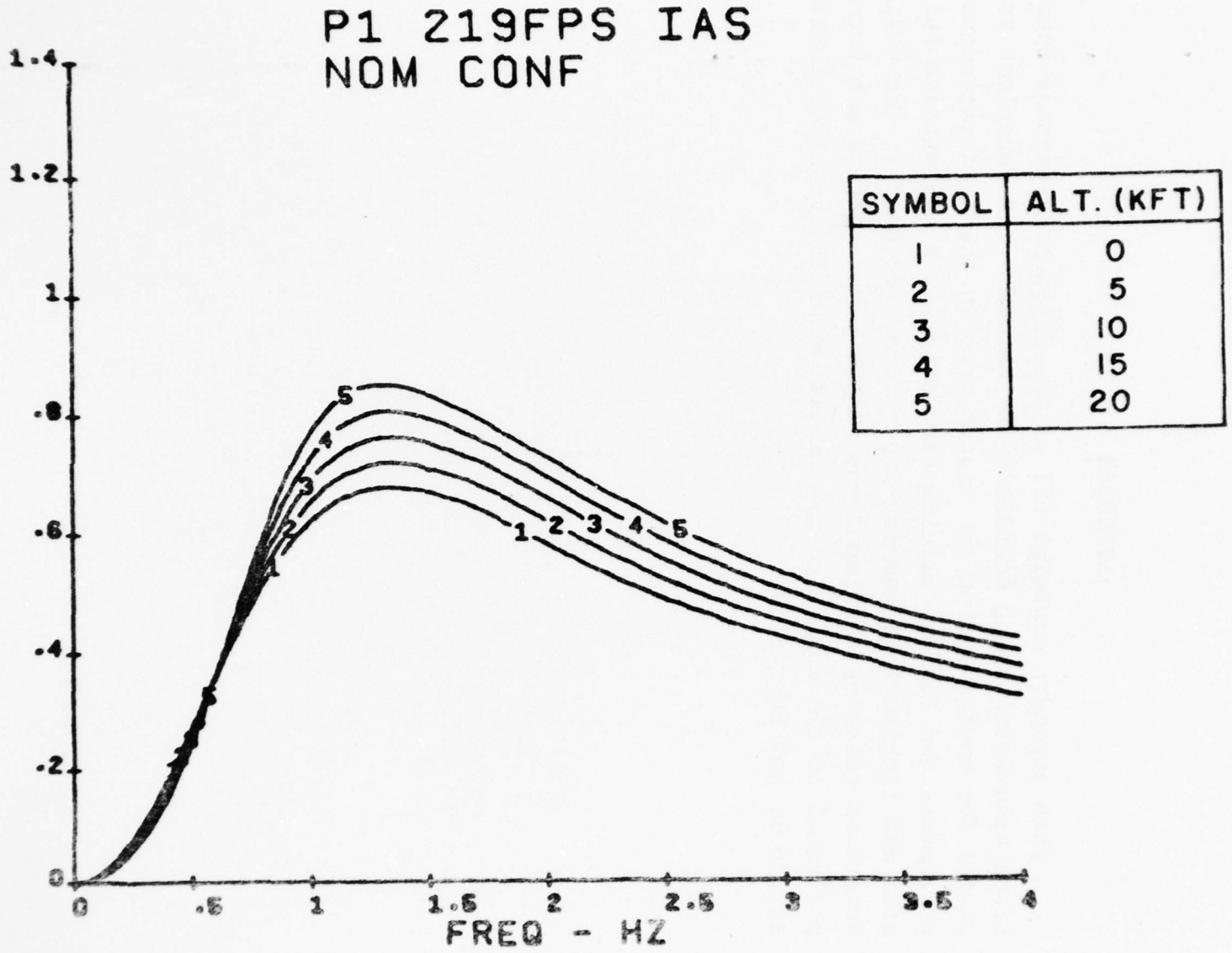

Figure B.1

PITCH RATE RESPONSE FUNCTION

P1 219FPS IAS
NOM CONF

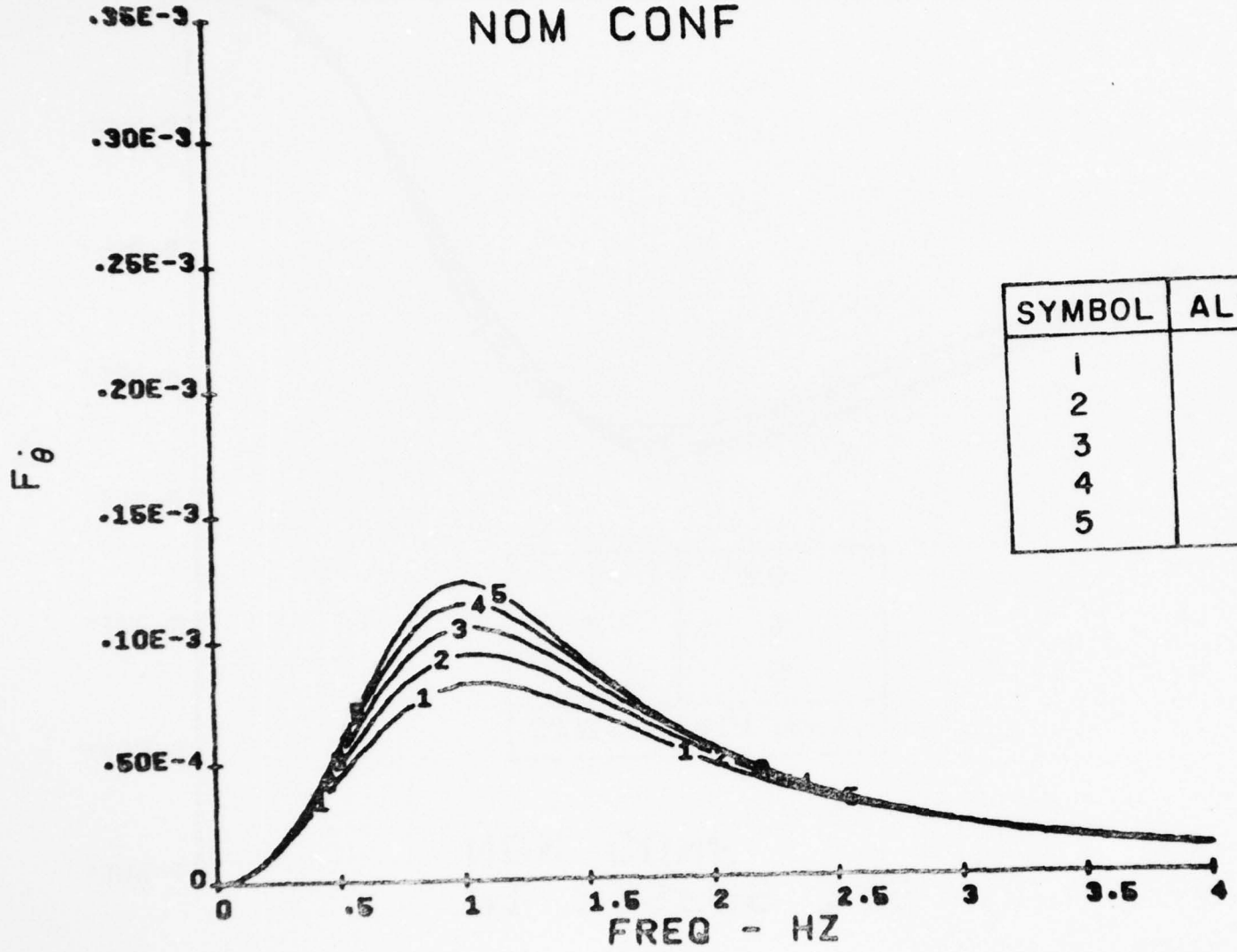

SYMBOL	ALT. (KFT)
1	0
2	5
3	10
4	15
5	20

Figure B.2

HORIZONTAL TAIL LOAD RESPONSE FUNCTION

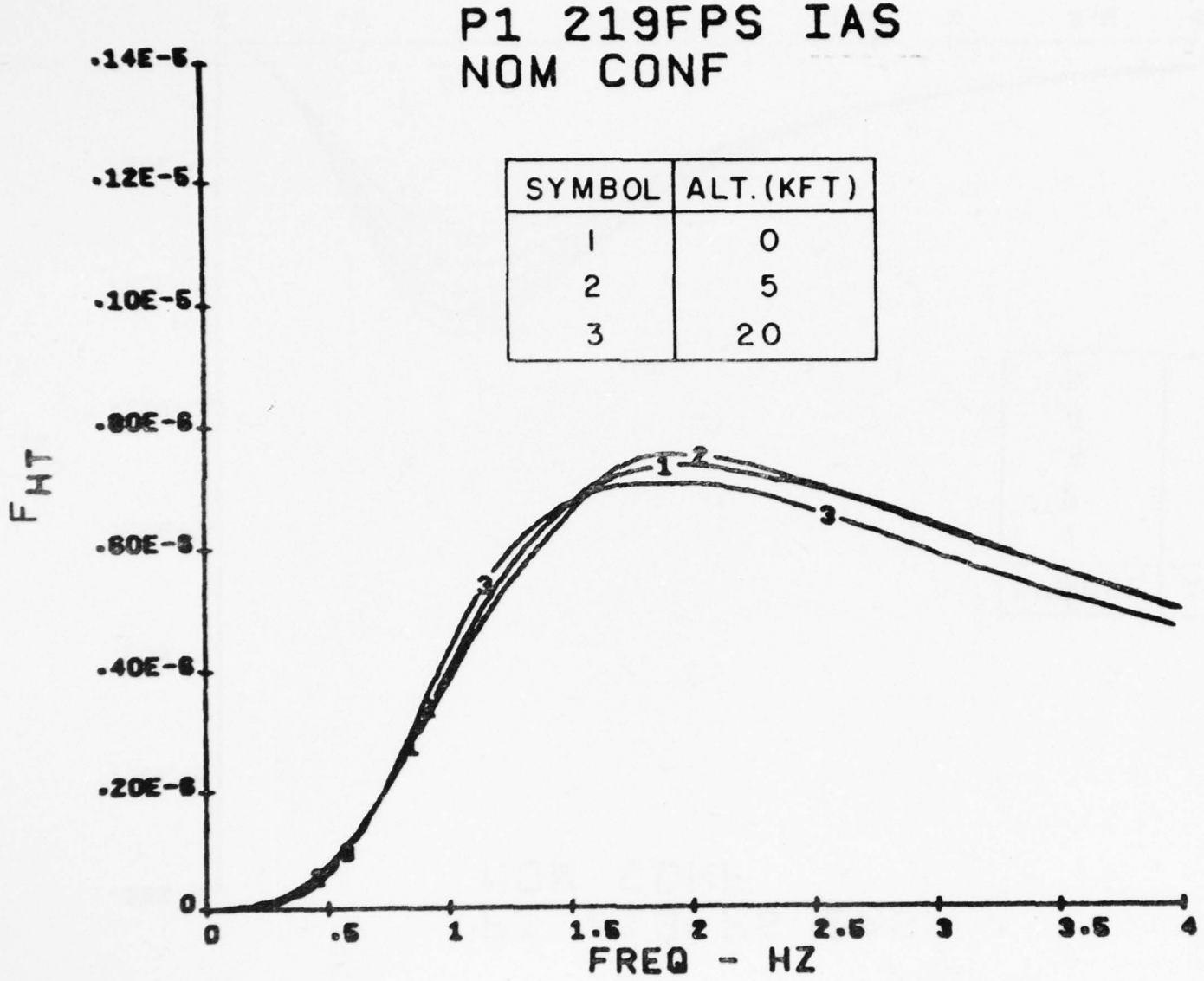

Figure B.3

LATERAL ACCELERATION RESPONSE FUNCTION

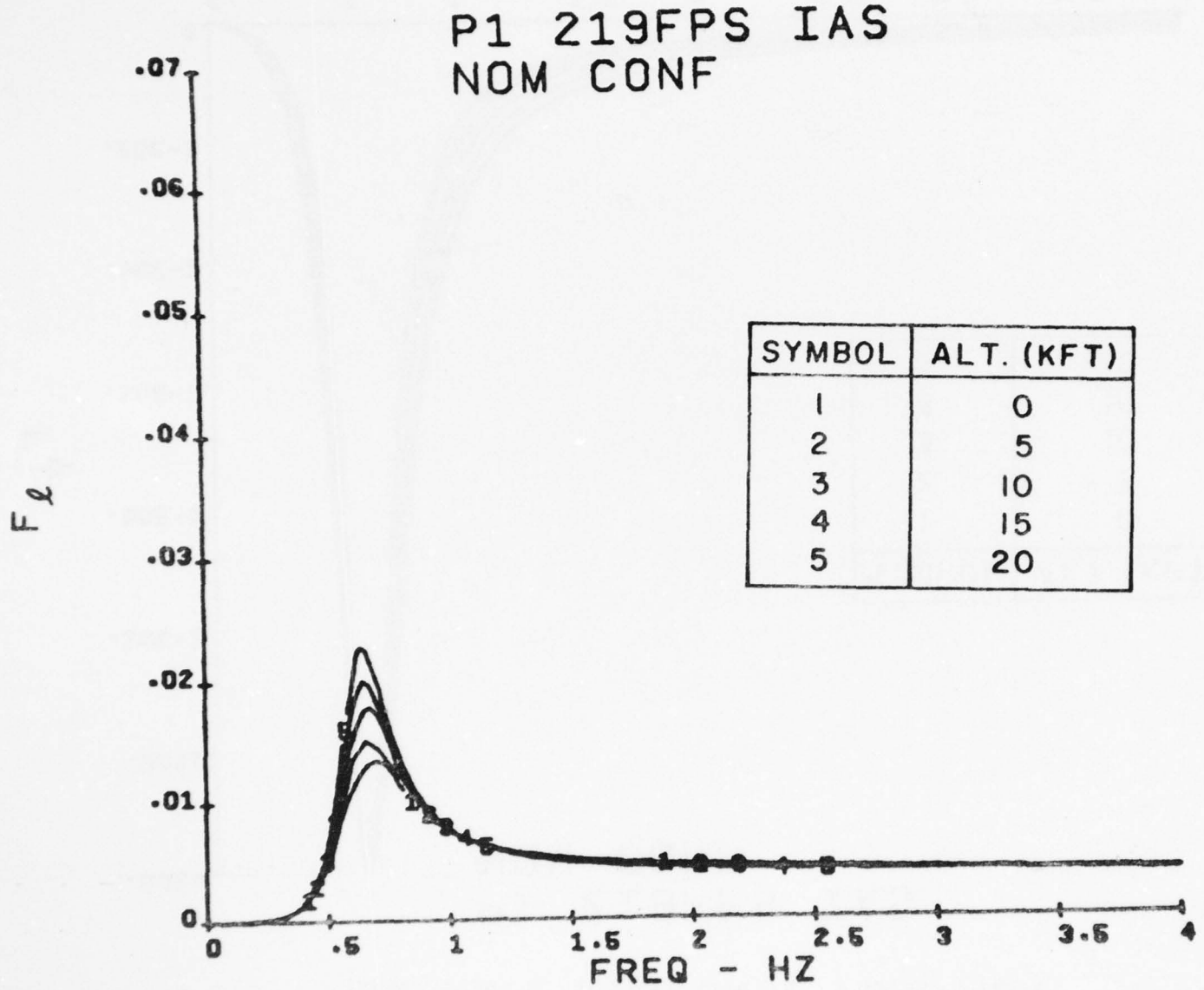

Figure B.4

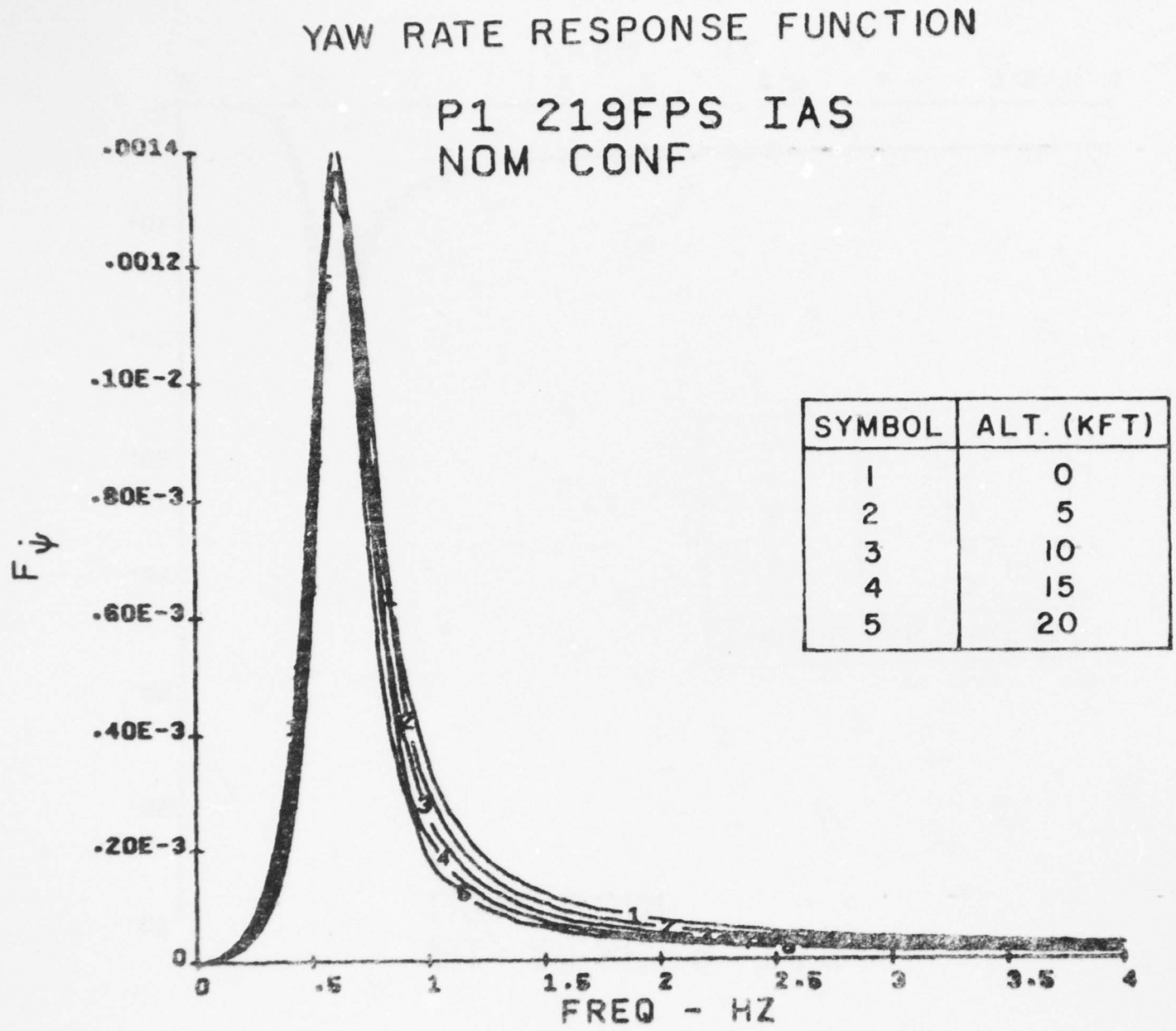
YAW RATE RESPONSE FUNCTION
P1 219FPS IAS
NOM CONF
.0014
.0012
.10E-2
.80E-3
.60E-3
.40E-3
.20E-3
0
Fψ̇
0
.5
1
1.5
2
2.5
3
3.5
4
FREQ - HZ
SYMBOL | ALT. (KFT)
1 | 0
2 | 5
3 | 10
4 | 15
5 | 20

Figure B.5

AD-A064 157 AERONAUTICAL RESEARCH ASSOCIATES OF PRINCETON INC N J F/G 1/2
GUST RESPONSE ANALYSES FOR TEN GENERAL AVIATION AIRCRAFT USING --ETC(U)
OCT 78 G G WILLIAMSON DOT-FA77WA-3972
UNCLASSIFIED ARAP-344 FAA-RD-78-117 NL

2 OF 2
AD
A064157

END
DATE
FILMED
3-79
DDC

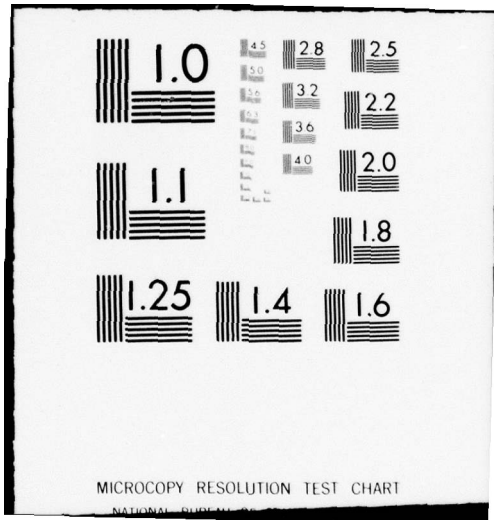
1.0
1.1
1.25
1.4
1.6
2.8
2.5
3.2
2.2
3.6
2.0
4.0
1.8
MICROCOPY RESOLUTION TEST CHART

VERTICAL TAIL LOAD RESPONSE FUNCTION

P1 219FPS IAS
NOM CONF

SYMBOL	ALT.(KFT)
1	0
2	5
3	20

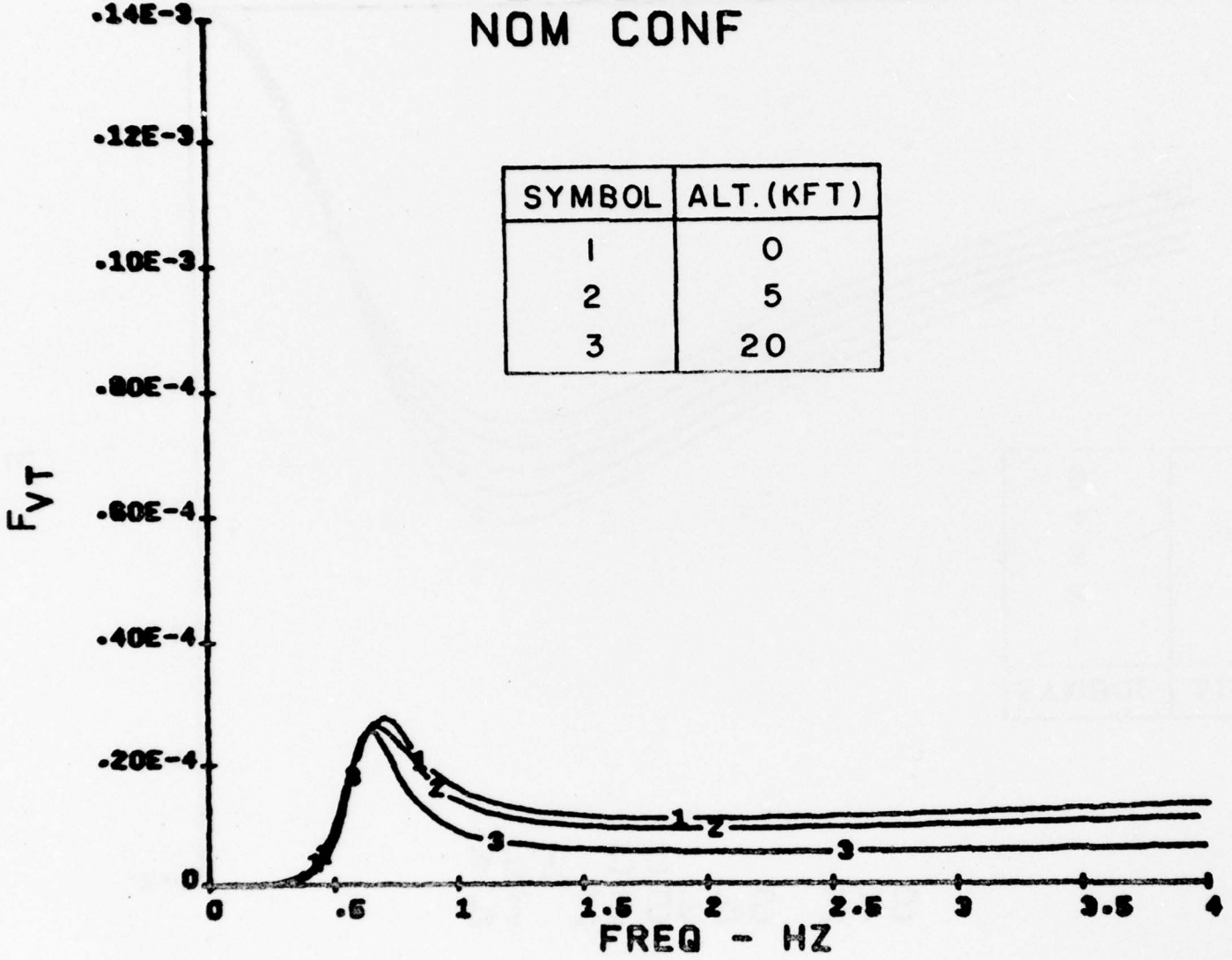

Figure B.6

NORMAL ACCELERATION RESPONSE FUNCTION

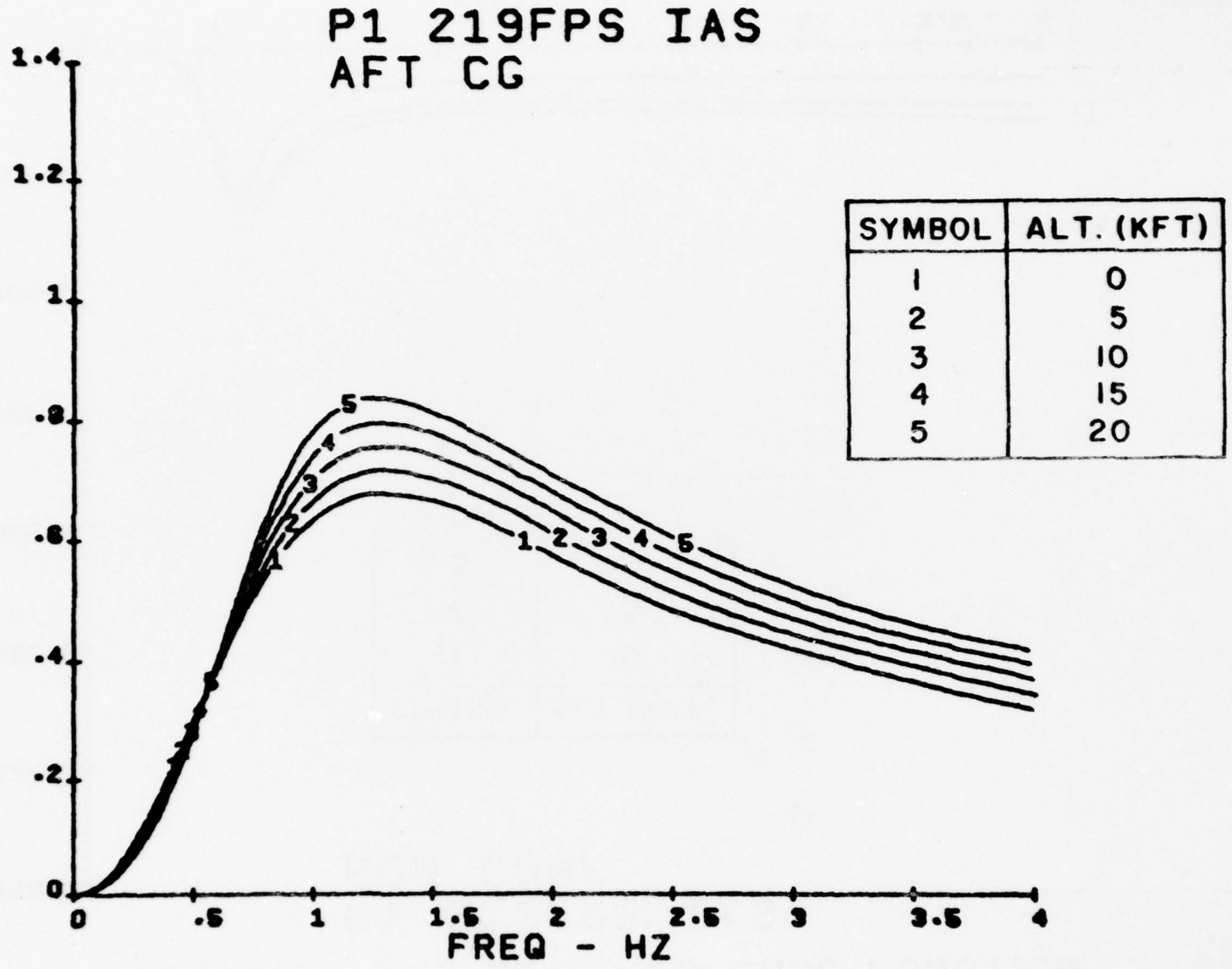

Figure B.7

PITCH RATE RESPONSE FUNCTION

P1 219FPS IAS
AFT CG

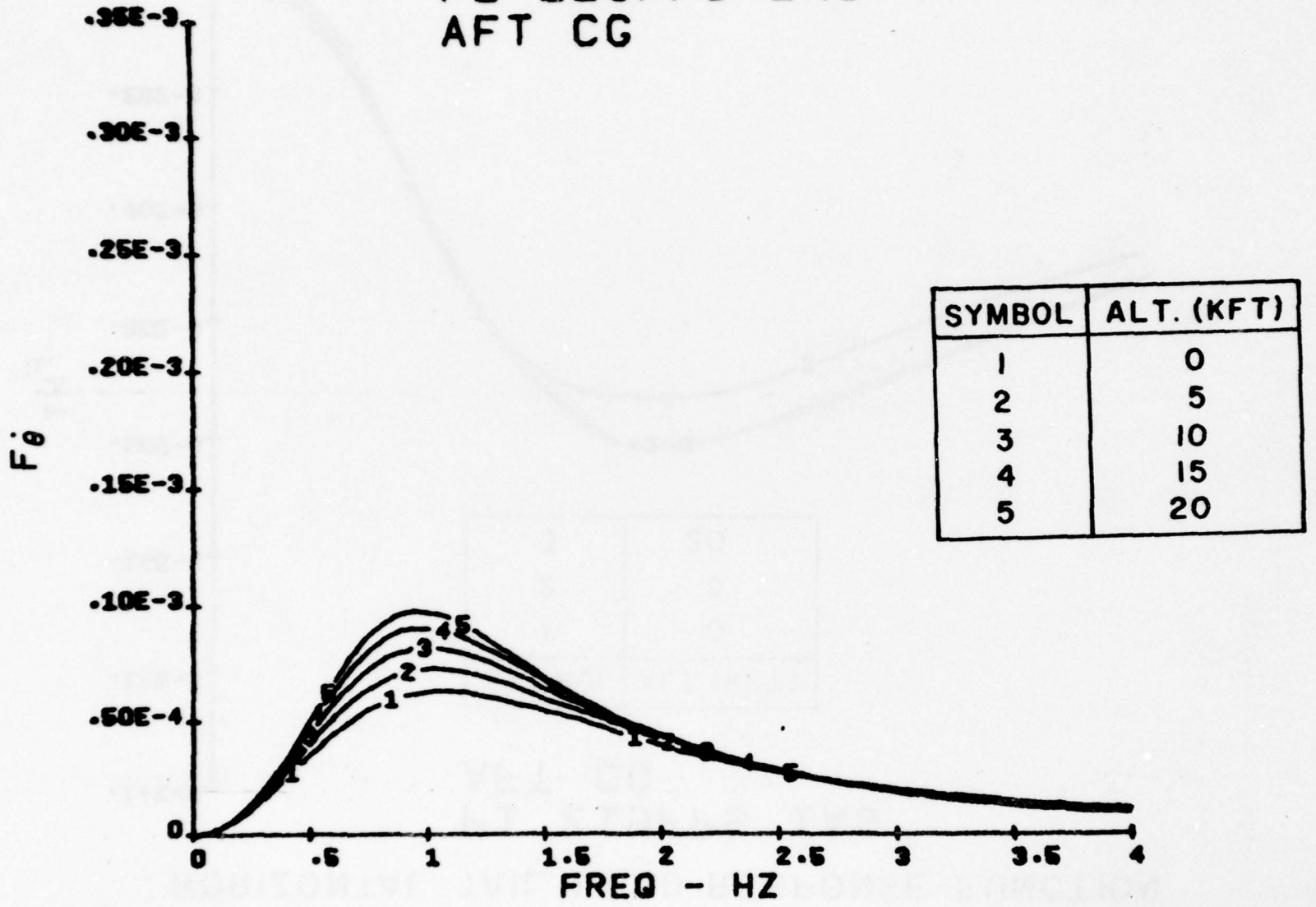

SYMBOL	ALT. (KFT)
1	0
2	5
3	10
4	15
5	20

Figure B.8

HORIZONTAL TAIL LOAD RESPONSE FUNCTION

P1 219FPS IAS
AFT CG

SYMBOL	ALT. (KFT)
1	0
2	5
3	20

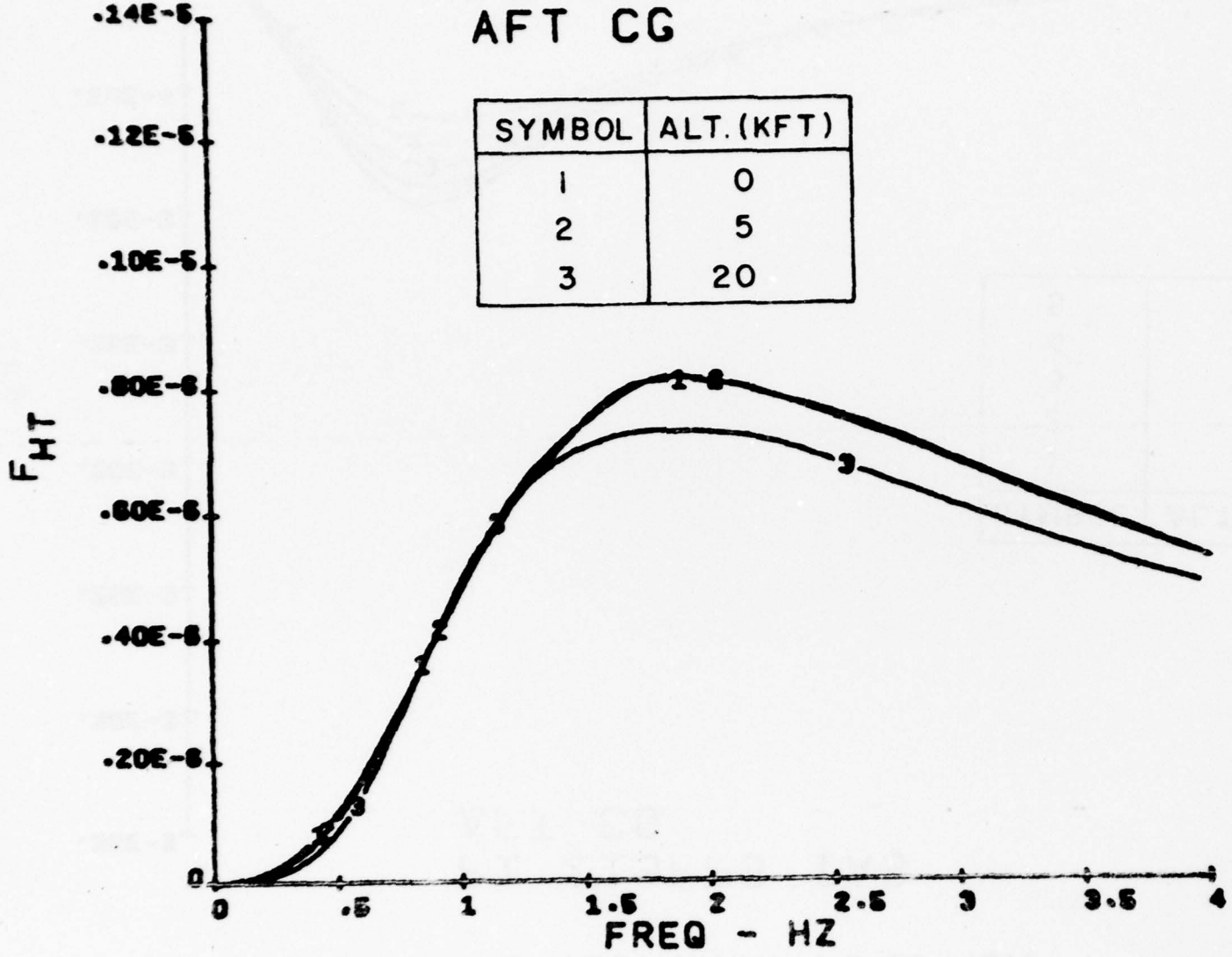

Figure B.9

LATERAL ACCELERATION RESPONSE FUNCTION

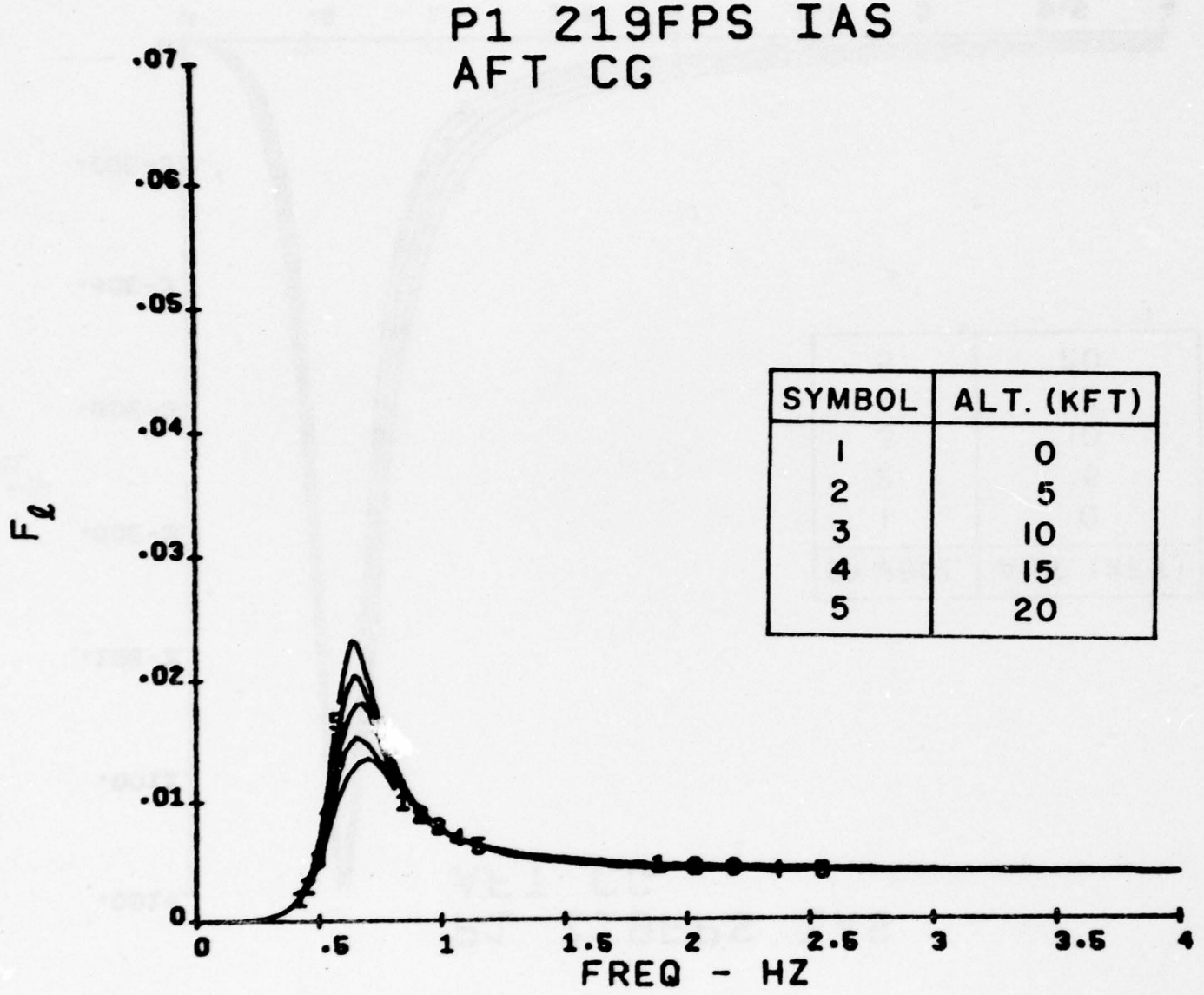

Figure B.10

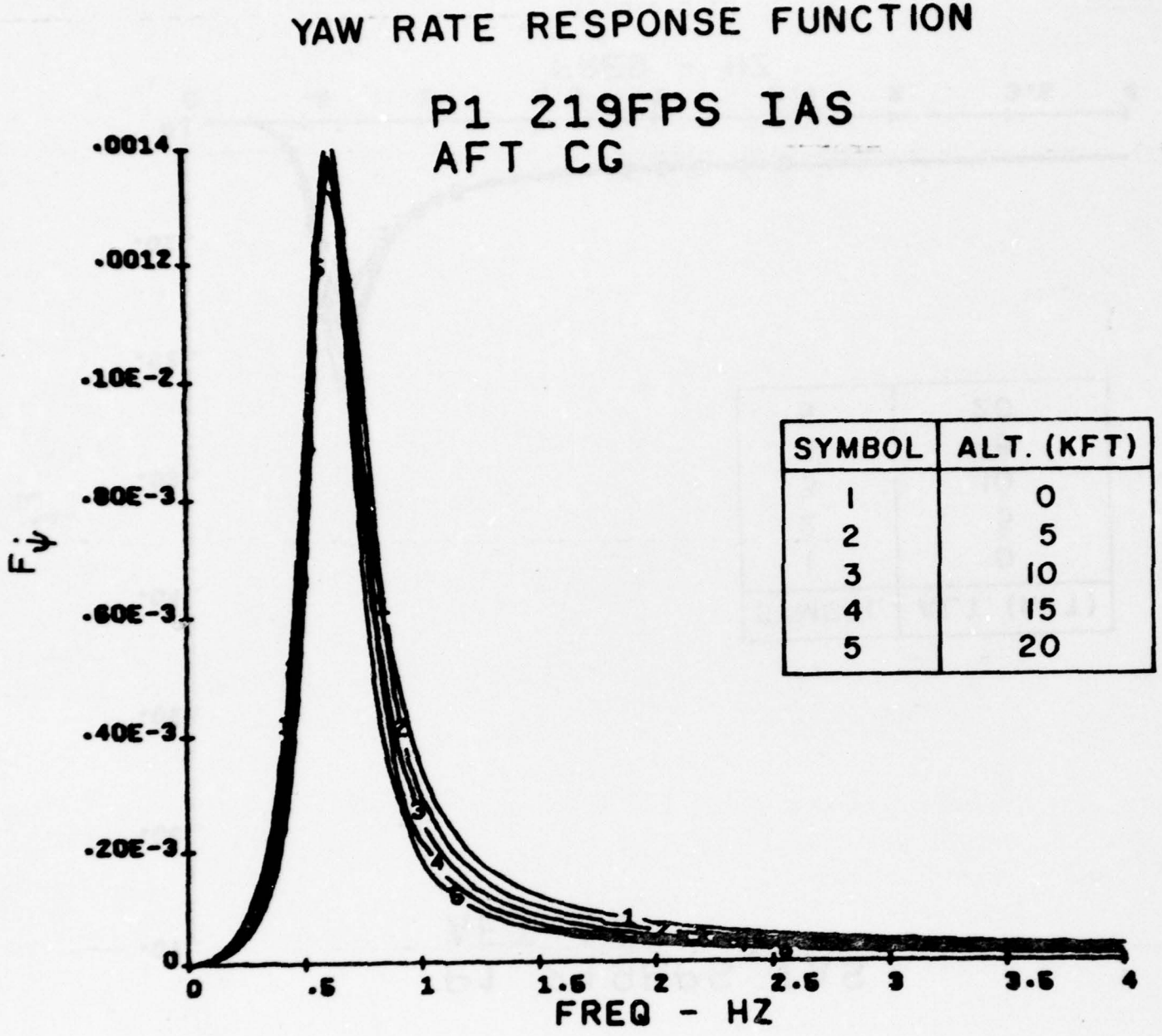
YAW RATE RESPONSE FUNCTION
P1 219FPS IAS
AFT CG
.0014
.0012
.10E-2
.80E-3
.60E-3
.40E-3
.20E-3
0
$F_{\dot{\psi}}$
0
.5
1
1.5
2
2.5
3
3.5
4
FREQ - HZ
SYMBOL | ALT. (KFT)
1 | 0
2 | 5
3 | 10
4 | 15
5 | 20

Figure B.11

VERTICAL TAIL LOAD RESPONSE FUNCTION

P1 219FPS IAS
AFT CG

SYMBOL	ALT.(KFT)
1	0
2	5
3	20

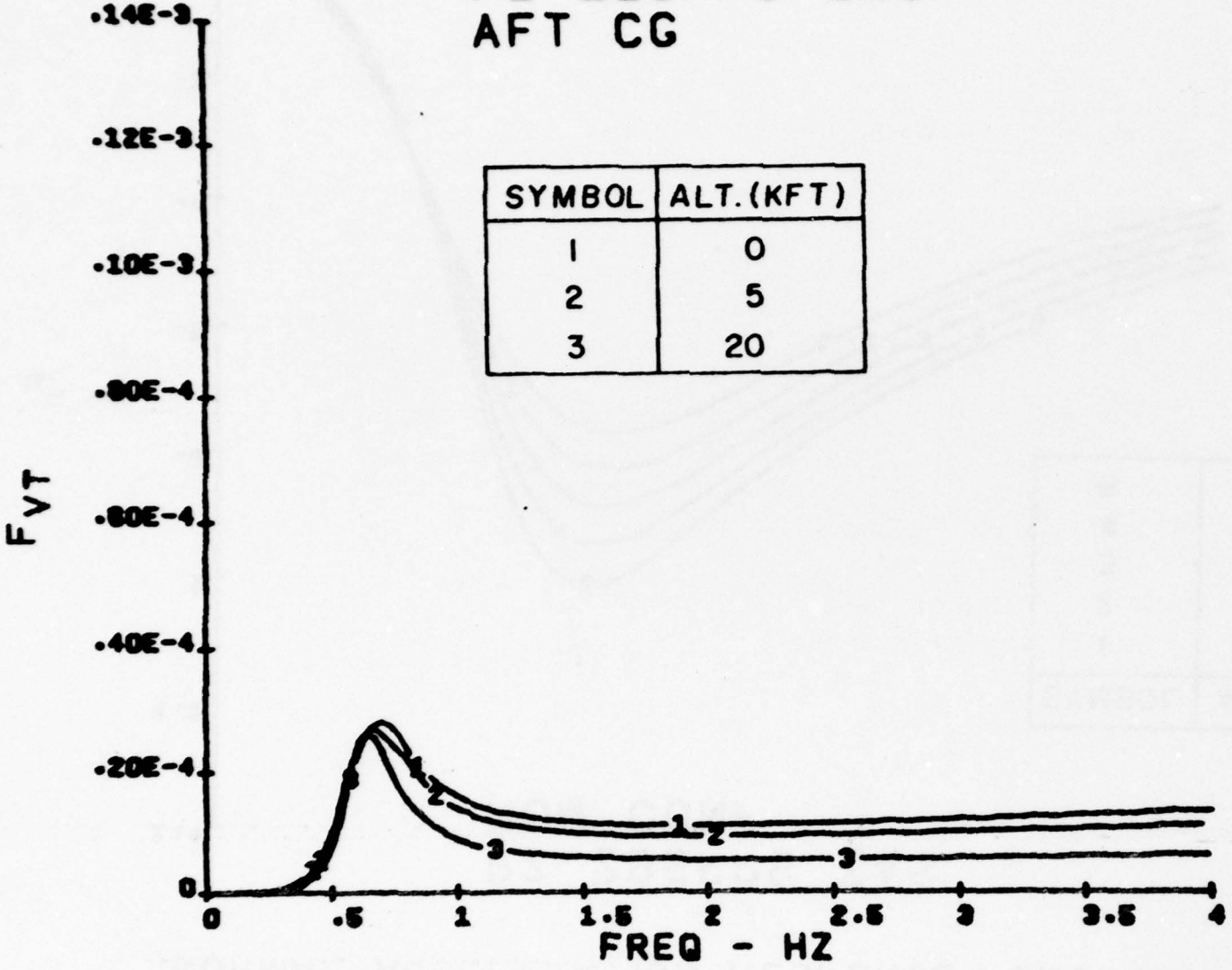

Figure B.12

NORMAL ACCELERATION RESPONSE FUNCTION

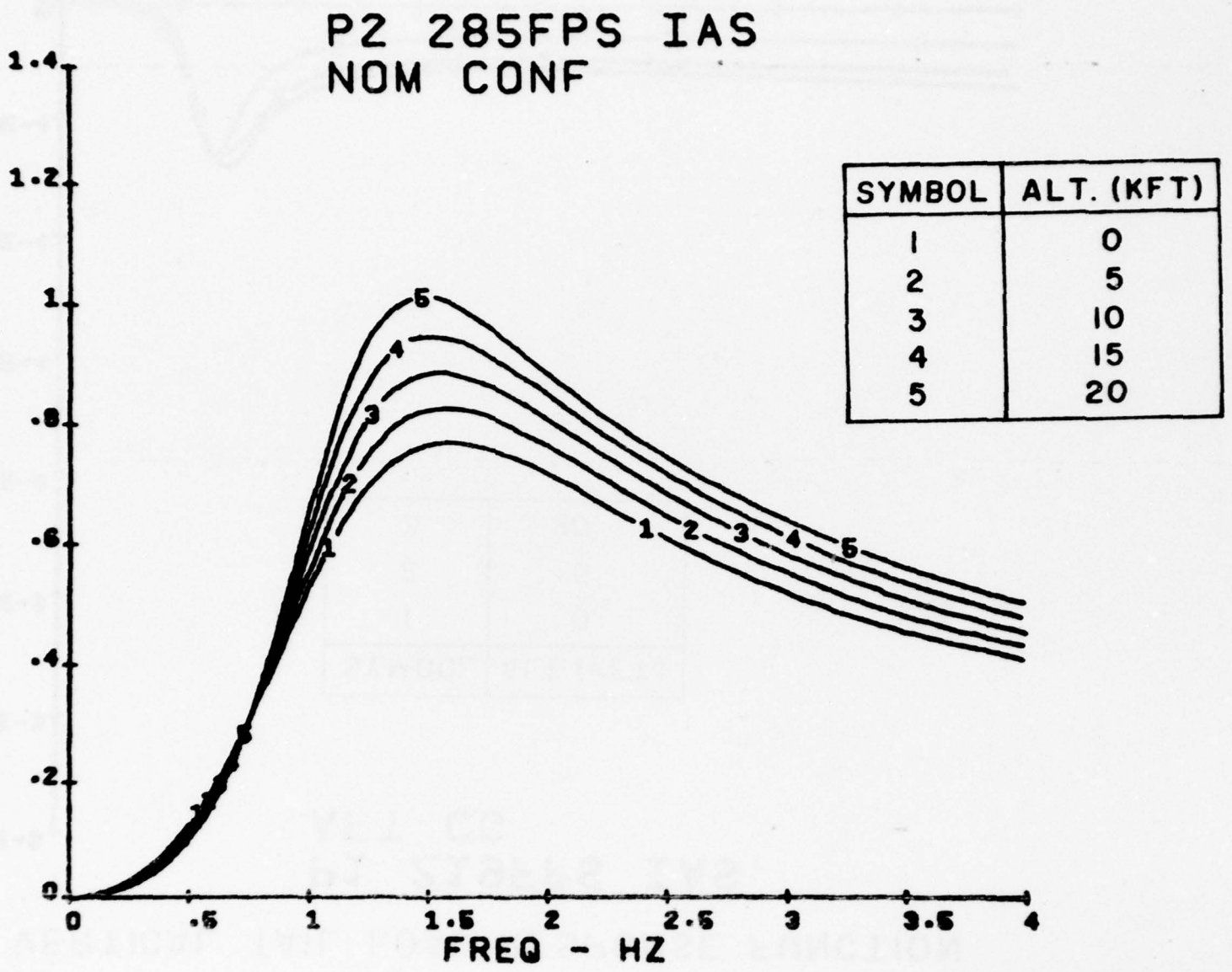

Figure B.13

PITCH RATE RESPONSE FUNCTION

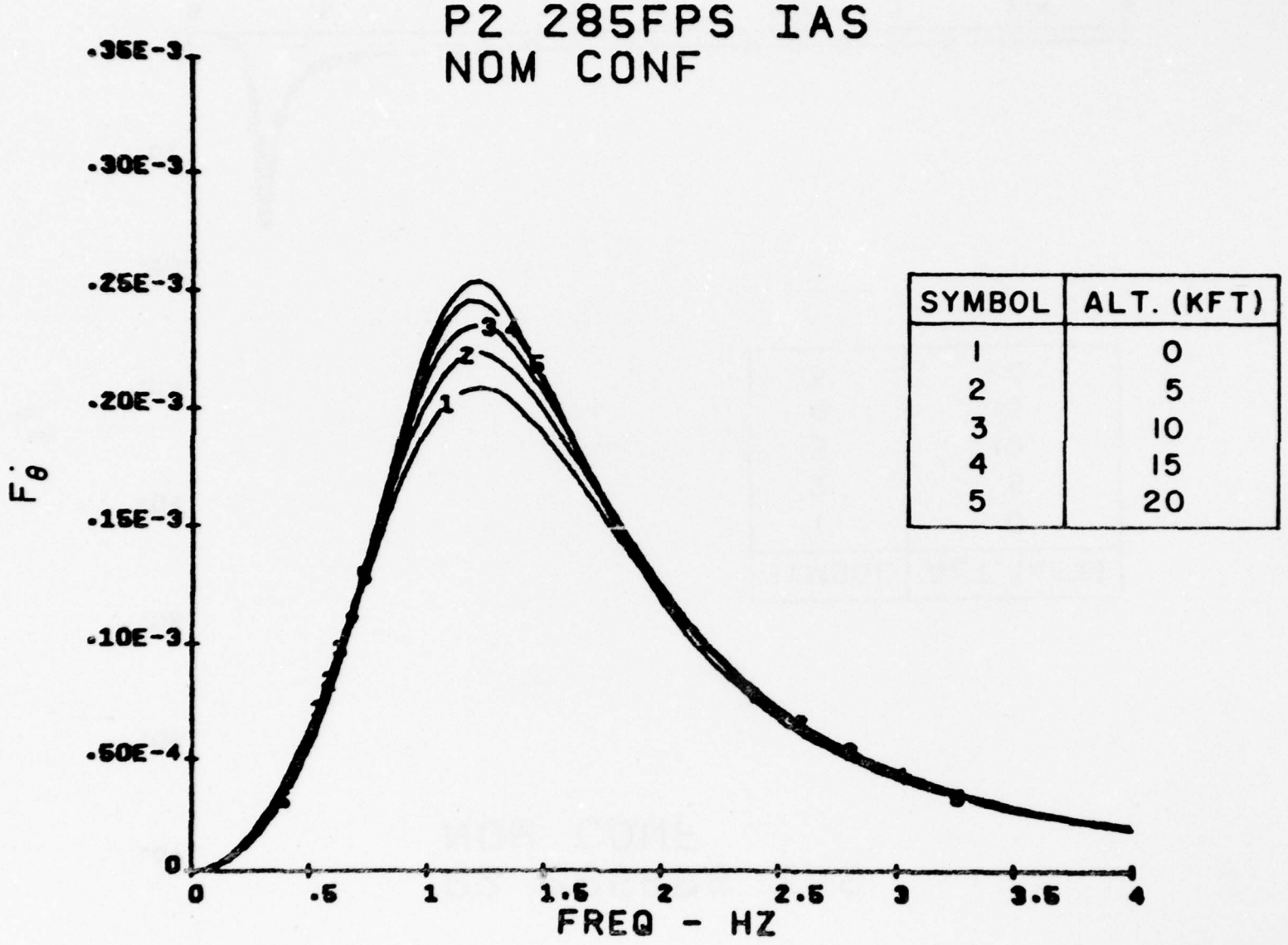

Figure B.14

LATERAL ACCELERATION RESPONSE FUNCTION

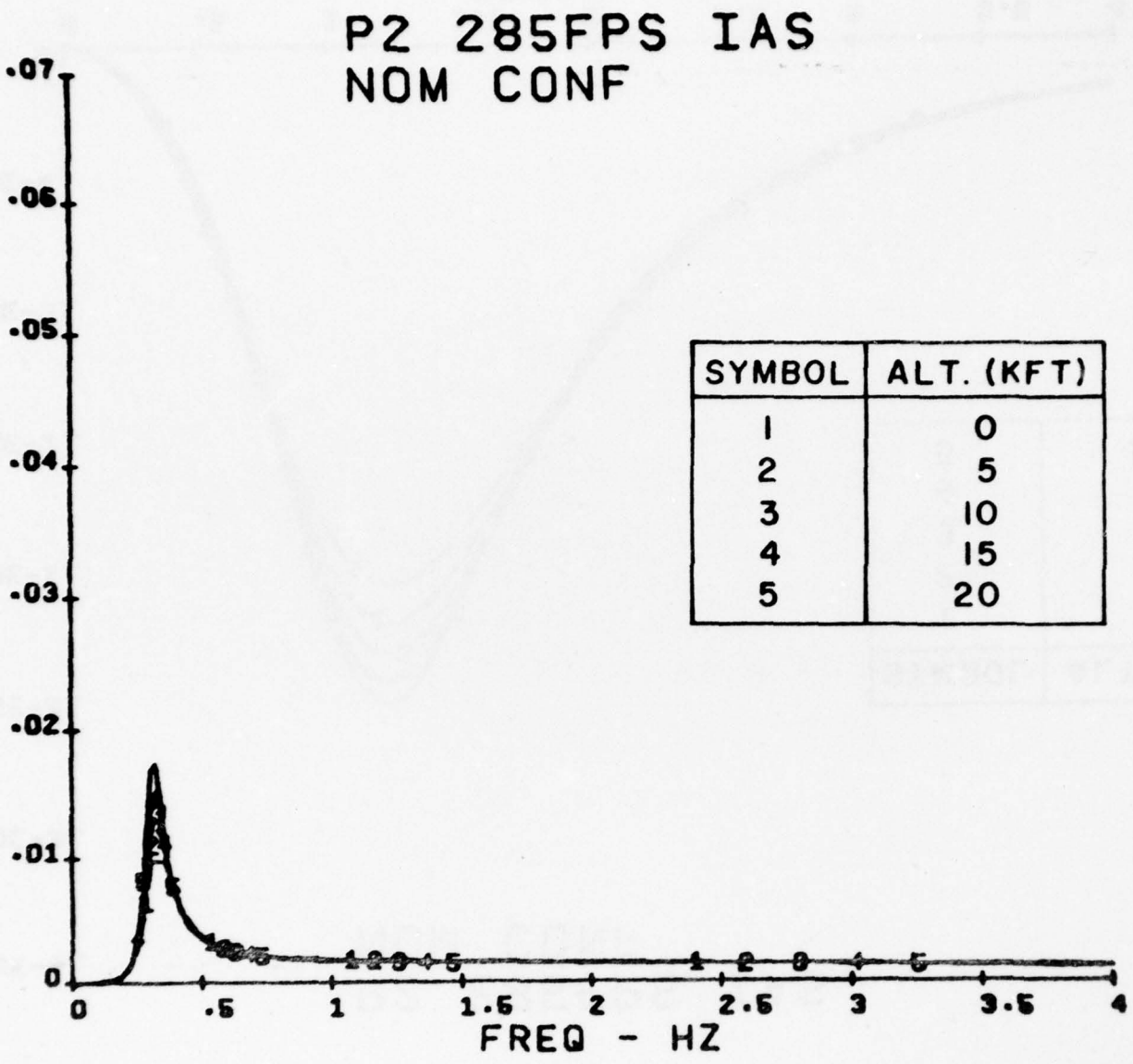

Figure B.15

YAW RATE RESPONSE FUNCTION

P2 285FPS IAS
NOM CONF

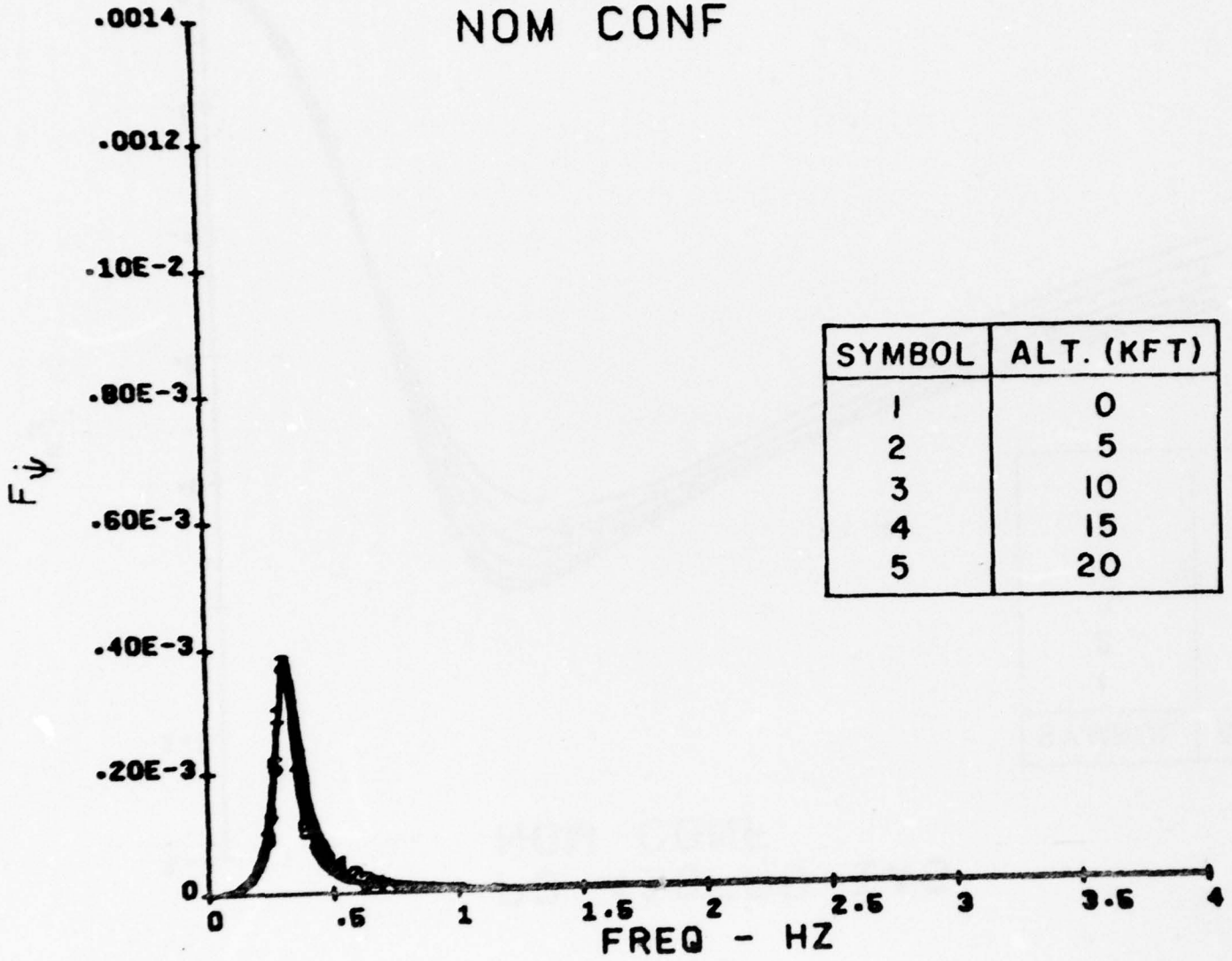

SYMBOL	ALT. (KFT)
1	0
2	5
3	10
4	15
5	20

Figure B.16

NORMAL ACCELERATION RESPONSE FUNCTION

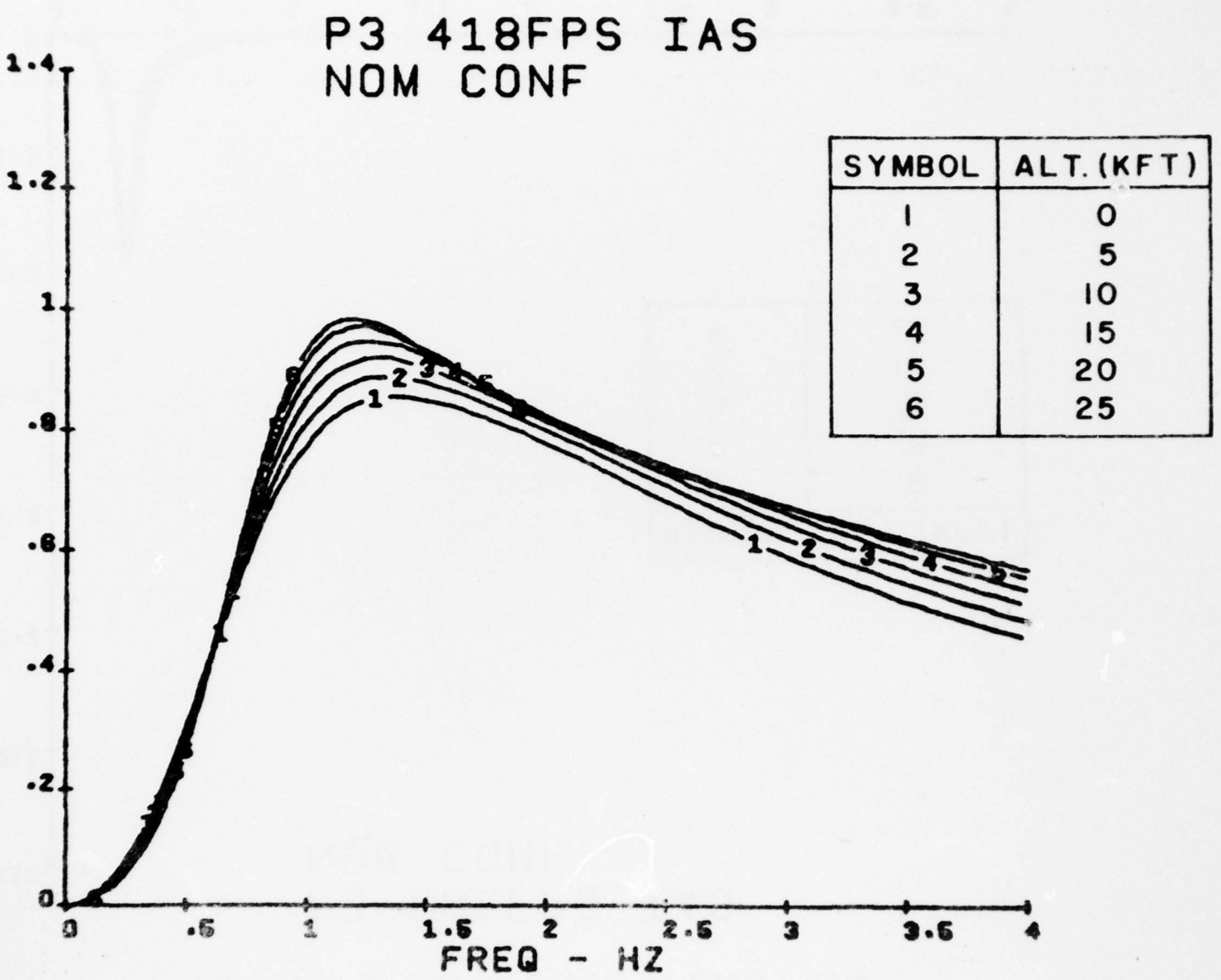

Figure B.17

PITCH RATE RESPONSE FUNCTION

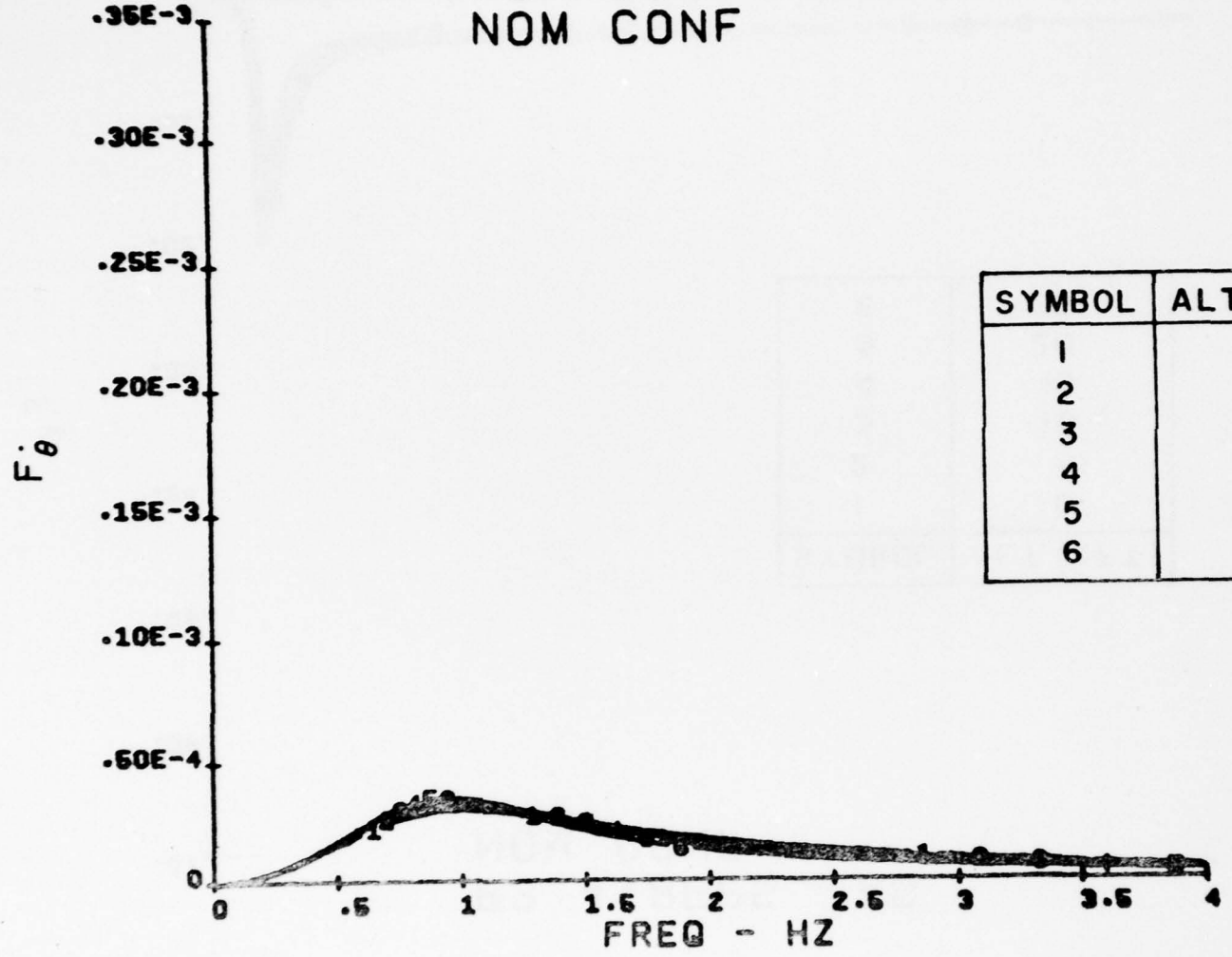

Figure B.18

LATERAL ACCELERATION RESPONSE FUNCTION

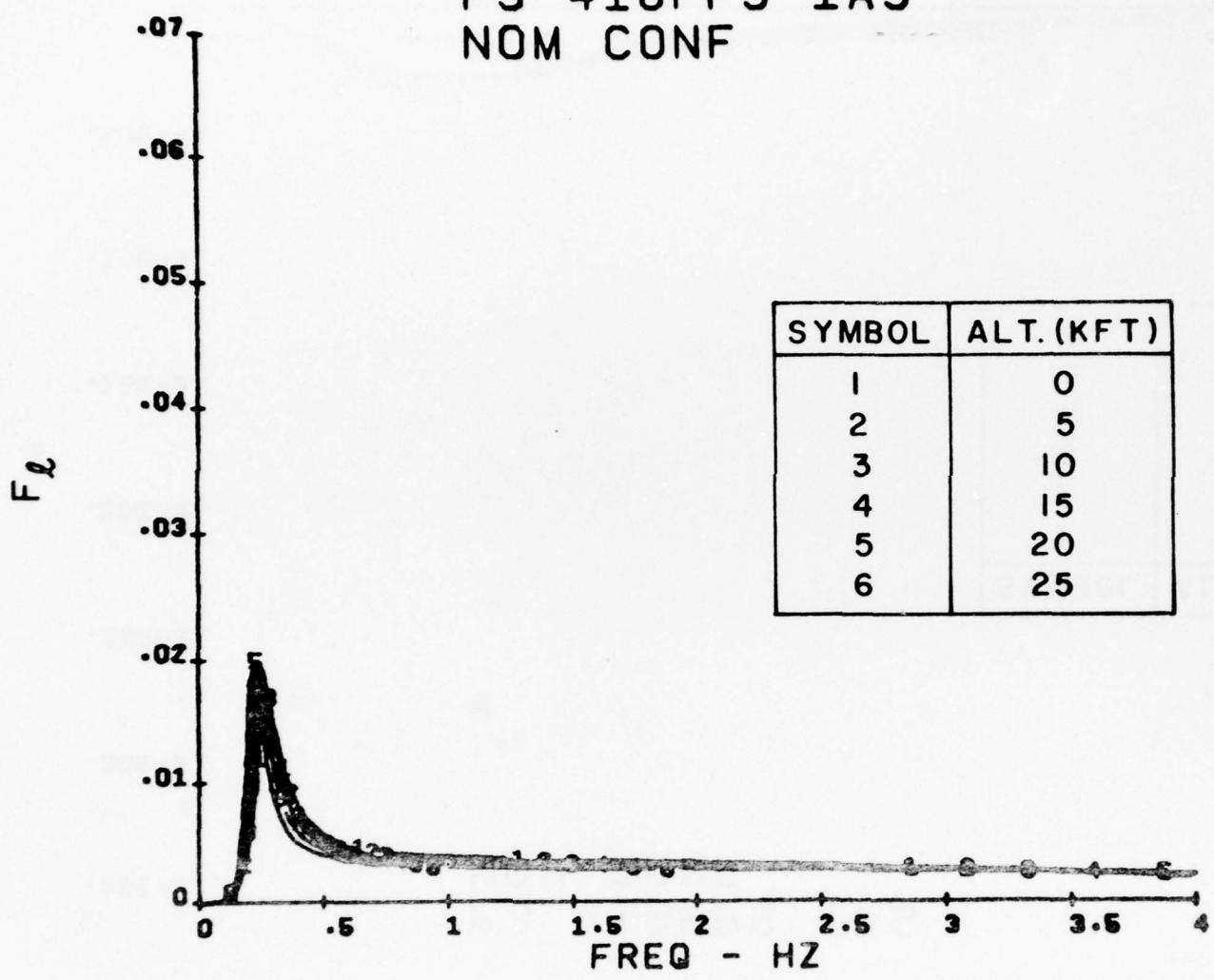

Figure B.19

YAW RATE RESPONSE FUNCTION

P3 418FPS IAS
NOM CONF

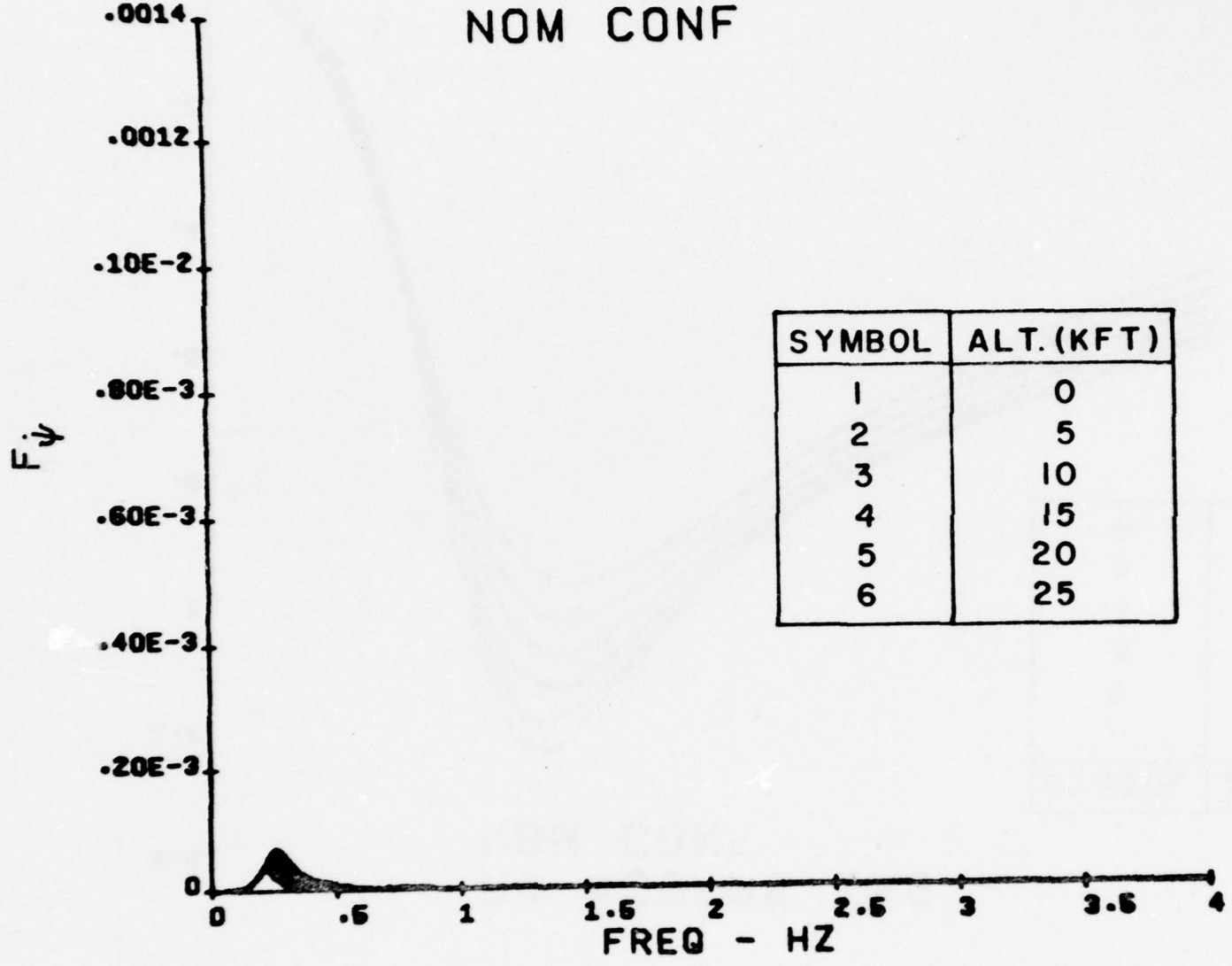

SYMBOL	ALT.(KFT)
1	0
2	5
3	10
4	15
5	20
6	25

Figure B.20

NORMAL ACCELERATION RESPONSE FUNCTION

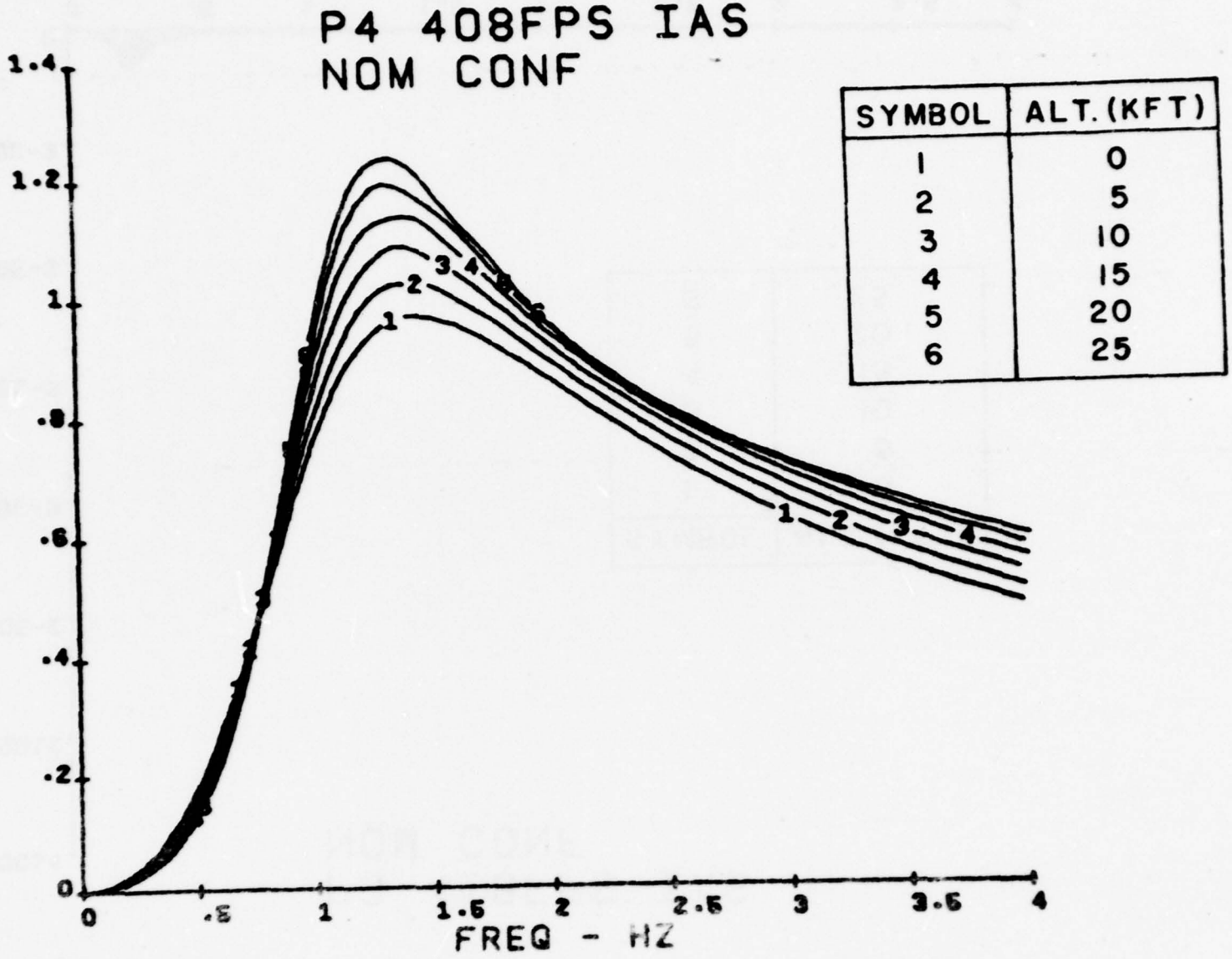

Figure B.21

PITCH RATE RESPONSE FUNCTION

P4 408FPS IAS
NOM CONF

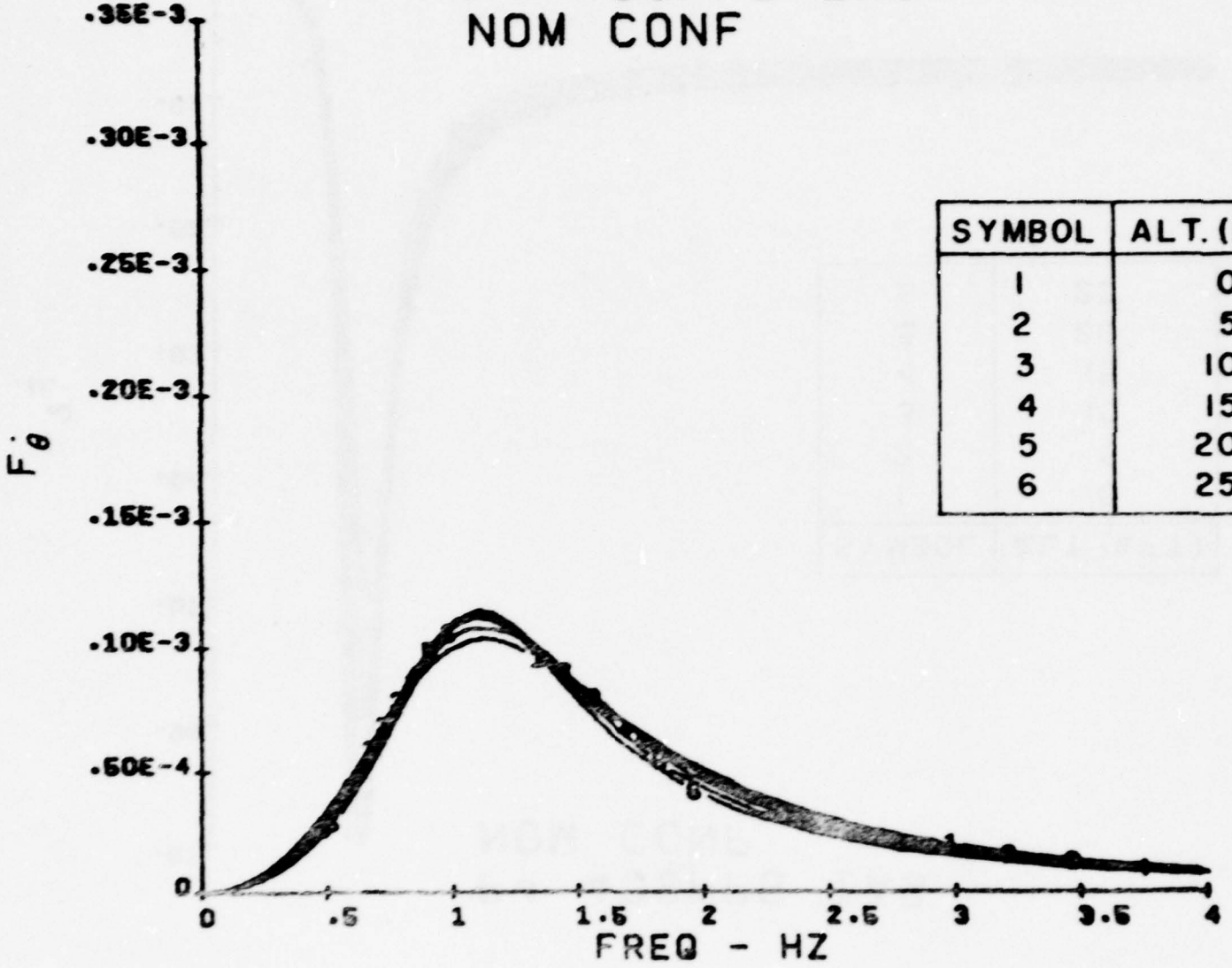

SYMBOL	ALT. (KFT)
1	0
2	5
3	10
4	15
5	20
6	25

Figure B.22

LATERAL ACCELERATION RESPONSE FUNCTION

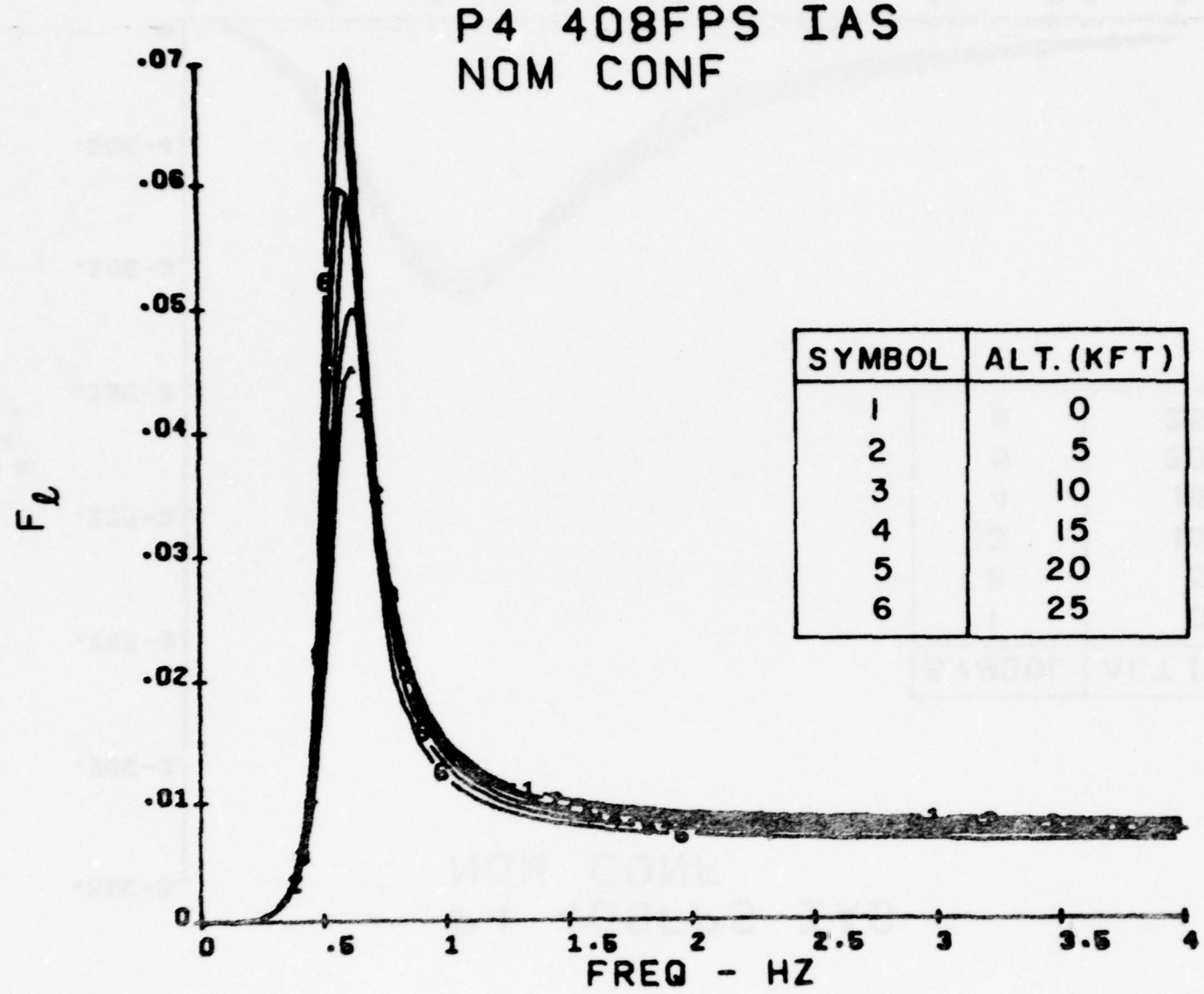

Figure B.23

YAW RATE RESPONSE FUNCTION

P4 408FPS IAS
NOM CONF

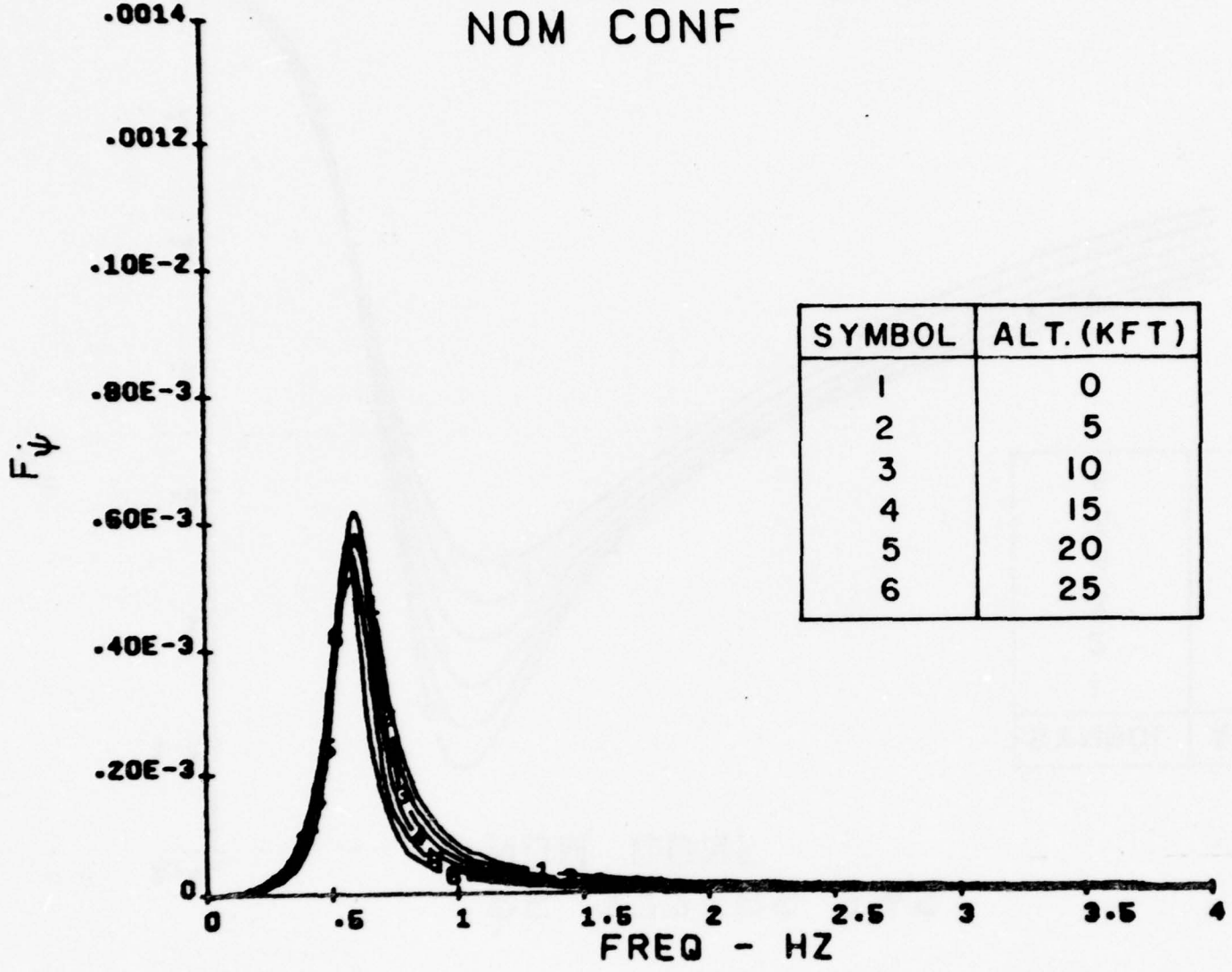

SYMBOL	ALT.(KFT)
1	0
2	5
3	10
4	15
5	20
6	25

Figure B.24

NORMAL ACCELERATION RESPONSE FUNCTION

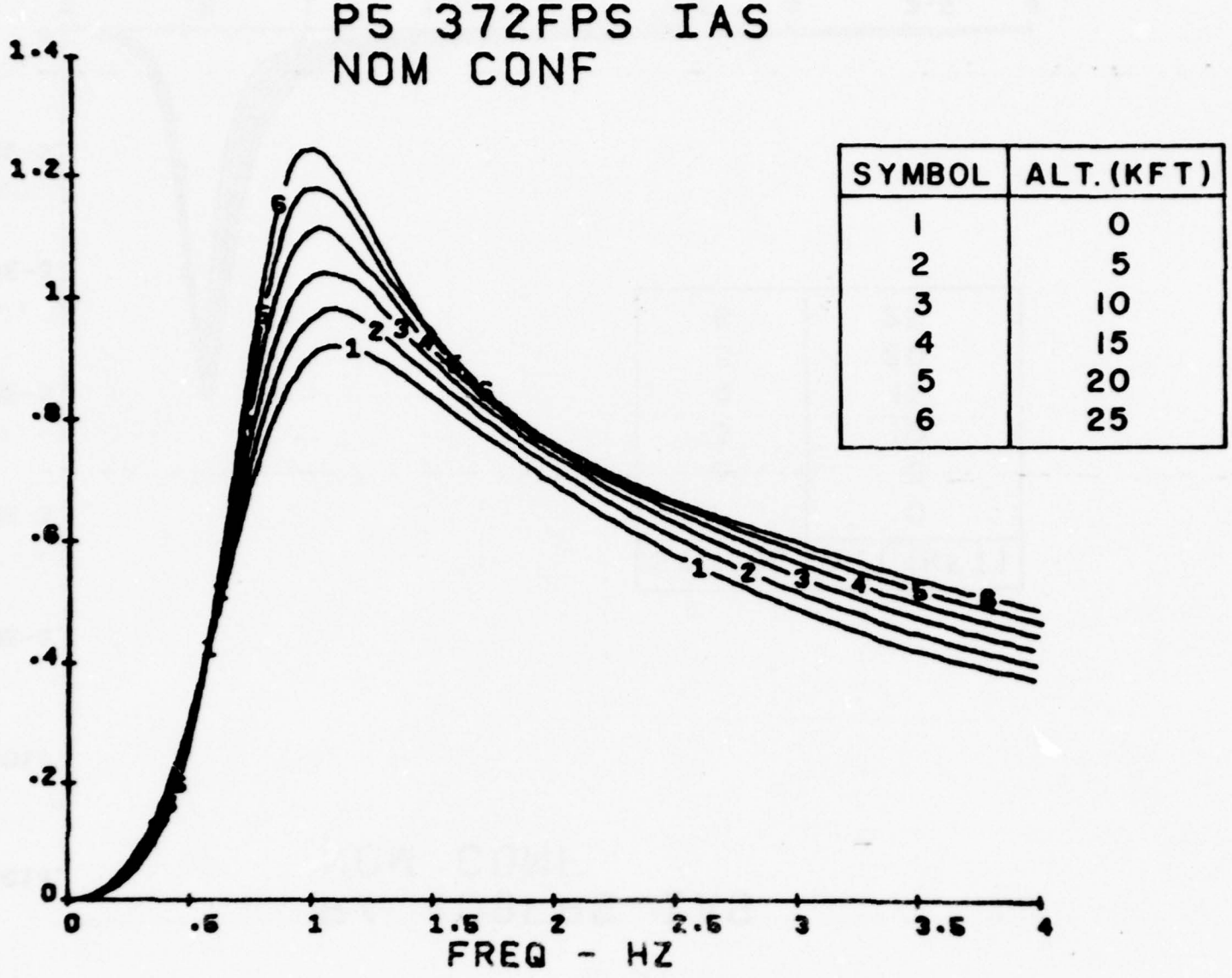

Figure B.25

PITCH RATE RESPONSE FUNCTION

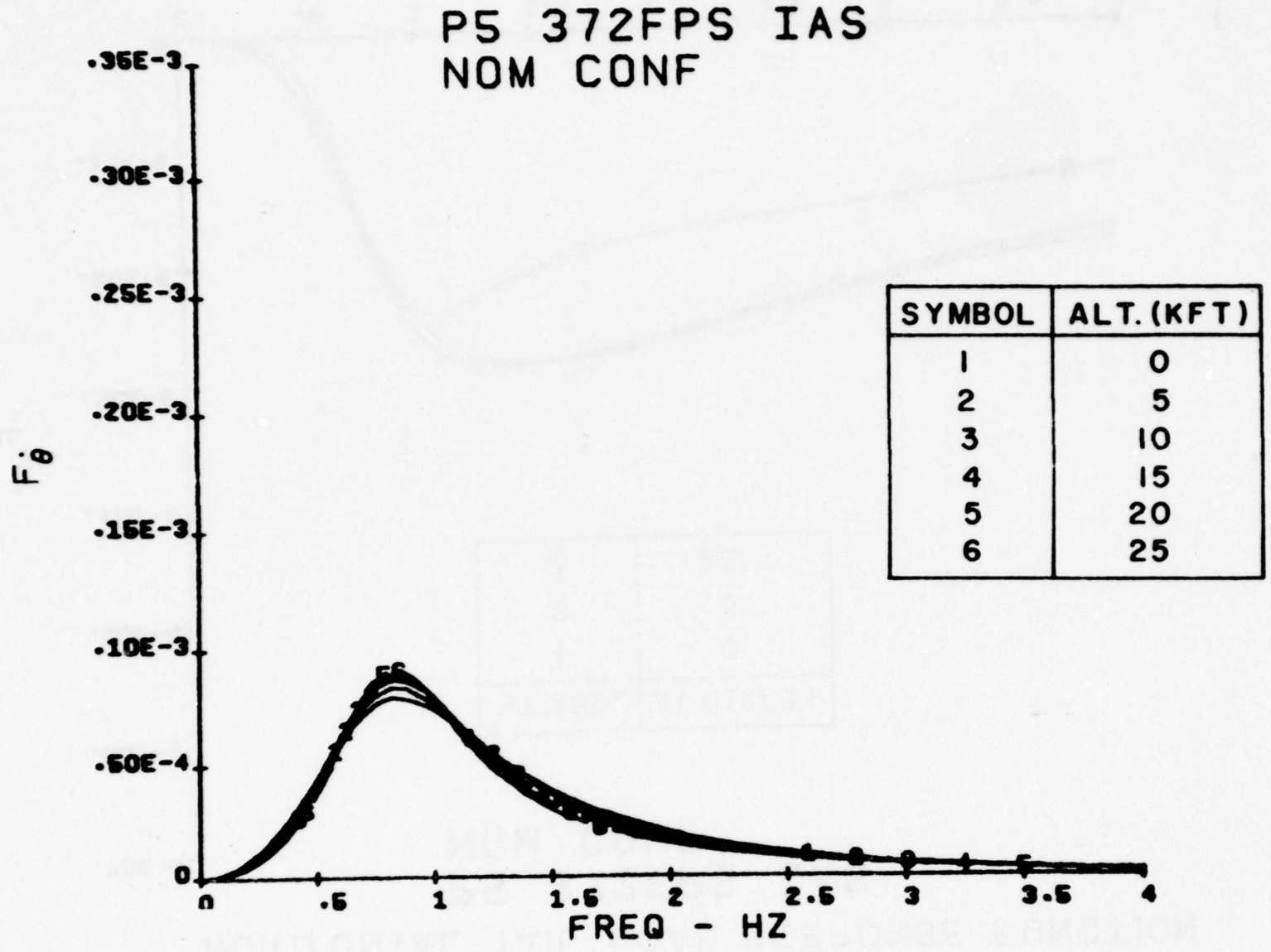

Figure B.26

HORIZONTAL TAIL LOAD RESPONSE FUNCTION

P5 372FPS IAS
NOM CONF

SYMBOL	ALT.(KFT)
1	0
2	5
3	25

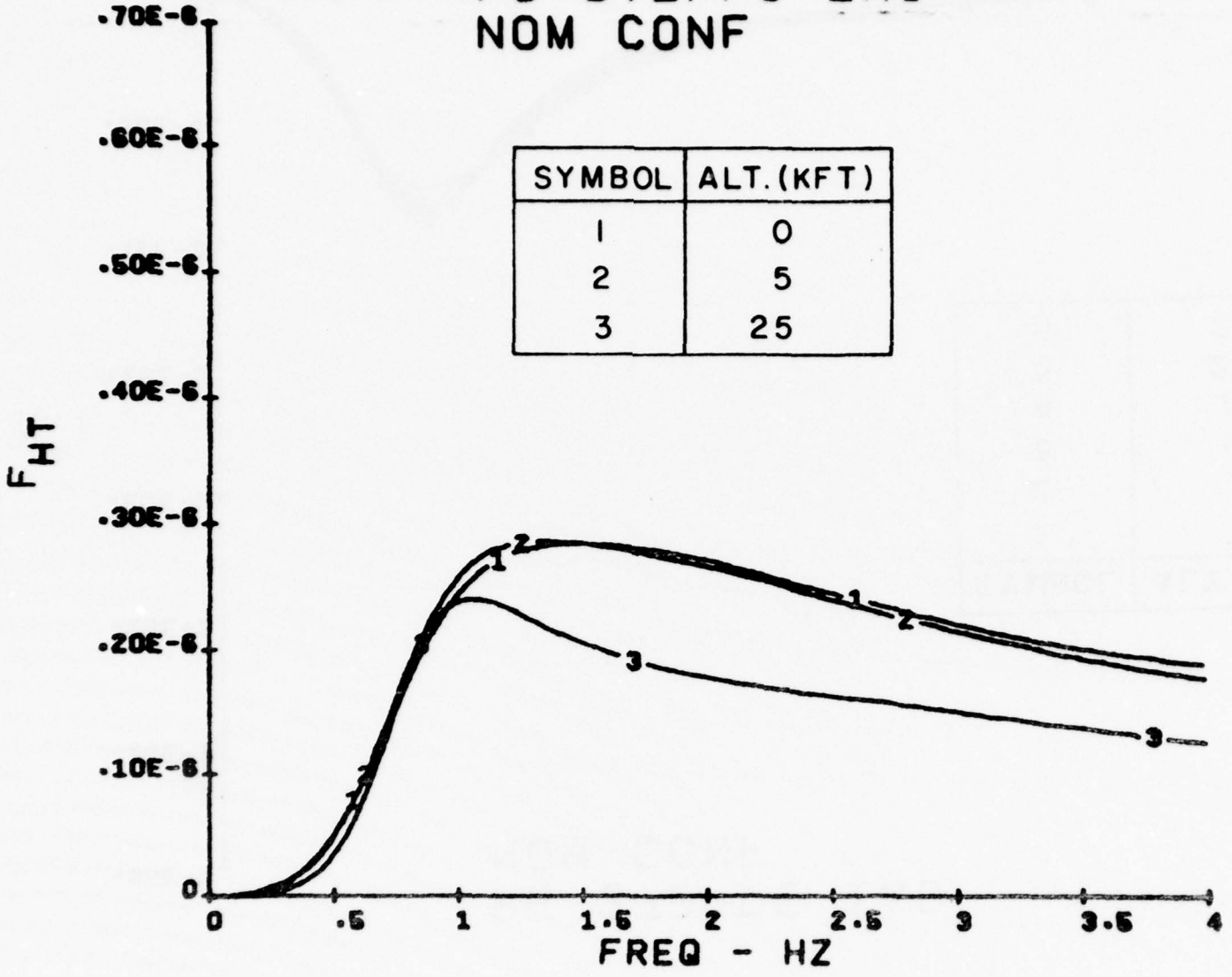

Figure B.27

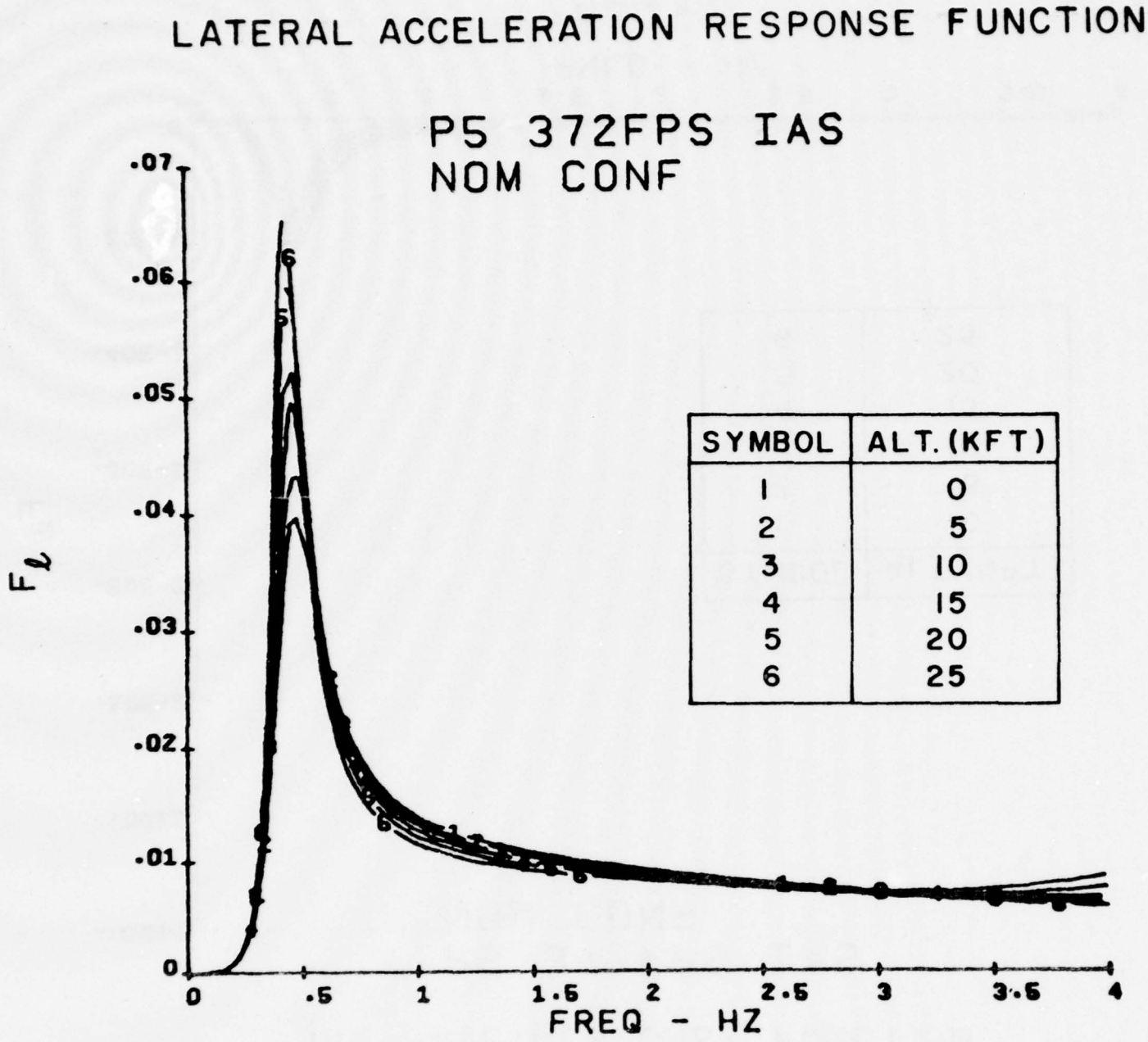
LATERAL ACCELERATION RESPONSE FUNCTION
P5 372FPS IAS
NOM CONF
F_{ℓ}
.07
.06
.05
.04
.03
.02
.01
0
0
.5
1
1.5
2
2.5
3
3.5
4
FREQ - HZ
SYMBOL | ALT.(KFT)
1 | 0
2 | 5
3 | 10
4 | 15
5 | 20
6 | 25

Figure B.28

YAW RATE RESPONSE FUNCTION

P5 372FPS IAS
NOM CONF

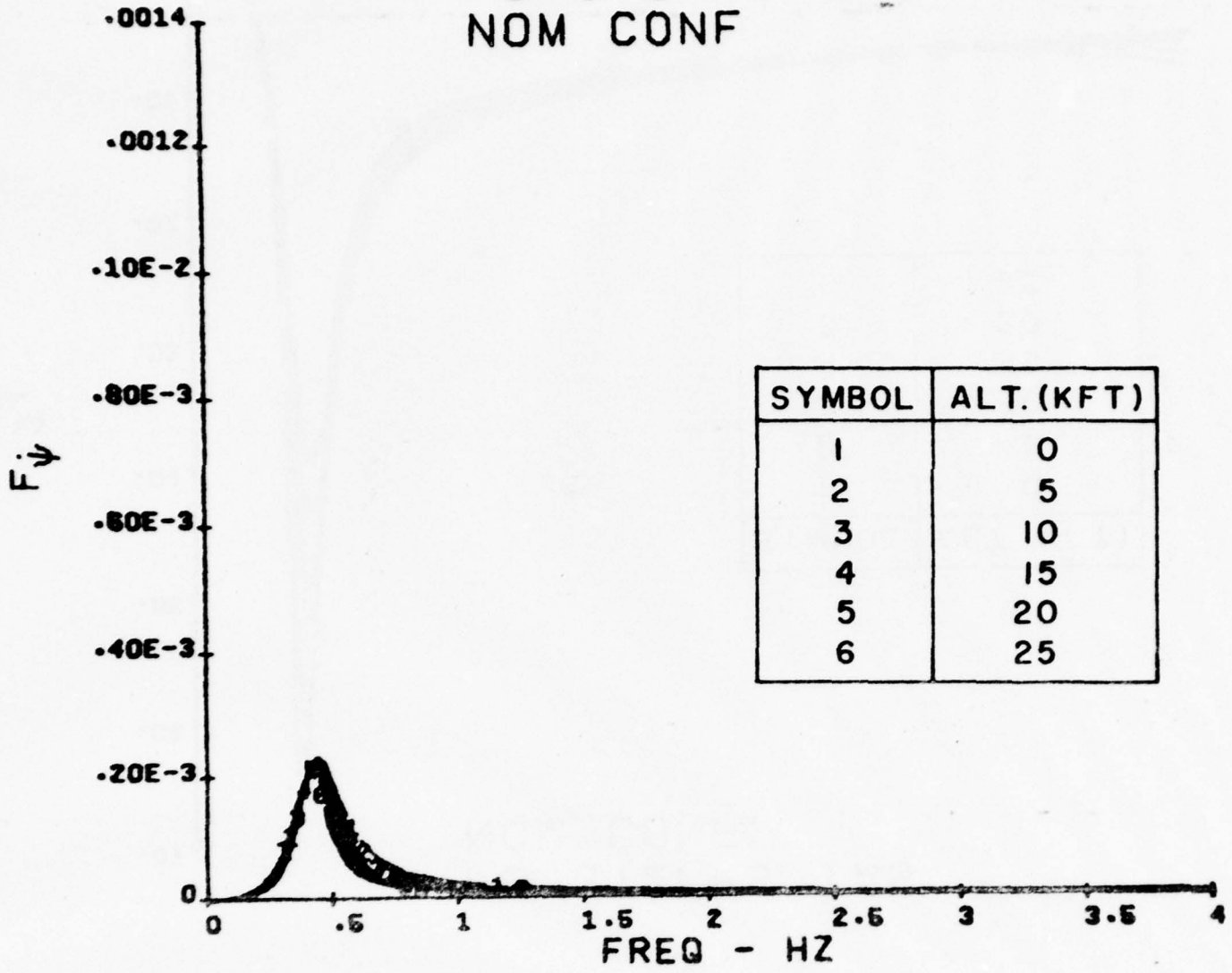

SYMBOL	ALT. (KFT)
1	0
2	5
3	10
4	15
5	20
6	25

Figure B.29

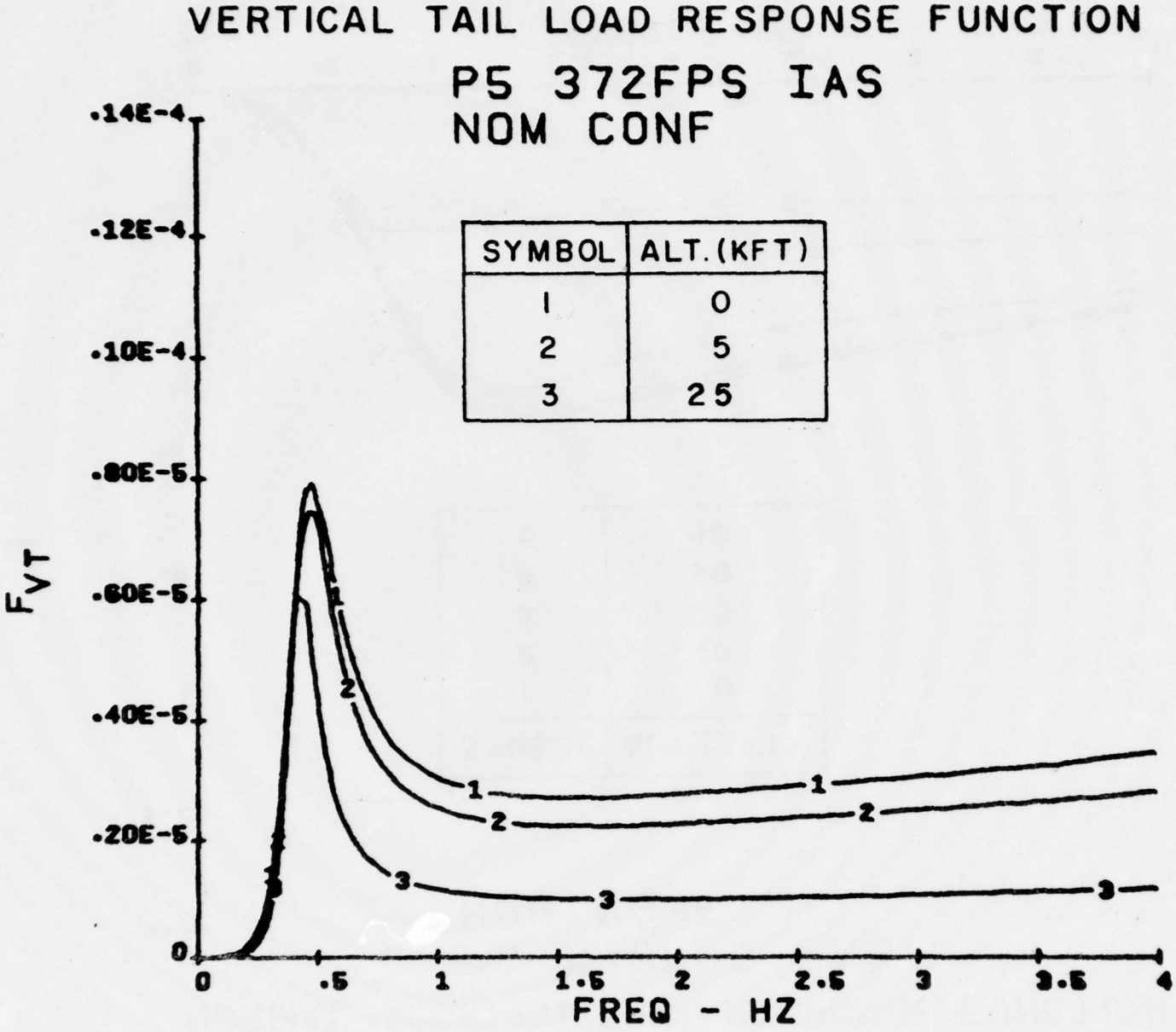
VERTICAL TAIL LOAD RESPONSE FUNCTION
P5 372FPS IAS
NOM CONF
SYMBOL | ALT.(KFT)
1 | 0
2 | 5
3 | 25
.14E-4
.12E-4
.10E-4
.80E-5
.60E-5
.40E-5
.20E-5
0
F_{VT}
0
.5
1
1.5
2
2.5
3
3.5
4
FREQ - HZ

Figure B.30

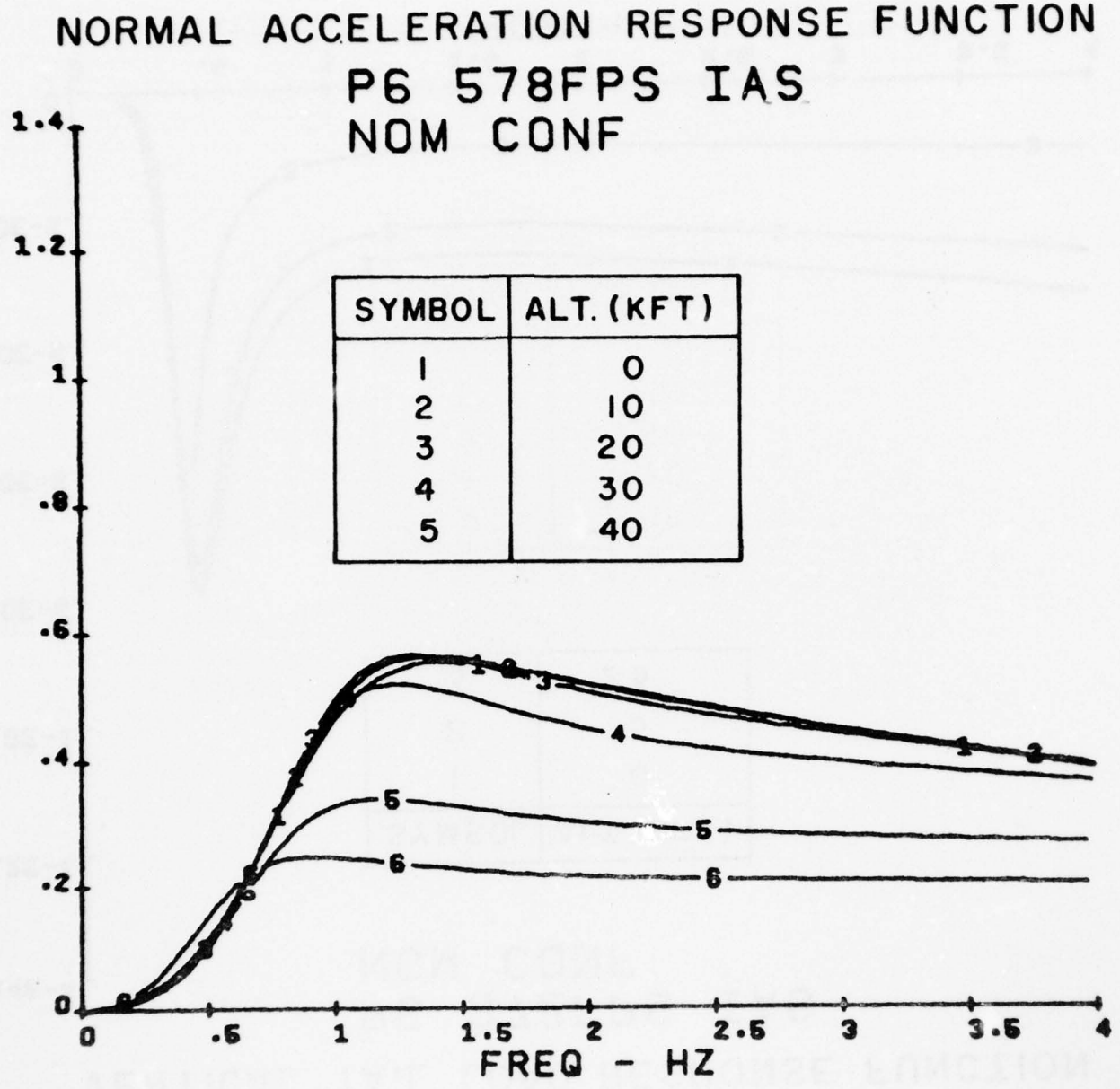
NORMAL ACCELERATION RESPONSE FUNCTION
P6 578FPS IAS
NOM CONF
SYMBOL | ALT. (KFT)
1 | 0
2 | 10
3 | 20
4 | 30
5 | 40
F_n
1.4
1.2
1
.8
.6
.4
.2
0
0
.5
1
1.5
2
2.5
3
3.5
4
FREQ - HZ

Figure B.31

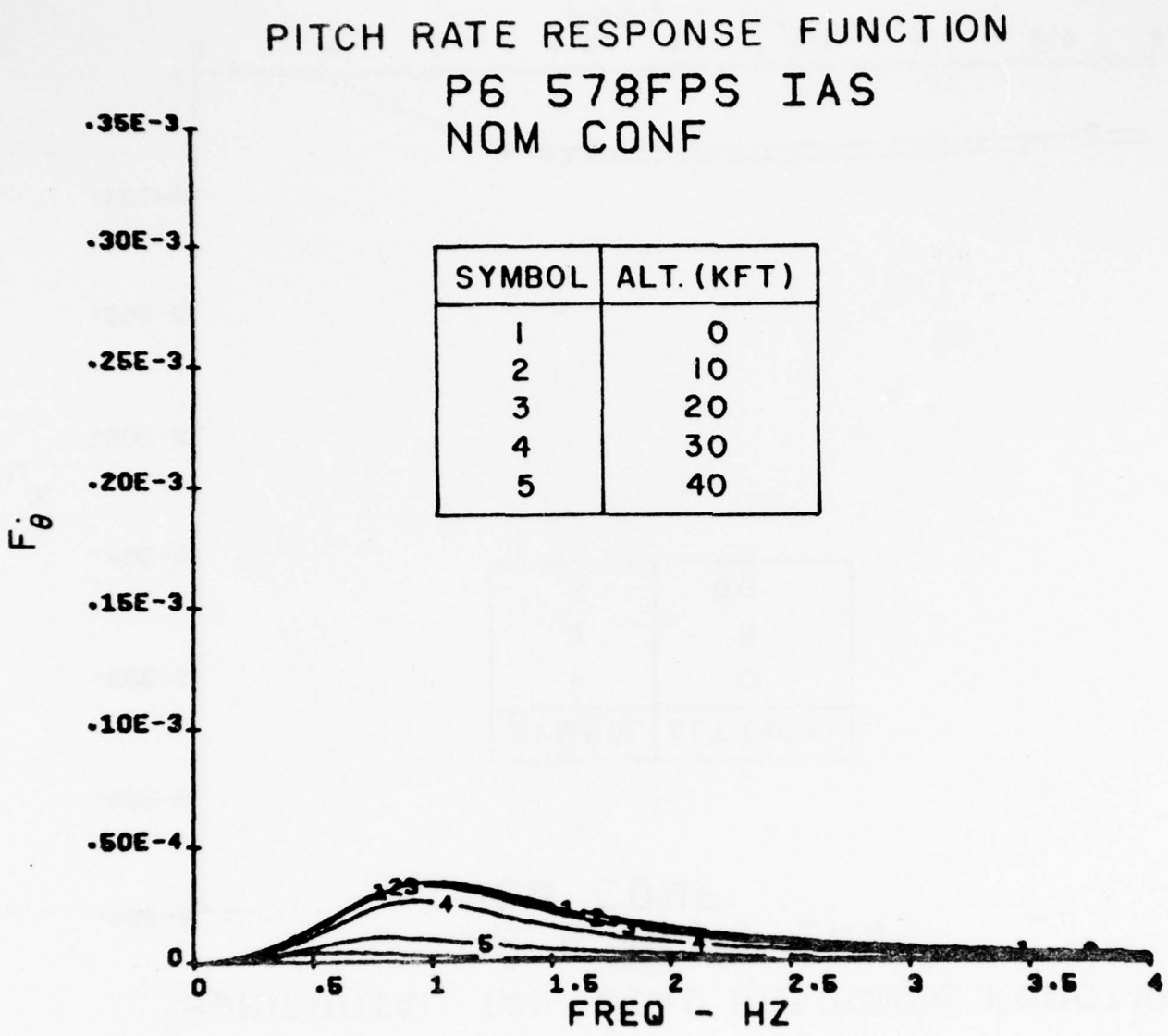
PITCH RATE RESPONSE FUNCTION
P6 578FPS IAS
NOM CONF
SYMBOL | ALT. (KFT)
1 | 0
2 | 10
3 | 20
4 | 30
5 | 40
.35E-3
.30E-3
.25E-3
.20E-3
.15E-3
.10E-3
.50E-4
0
$F_{\dot{\theta}}$
0
.5
1
1.5
2
2.5
3
3.5
4
FREQ - HZ

Figure B.32

HORIZONTAL TAIL LOAD RESPONSE FUNCTION

P6 578FPS IAS
NOM CONF

SYMBOL	ALT.(KFT)
1	0
2	5
3	40

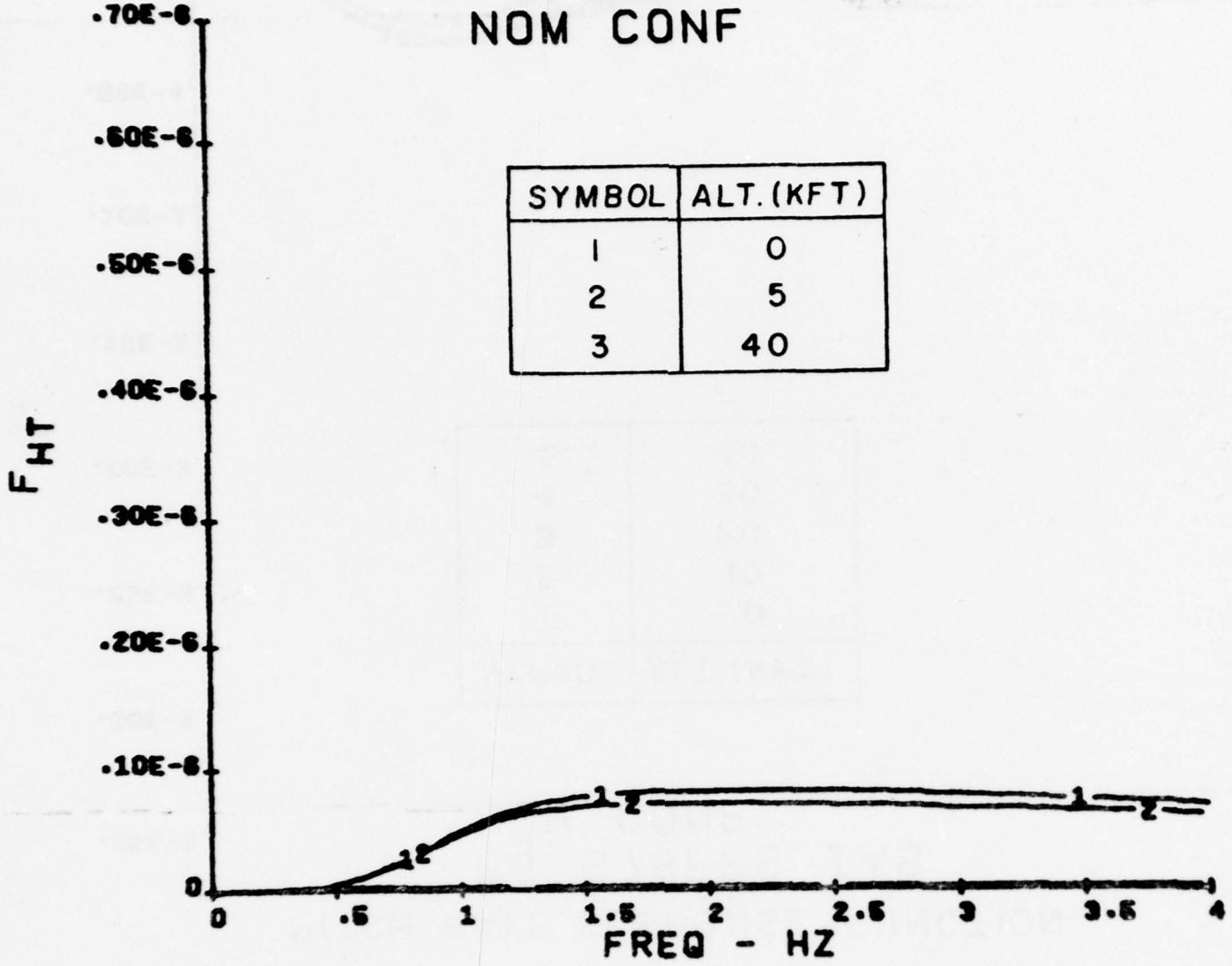

Figure B.33

LATERAL ACCELERATION RESPONSE FUNCTION

P6 578FPS IAS
NOM CONF

SYMBOL	ALT. (KFT)
1	0
2	10
3	20
4	30
5	40

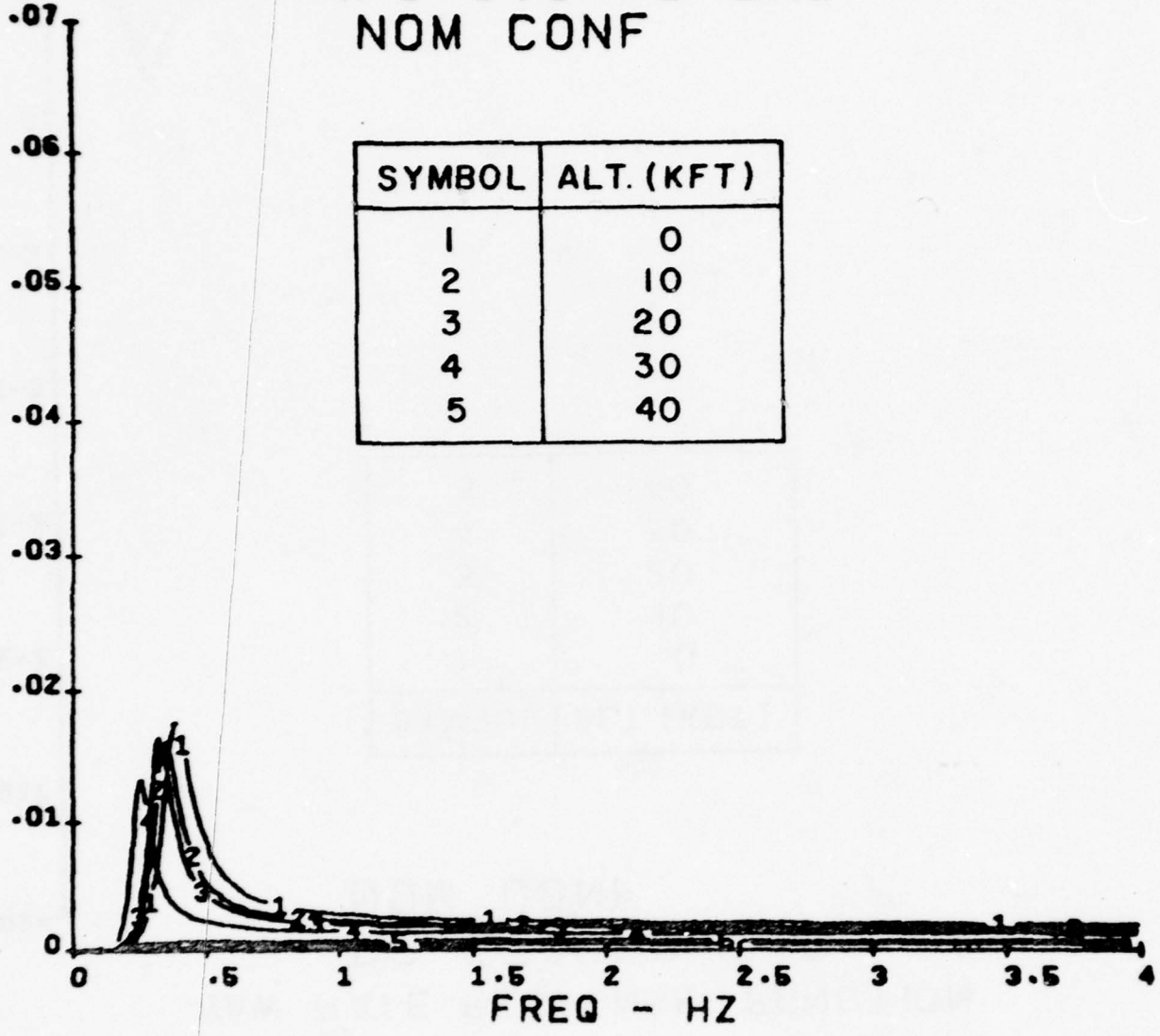

Figure B.34

YAW RATE RESPONSE FUNCTION
P6 578FPS IAS
NOM CONF

SYMBOL	ALT. (KFT)
1	0
2	10
3	20
4	30
5	40

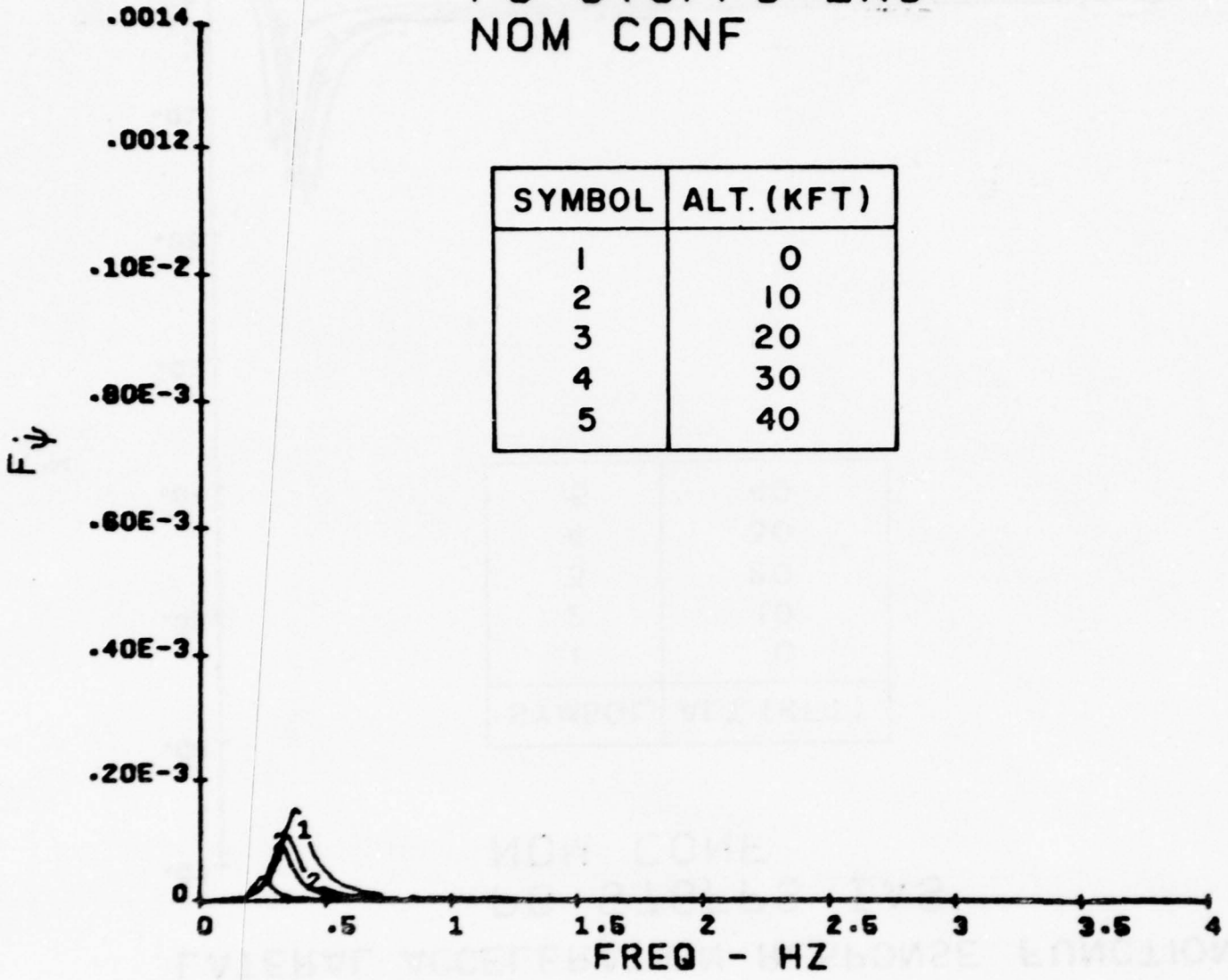

Figure B.35

VERTICAL TAIL LOAD RESPONSE FUNCTION

P6 578FPS IAS
NOM CONF

SYMBOL	ALT.(KFT)
1	0
2	5
3	40

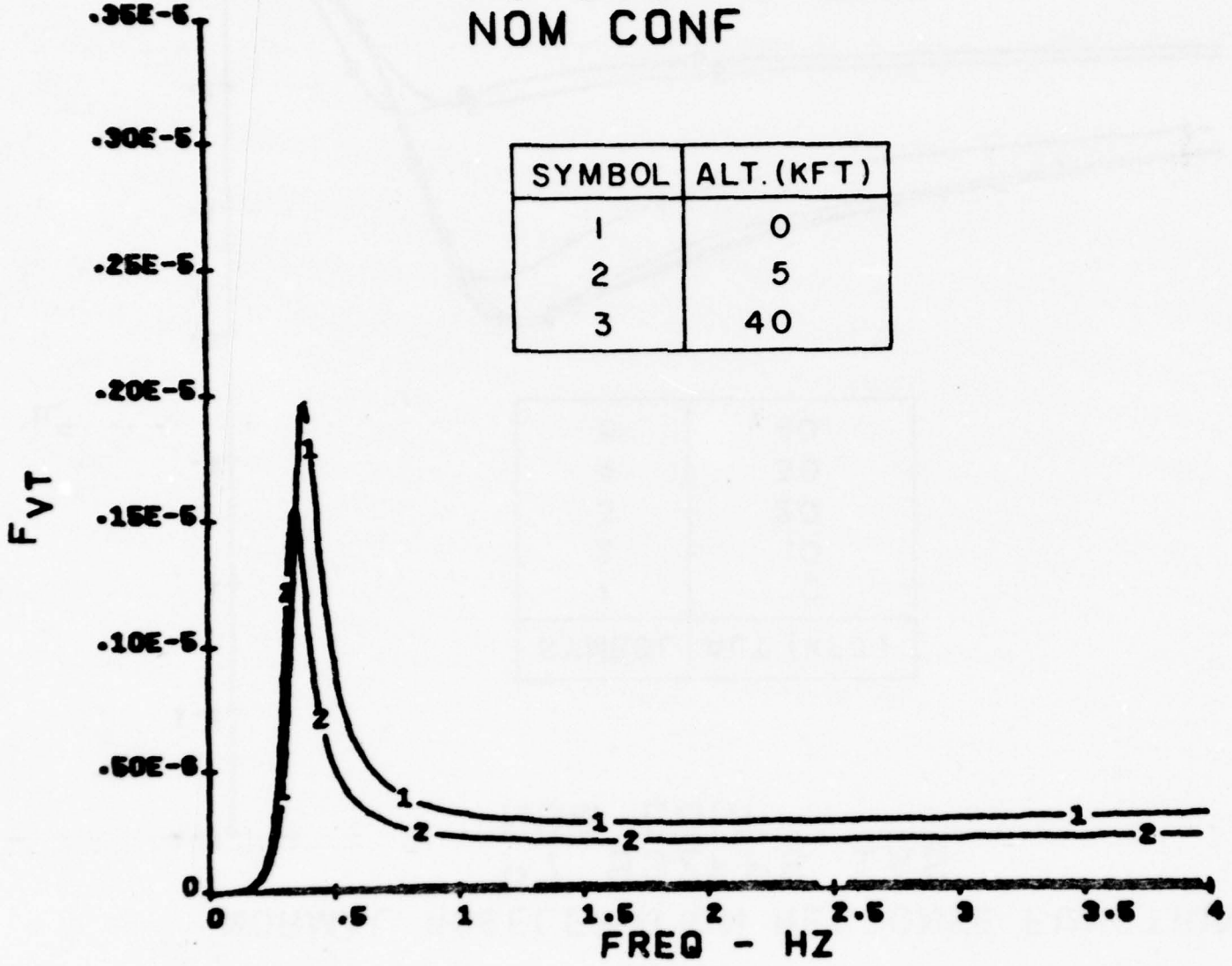

Figure B.36

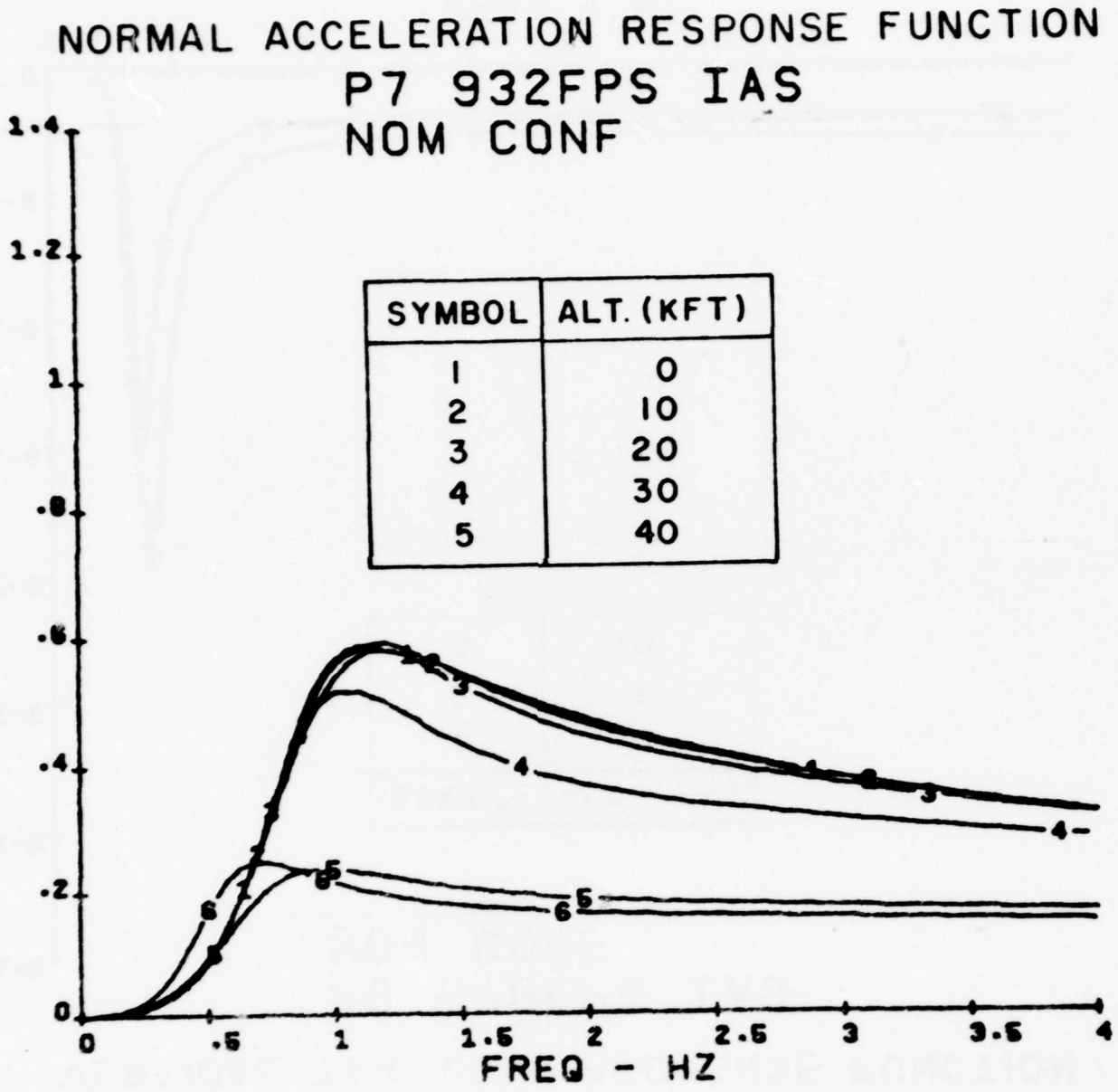
NORMAL ACCELERATION RESPONSE FUNCTION
P7 932FPS IAS
NOM CONF
SYMBOL | ALT. (KFT)
1 | 0
2 | 10
3 | 20
4 | 30
5 | 40
F_{n_z}
1.4
1.2
1
.8
.6
.4
.2
0
0
.5
1
1.5
2
2.5
3
3.5
4
FREQ - HZ

Figure B.37

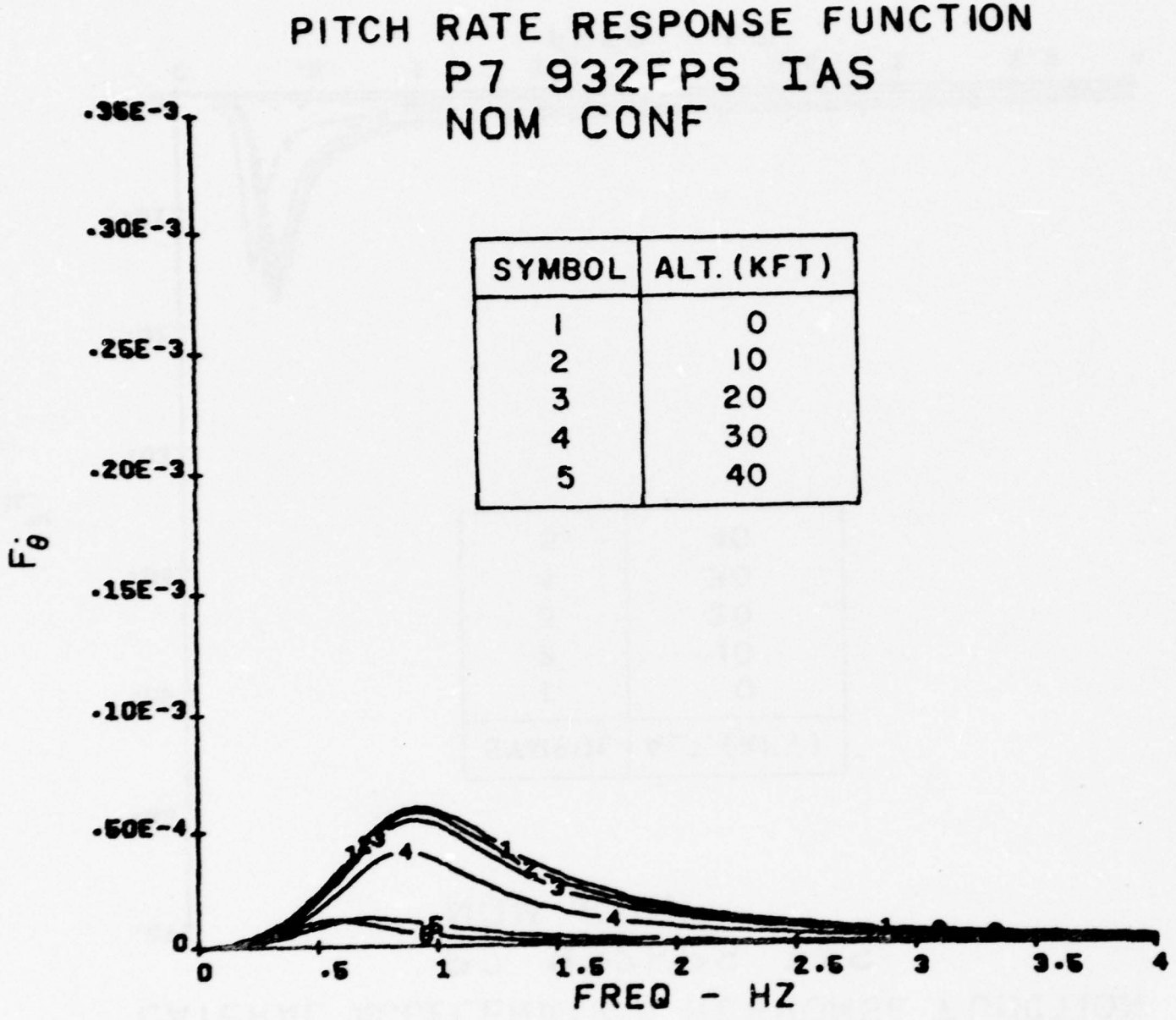
PITCH RATE RESPONSE FUNCTION
P7 932FPS IAS
NOM CONF
SYMBOL | ALT. (KFT)
1 | 0
2 | 10
3 | 20
4 | 30
5 | 40
.35E-3
.30E-3
.25E-3
.20E-3
.15E-3
.10E-3
.50E-4
0
$F_{\dot{\theta}}$
0
.5
1
1.5
2
2.5
3
3.5
4
FREQ - HZ

Figure B.38

LATERAL ACCELERATION RESPONSE FUNCTION

P7 932FPS IAS
NOM CONF

SYMBOL	ALT. (KFT)
1	0
2	10
3	20
4	30
5	40

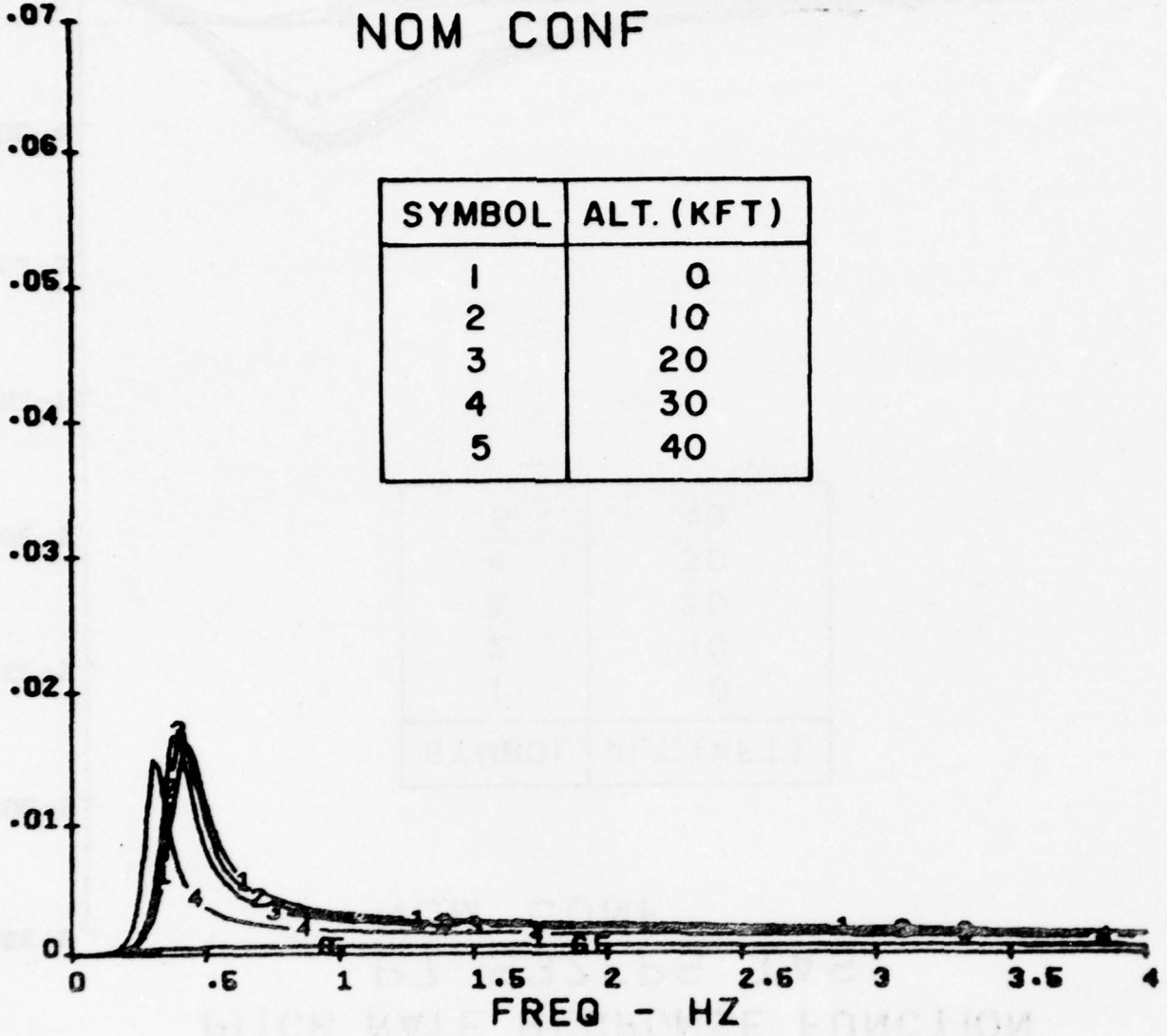

Figure B.39

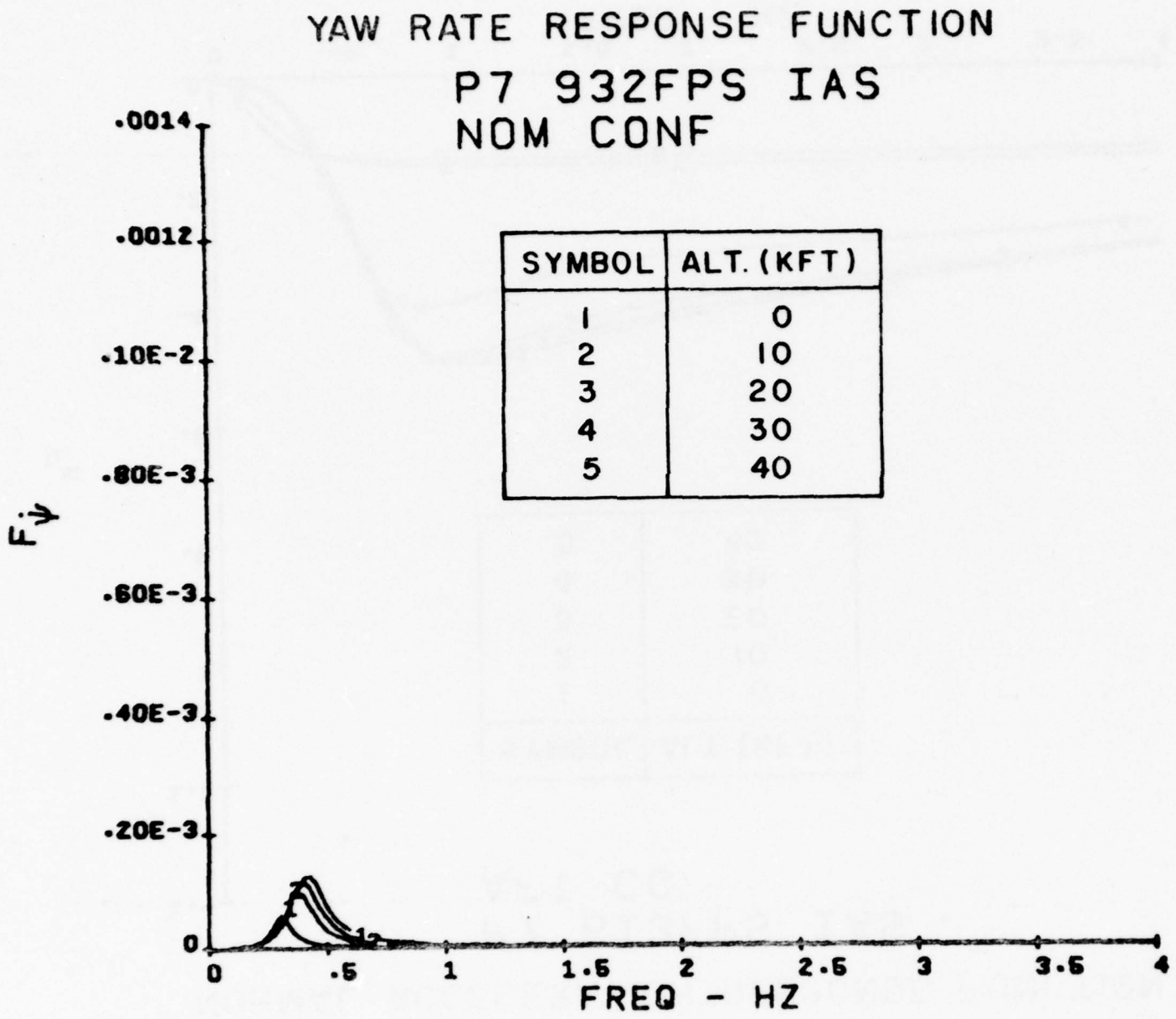
YAW RATE RESPONSE FUNCTION
P7 932FPS IAS
NOM CONF
SYMBOL | ALT. (KFT)
1 | 0
2 | 10
3 | 20
4 | 30
5 | 40
.0014
.0012
.10E-2
.80E-3
.60E-3
.40E-3
.20E-3
0
Fψ̇
0
.5
1
1.5
2
2.5
3
3.5
4
FREQ - HZ

Figure B.40

NORMAL ACCELERATION RESPONSE FUNCTION

P7 613FPS IAS
AFT CG

SYMBOL	ALT. (KFT)
1	0
2	10
3	20
4	30
5	40

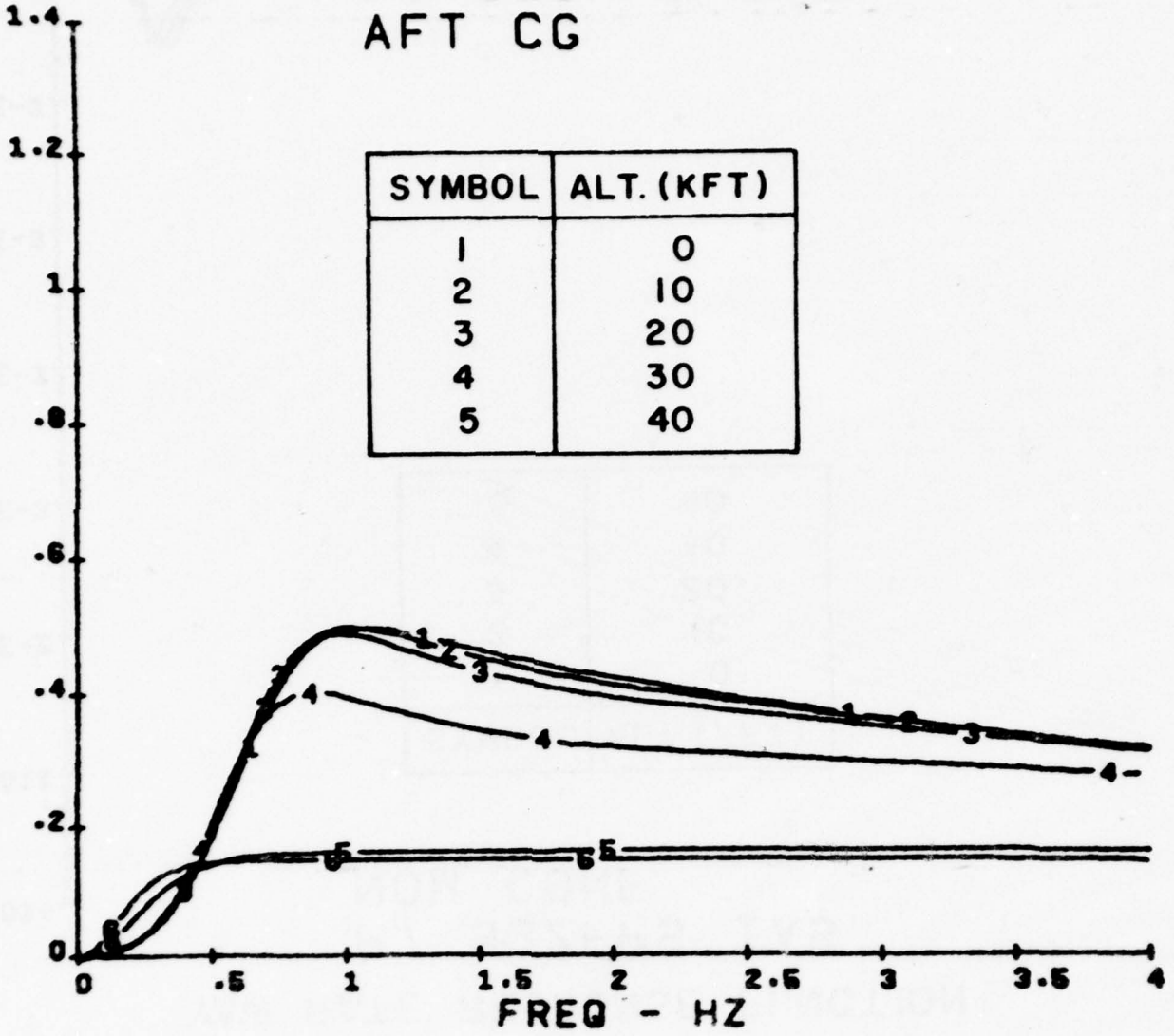

Figure B.41

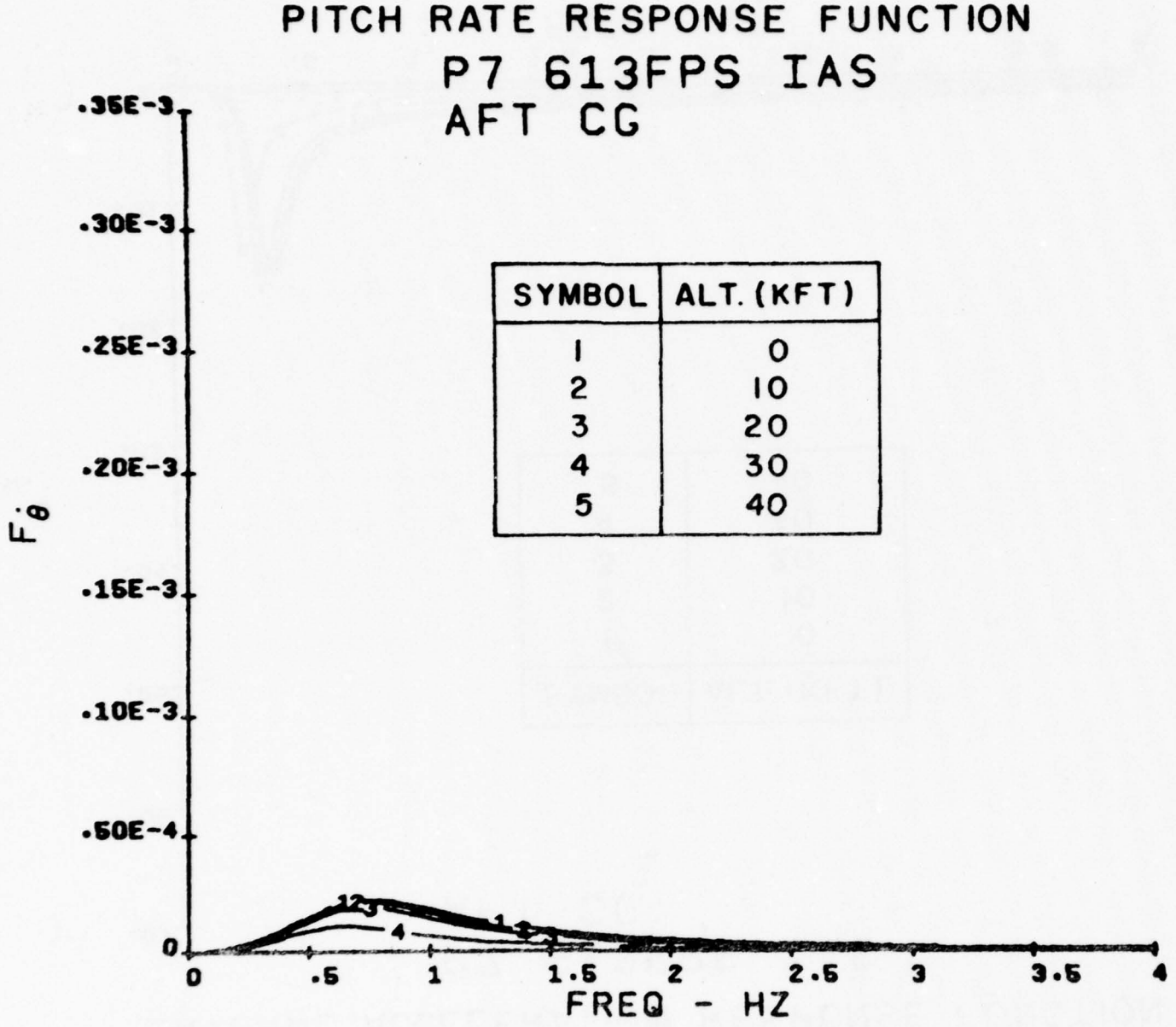
PITCH RATE RESPONSE FUNCTION
P7 613FPS IAS
AFT CG
SYMBOL | ALT. (KFT)
1 | 0
2 | 10
3 | 20
4 | 30
5 | 40
.35E-3
.30E-3
.25E-3
.20E-3
.15E-3
.10E-3
.50E-4
0
$F_{\dot{\theta}}$
0
.5
1
1.5
2
2.5
3
3.5
4
FREQ - HZ

Figure B.42

LATERAL ACCELERATION RESPONSE FUNCTION

P7 613FPS IAS
AFT CG

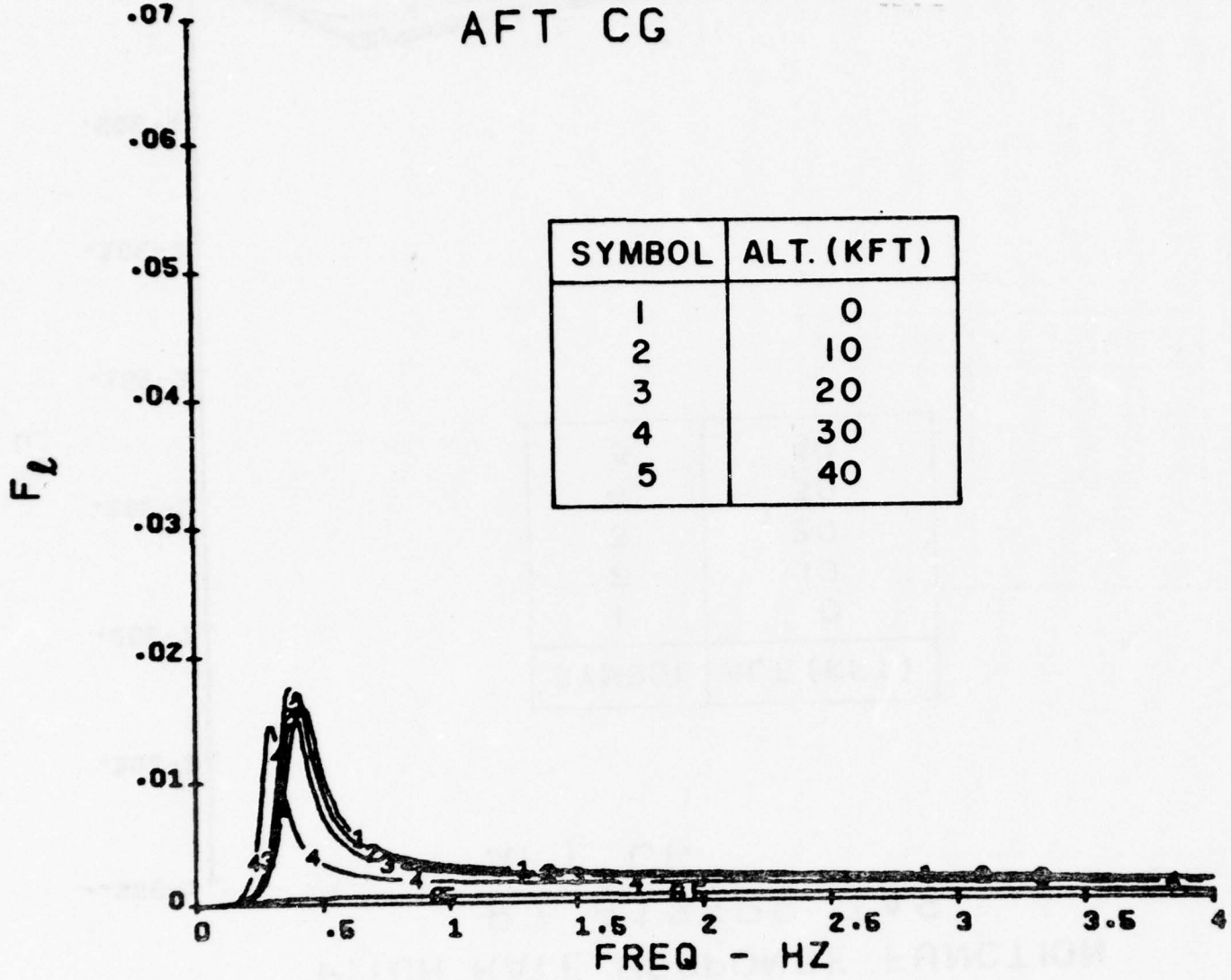

SYMBOL	ALT. (KFT)
1	0
2	10
3	20
4	30
5	40

Figure B.43

YAW RATE RESPONSE FUNCTION

P7 613FPS IAS
AFT CG

SYMBOL	ALT. (KFT)
1	0
2	10
3	20
4	30
5	40

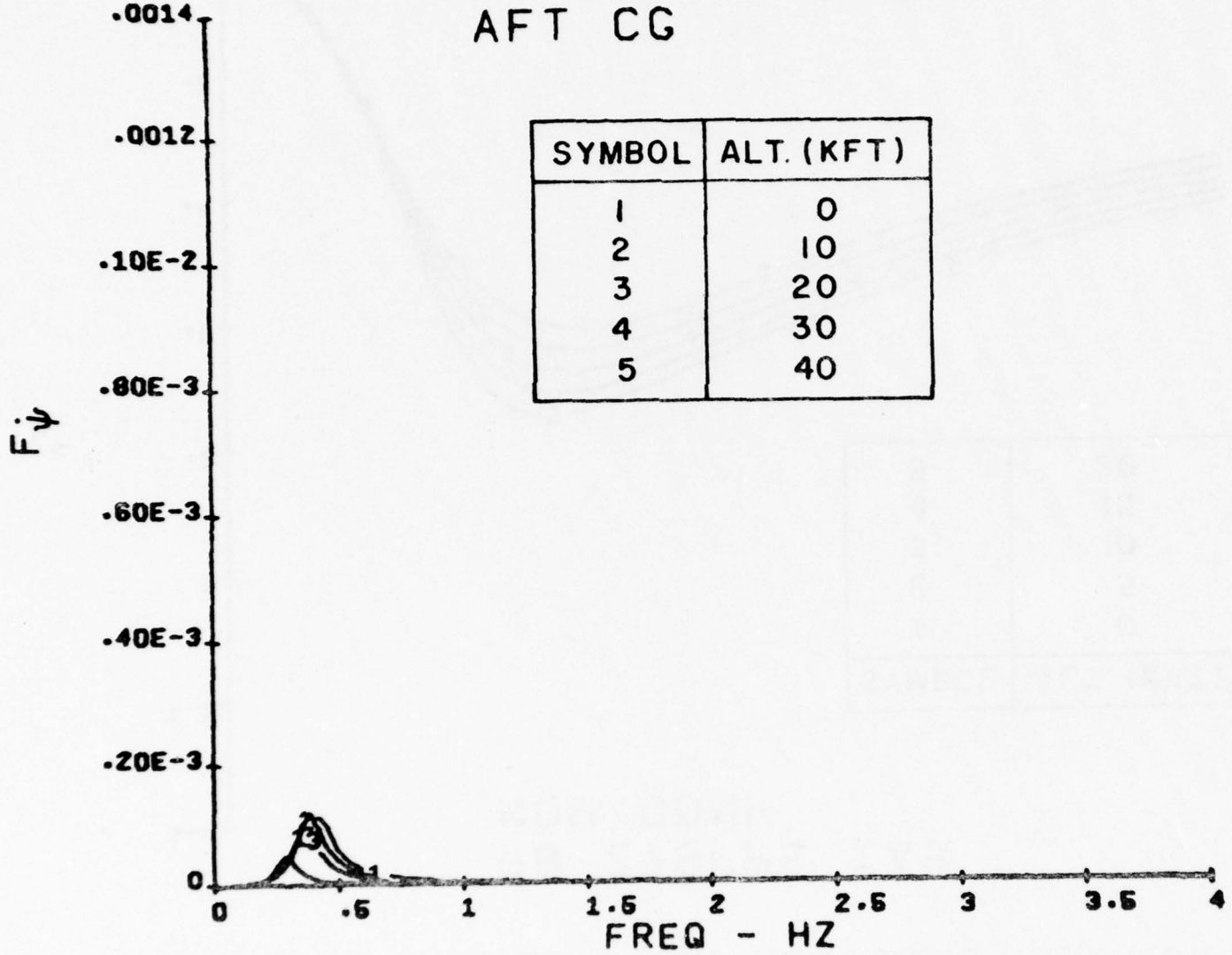

Figure B.44

NORMAL ACCELERATION RESPONSE FUNCTION

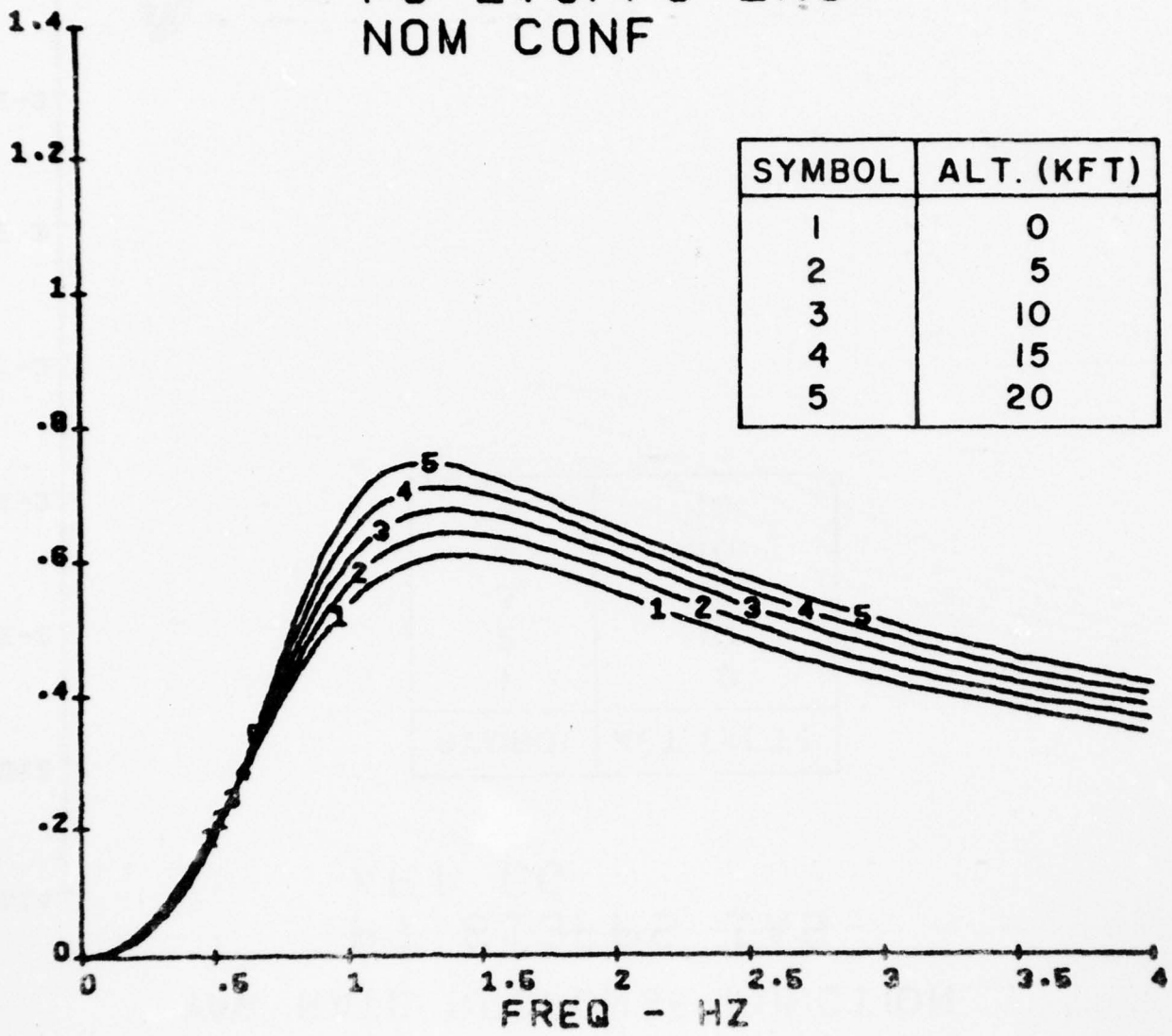

Figure B.45

PITCH RATE RESPONSE FUNCTION

P8 279FPS IAS
NOM CONF

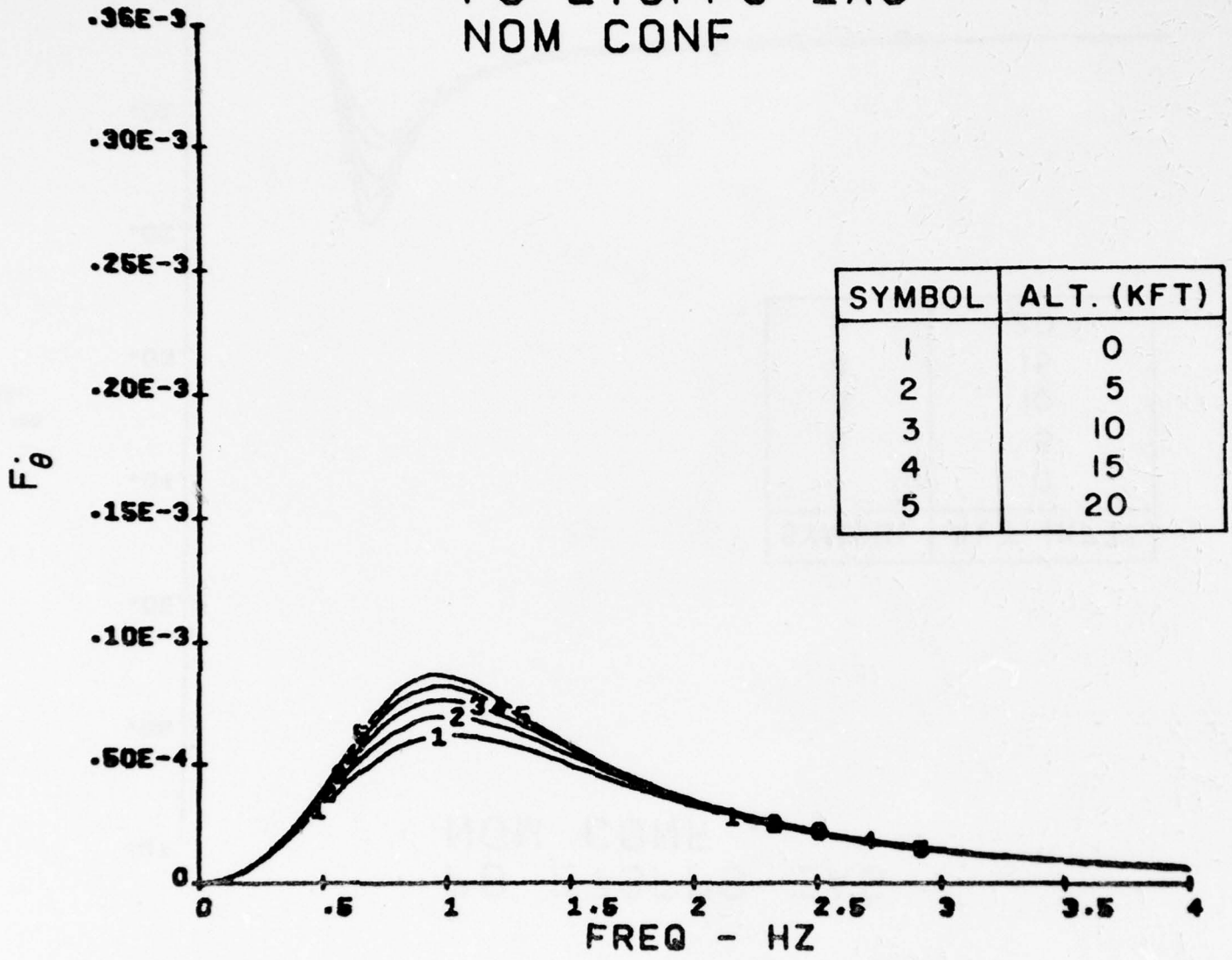

SYMBOL	ALT. (KFT)
1	0
2	5
3	10
4	15
5	20

Figure B.46

LATERAL ACCELERATION RESPONSE FUNCTION

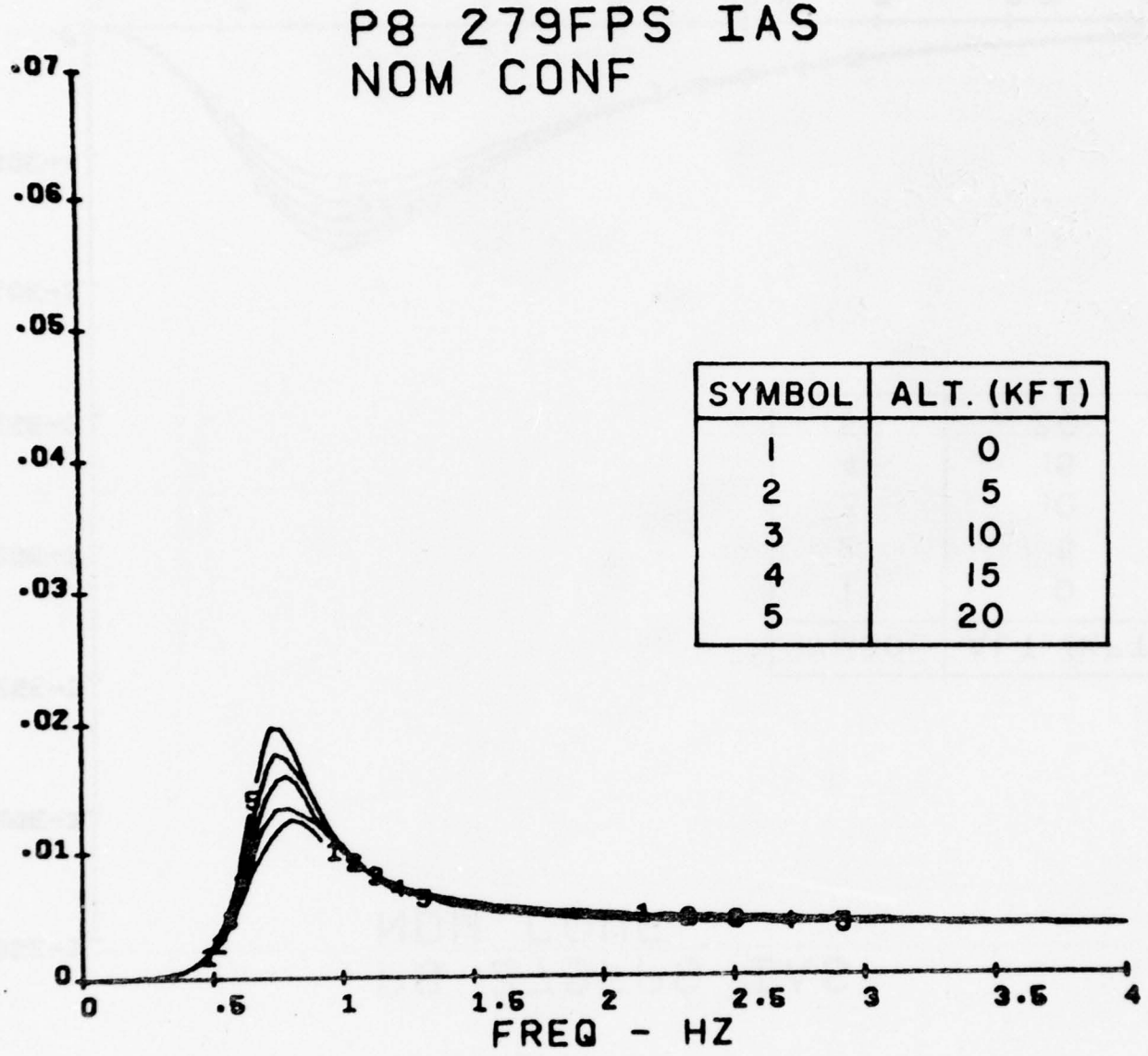

Figure B.47

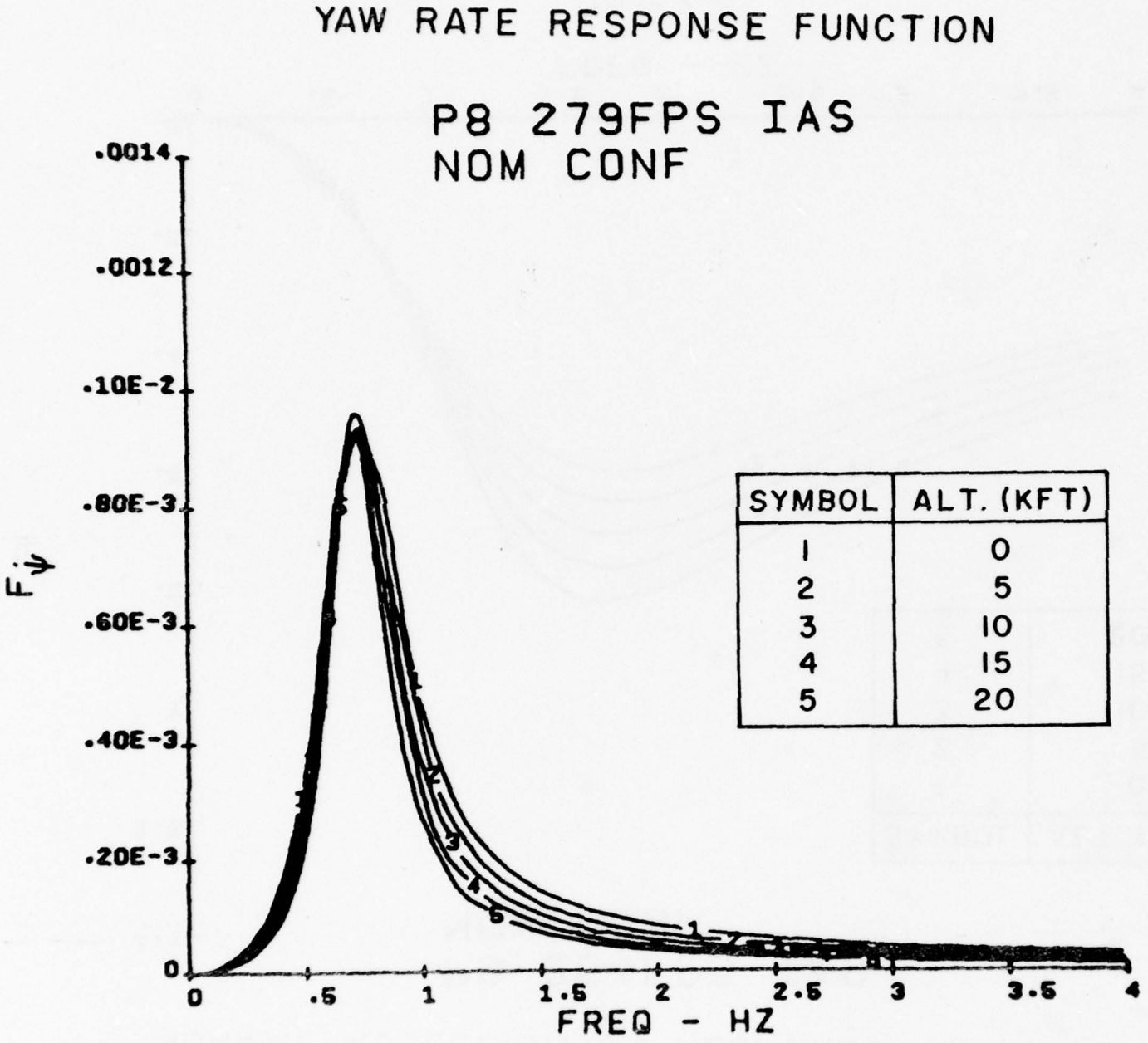
YAW RATE RESPONSE FUNCTION
P8 279FPS IAS
NOM CONF
.0014
.0012
.10E-2
.80E-3
.60E-3
.40E-3
.20E-3
0
$F_{\dot{\psi}}$
0
.5
1
1.5
2
2.5
3
3.5
4
FREQ - HZ
SYMBOL | ALT. (KFT)
1 | 0
2 | 5
3 | 10
4 | 15
5 | 20

Figure B.48

NORMAL ACCELERATION RESPONSE FUNCTION

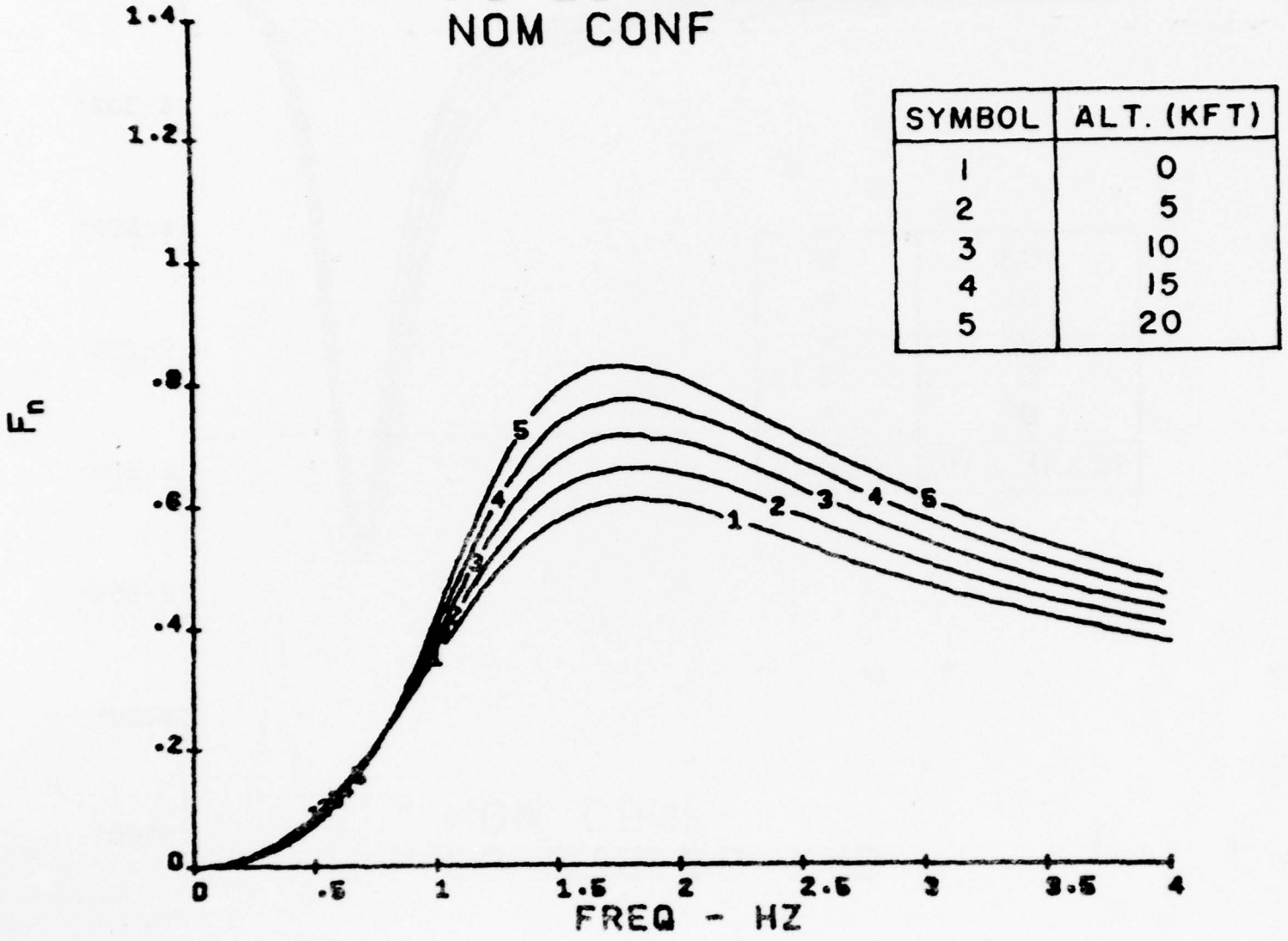

Figure B.49

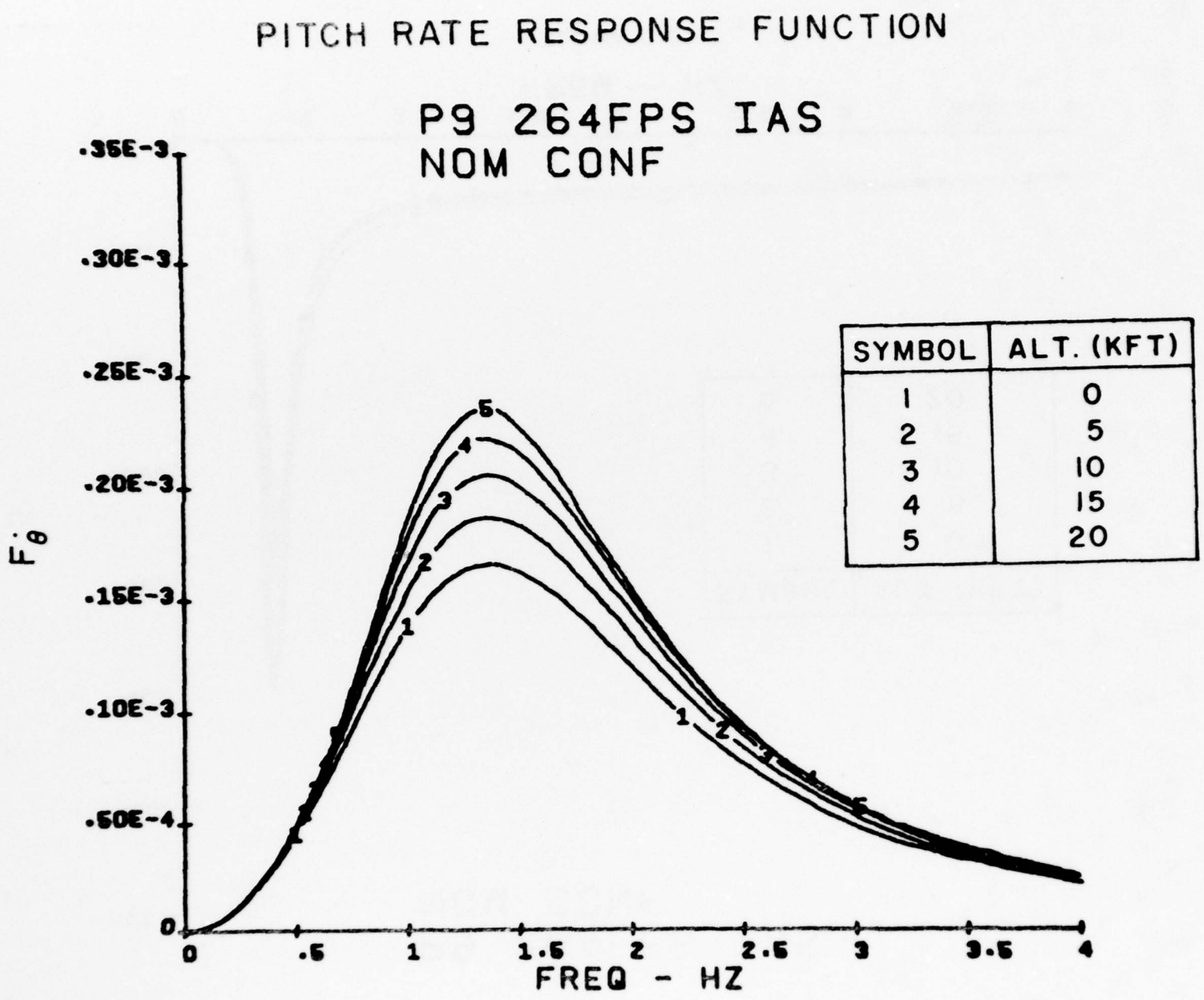
PITCH RATE RESPONSE FUNCTION
P9 264FPS IAS
NOM CONF
.35E-3
.30E-3
.25E-3
.20E-3
.15E-3
.10E-3
.50E-4
0
$F_{\dot{\theta}}$
SYMBOL | ALT. (KFT)
1 | 0
2 | 5
3 | 10
4 | 15
5 | 20
0
.5
1
1.5
2
2.5
3
3.5
4
FREQ - HZ

Figure B.50

LATERAL ACCELERATION RESPONSE FUNCTION

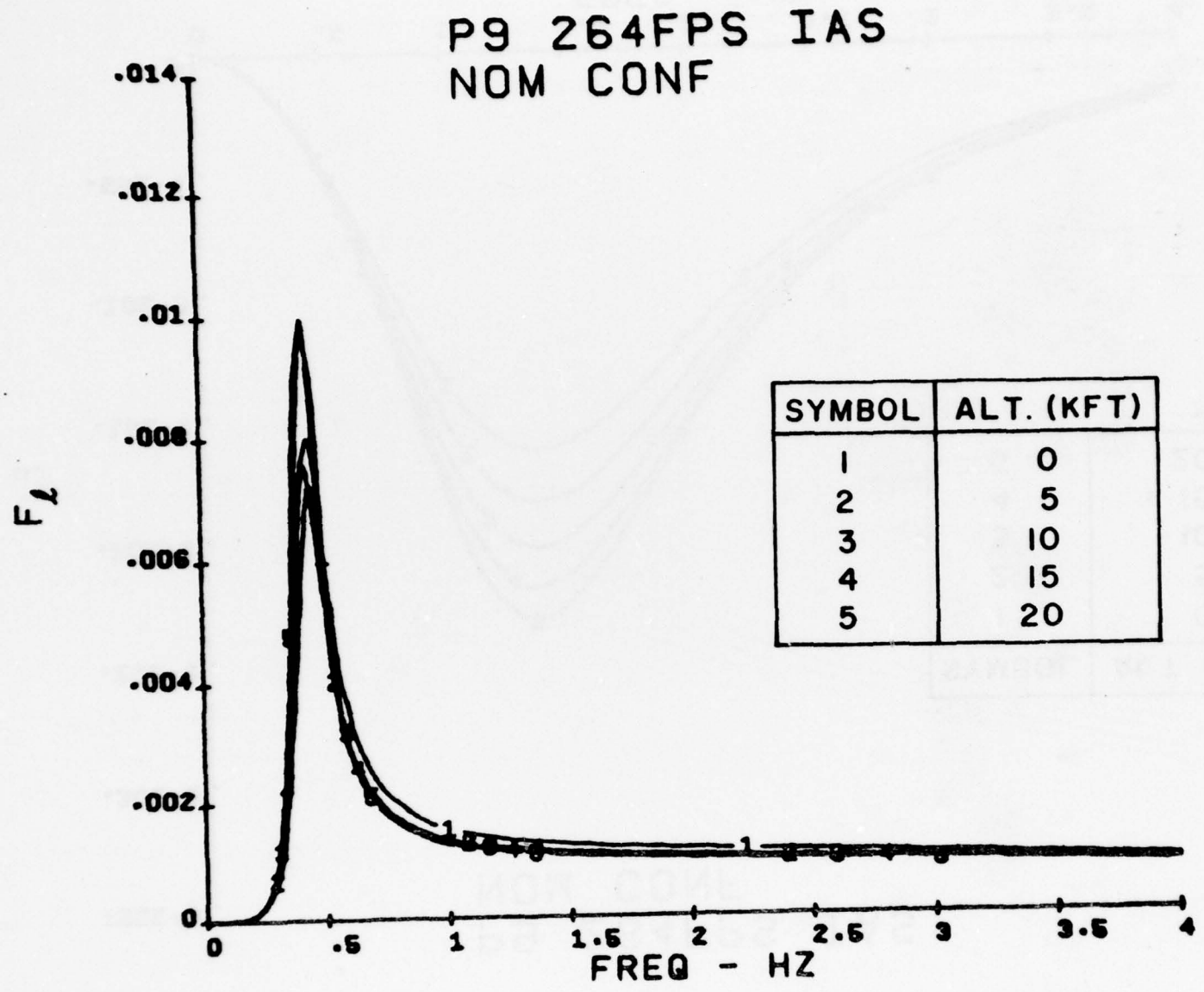

Figure B.51

YAW RATE RESPONSE FUNCTION

P9 264FPS IAS
NOM CONF

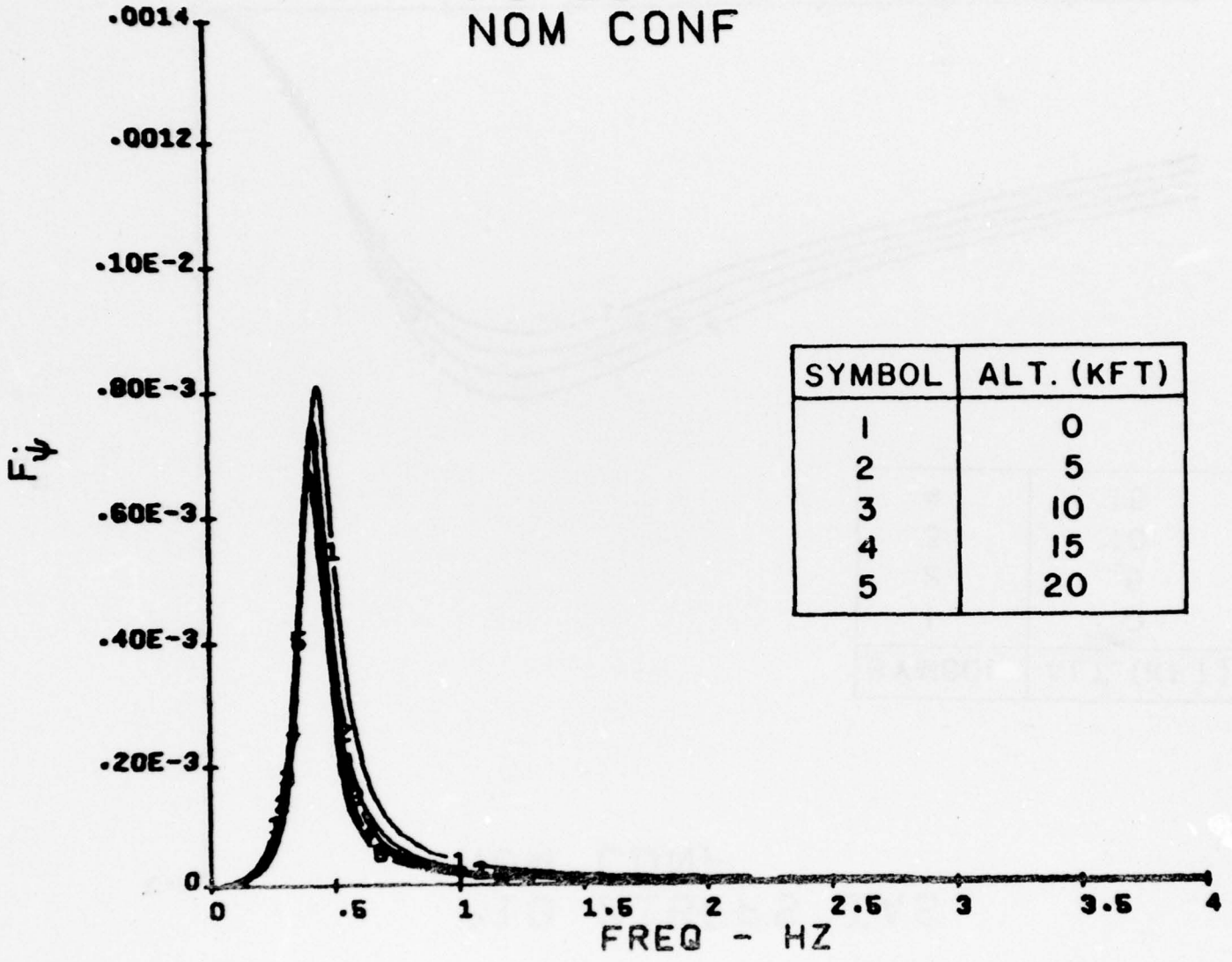

SYMBOL	ALT. (KFT)
1	0
2	5
3	10
4	15
5	20

Figure B.52

NORMAL ACCELERATION RESPONSE FUNCTION

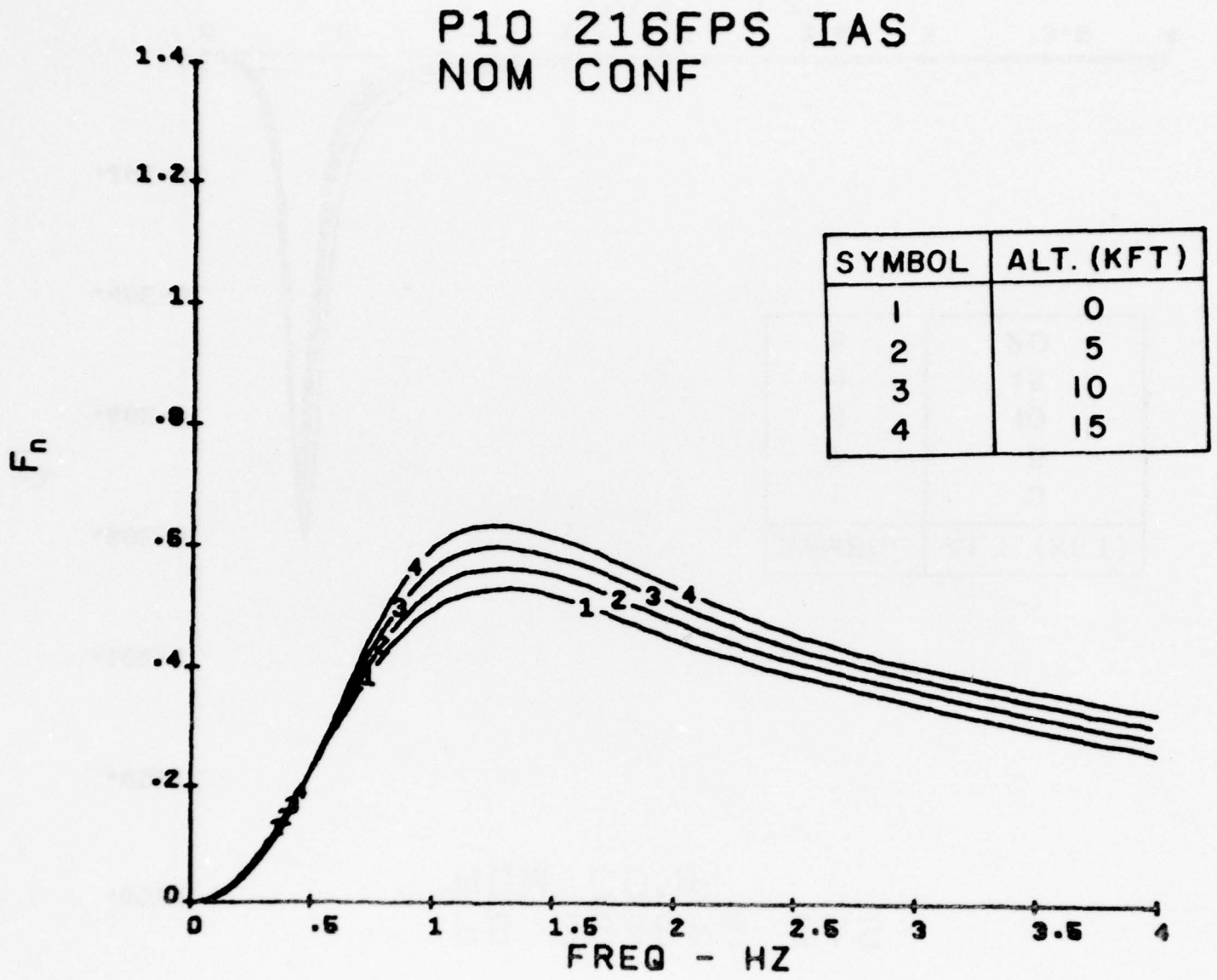

Figure B.53

PITCH RATE RESPONSE FUNCTION

P10 216FPS IAS
NOM CONF

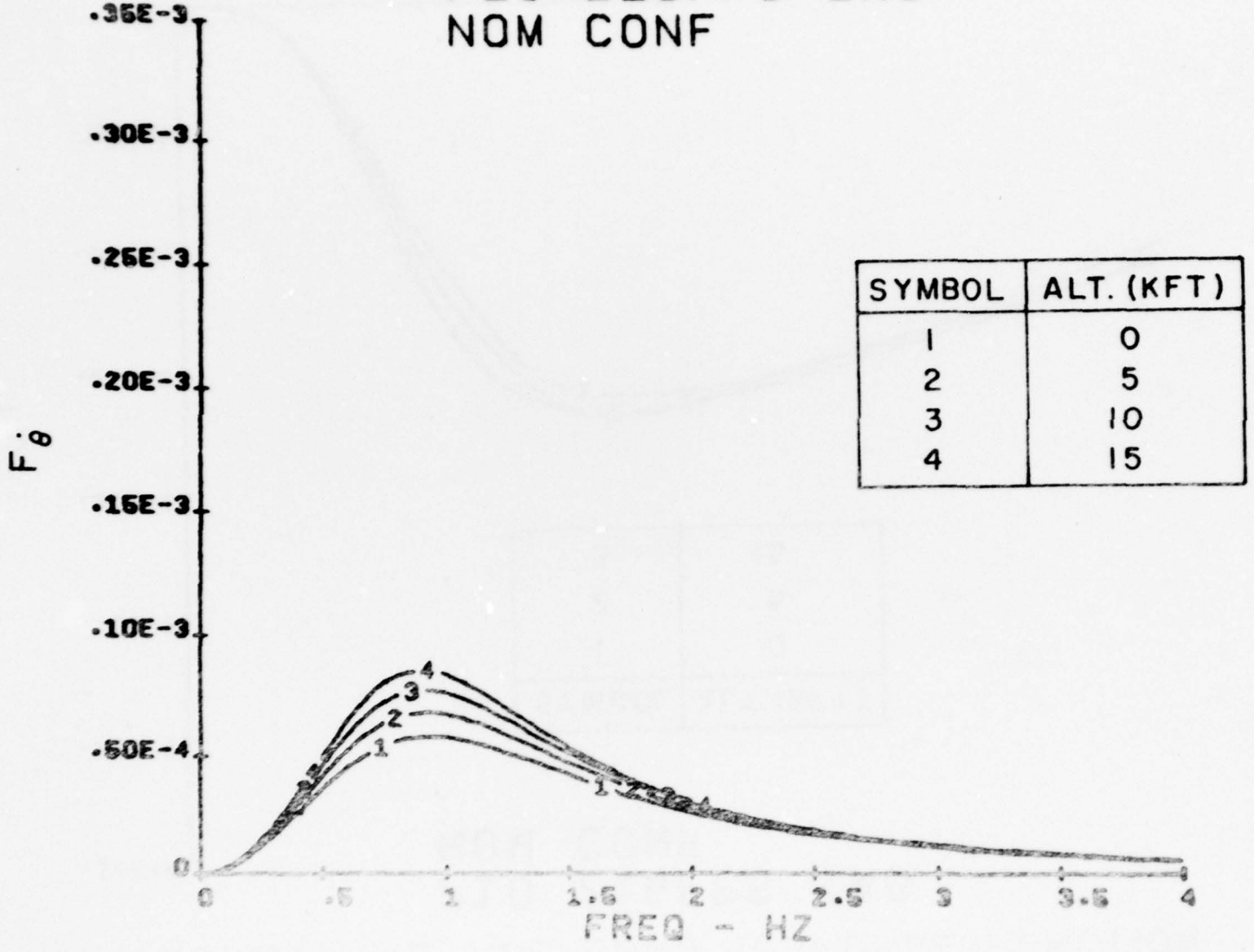

SYMBOL	ALT. (KFT)
1	0
2	5
3	10
4	15

Figure B.54

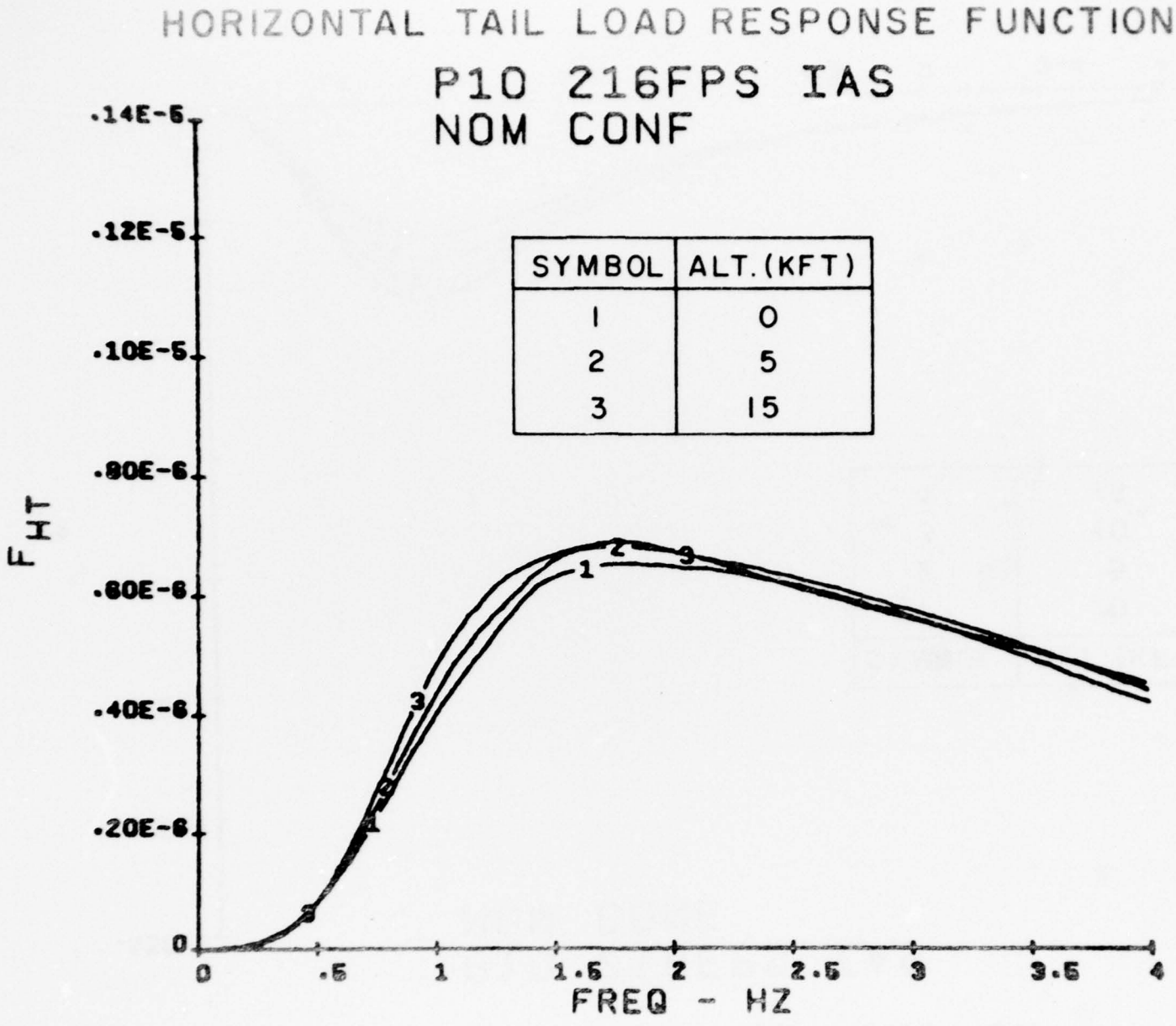
HORIZONTAL TAIL LOAD RESPONSE FUNCTION
P10 216FPS IAS
NOM CONF
SYMBOL | ALT.(KFT)
1 | 0
2 | 5
3 | 15
.14E-5
.12E-5
.10E-5
.80E-6
.60E-6
.40E-6
.20E-6
0
F HT
0
.5
1
1.5
2
2.5
3
3.5
4
FREQ - HZ

Figure B.55

LATERAL ACCELERATION RESPONSE FUNCTION

P10 216FPS IAS
NOM CONF

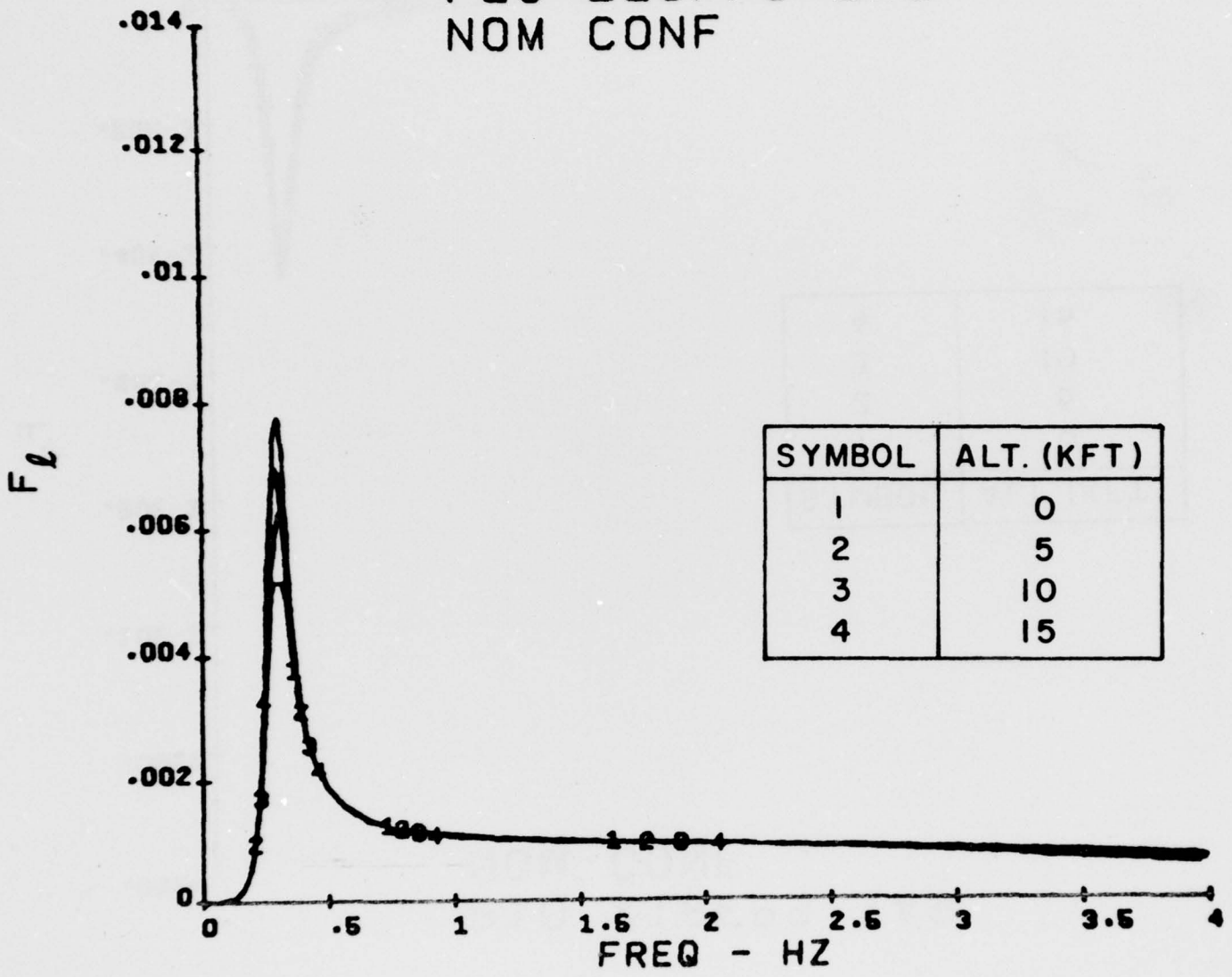

Figure B.56

YAW RATE RESPONSE FUNCTION

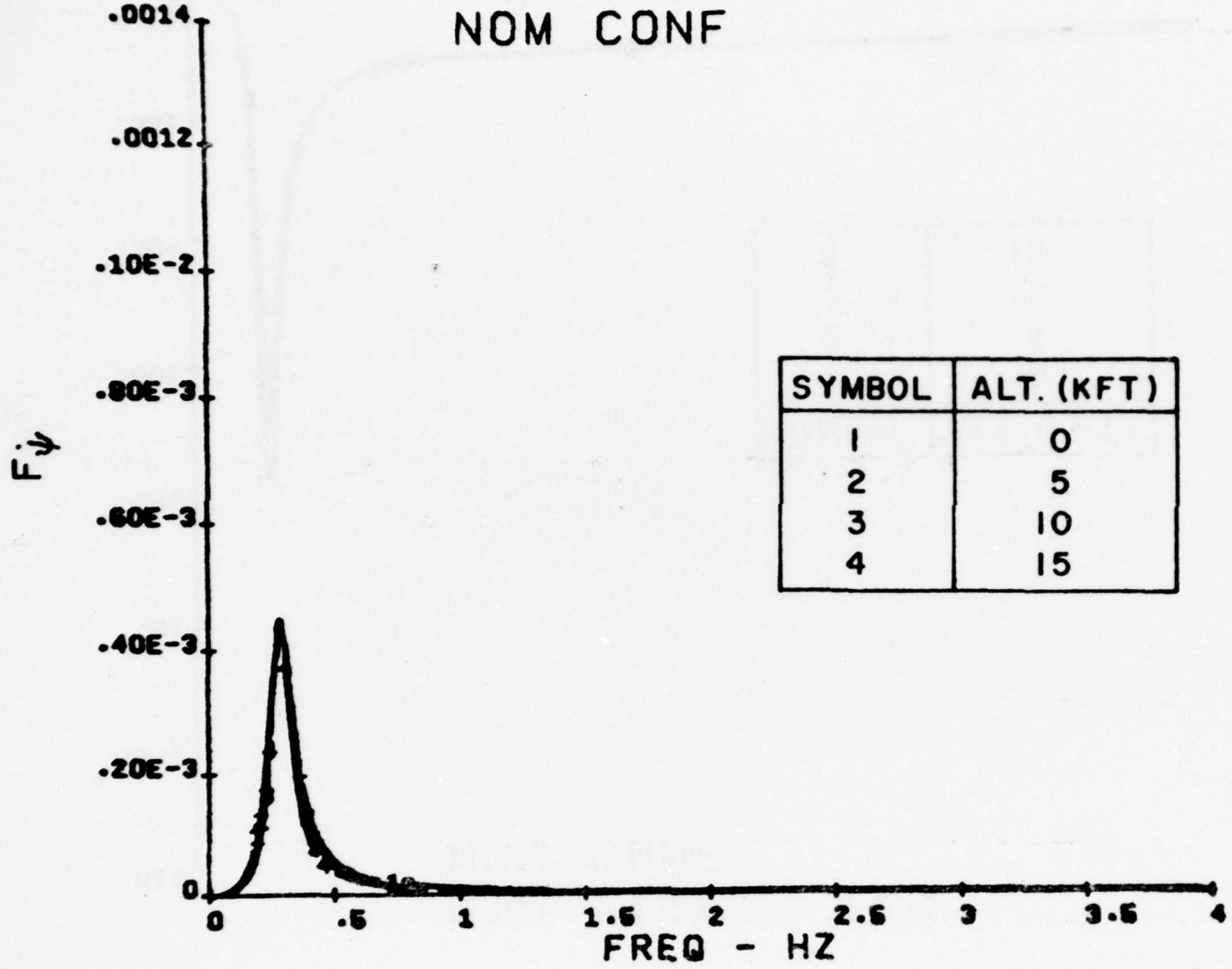

Figure B.57

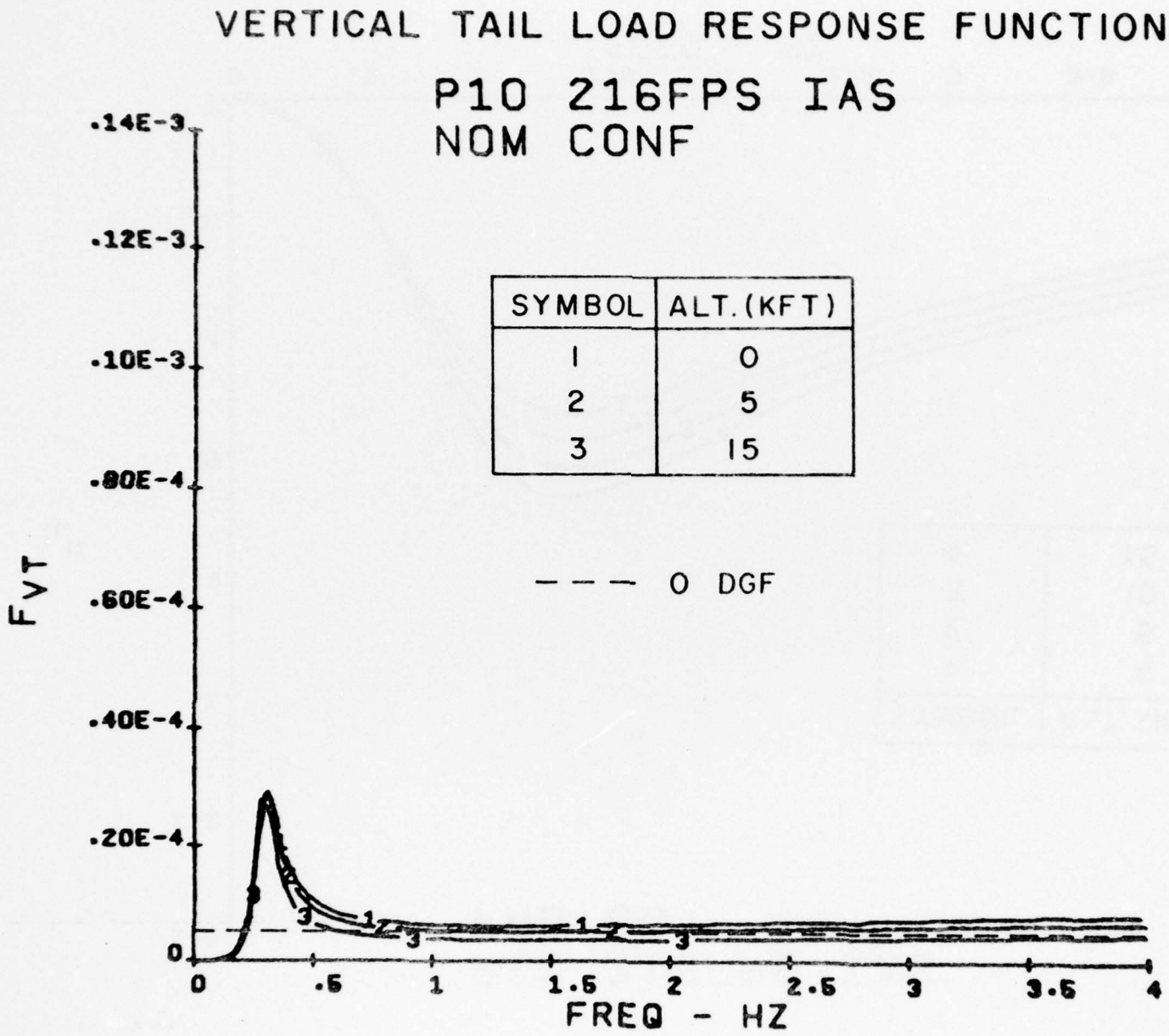
VERTICAL TAIL LOAD RESPONSE FUNCTION
P10 216FPS IAS
NOM CONF
SYMBOL | ALT.(KFT)
1 | 0
2 | 5
3 | 15
--- 0 DGF
F_{VT}
.14E-3
.12E-3
.10E-3
.80E-4
.60E-4
.40E-4
.20E-4
0
0
.5
1
1.5
2
2.5
3
3.5
4
FREQ - HZ

Figure B.58

NORMAL ACCELERATION RESPONSE FUNCTION

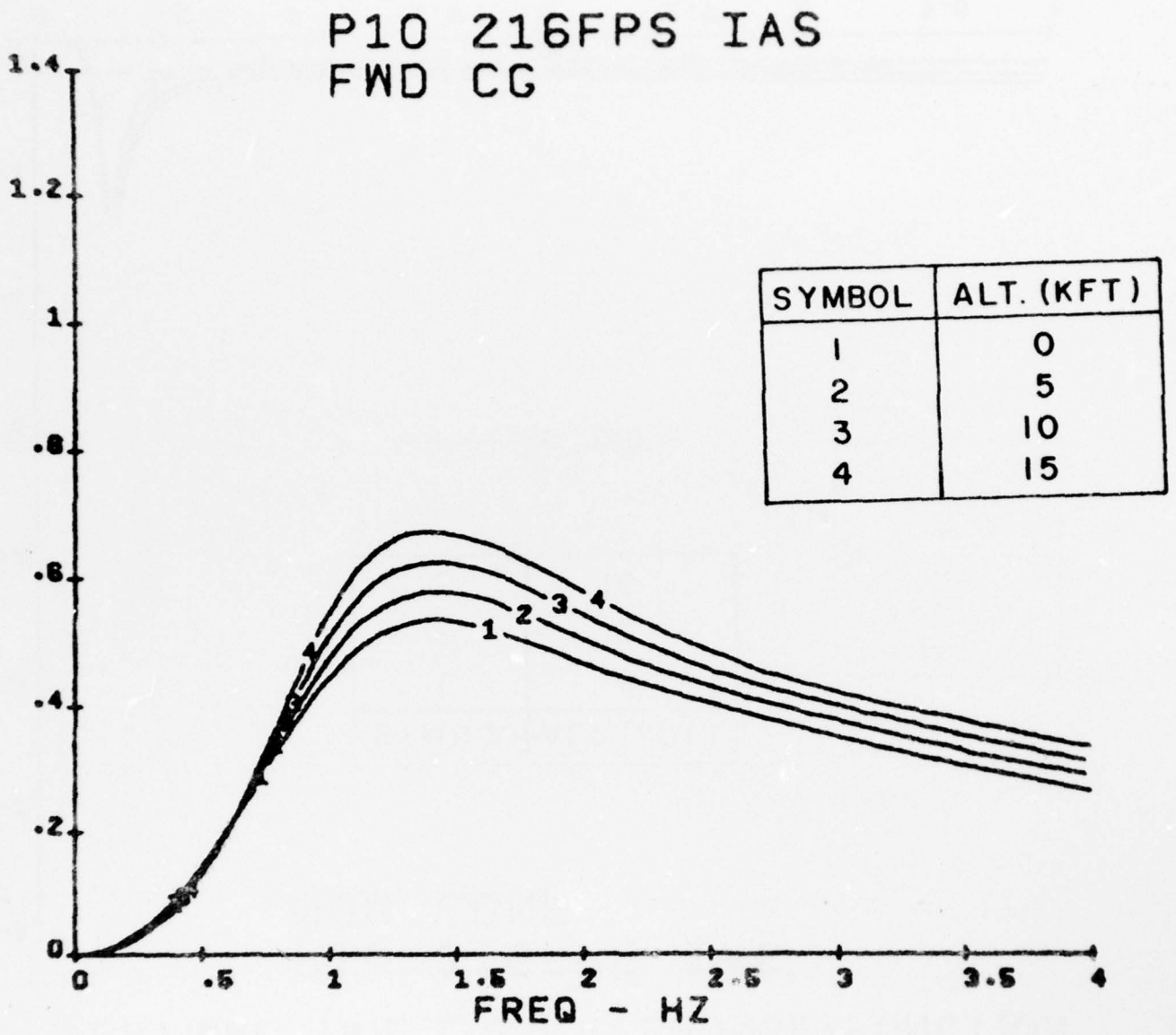

Figure B.59

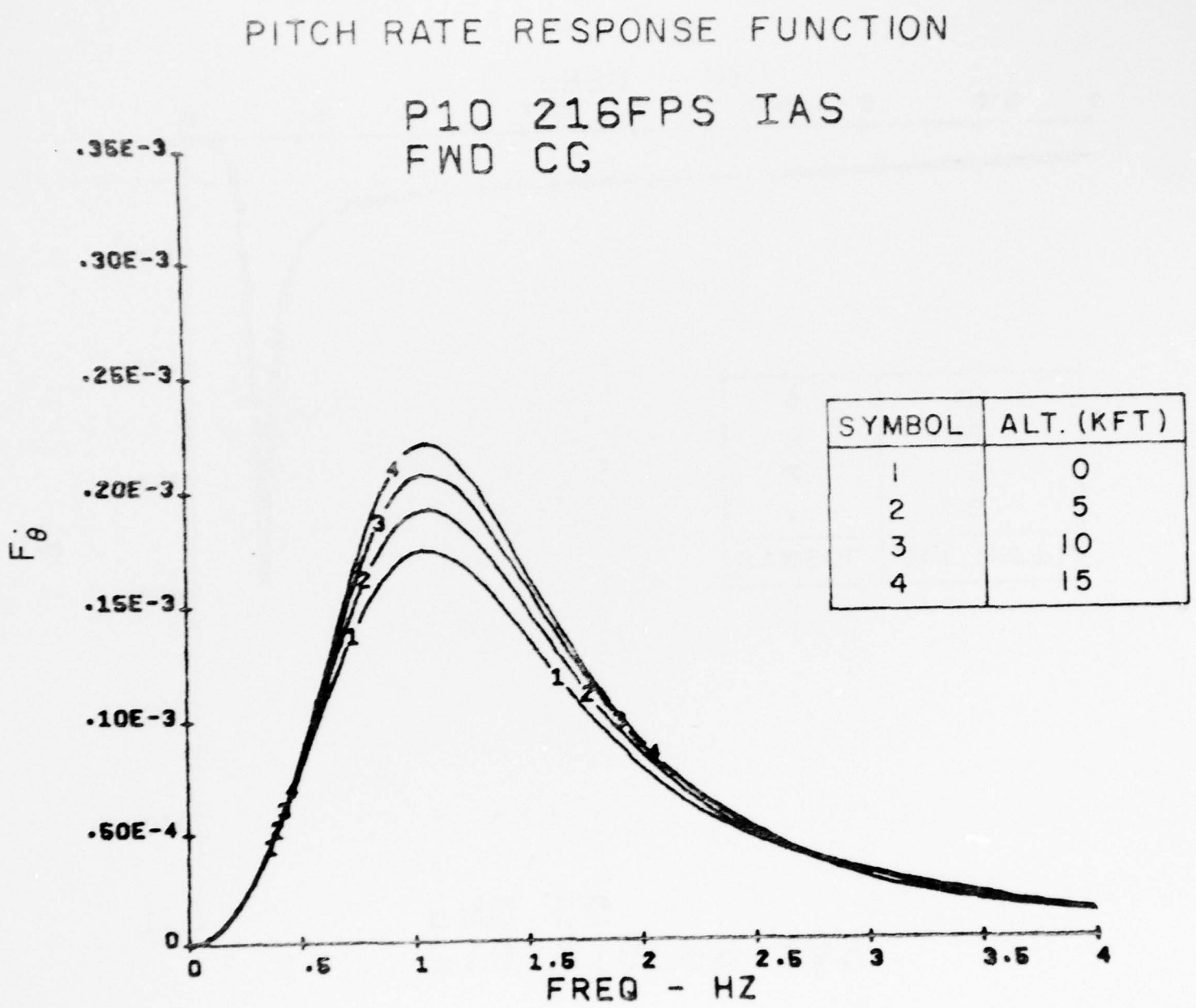
PITCH RATE RESPONSE FUNCTION
P10 216FPS IAS
FWD CG
.35E-3
.30E-3
.25E-3
.20E-3
.15E-3
.10E-3
.50E-4
0
$F_{\dot{\theta}}$
0
.5
1
1.5
2
2.5
3
3.5
4
FREQ - HZ
SYMBOL | ALT. (KFT)
1 | 0
2 | 5
3 | 10
4 | 15

Figure B.60

LATERAL ACCELERATION RESPONSE FUNCTION

P10 216FPS IAS
FWD CG

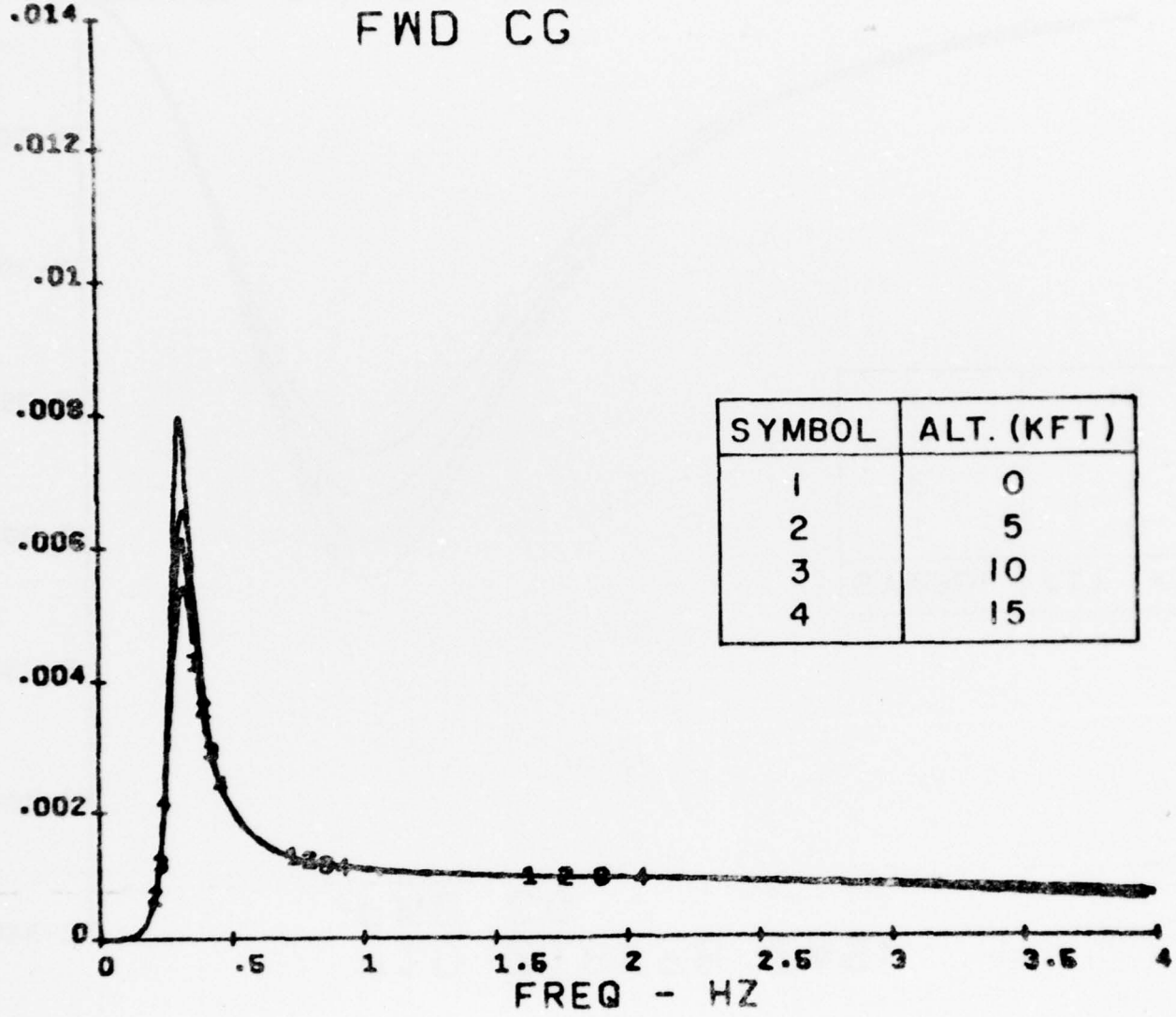

Figure B.61

YAW RATE RESPONSE FUNCTION

P10 216FPS IAS
FWD CG

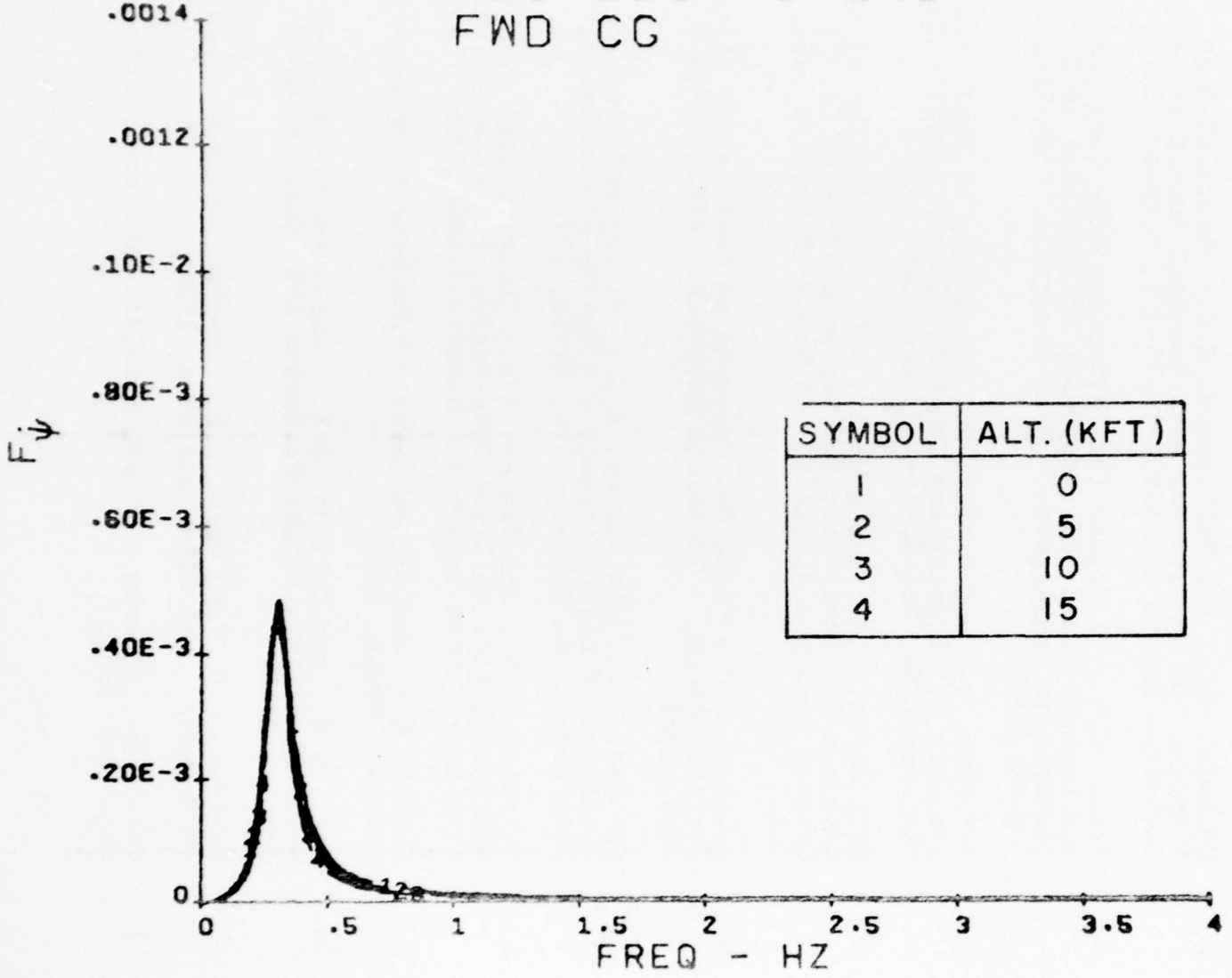

SYMBOL	ALT. (KFT)
1	0
2	5
3	10
4	15

Figure B.62

REFERENCES

1. Houbolt, J.C.: "Design Manual for Vertical Gusts Based on Power Spectral Techniques," Technical Report No. AFFDL-TR-70-106, December, 1970.

2. Houbolt, J.C., and Williamson, G.G.: "Spectral Gust Response for an Airplane with Vertical Motion and Pitch," Technical Report No. AFFDL-TR-75-121, October, 1975.

3. Peele, E.L.: "A Method for Estimating Some Longitudinal and Lateral Rigid-Body Responses of Airplanes to Continuous Atmospheric Turbulence," NASA Report No. NASA-TN-D-6273, August, 1971.

4. Petrakis, J., and Miller, N.: "Responses of Small Rigid Aircraft to Discrete and Continous Gust Analysis - Phase 1," FAA Report No. FAA-RD-74-160, December, 1975.

5. Williamson, G.G., and Houbolt, J.C.: "Evaluation of Gust Response Parameters for Two-Degree-of-Freedom for Seven General Aviation Aircraft," A.R.A.P. Report No. 282, June, 1976.

6. Houbolt, J.C.: "Some New Concepts in Oscillatory Lifting Surface Theory," Technical Report No. AFFDL-TR-69-2, June, 1969.

7. Smetana, F.O., and Summey, R.C.: "Riding and Handling Qualities of Light Aircraft - A Review and Analysis," NASA Report No. NASA-CR-;975, March, 1972.

8. Wolowicz, C.H., and Yancey, R.B.: "Longitudinal Aerodynamic Characteristics of Light Twin-Engine, Propeller-Driven Airplanes," NASA Report No. NASA-TN-D-6800, June, 1972.

9. Seckel, E.: *Stability and Control of Airplanes and Helicopters*, Academic Press, 1964.

10. Hoak, O.E., and Ellison, D.E.: *USAF Stability and Control Handbook, (DATCOM)*, Wright-Patterson AFB, Ohio, Revised August, 1968.

11. Perkins, C.D., and Hage, R.E.: *Airplane Performance Stability and Control*, John Wiley and Sons, 1958.

12. Etkin, B.: *Dynamics of Flight, Stability and Control*, John Wiley and Sons, 1967.